AD-A164 485

ADVANCED LPI INTERCEPT DETECTOR RESEARCH

DTIC

≣ Axiomatix

DTIC
ELECTE
FEB 21 1986
S D
D

86 2 7 005

12

ADVANCED LPI INTERCEPT DETECTOR RESEARCH

DTIC
SELECTED
FEB 2 1 1986
D

Final Report

Contract No. N00014-82-C-0585

Prepared for

Office of Naval Research

Prepared by

Dr. Andreas Polydoros

With Contributions by

Dr. C.L. Nikias
Dr. Kai T. Woo

Axiomatix
9841 Airport Boulevard, Suite 912
Los Angeles, California 90045

Axiomatix Report No. R8511-3
November 13, 1985

Tables of Contents

i

List of Figures

List of Tables

1.0 INTRODUCTION

We examine in this report the problem of wideband detection of a spread spectrum signal from an interceptor's viewpoint; our aim is to derive, evaluate and compare various detector structures whose purpose is to intercept a spread-spectrum communication transmitter. *The transmitter under surveillance employs a variety of modulation/ spreading/transmission techniques which are invariably assumed to emit the message-bearing signal in deep background noise or interference.* Thus, the challenging task of the intercepting detector is to reveal as best as possible any transmission of the unknown spread waveform in the presence of an obscuring noisy environment.

Naturally, the degree of success achieved by the interceptor when detecting the presence of the communicator's spread signal depends on the amount of information available to him regarding the structure of that signal. At one extreme, the interceptor's most fortunate situation would be to acquire the spreading code itself ("crack" the code). If this is too demanding, he must settle for less, such as approximate knowledge of the signal's carrier center frequency, code rate, code epoch, spreading bandwidth, etc., or a subset thereof. At the other extreme, he might know almost nothing,[1] in which case, he could resort to a simple energy discriminator device (i.e.,"radiometer") since it is, on many occasions, a low-SNR asymptotically optimal detector [1,2]. In this report our main interest is to investigate the possibility that the interceptor could do better by optimally processing whatever information is available to him between the two extremes cited above.

The detectability of the primary candidates for low-probability-of-intercept (LPI) waveforms, such as direct-sequence (DS), frequency-hopping (FH), time-hopping (TH) and their hybrids, is customarily related to two factors: (1) performance level of the interceptor's detector whose only function is to monitor the communicated messages and, (2) amount of signal processing (i.e., complexity) associated with such performance.

---

[1]Approximate spectral band location is a minimum prerequisite for any interceptor.

1

In subsequent sections, it will be shown that the detectability (exploitability) of a spread signal is greatly dependent on the interceptor's knowledge regarding the form of both the waveform and the interference. In other words, one should know not only the spreading format used (plus, possibly, some other parameters), but it is also very helpful to be able to identify the kind of background noise or interference involved. Although most of this report deals with white Gaussian noise as the dominant form of (omni-present) interference, a case is made in section 5.5. about the impact of nonwhite interference (random tones, in particular). It will be shown in Sections 3 through 5 that, when white noise is the only deterrent, the gains achieved by intelligent processing of the received waveform can vary from modest to significant (always as compared to the performance of a radiometer), depending on the scenario at hand. However, when random interfering tones are present and a DS or a hybrid FH/DS is detected, those gains could become impressive (many tens of decibels, for example). For details, see Section 5.5.

In searching for those structures which perform the aforementioned tasks, we start from the optimal solutions, as derived from applying the optimal likelihood-ratio rule. The results assume a good deal of knowledge about the signal parameters (although never the spreading code itself) and could thus become rather academic in most practical situations. Furthermore, they typically suffer from the common symptom of prohibitive implementational complexity. Thus, it is important to consider suboptimal structures and evaluate their relative loss with respect to the (unattainable) optimal performance; this has indeed been the spirit which permeated the present topic.

The report is organized as follows: In the remaining part of this section we classify the various receivers and briefly lay the theoretical groundwork for evaluating the forthcoming detector structures. In Section 3, 4 and 5, we develop the theory for DS, TH and FH signals, respectively.

There exists a wide variety of interceptor receiver structures, a rough classification of which is attempted below and is also depicted in Figure 1. The various factors

2

incorporated in the classsification include the spread spectrum signal whose interception (detection) is sought, the optimality or suboptimality of the interceptor's decision algorithm, the degree of knowledge of different system parameters, etc. Wideband detectors can first be classified as optimal or suboptimal. We term "optimal" those structures which result from a straightforward application of the generalized likelihood ratio theory to this problem and invoke a number of assumptions regarding the signal structure. For instance, optimal solutions typically assume knowledge of certain parameters (code rate or hopping rate, SNR, carrier frequencies, etc.) and average over the unknown ones (timing epochs, time hopping or code sequences, etc.). Since, however, optimal structures are often hard to implement, one resorts to "suboptimal" solutions whereby either one (or more) assumptions are removed or certain "atypical" nonlinearities such as the ln cosh (•) function, are substituted by simpler ones as, for instance, a square--law device.

A second classification results from the nature of the spread-spectrum signal for which the intercepting device is designed, so it can be a DS, FH, TH or hybrid detector. Also, DS and TH detectors can be coherent or noncoherent, depending on whether or not the carrier phase is known. FH detectors are assumed to be noncoherent from hop to hop due to the nature of the communicating channel and the transmitter wideband FH synthesizers.

The presence or absence of timing (epoch) information about the spreading code distinguishes detectors as synchronous or asynchronous. It is clear that timing is initially unavailable since the intercept detector does not even know if the signal is there; hence, asynchronous structures naturally attract more practical interest. However, synchronous and/or coherent detectors will also be considered -- not only because they provide useful upper bounds in performance -- but also because of the conceptual possibility of improved detector structure aided by the recursive estimation of pertinent parameters [9]. Furthermore, by quantizing the continuous-epoch uncertainty region into an adequate finite number of points, matched-detector structures can be devised that are synchronized to each
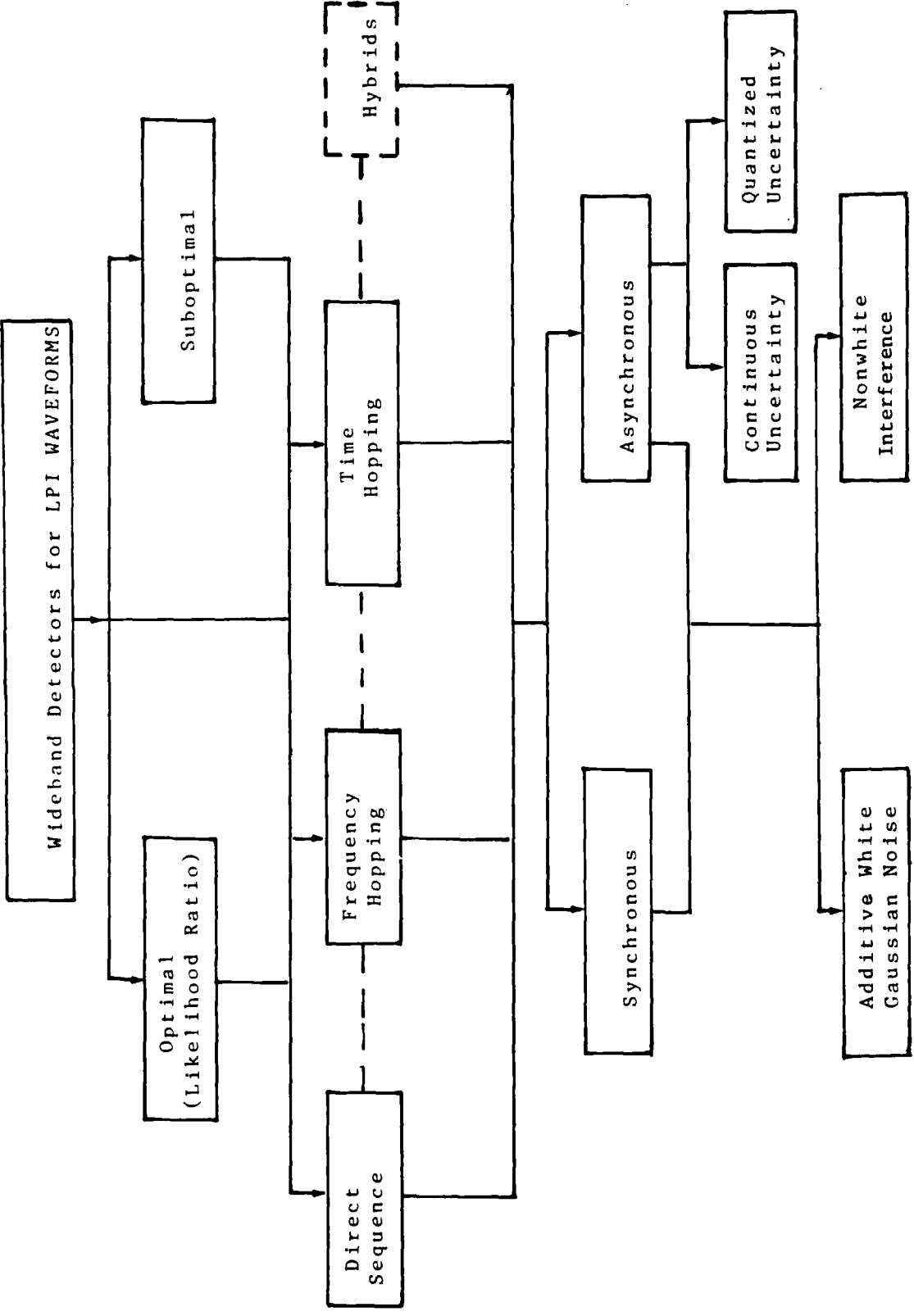
Figure 1. Classification of LPI Detectors

of those levels and whose outputs are combined to yield the final decision variable. Thus, since the maximum code-epoch uncertainty equals a chip or hop time,[2] one concludes that good nonsynchronous detectors can be constructed from combinations of a few synchronous ones. More discussion on this topic is provided in later sections.

Finally, we classify the detectors according to whether they expect to operate in the presence of _white_ (and typically Gaussian, such as thermal noise) or _nonwhite_ interference. The maximum-likelihood approach renders itself to the first case most easily, while its formulation is cumbersome for the second. Accordingly, the theory is fairly mature for AWGN interference, while it is still at the exploratory level for scenarios which involve more complicated interference forms. It is, nonetheless, a fact that most of the challenging practical problems reside in the "dense-interference-environment" area, where one or more wideband signals are to be intercepted amidst a large number of irrelevant, narrowband and wideband users, jammers, etc. Such interference should be excised to the best possible degree before the remaining detection and estimation tasks on the sought signal can be performed successfully. We shall not deal extensively with the excision problem in this report (a special case will be discussed in Section 5; rather, we shall assume that the remaining interference after excision consists of wideband Gaussian noise and focus on the performance of associated wideband detection algorithms. In terms of the block diagram in Figure 2, which shows the simplified flow of operations in a standard LPI receiver, the theory herein pertains to the "wideband signal detection" box, while interference excision, noise-level estimation, etc. are performed in the first box ("data collection and processing"), possibly aided by a continuously updated "signal history file". The ultimate goal of the LPI receiver is indicated in the last box ("signal analysis and modulation recognition"), wherefrom the information is made available to other interfaces.

---

[2]This clearly assumes a purely random code sequence for which a full chip (or hop) time-shift corresponds to another realization of the same stochastic process.
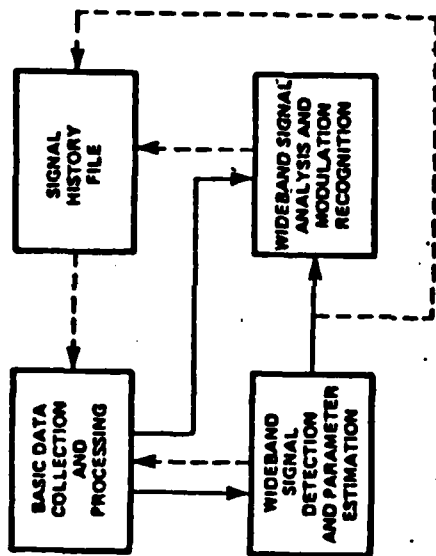
Figure 2.   Flow of Operations in the Simplified Diagram of a Standard
Intercept Receiver. (From Ref. [22], with permission)

6

We shall typically refer to the communicator's signals under interception threat as LPI signals. For the sake or clarity we should define here what we mean by such an LPI signal: it is a spread-spectrum waveform whose code is never identifiable (decipherable) from an interceptor's viewpoint; the latter is then forced to wideband processing throughout (as opposed to the communicator's narrowband processing after despreading). The detectability of such an LPI signal is a function of both scenario-dependent factors (topology, distances, power budgets, etc.) as well as scenario-independent quality factors, namely the structure of the interceptor's signal-processing algorithms (detection rule). The first five sections address the algorithmic aspects of the overall detectability/covertness issue and establish associated figures of merit parameterized by the spreading format, existing SNR and model dimensionality (time-bandwidth product). The ultimate quantity of interest, to be extracted from the analysis of these detection algorithms, is the required carrier-to-noise-ratio CNR $= (S/N_0)_{req}$ at the input to the detector in order to achieve a certain performance level (see Section 2). Then, any value of $(S/N_0)_{req}$ can be linked to the aforementioned scenario-dependent factors for a global, LPI vulnerability assessment. It is clear, however, that the two aspects of detectability can be treated separately. Furthermore, different detection algorithms can be compared on the basis of their associated $(S/N_0)_{req}$, their relative merit increasing as $(S/N_0)_{req}$ decreases; conversely, from the communicator's viewpoint, spreading waveforms with lower $(S/N_0)_{req}$ are more vulnerable to interception.

2.0. LIKELIHOOD RATIOS AND PERFORMANCE MEASURES

It is well known [3] that, under the common detection-performance criteria (most notably, the Neyman-Pearson philosophy), likelihood ratios yield optimal hypothesis-testing solutions, and performance is measured by the resulting pair of detection and false-alarm probabilities (P_D, P_{FA}). Furthermore it will be shown later that, in many models the overall likelihood ratio (LR) is expressible as the product of individual LR's due to the statistical independence of successive code chips (random DS code) or hopping slots (TH or FH). When the true model of the problem does not allow for such independence assumptions (as in the case of a random, but fixed, carrier phase), the resulting LR is too complicated for either exact analysis or implementation[3]. In this case, the performance of those (complicated) optimal decision schemes is assessed by upper and lower bounding arguments (see the following sections); in conclusion, the product LR can always be thought of as the analytical cornerstone. Since the log-likelihood ratio (LLR) is not only theoretically equivalent, but also more convenient to implement than an LR (it turns products into sums), it will serve as our point of departure.

The number of terms entering the summation of the LLR hops is typically large -- it equals the number of chips (DS), or time frames (TH) or frequency (FH) observed. Therefore, it is customary to model, via a central-limit-theorem (CLT)-type argument, the distribution of the resulting LLR as approximately Gaussian under either hypothesis. This constitutes a basic assumption upon which performance is derived in this report. However, the fact that no such LLR possesses an exact Gaussian distribution brings about certain ramifications, as explained below.

---

[3]In addition, it can be argued that the superposition of random data on DS or TH, such as PSK modulation, invalidates the modeling assumption of a fixed value of the signal phase over a multi-bit observation interval.

Furthermore, it should be pointed out here that the ensuing discussion, which is perfectly suited for DS waveforms, is also applicable to FH or TH only if the overall LR includes a large number of independent hops (FH) or frames (TH), so that the product-LR and some-LLR forms are valid and useful. As a suboptimal alternative to such optimal FH or TH detection procedures, it is possible (and many times preferable, from an implementation viewpoint) to perform individual LR decisions per hop (FH) or frame (TH) and combine afterwards these "tentative" LR-decisions over many hops or frames (post detection combing). In such cases, they one should address the quantitative properties of the LR directly; this will be further elaborated upon later.

Let us now return to the sum-LLR framework. To be specific, assume N independent, identically distributed (i.i.d.) measurements r_j, $j = 1,2,...,N$ and let $\Lambda(r)$ indicate the individual LR associated with any one of them. The corresponding individual LLR is denoted by

$$\ell(r) = \ln \Lambda(r) \tag{2.1}$$

The overall LR and LLR Λ and ℓ respectively, are

$$\Lambda = \prod_{j=1}^{N} \Lambda(r_j) \tag{2.2a}$$

and

$$\ell = \sum_{j=1}^{N} \ell(r_j) \tag{2.2b}$$

due to the i.i.d. assumption.

9

Let $\lambda(r)$ denote any "well-behaved" transformation[4] of r. Although it is convenient, in this context, to think of $\lambda(r)$ as an approximation to (or simplification of) $\ell(r)$ as per (2.1), it need not be so. Clearly,

$$\lambda \overset{\Delta}{=} \sum_{j=1}^{N} \lambda(r_j) \qquad (2.3)$$

constitutes another (typically suboptimal) decision statistic for the hypothesis testing at hand. Furthermore, the CLT approximation will be applicable to both ℓ and λ, as long as N is sufficiently large. With the resulting "Gaussian" performance or (2.2) or (2.3) in mind, consider the following model: Let X denote a Gaussian decision statistic under both hypotheses H_i; i = 0.1. The performance pair (P_D, P_{FA}), associated with the test

$$X \overset{H_1}{\underset{H_0}{\gtrless}} \text{threshold} \qquad (2.4)$$

is simply

$$P_D = Q\left[\frac{\sigma_{x,0} \; Q^{-1}\left[P_{FA}\right] + m_{x,0} - m_{x,1}}{\sigma_{x,1}}\right] \qquad (2.5)$$

where Q(x) is the Gaussian integral function

$$Q(x) = \int_x^\infty \frac{1}{\sqrt{2\pi}} \; \exp \; \left\{\frac{-z^2}{2}\right\} \; dz \qquad (2.6)$$

---

[4]For our purposes, this means that the transformation possesses finite first and second moments under either hypothesis.

with $Q^{-1}[x]$ its inverse, and $m_{x,i}$, $\sigma^2_{x,i}$; $i = 0,1$ are the means and variances of X under either hypothesis. In many cases where the inclusion of a weak signal does not alter the variance $\sigma^2_{x,0}$ significantly, i.e. $\sigma^2_{x,0} \approx \sigma^2_{x,1}$, equation (2.5) simplifies to

$$Q^{-1}[P_{FA}] - Q^{-1}[P_D] \cong \frac{m_{x,1} - m_{x,0}}{\sigma_{x,0}} \overset{\Delta}{=} d_x \qquad (2.7)$$

where the deflection (or distance) d_x has been appropriately defined in (2.7). Thus under the equal-variance Gaussian assumption, d_x quantifies performance uniquely. In other words, any desired performance level (P_D, P_{FA}) equivalently translates to a specific "desired" distance d_x via (2.7); the converse, however is not true.

The above discussion applies equally well to X representing a "Gaussian" ℓ or any other λ. Noting that, by definition,

$$d^2_\ell \overset{\Delta}{\approx} \frac{(m_{\ell,1} - m_{\ell,0})^2}{\sigma^2_{\ell,0}} \approx Nd^2_\ell \qquad (2.8\ a)$$

and similarly

$$d^2_\lambda = Nd^2_\lambda \qquad (2.8\ b)$$

where the distances d_ℓ and d_λ pertain to the individual statistics of ℓ and λ, respectively, we conclude that (2.5) - (2.8) provide a set of approximate performance estimates, reliable to the degree that the Gaussian assumption is itself sufficiently accurate. Simulation results, to be discussed later, confirm a very satisfactory accuracy for large values of N.

Use of the aforementioned distance measure hinges upon the evaluation of the appropriate moments. That is no particular problem for certain standard forms of λ (r); in fact, d^2_λ can be identified as an output-SNR measure for familar quadratic detectors (see, for instance, [4]-[8].

11

On the other hand, the exact calculation of d_ℓ^2 can be a formidable task indeed. Fortunately, this situation is remedied within the Gaussian framework due to results by Peterson, Birdsall and Fox [3]. For the sake of continuity and compactness, the main result is summarized below without substantation; however, the analytical reader is urged to go through Appendix A of this report. Therein, the tool of generating functions is employed to provide an independent proof of the aforementioned result, Chernoff bounds on detector performance,etc.

Theorem (P.B.F., 1954): Consider an LLR ℓ which is Gaussian under H_0. Then

(a) ℓ will be Gaussian under H_1

(b) $-m_{\ell,0} = m_{\ell,1} = \dfrac{d_G^2}{2}$

(c) $\sigma_{\ell,0}^2 = \sigma_{\ell,1}^2 \stackrel{\Delta}{=} d_G^2$

where d_G^2 is given by[5]

$$ d_G^2 = \ln (1 + \text{var}\{\Lambda \mid H_0\}) = \ln \mathscr{E}\{\Lambda^2 \mid H_0\} \tag{2.9}$$

and Λ is the LR associated with ℓ. Interestingly the moments Λ of are sometimes much easier to obtain than those of ℓ, hence the usefulness of (2.9). The quantity d_G will be referred to as the "Gaussian" distance.

Corollary: With N i.i.d. measurements, performance is uniquely quantified by

$$ d_\ell^2 = N \ln (1 + \text{var}\{\Lambda \mid H_0\}) \tag{2.10}$$

It is interesting that the Gaussianess of ℓ under H_0 suffices to specify everything else in terms of the single number d_G^2. Furthermore, (2.10) has been the basis of analytical evaluations for detectors employing optimal nonlinearities, whenever N is thought to be sufficiently large to support an approximate Gaussian assumption. We shall follow the

---

[5]Here $\mathscr{E}\{\cdot\}$ and var$\{\cdot\}$ stand for the mean variance, respectively.

same approach here, quickly cautioning however against two possible sources of inaccuracy and discrepancy, namely (I) different variances

$$\sigma^2_{\ell,0} = N \sigma^2_{\ell,0} \text{ and } \sigma^2_{\ell,1} = N\sigma^2_{\ell,1}$$

under two hypotheses, which would negate conclusion (c) of the theorem, and (II) intermediate values of N, coupled with low P_{FA} and/or high P_D, which would simply put the accuracy of the Gaussian approximation into question. It is clear that, for case (I) above, (2.5) would provide a more reliable answer; nonetheless, the difficulty in analytically evaluating $m_{\ell,i}$, $\sigma^2_{\ell,1}$; $i = 0.1$ remains. As for (II), it might be desirable to proceed with a numerical calculation of (P_D, P_{FA}) by computer via the analytical evaluation of characteristic functions, or resort to bounds. Again, the nontrivial aspect of this approach is the closed-form evaluation of the characteristic functions for the kinds of optimal nonlinearities encountered here.

In contrast to the above, suboptimal rules involve d^2_λ , which is typically straightforward to calculate. It is also quite useful for the purpose of comparing different suboptimal decision rules, applied to the same hypothesis testing model (see Section 3.3). Finally we shall use d^2_λ (or (2.5), whenever appropriate) to compare with $d^2_\ell = Nd^2_G$, in order to assess the cost of suboptimality, keeping always in mind our aforementioned reservations[6] . Note again that d^2_λ cannot be derived from the PBF theorem, since λ is not an LLR.

Finally, for the FH and TH cases mentioned above, where the appropriate tests come from individual LR's and not from LLR's, it is clear that distance measures based directly on Λ should be evaluated. A good such distance candidate is

---

[6]By this we refer to the appropriateness of (2.10) as a sound measure of "optimal performance; besides sources (I) and (II) mentioned above, we should not forget that, in this report, ℓ is never exactly Gaussian as the PBF Theorem requires.

$$d_\Lambda = \frac{\mathcal{E}\{\Lambda|H_1\} - \mathcal{E}\{\Lambda|H_0\}}{\text{var}^{1/2}\{\Lambda|H_0\}} \qquad (2.11)$$

provided, of course, that Λ is now the statistic which is approximately Gaussian and var $\{\Lambda|H_1\} \approx$ var $\{\Lambda|H_0\}$. Indeed, this is the case in certain scenarios to be explored later, making the evaluation of d_Λ in (2.11) a necesssary step.

Using properties of LR's, expression (2.11) can be simplified to

$$d_\Lambda = \sqrt{\text{var}\{\Lambda|H_0\}} = \sqrt{\mathcal{E}\{\Lambda^2|H_0\} - 1} \qquad (2.12)$$

which will be of use in section 5.

The theoretical groundwork laid out in this section will now be applied to a variety of LPI scenarios.

3.0 DIRECT-SEQUENCE WAVEFORMS

In this section, we consider and analyze wideband detectors for DS waveforms. It will be assumed throughout that the receiver has knowledge of the carrier frequency and code rate and that the code is biphase modulating the carrier. For the carrier phase, the two possibilities of it being known (coherent detection) and unknown (noncoherent detection) are examined separately in Section 3.1 and 3.2, respectively. A common assumption in both of these sections is that the detectors are synchronous, i.e., the code chip-timing epoch is known. In most practical situations this is rather unrealistic; the synchronous results can then be thought of as upper bounds on the performance of any asynchronous detector. Furthermore, by quantizing the continous-epoch uncertainty region into an adequate finite number of points, matched-detector structures can be devised which are synchronized to each of these points and whose outputs are combined to yield the final decision variable. The amount of quantization required depends upon the chip envelope; in this report we shall restrict attention to the constant-envelope case. Since the maximum code epoch-uncertainty for a random code equals a chip time, one concludes that good asynchronous detectors could be constructed from combinations of a few synchronous ones. More discussion on the cost of asynchronism is given in Section 3.3. Section 3.4 discusses some gains derived from correlation-combining of two independent receptions, ranks the performance of the aforementioned detectors, and compares them to that of the radiometer.

In order to introduce some notation, let the high-rate ±1-valued random spreading code $c(t)$ be represented by

$$c(t) = \sum_{n=-\infty}^{\infty} c_n p(t - nT_c - \varepsilon T_c) \qquad (3.1)$$

where $p(t)$ is a unit pulse of duration T_c seconds and $\{c_n\}_{-\infty}^{\infty}$ is a sequence of i.i.d. random variable (rv's) with $\Pr\{c_n = +1\} = \Pr\{c_n = -1\} = 0.5$. Note that the random sequence $\{c_n\}$, as modeled, does not distinguish between a pure random code and a code which is additionally modulated (in a synchronous fashion) by random binary data. Furthermore, the chip epoch is modeled by the rv ε, uniformly distributed over $(0,1)$. The waveform observed by the detector is therefore given by

$$ r(t) = \begin{cases} \sqrt{2S}\ c(t)\ \cos(\omega_0 t + \phi) + n(t) & (H_1) \\ \\ n(t) & (H_0) \end{cases} \quad (0 \le t \ge T) $$

$$(3.2)$$

where S, ω_0 and ϕ are the average signal power, carrier radian frequency and carrier phase, respectively and $n(t)$ is bandpass AWGN with one-sided power spectral density (PSD) of N_0 W/Hz. The observation time is T seconds, which we assume to be an integer multiple of the chip time, i.e., $T = NT_c$; N a positive integer. Such an assumption is the least restrictive since, in practice, N is generally a large number (of the order of hundreds or higher). However, a somewhat stronger restriction is embedded in (3.2)., namely the assumption that under hypothesis H_1, the signal is present during the whole observation interval. That excludes the possibility of the signal either starting or ending at any random time in $(0,T)$. Still, such a formulation is important because it provides meaningful and fairly simple comparative conclusions which (a) would otherwise be obscured by mathematical complexities and, (b) can be argued to extend to more general models.

In terms of the above notation, a synchronous detector implies that ε is identically zero, while a coherent one means that ϕ is known. The detector for which ϕ is unknown but constant over the observation interval duration is well within the coherence time of the spread-spectrum channel. For computational purposes, we also consider the fictitious chip-noncoherent detector, where phase is assumed to be totally random (uniform in

16

$(0,2\pi)$ and independent from chip to chip. Although this is not realistic for a biphase-system, it is discussed here because its readily derived performance serves as a useful lower bound to the performance of the carrier-noncoherent receiver. In addition, the random phase model becomes increasingly realistic if the DS modulation has four or more phase states.

3.1 Synchronous Coherent Detectors

When both the random phase ϕ and random chip epoch ε are assumed known, the detector is asked to perform the following composite hypothesis testing problem: Decide between the alternative H_0 and H_1, where

$$r(t) = \begin{cases} \sqrt{S}\, c(t) + n_I(t) & (H_1) \\ n_I(t) & (H_0) \end{cases} \quad (0 \le t \le NT_c) \quad (3.3)$$

Hypothesis H_1 is composite because it contains all possible patterns that the code can assume in NT_c seconds. Although we consider only random codes (in which case there are exactly 2^N such patterns), some of the steps below would also be valid for deterministic codes. The subscript I in $n_I(t)$ indicates that only the inphase component of the noise contributes with a flat two-sided PSD of $N_0/2$ W/Hz.

Well-known results about optimal detectors (see, for instance [12]) can be applied here to yield the composite likelihood ratio test:

$$\Lambda(r(t)) = \frac{\exp\{-N\gamma_c\}}{2^N} \sum_{i=1}^{2^N} \exp\left\{ \frac{2\sqrt{S}}{N_0} \int_0^{NT_c} r(t)\, c_i(t)\, dt \right\}$$

$$= \frac{\exp\{-N\gamma_c\}}{2^N} \sum_{i=1}^{2^N} \exp\left\{ \frac{2\sqrt{S}}{N_0} \sum_{j=1}^{N} r_j\, c_{ij} \right\} \underset{H_0}{\overset{H_1}{\gtrless}} \Lambda_0$$

$$(3.4)$$

where

$$\gamma_c = \frac{ST_c}{N_0} \quad (3.5)$$

18

is the predetection (or chip) SNR, $c_i(t)$; $i = 1,...,2^N$ is the ith code pattern, c_{ij} is the jth chip of the ith pattern, and r_j is given by

$$r_j \overset{\Delta}{=} \int_{(j-1)T_c}^{jT_c} r(t) \, dt \tag{3.6}$$

It is shown in Appendix B that an expression equivalent to (3.4) can be derived in terms of the cosh $(\cdot)$ function, where cosh $(x) = e^x + e^{-x})/2$. It is given by

$$\Lambda(r(t)) = \prod_{i=1}^{N} \exp\{-\gamma_c\} \cosh\left(\frac{2\sqrt{S}}{N_0} r_j\right) \underset{H_0}{\overset{H_1}{\gtrless}} \Lambda_0 \tag{3.7a}$$

which yields to optimal LLR test

$$\ln \Lambda(r(t)) = -N\gamma_c + \sum_{i=1}^{N} \ln \cosh\left(\frac{2\sqrt{S}}{N_0} r_j\right) \underset{H_0}{\overset{H_1}{\gtrless}} \ln \Lambda_0 \tag{3.7b}$$

as shown in Figure 3, we note that (3.7) could have been derived directly, based on the i.i.d. and AWGN assumptions, as per (2.2) (see also [5],[6],[8] for similar results). The method preferred here can be generalized to models with statistically dependent chips (c.f. Section 3.2) or nonrandom code

It can be shown that, the conditional mean of the random argument of the ln cosh $(\cdot)$ function in (3.7b), assuming $c_j = 1$ under H_1, is equal to $2\gamma_c$, which is also its variance

19
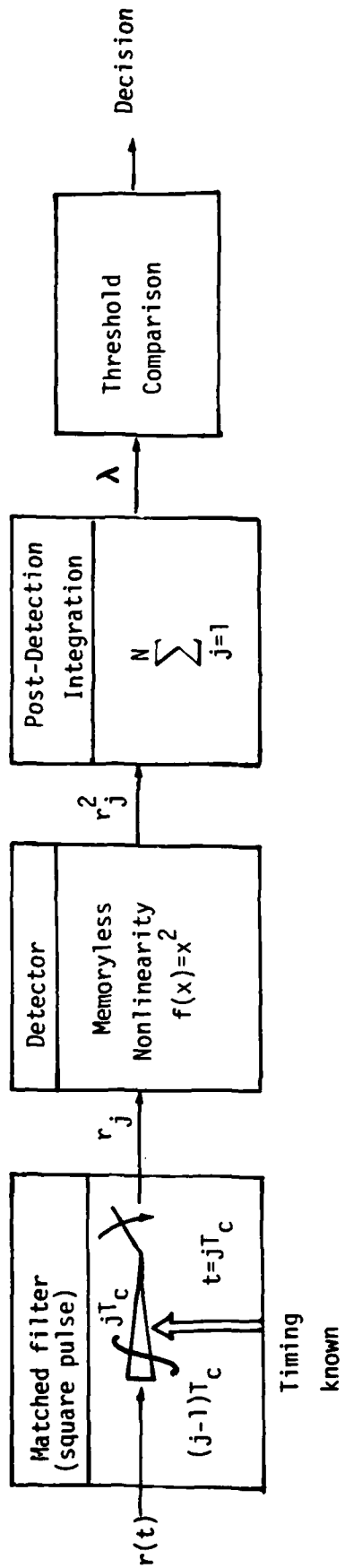
Figure 3.   Synchronous Coherent Detector for the Detection of
              Direct-Sequence Waveforms.

20

under H_0. Therefore, for typical predetection SNR values below -10 dB or so, the approximation ln cosh $(x) \approx x^2/2$ is well applicable, in which case (3.7b) reduces to the approximate (suboptimal) rule

$$\lambda = \sum_{j=1}^{N} r_j^2 \underset{H_0}{\overset{H_1}{\gtrless}} \lambda_0 \qquad (3.8)$$

depicted in Figure 3. Since the aforementioned approximation of the ln cosh(x) function becomes increasingly tight as $x \rightarrow 0$, it follows that (3.8) is asymptotically optimal as $\gamma_c \rightarrow 0$

Within the theoretical framework of Section.2, the performance of (3.8) is easily derived. The mean and variance of λ are given by (Appendix C)

$$\mathscr{E}\left\{\lambda \,|\, H_k\right\} = N\left(N_0 T_c\right)\left(\frac{1}{2} + \gamma_c \, \delta_{k1}\right) \qquad (k=0,1) \qquad (3.9a)$$

and

$$\text{var}\left\{\lambda \,|\, H_k\right\} = N\left(N_0 T_c\right)^2 \left(\frac{1}{2} + 2 \, \gamma_c \, \delta_{k1}\right) \qquad (3.9b)$$

respectively, where δ_{k1} is the Kronecker delta

$$\delta_{k1} = \begin{cases} 1 \, , \; k=1 \\ 0 \, , \; k=0 \end{cases} \qquad (3.9c)$$

21

Therefore, P_D and P_{FA} are related, as per (2.5) by

$$P_D \approx Q\left[\frac{Q^{-1}[P_{FA}] - a\sqrt{N}\,\gamma_c}{\sqrt{1 + b\gamma_c}}\right] \qquad (3.10a)$$

with

$$a = \sqrt{2}\ ; \quad b = 4 \quad \text{(synchronous coherent detector).} \qquad (3.10b)$$

Since $b\gamma_c$ is typically much less than one, (3.10) can be combined with (2.7) to yield

$$d_\lambda \approx \sqrt{2}\ \sqrt{N}\ \gamma_c \qquad (3.11)$$

We note that performance is dictated by the product $\sqrt{N}\ \gamma_c$, which is typical of schemes employing post-detection integration. In contrast, detection of a <u>known</u> waveform would involve the factor $\sqrt{N\gamma_c}$; the losses in performance, due to the composite test (since the signal pattern is unknown) for low values of SNR, are evident by comparison. Note also that rule (3.8) <u>could</u> have been analyzed exactly, but this issue is deferred until noncoherent detectors are discussed in the following section.

In terms of the overall observation time T and the null-to-null spread spectrum bandwidth $W_s = 2T_c^{-1}$ (Hz), (3.11) can be rewritten to establish the required $(S/N_0)_{req}$ in order to achieve the performance level d_λ as

$$\left(\frac{S}{N_0}\right)_{req} \approx \left(\frac{1}{2}\right)\sqrt{\frac{W_s}{T}}\,d_\lambda \qquad (3.12)$$

The above refers to the suboptimal rule (3.8). The Gaussian distance d_ℓ of (2.7) for the optimal rule (3.7b) can also be derived. Let

$$y_j \triangleq \frac{2\sqrt{S}}{N_0} \, r_j$$

with r_j as per (3.6). Under H_0, y_j is a zero-mean Gaussian rv with variance $\sigma_y^2 = 2\gamma_c$. Using the fact that $\mathscr{E}\{\cosh(y_j)\} = \exp\{\sigma_y^2 / 2\}$ in conjunction with (3.7a) results in

$$d_\ell = \sqrt{N \, \ln \cosh(2\gamma_c)} \tag{3.13}$$

For small x, $\ln \cosh(x) \approx x^2/2$, which, upon substitution in (3.13), verifies that $d_\ell \rightarrow d_\lambda$ of (3.11) as $\gamma_c \rightarrow 0$. In conclusion, the approximate rule is well suited for the low prediction SNR range of interest.

The performance (P_D, $P_{FA} = 10^{-2}$) of the optimal and suboptimal decision rules (3.7b) and (3.8); respectively, as predicted by (3.13) and (3.11), is shown in Figure 4. The two values of N chosen, a high (1000) and a low (50), are meant to illustrate the qualities and limitations of the Gaussian assumption. The $P_{FA} = 10^{-2}$ value, used here for exemplary purposes, was fixed both in theory and simulation. Although this P_{FA}, if considered by itself, would correspond to unacceptable false-alarm rates[7], it is typically true that multiple tests are employed before a final decision is reached, thus lowering the overall P_{FA} to the desired levels.

The simulation results for both rules, also included in Figure 4, confirm the expected trend of the CLT-Gaussian approximation to improve as N and P_D increase, for fixed P_{FA}. This improvement is manifested in the increased quality of both performance estimates, i.e. eqns. (3.11) and (3.13), each pertaining to its own test.[8] Interestingly, the approximate estimate (3.11) seems satisfactory for both optimal and suboptimal tests. This should be

---

[7]For a 10 Mchips/sec code and $N = 1000$, the number $P_{FA} = .01$ corresponds to an average false-alarm rate of 100 FA/second.

[8]This is certainly true for increasing N; for small values of N, the applicability of (3.13) becomes more questionable as P_D increases.

Figure 4.   (a) P_D vs. γ_c for the synchronous coherent detector, optimal and suboptimal tests, $P_{FA} = 10^{-2}$.

N = 1000
$P_{FA} = 10^{-2}$
SIM: 2,000 RUNS

γ_C (dB)
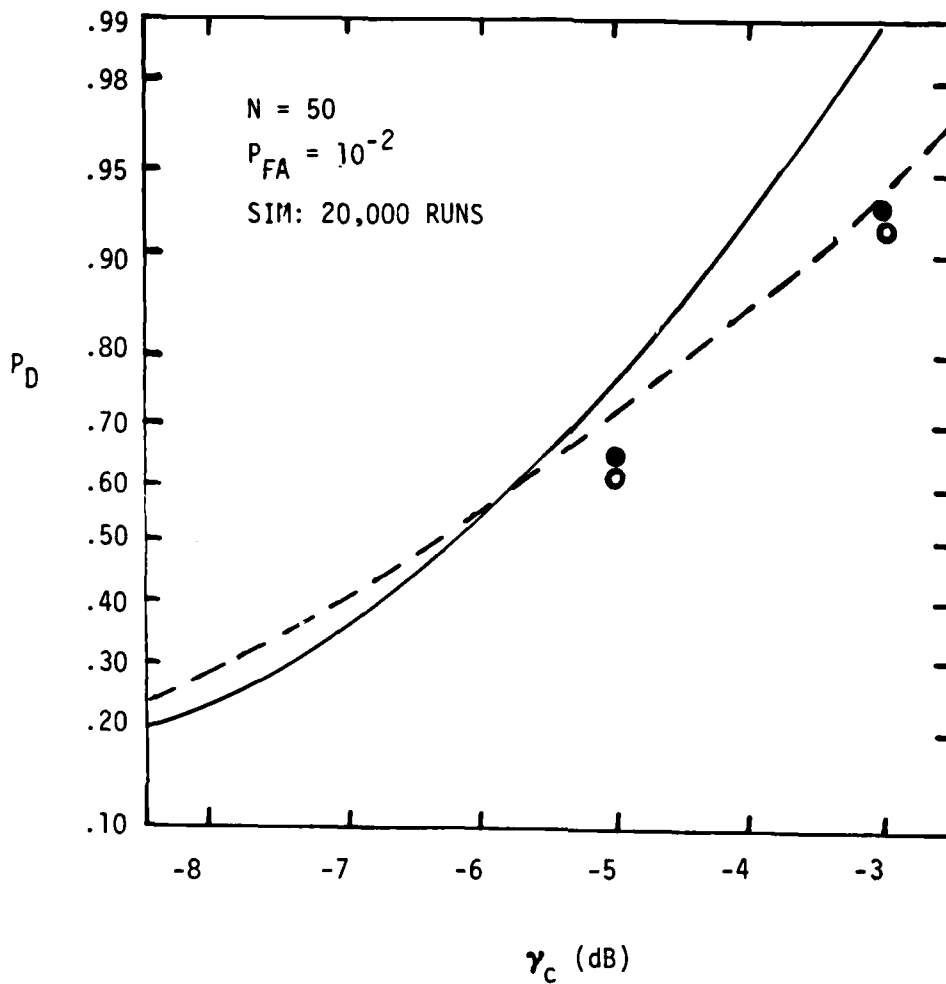
———————— d_ℓ performance prediction for LLR test (3.7b)

— — — — approximate Gaussian prediction (3.10)

● simulation results for LLR test (3.7b)

○ simulation results for suboptimal test (3.3)

(b) N = 1000

Figure 4. (b) P_D vs. γ_C for the synchronous coherent detector, optimal and suboptimal tests, $P_{FA} = 10^{-2}$.

attributed to the low chip-SNR γ_c, which renders rules (3.7b) and (3.8) almost equivalent, as attested also by the closeness of the respective simulation results. In different environments however, (eg.,FH or TH), corresponding to higher hop-SNR's, the cost of suboptimality should be more pronounced (see Section 4 and 5).

3.2 Synchronous Noncoherent Detectors

Let us now relax the assumption that the carrier phase of the DS waveform is known by the interceptor, but still retain the assumption of a known code epoch. We shall state the optimal decision rule for a carrier-noncoherent system, whose *exact* analysis, however, appears unattainable. Instead, a chip-noncoherent detector will be derived and analyzed, whose performance can serve as an asymptotically tight (as $\gamma_c \to 0$) lower bound for the carrier-noncoherent system.[9] Thus, the performance of the latter can be nicely bracketed between that of the former and the upper bounding performance of the synchronous coherent detector[10] in the previous Section 3.1.

Consider first the carrier-noncoherent system. Under the usual narrowband assumption $\omega_0 \gg 2\pi/T$, the resulting decision rule is

$$\Lambda = \frac{\exp\{-N\gamma_c\}}{2^N} \sum_{i=1}^{2^N} I_0\left(\frac{2\sqrt{S}}{N_0} R_i\right) \mathop{\gtrless}_{H_0}^{H_1} 0 \tag{3.14}$$

where $I_0(\cdot)$ is the zeroth-order modified Bessel function and R_i is the ith correlation envelope

$$R_i = \sqrt{e_{I_i}^2 + e_{Q_i}^2} \; ; \; i=1,2,\ldots,2^N \tag{3.15a}$$

In (3.15a); the two components are given by

$$e_{a_i} = \sum_{j=1}^{N} r_{a_j} c_{ij} \triangleq \mathbf{r}_a \cdot \mathbf{c}_i \; ; \; a=I,Q \tag{3.15b}$$

---

[9] Since a chip-noncoherent detector utilizes less statistical information than a carrier-noncoherent detector, it is inferior to the latter for all SNR values.

[10] In fact, it was argued in [4] that the coherent upper bound is asymptotically achieved, for large distance d, by an approximate version of the carrier-noncoherent detector, because the (unknown) constant phase can be estimated reliably at high SNR.

with

$$\begin{bmatrix} r_{I_j} \\ r_{Q_j} \end{bmatrix} \triangleq \sqrt{2} \int_{(j-1)T_c}^{jT_c} r(t) \begin{bmatrix} \cos \omega_0 t \\ \sin \omega_0 t \end{bmatrix} dt \; ; \; j=1,\dots,N \tag{31.5c}$$

The optimal rule (3.14) - (3.15) is hard to mechanize. Instead, suppose that the received waveform r(t) is represented under H_1 by

$$r(t) = \sqrt{2S} \sum_{j=-\infty}^{\infty} c_j \, p\left(t-jT_c\right) \cos\left(\omega_0 t + \phi_j\right) + n(t) \tag{3.16}$$

where $\{\phi_j\}$ is a sequence of i.i.d. uniform phases, thus modeling the aforementioned chip-noncoherent system. It is then straightforward to show the independence of chips, using a procedure analogous to Section 3.1 or directly (see also [4], [8]), that the optimal decision rule is

$$\ell = -N\gamma_c + \sum_{j=1}^{N} \ln I_0\left(\frac{2\sqrt{S}}{N_0} r_j\right) \underset{H_0}{\overset{H_1}{\gtrless}} \ell_0 \tag{3.17}$$

where r_j is the envelope of the jth chip

$$r_j = \sqrt{r_{I_j}^2 + r_{Q_j}^2} \tag{3.18}$$

with r_{I_j}, r_{Q_j} as per (3.15b). Again, under the small-argument approximation in $I_0(x \approx x^2/4$, it follows that (3.17) reduces to the suboptimal rule

$$\lambda = \sum_{j=1}^{N} r_j^2 \underset{H_0}{\overset{H_1}{\gtrless}} \lambda_0 \tag{3.19}$$

28

Rule (3.19) is formally identical to (3.8), the difference being that r_j here corresponds to a noncoherent-chip integration. Furthermore, it is shown that as $\gamma_c \to 0$ (namely for small arguments of the $I_0(\cdot)$ function), the optimal carrier-noncoherent rule (3.14), which involves averaging over all possible 2^N N-tuples of the code, reduces to the simple suboptimal decision rule (3.19) for the chip-noncoherent system. It can thus be concluded that the performance associated with (3.19) is asymptotically close to that of (3.14) on the low-SNR side; however, this probably occurs at an unacceptably poor overall performance level.

Although the distance d_ℓ for the exact rule (3.17) can be derived (see Section 4.0 for a closely related case), we shall be content with d_λ of (3.11) in view of the low-SNR conclusions of the previous section. The random envelope r_j in (3.18) possesses a Rayleigh pdf under H_0

$$f(r_j \mid H_0) = \frac{r_j}{\sigma^2} \exp\left\{ -\frac{r_j}{2\sigma^2} \right\}; \quad r \geq 0 \tag{3.20a}$$

and a Rician under H_1

$$F(r_j \mid H_1) = \frac{r_j}{\sigma^2} \exp\left\{ -\tfrac{1}{2}\left(\frac{r_j}{\sigma^2} + 2\gamma_c \right) \right\} I_0\left(\frac{r_j}{\sigma^2} \sqrt{2\gamma_c} \right); \quad r \geq 0 \tag{3.20b}$$

with $\sigma^2 = N_0 T_c / 2$. Then, the statistics of the r.v. (λ/σ^2) in (3.19) are known exactly [19]: under H_0, (λ/σ^2) is a central chi-square r.v. with 2N degrees freedom while, under H_1, (λ/σ^2) is a noncentral chi-square with 2N degrees of freedom and noncentrality parameter $\theta = 2N\gamma_c$. Following Marcum's expressions [15] for the performance analysis of pulsed radar, which involves an analogous detection model, we conclude that the probabilities of interest are

$$P_{FA} = \frac{1}{(N-1)!} \int_{\lambda_0/2\sigma^2}^{\infty} x^{N-1} e^{-x} \, dx = 1 - I\left(\frac{\lambda_0}{2\sigma_0^2 \sqrt{N}}, \, N-1 \right) \tag{3.21a}$$

where I(u,p) is the incomplete Gamma function and

$$P_D = Q_N \left(\sqrt{2\gamma_c}, \frac{\sqrt{2}}{\sigma} \right)$$ (3.21b)

where $Q_N(\alpha, \beta)$ is the Nth order generalized Q function [15, 16]

Although the above results are exact, they are cumbersome to use from a computational viewpoint, especially for large N. In addition, the Gaussian approximation yields satisfactory results in the range of N of interest and thus becomes our alternative simpler route.

It is shown in Appendix D that

$$\mathscr{E}\left\{ r_j^2 \middle| H_k \right\} = \left(N_0 T_c \right) \left[1 + \gamma_c \, \delta_{kl} \right]$$ (3.22a)

and

$$\text{var}\left\{ r_j^2 \middle| H_k \right\} = \left(N_0 T_c \right)^2 \left[1 + 2\gamma_c \, \delta_{kl} \right]$$ (3.22b)

Combining (3.19) and (3.22) and employing Gaussian assumption results in (3.10a) where now

$$a = 1; \quad b = 2 \qquad \text{(Syncrochronous chip-noncoherent detector).}$$ (3.23)

Equivalently,

$$\left(\frac{S}{N_0} \right)_{req} = \frac{1}{\sqrt{2}} \sqrt{\frac{W_s}{T}} \, d_\lambda$$ (3.24)

which reveals a loss factor of $\sqrt{2}$, or 1.5 dB, with respect to the coherent detectors. This is the penalty paid for the lack of coherency. Furthermore, since the performance of the carrier-noncoherent system is bracketed between the coherent (upper bound) and the chip-noncoherent (lower bound) ones that differ by only 1.5 dB, it is concluded that any implementational complexity beyond that of rule (3.19) is not justified from a practical standpoint.

3.3 Asynchronous Detectors

In the most natural problem formulation, the code timing (epoch) ε is a random variable uniformly distributed within a chip interval. We shall first show in this section how a cascade of analog devices and nonlinearities can be configured, in principle, to optimally average the likelihood ratio over the epoch uncertainty. The derivation follows the basic steps illustrated by Krasner [8] in a somewhat simplified and expanded manner. Then, practical suboptimal detectors of reduced complexity will be derived, analyzed and compared with the optimal one. The main purpose here, besides obtaining useful quantitative performance estimates, is to establish a certain performance-bounding philosophy; although attention is confined to constant-envelope DS signals, the line of thought is also applicable to nonconstant envelope waveforms, for which the effect of epoch mismatch could be much more pronounced.

For the sake of simplicity, the coherent case is analyzed herein. Most of the ensuing steps, however, carry without change to the noncoherent rule. The starting point is the coherent likelihood ratio (3.7a), which is now interpreted as a conditional LR, given the value of the random offset ε. In other words, we can write

$$\Lambda\left(r(t)|\varepsilon\right) = \prod_{j=1}^{N} \exp\left\{-\gamma_c\right\} \cdot \cosh\left(\frac{2\sqrt{S}}{N_0}\left(r_j(\varepsilon)\right)\right)$$

$$(3.25a)$$

where the coherent integration (3.6) is adjusted to reflect the knowledge of ε.

$$r_j(\varepsilon) = \int_{(j-1)T_c+\varepsilon}^{jT_c+\varepsilon} r(\tau)\, dt$$

$$(3.25b)$$

Furthermore, the unconditional LR results from (3.25) by averaging with respect to the rv ϵ in the following manner:

$$\Lambda(r(t)) = \mathscr{E}_{\epsilon}\{\Lambda(r(t)|\epsilon)\} = T_c^{-1} \cdot \int_0^{T_c} \exp\left\{ \ln \Lambda\, r(t)|\epsilon) \right\} d\epsilon$$

$$= \int_0^{T_c} \exp\left\{ -N\gamma_c + \sum_{j=1}^{N} \ln \cosh\left[\int_{(j-1)T_c+\epsilon}^{jT_c+\epsilon} r(\tau)\, d\tau \right] \right\} d\epsilon$$

(3.26)

Complicated as it may seem, rule (3.26) can indeed be implemented exactly by the means shown below. First, we define the waveform $y(t)$ as

$$y(t) = \int_{t-T_c}^{t} r(\tau)\, d\tau$$

(3.27)

This process $y(t)$ is easily mechanized as the output, due to an input $r(t)$, of a linear filter matched to the chip-envelope pulse[11] $p(t) = u(t) - u(t - T_c)$, since

$$\int_{t-T_c}^{t} r(\tau)\, d\tau = \int_{-\infty}^{\infty} r(\tau)\, p(t-\tau)\, d\tau$$

(3.28)

Note from (3.27) that the argument of the ln cosh($\cdot$) function in (3.26) is just $y(jT_c + \epsilon)$. Thus, the next step involves creating the sum of samples $\sum_{J=1}^{N} \ln \cosh\,[y(jT_c + \epsilon)]$ of the new, transformed process ln cosh $[y(t)]$. To do that, consider that the convolution of ln cosh $[y(t)]$ with the impulse response.

$$h(t) = \sum_{m=0}^{N-1} \delta\left(t - mT_c\right)$$

(3.29)

---

[11]Here, $u(t)$ stands for the *unit-step function.*

namely,

$$g(t) \triangleq h(t) \circledast \ln\cosh(y(t)) = \int_{-\infty}^{\infty} \left(\sum_{m=0}^{N-1} \delta(\tau - mT_c) \right) \ln\cosh(y(t-\tau))d\tau$$

$$= \sum_{m=0}^{N-1} \ln\cosh\left[y(t - mT_c) \right]$$

(3.30)

which, sampled at $t = kT_c + \varepsilon$ yields

$$g(kT_c + \varepsilon) = \sum_{m=0}^{N-1} \ln\cosh\left[y((k-m)T_c + \varepsilon) \right]$$

$$= \sum_{j=k-N+1}^{k} \ln\cosh\left[y(jT_c + \varepsilon) \right]$$

(3.31)

where the change of variables $j = k-m$ has been used. At $k = N$, i.e. when g(t)is sampled at $t_s = NT_c + \varepsilon$, the desired sum $\sum_{j=1}^{N} \ln\cosh[y(jT_c + \varepsilon)]$ is formed. Since $0 \leq \varepsilon \leq T_c$, the sampling times t_s belongs to the interval $NT_c \leq t_s \leq (N+1) T_c$. Therefore, the above sum (or its exponent, according to (3.26)) can be averaged with respect to ε by simply integrating g(t) (or exp{g(t)}) over the interval $NT_c \leq t \leq (N+1)T_c$. Again, such an integration with a uniform "weight" function can be directly interpreted and performed as a convolution with the square chip-pulse p(t) similar to (3.28). (A possible analog implementation of this convolutor with a square-pulse impulse response, also called a "moving average" filter, is shown in Figure 5 . It should be emphasized here, however, that the use of the same pulse shape for the two convolutions is coincidental, owing to the square-pulse, biphase-modulated pseudo-random code considered. Arbitrary code pulse-shapes would require general, matched-filter structures for y(t) in (3.25) - (3.28), while the averaging with respect to the "uniform" r v ε can always be performed via the aforementioned square-pulse convolution. The general case is treated in depth by Krasner [8].

34
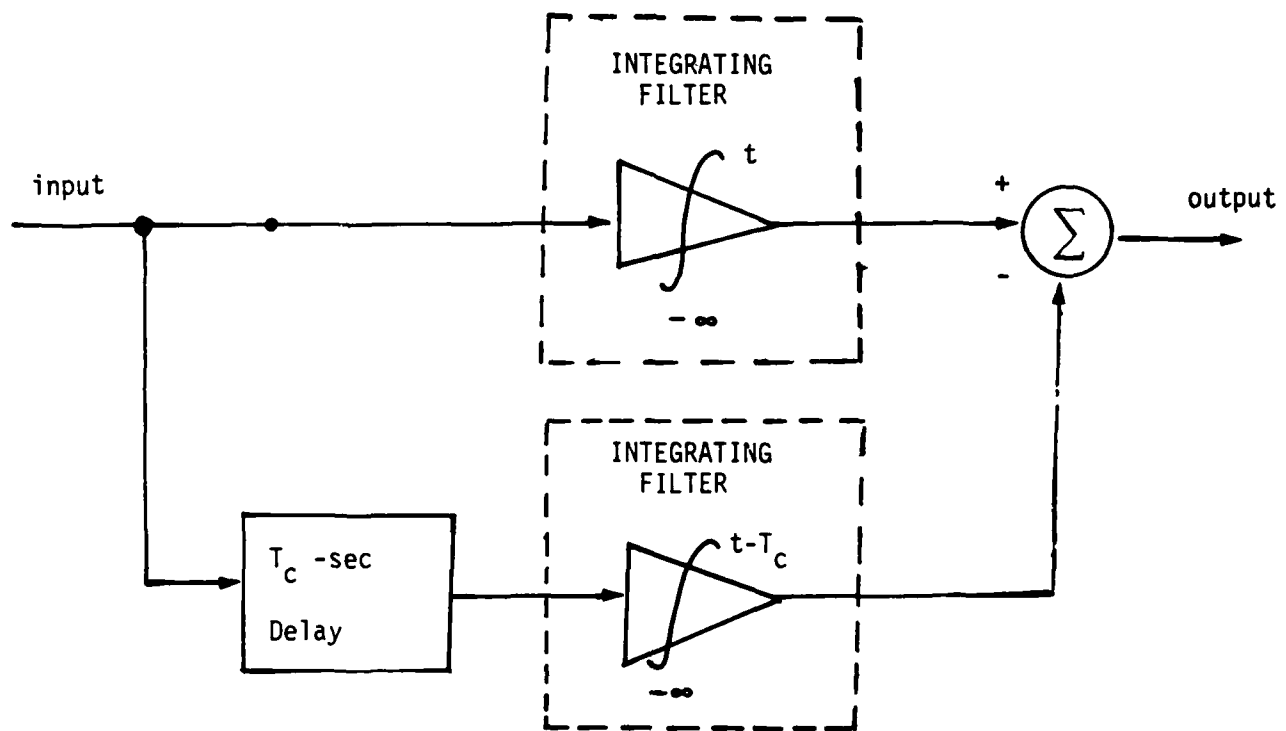
Figure 5.   Moving-Average Filter with a square-pulse impulse response

The coherent optimal LR detector structure for the continuous-epoch uncertainty case is shown in Figure 6, explicitly indicating the series of linear filtering and nonlinear operations required to implement it. Note that the impulse response h(t) of (3.29) and the subsequent convolution (3.30) are associated with the tapped-delay-line box in Figure 6, which calls for (N-1) delay elements, T_c seconds apart Figure 7(a). Such an implementation, however, is not recursive and would require more delay elements for higher N. As an alternative, the feedback structure of Figure 7(b) can be employed, which only needs a single delay element in the feedback path. Ideally, the impulse response of the latter structure would be an infinite-length delta train; thus, N need not be specified a priori. However, stability considerations, due to component noise, parasitics, etc. typically require the insertion of a gain $\alpha < 1$ (dotted lines in Figure 7(b)), which practically limits the "effective" length NT_c of the resulting impulse response.

As witnessed from Figure 6, a number of (possibly costly) linear and nonlinear devices are involved in the optimal asynchronous processor. One step towards reducing the complexity is to quantize the epoch uncertainty region of T_c seconds into a (small) finite number of alternatives, i.e., points. This is equivalent to pretending that the epoch r v can take on only those values and accordingly develop the optimal or near-optimal detector for the resulting finite hypothesis problem. The quality (as well as complexity) of such an approximation will obviously increase with the number of points considered. It will soon be clear, however that, for constant-envelope waveforms, the simplest case of only a two-point quantization, which will be the one we analyze herein, provides quite adequate performance with respect to the ideal (synchronous) detector; thus, higher level quantization and complexity might even be undesirable from a practical standpoint. In addition, a suitable interpretation of this analysis can simultaneously serve as a bounding technique (upper and lower) for the optimal, continuous-epoch uncertainty detector whose exact analysis is intractable.
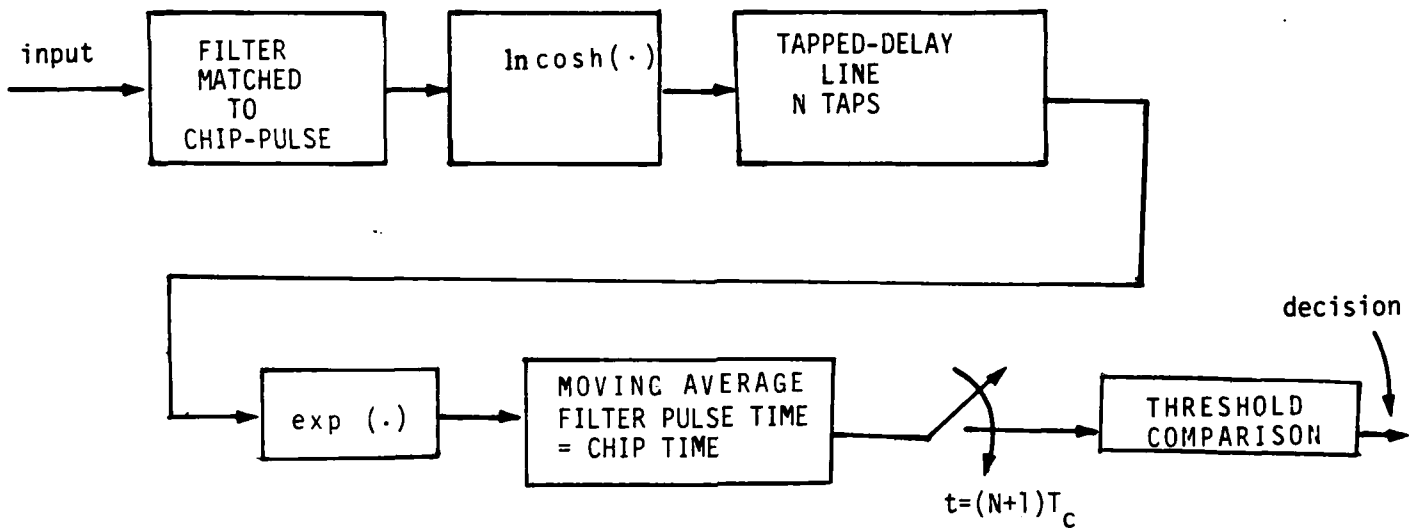
Figure 6.   Optimal, Continuous Epoch Uncertainty, Likelihood Ratio
Detector for the Coherent Case
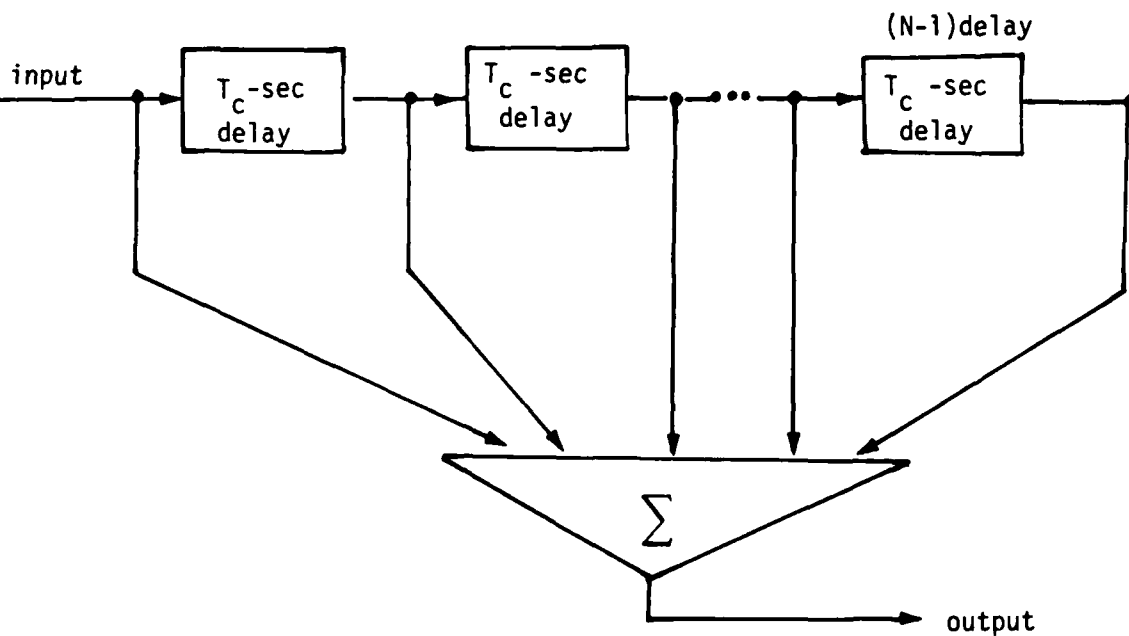
(a) Tapped Delay line with (N-1) delay elements
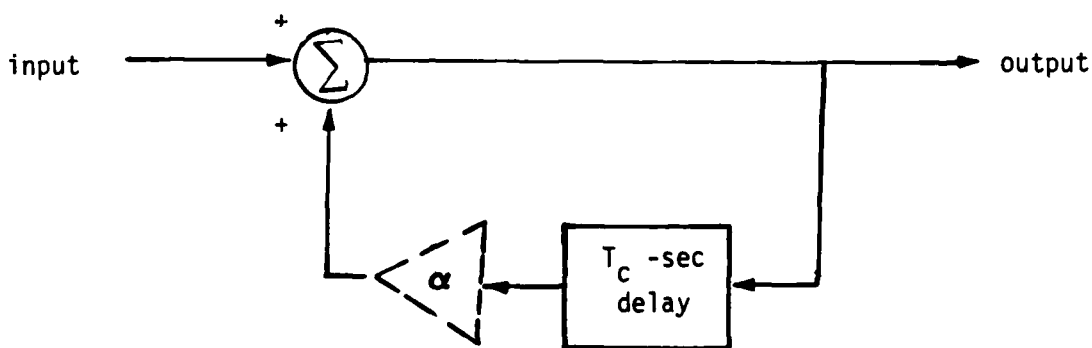
(b) Alternative Implementation through an Infinite Impulse Response (IIR) Filter

Figure 7.   Filters providing an impulse-train impulse response.

38

Let us assume that the two points comprising the epoch uncertainty[12] are ε_0 and $\varepsilon_{1/2}$, corresponding to the offsets $\varepsilon = 0$ and $\varepsilon = 1/2$ in (3.1); that is to say, the incoming code chips are likely to arrive either in perfect synchronization ($\varepsilon = 0$) or half a chip off ($\varepsilon = 1/2$) with respect to the local chip-timing reference, and they are both equally probable to occur. A variation of the optimal-likelihood ratio (3.7a) for the coherent case, adapted for the above scenario, would imply that the decision rule should be

$$\Lambda = \frac{1}{2}\left[\exp\{\sum_{j=1}^{N} \ln\cosh\ (\frac{2\sqrt{S}}{N_0}\ r_j(\varepsilon_0))\} + \exp\{\sum_{j=1}^{N} \ln\cosh\ (\frac{2\sqrt{S}}{N_0}\ r_j(\varepsilon_{1/2}))\}\right]$$

$$\cdot \exp\{-N\gamma_c\} \underset{H_0}{\overset{H_1}{\gtrless}} \Lambda_0 \tag{3.32}$$

where

$$r_j(\varepsilon_0) \triangleq \int_{(j-1)T_c}^{jT_c} r(\tau)d\tau; \quad r_j(\varepsilon_{1/2}) \triangleq \int_{(j-1)T_c+T_c/2}^{jT_c+T_c/2} r(\tau)d\tau \tag{3.33}$$

Clearly, the chip-noncoherent detector would form the envelopes r_j in place of the coherent integrations (3.33) and would proceed in an analogous way from equation (3.17). We should note here that the two NT_c-second observation intervals for the two corresponding exponential terms of (3.32) are slightly off by half a chip. For large N, such "edge effects" are insignificant and will be neglected in the following.[13]

Equation (3.32) can be simplified by employing the small-argument approximation to the ln cosh ($\cdot$) function as in Section (3.1), resulting in the (non-LR) test

$$L = (\frac{1}{2})\left[\exp\{\frac{2S}{N_0^2}\sum_{j=1}^{N} r_j^2(\varepsilon_0)\} + \exp\{\frac{2S}{N_0^2}\sum_{j=1}^{N} r_j^2(\varepsilon_{1/2})\}\right] \underset{H_0}{\overset{H_1}{\gtrless}} L_0 \tag{3.34}$$

---

[12]So, at this pont, the epoch uncertainty is assumed to be discrete by nature, not by quantization.
[13]For that purpose, small adjustments will be made for convenience without explicit acknowledgment

In view of the findings of Section (3.1) it could be argued that the test (3.34) albeit suboptimal, should perform close to the LR test (3.32). Nevertheless, it is shown below that the former can be outperformed by another suboptimal test, at least under certain circumstances, which is in fact a further simplification to (3.34). In other words, one should not automatically conclude that, in the realm of suboptimal tests, a "simpler" rule necessarily implies a deterioration in performance. Towards that end, let r_{j1} and r_{j2} indicate the coherent integrations during the first and second halves of the jth chip interval, respectively, i.e.

$$r_{j1} \triangleq \int_{(j-1)T_c}^{(j-1/2)T_c} r(\tau)d\tau; \quad r_{j2} \triangleq \int_{(j-1/2)T_c}^{jT_c} r(\tau)d\tau \tag{3.35}$$

and define

$$A_0 \triangleq \frac{2S}{N_0^2} \sum_{j=1}^{N} r_j^2(\epsilon_0) = \frac{2S}{N_0^2} \sum_{j=1}^{N} (r_{j1} + r_{j2})^2 \tag{3.36a}$$

$$A_{1/2} \triangleq \frac{2S}{N_0^2} \sum_{j=1}^{N} r_j^2(\epsilon_{1/2}) = \frac{2S}{N_0^2} \sum_{j=1}^{N} (r_{j2} + r_{j+1,1})^2 \tag{3.36b}$$

and

$$z \triangleq \frac{A_0 + A_{1/2}}{2}; \quad w \triangleq \frac{A_0 - A_{1/2}}{2} \tag{3.37}$$

Then, (3.34) can be written as

$$L = \left(\frac{1}{2}\right)\left[\exp\{A_0\} + \exp\{A_{1/2}\}\right] = \exp\{Z\} \cosh(W) \mathop{\gtrless}_{H_0}^{H_1} L_0 \tag{3.38}$$

40

or, through the transformation $\lambda_1 \triangleq \ln L$.

$$\lambda_1 = Z + \ln\cosh(W) \underset{H_0}{\overset{H_1}{\gtrless}} \text{threshold} \tag{3.39}$$

which is thus equivalent to (3.34)

An approximation (3.39) is obtained by simply omitting the second term,

$$Z \underset{H_0}{\overset{H_1}{\gtrless}} L_0 \text{ threshold} \tag{3.40}$$

which, by substituting (3.36) into (3.37) expanding terms and absorbing constants into the threshold, reduces to

$$\lambda_2 = \sum_{j=1}^{N} r_{j1}^2 + r_{j2}^2 + r_{j2}\left(r_{j1} + r_{j+1,1}\right) \underset{H_0}{\overset{H_1}{\gtrless}} L_0 \text{ threshold} \tag{3.41}$$

An examination of the decision rule (3.41) reveals the source of inferiority of the asynchronous coherent detector in comparison with its synchronous counterpart, namely, rule (3.8). The latter rule can be obtained from (3.41) if the factor $r_{j+1,1}$ in the last term is substituted by r_{j1}, because the resulting expression is then the perfect square $(r_{j1} + r_{j2})^2 = r_j^2$ of (3.8). Since r_{j1} and $r_{j+1,1}$ are independent r.v.'s (they belong to different random chips) regardless of the true epoch value, it follows after some thought that such a substitution would increase the mean of the decision statistic λ_2 under H_1 and slightly reduce the variance--the effect of which is a net improvement in performance for synchronous detector.

We now turn to evaluating and comparing (3.39) and (3.41). Let us first look at λ_2 and return to λ_1 later. Without any loss in generality, we can assume that the true epoch is $\varepsilon = 0$. The symmetry of the problem suggests that the results to be derived under such

41

conditioning also represent the unconditional (average) performance in this two-possible-value case. Using the familiar type of Gaussian analysis, it can be shown that

$$d_{\lambda_2}\Big|_{\varepsilon=0} = \sqrt{\frac{3}{2}}\ \sqrt{N}\ \gamma_c \qquad (3.42)$$

which, when compared with its synchronous counterpart (3.11) reveals a loss factor of $\sqrt{4/3}$, or 0.63 dB, as the SNR penalty (in γ_c) associated with the aforementioned asynchronous detector.

The above estimated loss can also be viewed as a lower bound on the performance losses of the continuous-epoch-uncertainty detector illustrated in Figure 6. This is because the two-point uncertainty coherent detector discussed so far assumes a random epoch that can take on only two values; thus, it faces less uncertainty than any other multipoint or continuous type of epoch-randomness. Therefore, it is bound to outperform any other asynchronous detector, including the aforementioned continuous-uncertainty one.

It is also possible to derive an upper bound on the performance losses of the continuous-uncertainty detector. This can be done by assuming a truly continuous epoch and viewing the two-point detector as a suboptimal quantized implementation of the optimal continuous-uncertainty one. The performance losses of the suboptimal detector under a worst-case choice of the unquantized epoch will then clearly upper-bound the losses of any other, higher complexity, multipoint or continuous detector.

Some reflection could persuade us that the worst epoch for the two-point quantized detector is the one straddling between $\varepsilon = 0$ and $\varepsilon = 1/2$, namely, $\varepsilon = 1/4$ (or, equivalently, $\varepsilon = 3/4$, whose performance, however, is identical). This is because, under H_1, r_{j1} will then have the lowest possible mean (namely, zero) half of the time, while r_{j2} remains unaffected. Any other offset will yield a higher overall average for r_{j1}, thus improving performance. The steps of this worst-case analysis are summarized in Appendix E, wherein it is shown that

$$d_{\lambda_2}\Big|_{\varepsilon=\frac{1}{4}} = \sqrt{\frac{25}{24}}\ \sqrt{N}\ \gamma_c \qquad (3.43)$$

Thus, the upper-bounding loss is $(4 \sqrt{3/5})$, or 1.42 dB, with respect to the synchronous structure. In summary, lack of synchronism in the coherent case costs anywhere from 0.63 dB (lower-bound) to 1.42 dB (upper bound) Tighter bounds can be obtained by reiterating the above arguments for epoch-quantized detectors with more than two quantization points. As the number of points increases, one asymptotically converges to the actual performance of the continuous-epoch detector. In any case, a rough figure of an average 1 dB loss due to asynchronism should not be far from exact. Similar conclusions can be drawn for noncoherent detectors.

Finally, let us briefly return to the test (3.39). In order to assess the impact of the ln cosh(W) term, consider the rv W as defined in (3.36), (3.37), and assume a worst-case offset $(\varepsilon = 1/4)$. It is clear from the symmetry of the problem that the rv's A_0 and $A_{1/2}$ have identical first and second moments under either hypothesis.

Furthermore, for large N, the summations in (3.36) will make them approximately jointly Gaussian, correlated rv's. It is then well known that the transformations defined by (3.37) render Z and W approximately Gaussian and independent rv's. Thus, Z and ln cosh(W) are also approximately independent. The mean of W is zero and its variance $\sigma^2_{W|H_k}$ is essentially the same under either hypothesis H_k. Since, for zero-mean W, the expected value $\varepsilon\{\ln \cosh(W)|H_k\}$ is only a function of $\sigma^2_{W|H_k}$ it follows that the second term in (3.39) does not contribute to the difference of the means of λ_1 under H_0 and H_1 while it does contribute to the variance. The net result is that $d_{\lambda 1} < d_{\lambda 2}$, i.e. the detector is better off by neglecting ln cosh(W). This conclusion, is true for the worst offset $\varepsilon = 1/4$; although other offsets will require somewhat more complicated arguments, the same supremacy of λ_2 over λ_1 is likely to hold.

Some asynchronous simulation results are presented in Figure 8 for (a) N = 50 and (b) N = 1000, along with the synchronous (suboptimal detector) simulation points from Figure 4 are used here for reference. The simulation model was coherent, worst-case offset for both rules (3.39) and (3.41). As seen, the agreement with the theory is quite satisfactory.
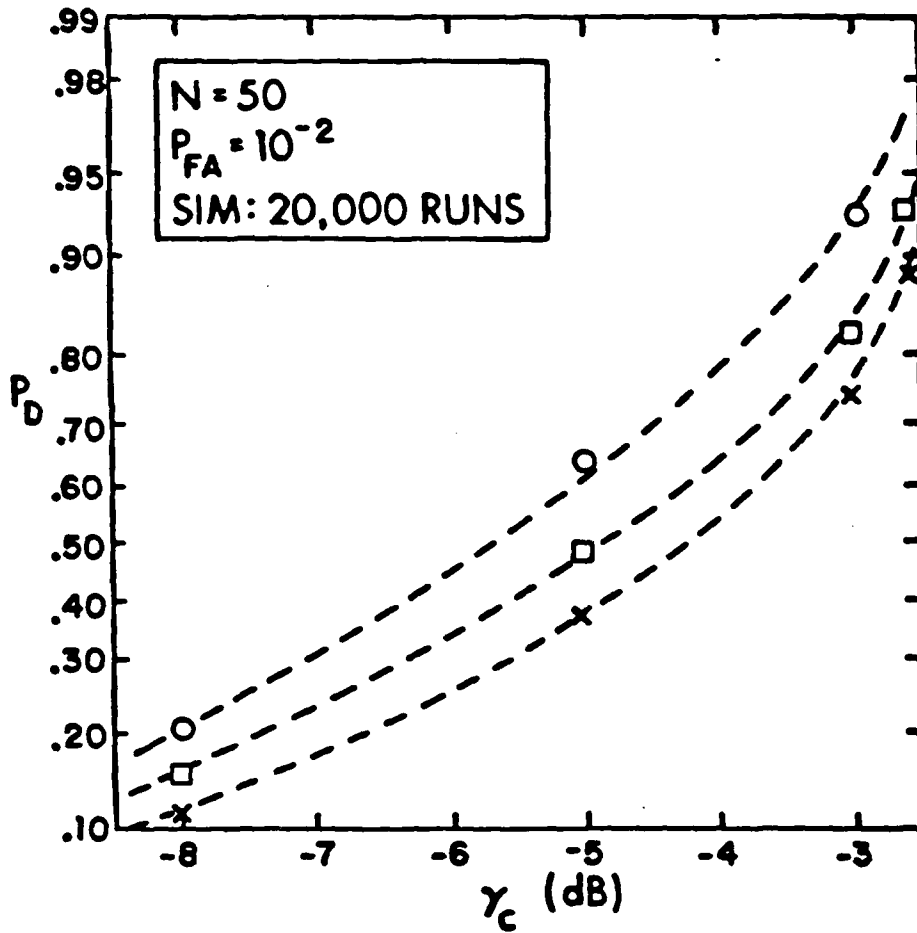
43

◯ simulation results for synchronous test (3.8)

▢ simulation results for asynchronous test (3.41)
                                    worst offset

✕ simulation results for asynchronous rule (3.39)
                                    worst offset

(a) N = 50

Figure 8a   Simulation results for P_D vs. γ_c, asynchronous detectors, worst-case offset, $P_{FA} = 10^{-2}$, N=50.
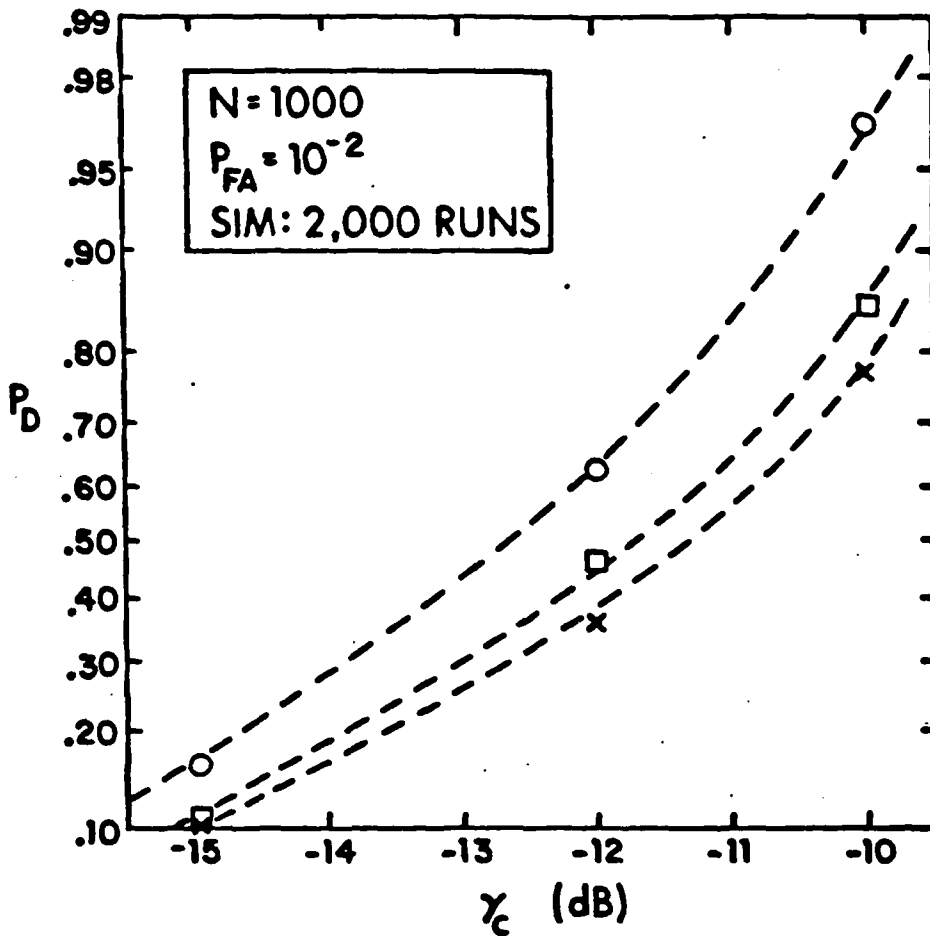
$\bigcirc$ simulation results for synchronous test (3.8)

$\square$ simulation results for asynchronous test (3.41)
                    worst offset

$\times$ simulation results for asynchronous rule (3.39)
                    worst offset

(b) N = 1000

Figure 8b   Simulation results for P_D vs. γ_c, asynchronous detectors, worst-case offset, $P_{FA} = 10^{-2}$, N=1000.

3.4 Radiometric and Correlation Detectors

Thus far we have explored structures which result from likelihood-ratio considerations and variations thereof. We shall now take a look at some other detector structures widely used in practice. Those are (a) the energy detector or radiometer, (b) the product or crosscorrelation detector from two independent receptions and (c) the single-log autocorrelation or chip-rate detector.

Although all three are basedband detectors, with respect to the carrier harmonics, they differ in that the first two utilize the DC compont of the output as a decision statistic while the third filters and detects at the chip rate. Another grouping yet results from the fact that, although all three rely upon a good measurement of the noise level for precise threshold setting, the last two avoid a total-noise-power factor in the output mean thus being more robust to noise fluctnations than the first. These facts are all borne out in the ensuing analysis. We should clarify here that the term "correlation" above is not to be intepreted in the statistical sense; rather, it signifies a product-and-filtering (averaging) mechanism in the time domain. Such correlation operations comprise standard suboptimal[14] timing-recovery methods in Pulse-Analog (PAM) and Digital Modulation schemes (see[17]; also, the section bit synchronizers in [18]). Furthermore, the correlation detectors presented herein may be viewed as a single-point ("single-lag") special case of the general multi-lag correlation algorithms to be analyzed in Section 5. Nonetheless, because of their popularity and implementational simplicity, they will be treated here separately. Let us note that the analyses and conclusions herein, although described in terms of DS waveforms, basically carry over to TH and FH waveforms with only notational changes.[15]

---

[14]Suboptimality results from the fact that the received noisy waveform is not correlated against a local replica of the useful signal or an estimated version, thereof, but rather against itself after a proper delay.

[15]This statement neglects second-order effects (for low input-SNR) created from signal self-noise and signal-cross-noise contributions.

Detection based on an energy measurement is an optimal LR procedure, when both signal and noise are independent Gaussian processes [12]; it is, therefore, suboptimal in principle, when the sought signal is not Gaussian, but rather a BPSK (or any other type of digitally modulated) waveform. The performance of the radiometric detector, shown in Figure 9, has been analyzed. It can be shown that

$$\mathcal{E}\{\lambda | H_k\} = (NT_c)(\alpha_{BP}^2 S\delta_{k1} + N_0 W_{BP}) \tag{3.44a}$$

and

$$var\{\lambda | H_k\} = (NT_c)(N_0^2 W_{BP} + 2\alpha_{BP}^4 SN_0\delta_{k_1}) \tag{3.44b}$$

where the __attenuation factor__ α_{BP}^2 is defined as

$$\alpha_{BP} = \frac{\int_{-\infty}^{\infty} |H_L(f)|^2 S_c(f)df}{\int_{-\infty}^{\infty} S_c(f)df} = \left(\frac{2}{\pi}\right) \int_0^{\pi W_{BP}T_c/2} \left(\frac{\sin x}{x}\right)^2 dx \tag{3.44c}$$

and is a measure of the energy loss due to filtering. In (3.44c), $H_L(f)$ stands for the low pass equivalent of the BP filter $H_{BP}(f)$ and $S_c(f)$ is the power spectral density of the code sequence $c(t)$. Again, assuming that $W_{BP} \approx T_c^{-1}$ and that the time-bandwidth product $W_{BP}(NT_c) \cong N$ is large, (3.44) can be combined with the "Gaussian" performance of (2.5). The result is (3.10a), with
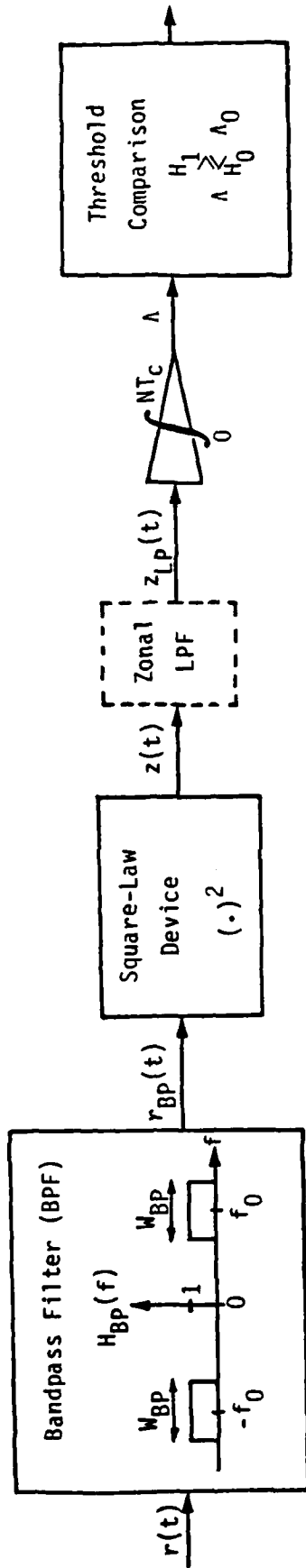
Figure 9. Energy Detector (Radiometer)

48

$$a = \frac{\alpha^2_{BP}}{\sqrt{W_{BP}T_c}} \; ; \; b = 2a^2 \text{ (Radiometer)} \qquad (3.45)$$

The radio $a = \alpha^2_{Bp}/\sqrt{W_{Bp}T_c}$ can be plotted versus $(W_{Bp}T_c)$, and the optimal choice can be shown to be approximately $W_{BP}T_c \approx 1$, from which it follows that $a_{max} \approx 0.77$. This corresponds to a minimum loss of -1.1 dB with respect to the chip noncoherent detector (3.23). Since the above conclusions are based strictly on energy considerations and interchip-interference effects, due to filtering, which have not been taken into account, the actual losses are somewhat higher. In the following comparisons, we select a nominal loss figure of -1.5 dB. We note that the above losses pertain to a rectangular BPF; other filter ships will result in different loss figures, typically of the same order. For the effect of filtering on a baseband rectangular pulse (in terms of output-SNR losses) with respect to a matched filter, the interested reader is referred to [12].

We now turn to examine whether benefits can be extracted from utilizing <u>two</u> independent receptions of the same signal, resulting from two RF circuits with independent thermal noises. Although only the synchronous coherent case is covered here, similar conclusions are expected from the other models.

Let

$$r_1(t) = \sqrt{S} \, c(t)\delta_{k1} + n_1(t); \; 0 < t \leq T$$

$$r_2(t) = \sqrt{S} \, c(t-\Delta)\delta_{k1} + n_2(t); \quad k = 0,1 \qquad (3.46)$$

represent the two receptions. Here, the two noise processes $n_m(t)$; $m = 1,2$ are Gaussian and independent, while the signal component is the same in both waveforms. Furthermore, the second signal has a delay of Δ seconds with respect to the first. If Δ were exactly known, the two receptions could be adjusted to align in time and be coherently combined with a resultant 3 dB gain in SNR. In many cases, Δ is unknown and its estimation is of interest as it relates to path differentials and, therefrom, to direction finding.

A simple cross correlation receiver which performs this estimation/detection problem is shown in Figure 10a. The corresponding decision rule is

$$\lambda = \int_0^{NT_c} r_1(t) \, r_2(t) \, dt \underset{H_0}{\overset{H_1}{\underset{<}{>}}} \lambda_0 \tag{3.47}$$

To simplify, let us assume that detection occurs only when $\Delta = 0$; then, (3.47) can be analyzed exactly by evaluating the second-order statistics of the product waveform $g_{12}(t) = r_1(t)r_2(t)$ under either hypothesis. Such a procedure will be applied below in analyzing the chip-rate detector. Here, for the sake of brevity, let us just consider the alternative structure of Figure (10b) which can be thought of as an approximation to Figure (10a). Obviously, the constraint of individual chip-synchronism per channel has been imposed on the second structure, in addition to the delay-sync between the two channels. The rule corresponding to Figure (10b) is

$$\lambda = \sum_{j=1}^{N} r_j^{(1)} \, r_j^{(2)} \underset{H_0}{\overset{H_1}{\underset{<}{>}}} \lambda_0 \tag{3.48}$$

where

$$r_j^{(m)} = \int_{(j-1)T_c}^{jT_c} r_m(t) \, dt \tag{3.49}$$

are synchronous, chip-by-chip integrations.

Equation (3.48) is analogous to (3.8) once r_j is substituted $r_j^{(1)} r_j^{(2)}$. Clearly, in the absence of thermal noise, both (3.8) and (3.48) produce the same quantity NST_c^2; however, performance is different in noise. Indeed, from (3.48), it easily follows that

$$\mathscr{E}\{\lambda|H_k\} = N(N_0T_c)\gamma_c\delta_{k1} \tag{3.50}$$

50
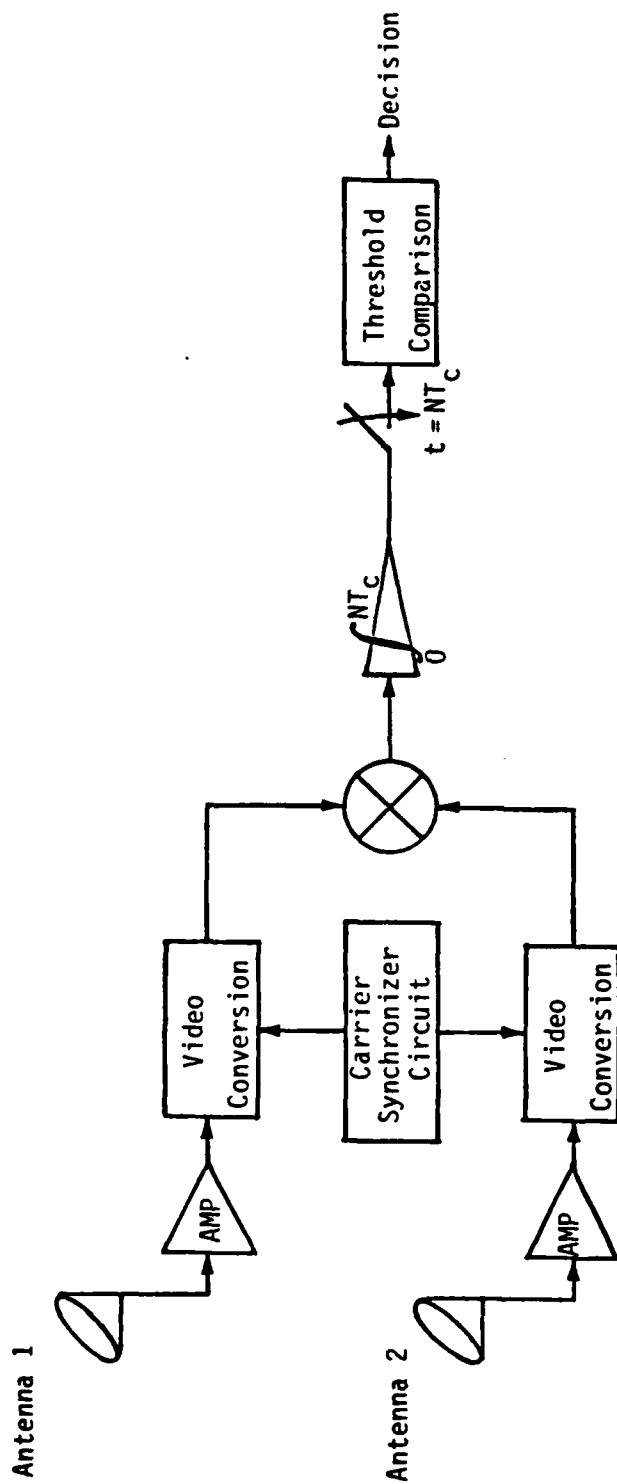
Figure 10a. A Coherent, Two-Reception, Cross-correlation Detector

51
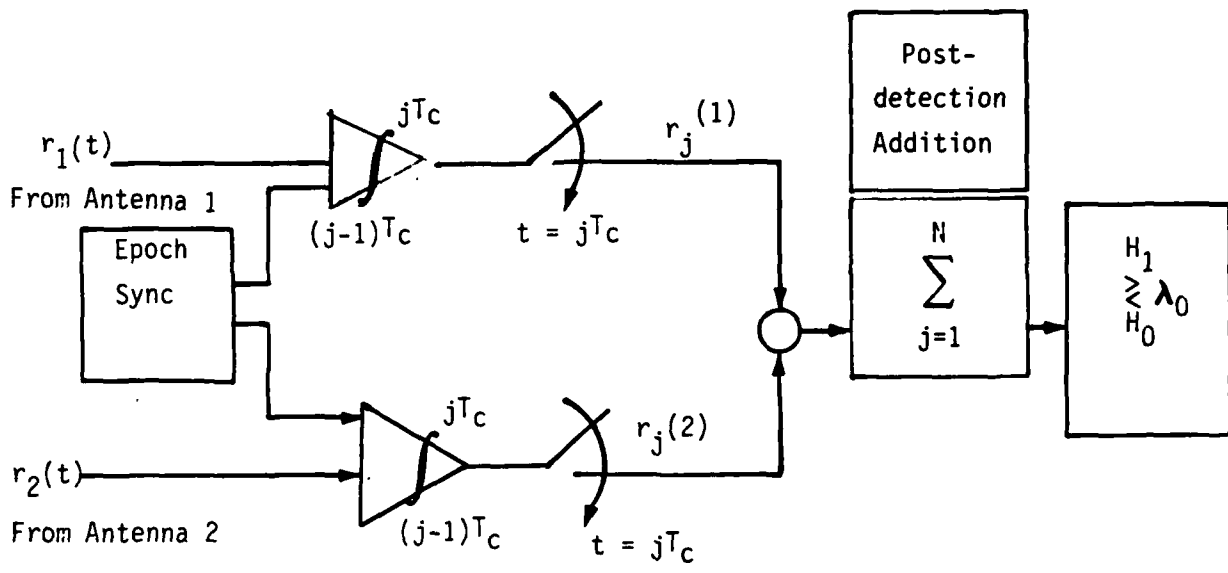
Figure 10b: An approximate version of the crosscorrelation detector in Figure 10a.

and

$$\text{var}\{\lambda|H_k\} = N(N_0T_c)^2 \, [1/4 + \gamma_c\delta_{k1}] \tag{3.51}$$

The resulting performance is again described by (3.10a), where now

$$a = 2; \quad b = 4 \quad \text{(Two independent coherent receptions)}. \tag{3.52}$$

Thus, a comparison with the corresponding performance parameters (3.10b) for the (one-reception) synchronous coherent detector reveals a gain factor of $\sqrt{2}$, or 1.5 dB in SNR for the present system. However, this gain is clearly attained at the cost of higher complexity. Similar conclusions are true for noncoherent reception detectors.

Finally, we consider the chip-rate detector, a noncoherent BP version which is shown in Figure 11. This is an one-antenna system (like the radiometer) which, however, detects power at the first harmonic of the "signal x signal" term. Clearly, this structure could also detect power at DC and serve as a "generalized" radiometer where the $\Delta = 0$ case would correspond to the familiar square-law energy detector (Figure 9). This possibility is explored below, where it is shown that, aside from sensitivity considerations, SNR performance increases monotonically as $\Delta \to 0$. Thus, the standard radiometer is probably the most meritorious device to consider at DC; contrary to that, detection at the first harmonic is worth exploring.

We note, however, that the robustness gains to be shown below are predicated upon the knowledge of the sought signal rate, a requirement not present in the radiometric analysis. We can, therefore, conclude that the chip-rate detector trades increased parametric knowledge with a certain robustness to noise fluctuations, something that an energy detector is not equipped to do.

Under H_1, the filtered input is r(t), given by

53
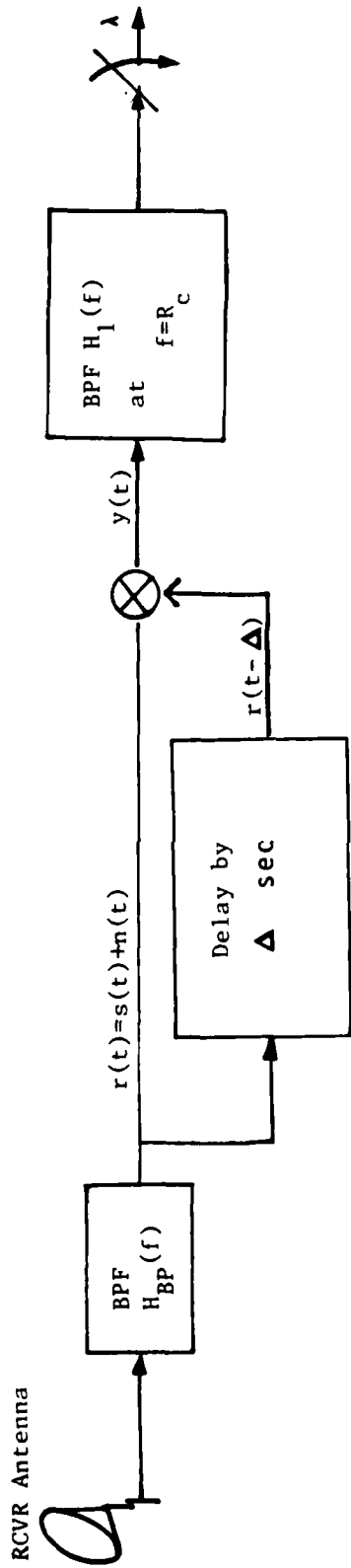
Figure 11: A chip-rate detector used for LPI purposes

$$r(t) = \sqrt{2\alpha_{BP}^2 S} \; c(t) \cos(\omega_0 t + \phi) + n(t) \qquad (3.53)$$

where the BP nature of the noise process is reflected in its PSD $S_n(f) = (N_0/2) |H_{BP}(f)|^2$ and the standard modeling for the filtered signal via the factor α_{BP} has been assumed.

The product output $y(t) = r(t)r(t-\Delta)$ has a correlation function

$$R_y(\tau) = R_{s \times s}(\tau) + R_{S \times N}(\tau) + R_{N \times N}(\tau) \qquad (3.54)$$

where the "signal x signal" correlation is

$$R_{sxs}(\tau) = \alpha_{BP} S^2 \left(\cos^2 \omega_0 \Delta + \frac{\cos 2\omega_0 \tau}{2} \right) R_g(\tau) \qquad (3.55a)$$

In (3.55a), $R_g(\tau)$ signifies the corrlation of the code-product process $g(t) = c(t) \, c(t-\Delta)$. Furthermore, the "noise x noise" correlation is

$$R_{NxN}(\tau) = \mathcal{E}\{n(t)n(t-\Delta)n(t-\tau)n(t-\Delta-\tau)\}$$
$$= R_n^2(\Delta) + R_n^2(\tau) + R_n(\tau + \Delta) \cdot R_n(\tau - \Delta) \qquad (3.55b)$$

while the "signal x noise" term $R_{SxN}(\tau)$ includes all other remaining terms. For low input-SNR, the signal x noise term will be neglected in comparison to the noise x noise term; thus, the PSD $S_y(f)$ of $y(t)$ can be approximately written as

$$S_y(f) = \alpha_{BP} S^2 [\cos^2(\omega_0 \Delta) S_g(f) + 1/4(S_g(f-2f_0) + S_g(f+2f_0))$$
$$+ R_n^2(\Delta)\delta(f) + S_n(f) \circledast S_n(f)$$
$$+ [S_n(f)e^{-j2\pi f\Delta}] \circledast [S_n(f)e^{j2\pi f\Delta}] \qquad (3.56)$$

55

where $S_g(f)$ is the PSD of $g(t)$.

In order to pursue any further and derive the second-order statistics of the narrowband output λ, one has to specify $S_g(f)$, $S_n(f)$ and the output-filter characteristic. For a purely random code, $S_g(f)$ was derived to be

$$
S_g(f) = \left(1 - \left|\frac{\Delta}{T_c}\right|\right)^2 \delta(f) + \left(\frac{\Delta}{T_c}\right)^2 \sum_{\substack{m=-\infty \\ m \neq 0}}^{\infty} S_a^2\left(\frac{\pi m \Delta}{T_c}\right) \delta\left(f + \frac{m}{T_c}\right)
$$

$$
+ \frac{\Delta^2}{T_c} \cdot S_a^2(\pi f \Delta)
\tag{3.57}
$$

where the offset Δ is restricted to $0 \leq |\Delta| < T_c$. Note, the presence of the "signal self-noise" term, the third in (3.57). Because of the weak input-SNR assumption, this term will be neglected in terms of its contribution to the total noise level. However, for high input-SNR environments (as, for instance, in certain FH scenarios), this term will be the major limiting factor and deserves due attention. To prove further, let us evaluate the contribution $S_{NxN}(f)$ for a standard "brick-wall" noise PSD

$$
S_n(f) = \begin{cases} \dfrac{N_0}{2} & \ldots, \ \left| |f| - f_0 \right| \leq \dfrac{W_{BP}}{2} \\[3mm] 0 & \ldots, \ \text{otherwise} \end{cases}
\tag{3.58}
$$

which can be shown to be

$$
S_{NxN}(f) = (N_0 W_{BP})^2 S_a^2(\pi W_{BP}\Delta)\cos^2\omega_0\Delta \delta(f) +
$$

$$
\frac{N_0^2}{2}(W_{BP} - |f|)[1 + \cos(2\omega_0\Delta) S_a(2\pi\Delta(W_{BP} - |f|))]
$$

$$
\text{for } |f| \leq W_{BP}
\tag{3.59}
$$

We shall restrict attention to the two baseband possibilities: (a) DC filtering by $H_{DC}(f)$ and (b) chip-rate filtering by $H_1(f)$, the latter corresponding to the $m = \pm1$ terms in (3.57). In both cases, the postdetection filter will be assumed to be very narrow with respect to R_c ; for instance, if $H_{DC}(f)$ corresponds to an NT_c integrator, this implies that $N >> 1$. Note that Figure 11 refers to case (b) only. Furthermore, the terms around $2f_0$ will be filtered out from (3.56) (they have already been excluded from (3.59)).

For a narrowband integrator-LPF(case(a)), the output SNR

$$d_\lambda^2 \overset{\Delta}{=} (\mathscr{E}\{\lambda | H_1\} - \mathscr{E}\{\lambda | H_0\})^2 / var\{\lambda | H_0\}$$

is easily derived from (3.56) - (3.59) to be

$$d^2_{\lambda \, bc} = (NT_c) \frac{\alpha_{BP}^4 \, S^2 \, cos^2(\omega_0 \Delta)(1 - |\frac{\Delta}{T_c}|)^2}{(N_0^2 W_{BP}/2)[1 + cos(2\omega_0 \Delta) \, S_a(2\pi W_{BP}\Delta)]}$$

(3.60)

since the "noise x noise" DC contribution cancels out in the different $\mathscr{E}\{Z|H_1\} - \mathscr{E}\{Z/H_0\}$. Certain interesting observations can be made from (3.60), especially in connection with the radiometric output-SNR $d_{\lambda,rad}^2$ from (3.44); if we form the ratio

$$\frac{d^2_{\lambda; \Delta \neq 0}}{d^2_{\lambda, rad \atop (\Delta=0)}} = \frac{2 \, cos^2(\omega_0 \Delta)\left(1 - |\frac{\Delta}{T_c}|\right)^2}{1 + cos(2\omega_0 \Delta) \cdot S_a(2\pi W_{BP}\Delta)}$$

$$= \left(1 - |\frac{\Delta}{T_c}|\right)^2 \left[\frac{1 + cos(2\omega_0 \Delta)}{1 + cos(2\omega_0 \Delta) \, S_a(2\pi W_{BP}\Delta)}\right]$$

(3.61)

57

then it is immediately clear that the ratio tends to 1 as $\Delta \to 0$, as it should. Furthermore, if $\Delta \ll (2W_{BP})^{-1}$ so that the $S_a(\cdot)$ function in the denominator of (3.61) is approximately one, the ratio is roughly equal to $(1 - |\Delta/T_c|)^2$, independent of the signal carrier frequency f_0. Thus, in this range of Δ, the ratio is maximized by choosing $\Delta = 0$, i.e., square-law energy detection yields the highest output SNR. The same conclusion holds far higher values of Δ, say, $\Delta \geq 1/2W_{BP}^{-1}$, the $S_a(\cdot)$ function diminishes and the ratio tends to

$$2(1-|\Delta/T_c|)^2 \cos^2(\omega_0\Delta)$$

However, since, typical values for the filter BW are $W_{BP} > R_c$, it follows that $\Delta \geq T_c/2$, which implies that the ratio is upperbounded by $(1/2)\cos^2\omega_0\Delta \leq 1/2$ or a 3 dB loss of the correlator versus the radiometer. In addition, one has to worry in the latter case about the exact relationship between f_0 and Δ. If $f_0\Delta \neq k/2$, k an integer, servere loss of "signal" power can occur due to the cosine term. Clearly, in an LPI environment where the signal parameters are hardly at the disposal of the interceptor, such limitation is of concern. On the other hand, the mean "noise x noise" contribution at DC (the first term in (3.59)) also diminishes with increasing values of $(W_{BP}\Delta)$, a factor which, although not directly reflected in the SNR computations, could affect the sensitivity of the system in an actual implementation with imperfect AGC's.

Let us now turn to the chip-rate filter (case(b)). Evaluating the S x S and N x N narrowband terms at $f = R_c$, we get the following SNR expression.

$$d_\lambda^2 = \left[\left(\frac{1}{W_1}\right)\frac{\alpha_{BP}^4 P S^2}{N_0^2 W_{BP}}\right]\left\{\frac{(1 + \cos 2\omega_0\Delta)\left[\left(\frac{\Delta}{T_c}\right)^2 S_a^2\left(\frac{\pi\Delta}{T_0}\right)\right]}{(1-\rho)[1+\cos(2\omega_0\Delta)S_a(2\pi\Delta W_{BP}(1-\rho))]}\right\}$$

(chip-rate detector)   (3.62)

58

where W_1 is the BW of the narrowband filter H (f) and the ratio $\rho = R_c/W_{BP}$ is assumed to be in the range $0 < \rho < 1$. Note that if $W_1 \approx (NT_c)^{-1}$, then the first bracketed term corresponds to the radiometric SNR; thus, the fraction in the second brackets represents an SNR-ratio similar to (3.61). It is further shown that the numerator of this ratio (i.e., the S x S portion) is maximized for $\Delta = T_c/2$, assuming that the condition $f_0\Delta = k/2$; k = integer, is satisfied. For that "optimal" choice of the offset, the resulting SNR is

$$d_\lambda^2 = \left(d_{\lambda,rad}^2\right)\left(\frac{2}{\pi^2}\right)\frac{1}{(1-\rho)[1 + S_a \pi(1-\rho)/\rho]}$$

(chip-rate detector)

$$(\Delta = T_c/2; \; f_0\Delta = k/R) \tag{3.63}$$

Note that the SNR of the chip-rate detector increases as $\rho \to 1$, i.e., as $W_{BP} \to R_c$; in fact, for $W_{BP} \approx 1.25\, R_c$, *the two detectors (chip-rate and radiometric) are roughly equivalent.* Since much smaller values of W_{BP} are rather inappropriate to consider in view of Doppler uncertainties, signal filtering, etc., such equivalence can be considered a practical fact. Again, the aforementioned tradeoffs between robustness to noise fluctuations, knowledge of chip-rate and adjustment of carrier frequency should be kept in mind for a true comparative assessment of the various detectors.

As mentioned, a complete analysis for all values of the input SNR should incorporate the signal self-noise contribution from (3.57), as well as the signal x noise terms.

Furthermore, the dependence on the carrier frequency can be totally eliminated by using the alternative structure; the penalty there, of course, will be a somewhat lower output SNR. Finally, let us note that variations of the schemes herein are also possible,

involving different intermediate frequencies (IF) for the undelayed and delayed versions, respectively. We shall not pursue the topic here any further.

3.5 Comparisons and Discussion

The performance of any of the schemes discussed, so far, will always be upper-bounded by that of a perfectly code-matched system (i.e., one where the code is totally known) and lower-bounded by the performance of the radiometer. The distance d_{UB} corresponding to the (unattainable from an LPI viewpoint) upper bound is easily shown to be

$$d_{UB} = \sqrt{2N\gamma_c} \qquad\qquad (3.64)$$

where a coherent system has been assumed. Comparing (3.64) with (3.11) implies that the lack of code knowledge amounts to an SNR loss of $\sqrt{\gamma_c}$ between two synchronous coherent detectors, one equipped with the code and the other not; in dB, this means that knowledge of the code reduces in half the input SNR (dB) required to achieve a certain performance level.[17] This is depicted in Figure 12 (compare curves ① and ③) along with the performance of the other alternative schemes. We observe that the difference between ② and ③ is roughly 1.5 dB, which is also the difference between ③ and ④ as well as ④ and ⑤. It follows that, under fairly ideal conditions, i.e., two independent synchronous coherent receptions, one could utilize up to 4.5 dB gain above the radiometer; each of the added features (i.e., two receptions, synchronism and coherence) can be thought of as contributing 1.5 dB to the gain. We note that, in arriving at these gain figures, system imperfections and noncalibrated parameters such as Doppler frequency offset have not been accounted for.

It is, therefore, seen that certain gains are plausible with respect to the radiometer if careful designs are employed, but they are certainly not overwhelming--at least in the SNR

---

[17] For example, if the unknown-code detector requires -15 dB for certain performance level, the known-code system will achieve the same level at - 30 dB

61
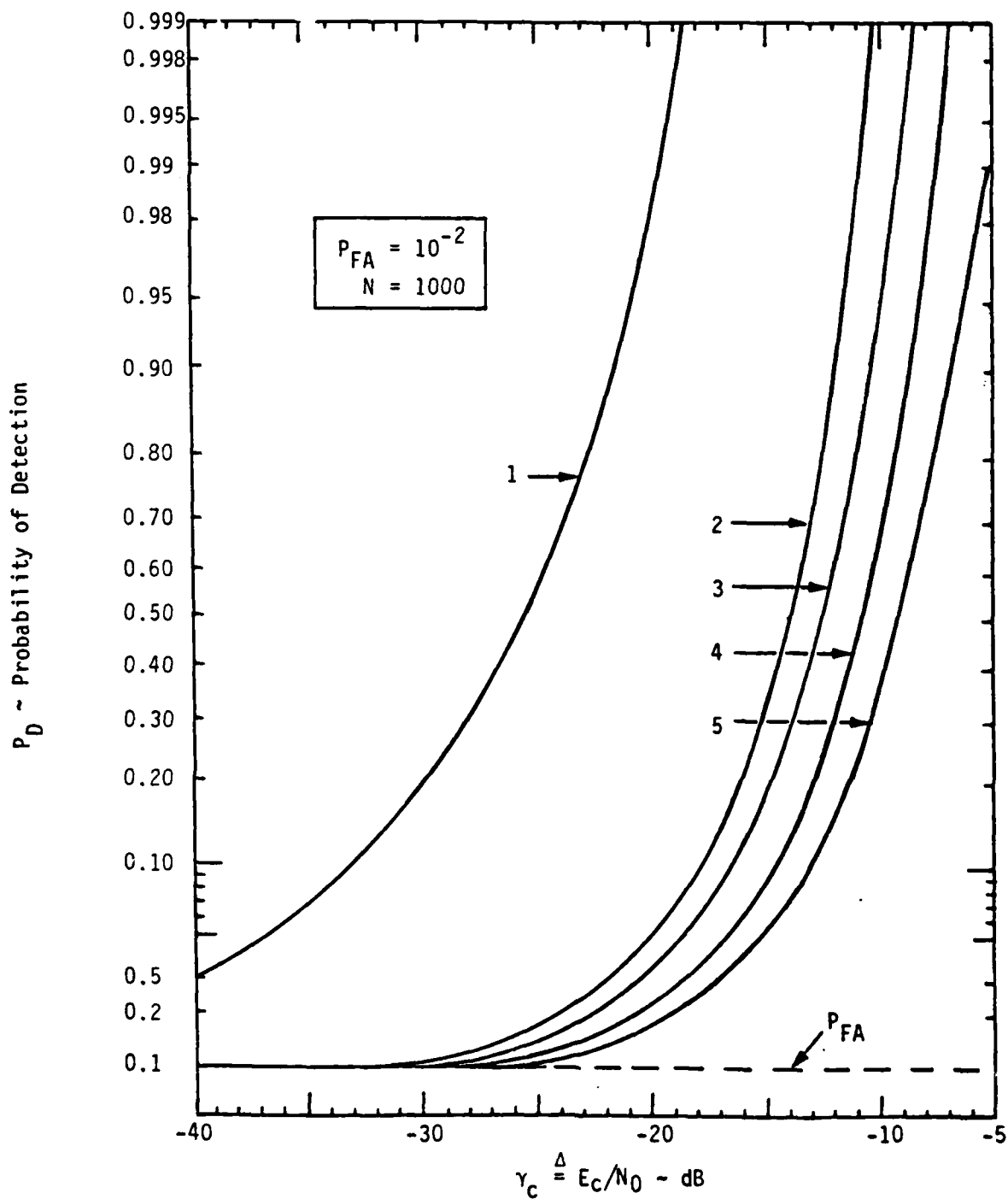
1. Completely known waveform
2. Two independent receptions, synchronous coherent detector
3. Synchronous coherent energy detector
4. Synchronous chip-noncoherent energy detector
5. Radiometer

Figure 12.   Performance Comparisons for the Detection of DS Waveforms

range of interest and for constant-envelope signals. This is because a high-rate DS waveform is not very distinguishable from the background thermal AWG noise in which it is detected and, as is well known, the radiometer then becomes an asymptotically optimal detector. This is also in accordance with Krasner's approximate result regarding biorthogonal waveforms [8], which establishes the DS signals as uniformly good LPI choices almost independent of the prevailing system parameters (SNR and N). However, if one removes the biorthogonality of the signal set and/or the AWG nature of the noise, the results can differ substantially. An illustration of the former can be found in the following sections which pertain to time-hopping and frequency-hopping waveforms. As for the latter, it is clear that the white-noise theory as developed herein can be grossly inadequate in a dense environment, loaded with a mixture of wideband and narrowband waveforms. As mentioned in the introduction, the presence of narrowband interference prediction and excision algorithms will then become crucial to the success of any detection scheme. The example of section 5.5 is meant to illustrate the dramatic difference between a somewhat "intelligent" algorithm and the "naive" radiometer in such a narrowband environment which, of course, comes as no surprise. We note that a general theory of LPI performance in an unpredictable-interference scenario has not yet matured (at least in the open literature) and thus constitutes an area of significant interest.

We conclude by noting that the implicit assumption of "message-synch" (i.e., signal occupying exactly the observation interval) should and could be removed in a realistic evaluation of an LPI detecting system.. However, the relative ranking. in terms of merit of the various detectors discussed herein is not expected to change under such alteration of the underlying scenario.

4.0   TIME-HOPPING WAVEFORMS

We now focus on the wideband detection of a particular type of orthogonal signalling, namely TH waveforms, where the code dictating the hopping is again random. We shall consider only synchronous detectors (i.e., the timing or epoch of the hopping slot will be assumed known); asynchronism can be treated with methods similar to those used in Section 3.3. Furthermore, both carrier-coherent and carrier-noncoherent systems will be examined. In particular, the former will assume a known carrier phase combined with a pulse-position-modulation (PPM) format while, for the latter, any modulation that randomizes the phase form frame to frame (e.g., BPSK) is well suited. We term such cases "pulse noncoherent". Of course, one could hypothesize a noncoherent PPM system with an unknown, but constant carrier phase, and derive the optimal detection rule. However, the resulting receiver and pertinent analysis are again complicated (for a similar situation, refer to section 3.2 for DS); therefore, only pulse-noncoherent systems will be discussed here. Again, the lower-bounding performance of the radiometer will indicate that little is lost by using this simplification.

For our purposes, the received waveforms (TH signal plus noise) can be written as

$$r(t) = \sqrt{2S} \sum_{k=-\infty}^{\infty} p\left(t - kT_F - \rho_k T_H\right)\cos\left(\omega_0 t + \theta_k\right) + n(t) \qquad (4.1)$$

where T_F is the frame length, T_H is the hop length (width of each time slot), and ρ_k, θ_k are random variables which are independent from frame to frame[18] and of each other, denoting the slot location and carrier phase, respectively, during the kth frame. Here, ρ_k can take on any one of the equiprobable values $\rho_k = 0,..., N_F -1$, where $N_F = T/T_H$ is the total number of slots per frame and θ_k summarizes both the unmodulated carrier phase ϕ plus

---

[18] The independence of θ_k is within the aforementioned spirit of a "pulse-noncoherent" system.

64

any superimposed PSK modulation. For coherent systems, θ_k is assumed known for every k. Finally, p(t) is a unit pulse of duration T_H seconds, while n(t) is the usual bandpass AWGN. A noiseless sample waveform (realization) of the T_H signal is shown in Figure 13. We shall assume that the total observtation interval consists of Q frames, ie., $T = QT_F = QN_FT_H$. Note that the average signal power in (4.1) is $S_{av} = S/N_F$.
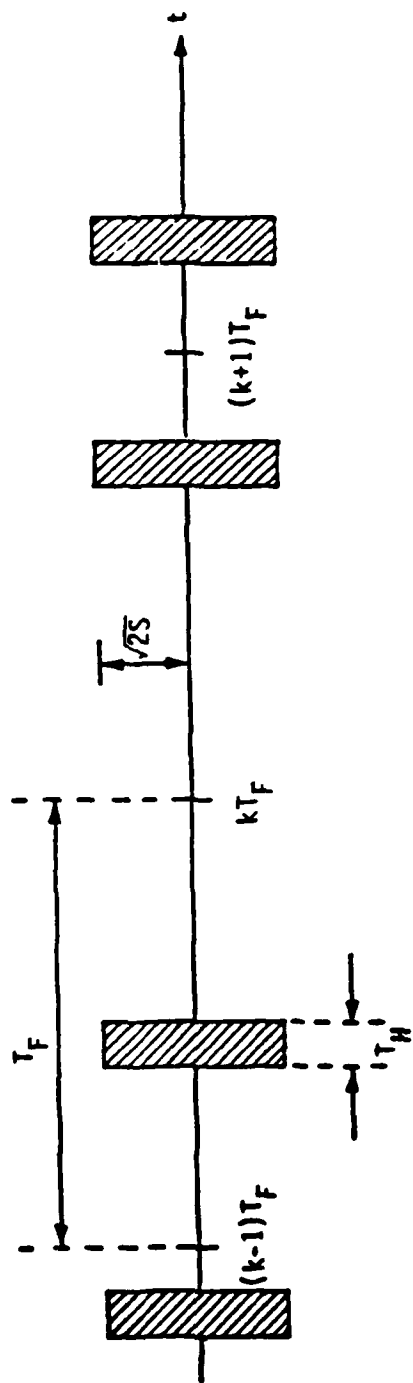
Figure 13. A Time-Hopping Signal with N_F = 10 and Random RF Phase from Frame to Frame

4.1 Synchronous Coherent Detectors

Under the coherent assumption, $\sqrt{2}\cos(\omega_0 t + \theta_k)$ in (4.1) is substituted by one. Then, a straightforward application of the composite likelihood ratio yields

$$\Lambda(r(t)) = \prod_{m=1}^{Q}\left\{\frac{\exp\{-\gamma_H\}}{N_F}\sum_{k=1}^{N_F}\exp\left\{\frac{2\sqrt{S}}{N_0}r_{km}\right\}\right\} \underset{H_0}{\overset{H_1}{\gtrless}} \Lambda_0 \qquad (4.2)$$

where

$$\gamma_H \triangleq \frac{ST_H}{N_0} \qquad (4.3)$$

is the SNR per time hop (slot) and

$$r_{km} = \int_{(m-1)T_F+(k-1)T_H}^{(m-1)T_F+kT_H} r(t)\, p(t - kT_H)dt \qquad (4.4)$$

is the integral of r(t) in the kth slot of the mth frame. If γ_H is a small number so that $\exp\{x\} \approx 1 + x$, (4.2) can be simplified to the approximate rule

$$\Lambda(r(t)) \approx \int_0^T r(t)dt \underset{H_0}{\overset{H_1}{\gtrless}} \lambda_0 \qquad (4.5)$$

i.e., just the coherent integral of r(t). However, since γ_H is typically above 0 dB (much larger than γ_c), such approximations are not as successful as in the DS case -- a fact to which the comparisons in Section 4.3 will attest.

The Gaussian distance $d_{\ell,coh}$ associated with the optimal coherent rule (4.2) can be derived based on (2.9) and the following steps:

$$d_{\ell,coh}^2 = \ln \mathscr{E}\{\Lambda^2|H_0\} = Q\ln \mathscr{E}\{\Lambda_F^2|H_0\} \qquad (4.6)$$

where Λ_F is the likelihood ratio per frame. But,

$$
\ln \mathscr{E}\left\{\Lambda_F^2 \big| H_0\right\} = \ln\left[1 + \operatorname{var}_{H_0}\left\{\frac{\exp\{-\gamma_H\}}{N_F} \sum_{k=0}^{N_F-1} \exp\left\{\frac{2\sqrt{S}}{N_0} r_{km}\right\}\right\}\right]
$$

$$
= \ln\left[1 + \frac{\exp\{-2\gamma_H\}}{N_F} \operatorname{var}_{H_0}\left\{\exp\left\{\frac{2\sqrt{S}}{N_0} r_{km}\right\}\right\}\right]
$$

$$
= \ln\left[1 + \frac{\exp\{-2\gamma_H\}}{N_F}\left(\exp\{4\gamma_H\} - \exp\{2\gamma_H\}\right)\right] \tag{4.7}
$$

Since r_{km} is a zero-mean Gaussian random variable (rv) under H_0. Combining (4.6) and (4.7) results in

$$
d_{coh} = \sqrt{Q \ln\left[1 + \frac{1}{N_F}\left(e^{2\gamma_H} - 1\right)\right]} \tag{4.8}
$$

The distance $d_{\lambda,coh}$ for approximate rule (4.6) is derived much easier since

$$
\mathscr{E}\{\lambda|H_0\} = 0, \quad \mathscr{E}\{\lambda|H_1\} = \sqrt{S}\, Q T_H \text{ and } \operatorname{var}\{\lambda|H_0\} = \left(N_F Q T_H\right) N_0/2.
$$

Therefore,

$$
d_{\lambda.coh} = \frac{\mathscr{E}\{\lambda|H_1\} - \mathscr{E}\{\lambda|H_0\}}{\left(\operatorname{var}\{\lambda|H_0\}\right)^{1/2}} = \sqrt{2\left(\frac{Q}{N_F}\right)}\, \gamma_H \tag{4.9}
$$

It is clear from (4.8) and (4.9) that $d_{\ell,coh}$ asymptotically approaches $d_{\lambda,coh}$ as $\gamma_H \to 0$ an expected result. Furthermore, we can compare the approximate coherent rules (3.8) for DS versus (4.6) for TH and note that the first involves a nonlinear operation on the data prior to integration, while the second does not. This has a reflection on their corresponding distances, as (3.11) is directly proportional to γ_c while (4.9) is proportional to γ_H. Thus, for the very-low-SNR case, the latter would outperform the former.

68

4.2 Synchronous-Noncoherent Detectors

Starting from (4.1) and invoking the independent phase assumption results in the decision rule

$$\Lambda = \prod_{m=1}^{Q} \left\{ \frac{\exp\{-\gamma_H\}}{N_F} \sum_{k=1}^{N_F} I_0\left(\frac{2\sqrt{S}}{N_0} R_{km}\right) \right\} \underset{H_0}{\overset{H_1}{\gtrless}} \Lambda_0 \qquad (4.10)$$

where R_{km} is the kth slot, m_{th} frame envelope

$$R_{km} = \sqrt{e_{I,km}^2 + e_{Q,km}^2} \qquad (4.11a)$$

and

$$\begin{bmatrix} e_{I,km} \\ e_{Q,km} \end{bmatrix} = 2 \int_{(m-1)T_F+(k-1)T_H}^{(m-1)T_F+kT_H} r(t) \begin{bmatrix} \cos \omega_0 t \\ \sin \omega_0 t \end{bmatrix} dt$$

$$k=1,\ldots,N_F \quad ; \quad m=1,\ldots,Q \qquad (4.11b)$$

The distance $d_{\ell,noncoh}$ associated with (4.10) is derived by steps identical to (4.7) as

$$d_{\ell,noncoh} = \sqrt{Q \ln\left[1 + \frac{1}{N_F}\left(I_0(2\gamma_H) - 1\right)\right]} \qquad (4.12)$$

Since $I_0(x) < \exp\{x\}$ for every $x > 0$, it follows from the comparison of (4.8) and (4.12) that $d_{\ell,coh} > d_{\ell,noncoh}$ for every γ_H, as expected. We note further that, unlike the coherent distance (4.8) or its approximate counterpart (4.9). $d_{\ell,noncoh}$ of (4.12) is proportional to γ_H at low SNR.

Instead of analyzing the noncoherent rule which approximates (4.10) for low SNR, let us just consider the performance of the radiometer which operates on the time-hopped

waveform (4.1) for T seconds. Following the steps outlined in Section 3.4 it can be be shown that

$$d_{rad} \approx \sqrt{K_{rad}\left(\frac{Q}{N_F}\right)}\gamma_H$$

(4.13)

where the constant $K_{rad} = \alpha^4/(W_{BP}T_H)$ again measures the loss due to filtering. As was done in Section 3.4, K_{rad} can be set at its optimal value $K_{rad} = (0.77)^2 \approx 0.6$. We should note here that (4.13) is actually an optimistic prediction (i.e., an upper bound) of the radiometric performance since it is based on the assumption that the variance of the test statistic under H_1 is approximately the same as under H_0. For medium to high input SNR, this is not true; although a more meaningful performance description can easily be derived , we shall be content with (4.13) for comparison purposes.

4.3   Comparisons and Discussion

First, we are interested in comparing the relative loss of the approximate coherent rule (4.5) versus the exact (4.2), since the former can be implemented easily (a simple integrator) in contrast to the significant complexity of the latter. The comparison is in terms of the relative SNR values γ_H (in dB) required by each in order to achieve the same performance level (d_λ^2) for the same fixed values of Q and N_F. It is based on (4.8) and (4.9) and is shown in Figure 14 ($N_F = 10$). As expected, the difference diminishes at low SNR, but is rather pronounced at medium to high SNR. So, $\gamma_H^{coh,opt} = 0$ dB corresponds to $\gamma_H^{coh,appr} = 3.9$ dB -- a gap that increases rapidly as $\gamma_H^{coh,opt}$ increases.

Second we look at the gains brought about by the coherent assumption versus the noncoherent by comparing the Gaussian distances in (4.8) and (4.12) . The result, again in terms of the required SNR's for the same performance level, is shown in Figure 15. (Note that this comparison is independent of N_F). The difference here diminishes as SNR increases, while it can be substantial at low SNR. The final comparison is between the noncoherent optimal performance (4.12) (or its equivalent log-likelihood sum) versus the radiometer performance estimate (4.13). It is shown in Figure 16 for $K_{rad} = 0.6$ and $N_F = 10$. The irreducible distance of 1.1 dB, as the SNR goes to zero, is due to the $\sqrt{K}_{rad}$ factor[19]. Again, we should keep in mind that the actual SNR losses of the radiometer are higher than those shown in Figure 16 by an amount that increases with SNR due to previously discussed reasons. Furthermore, a common trend is evident from Figures 14 and 16, namely, that the simplifying deviations from the optimal decision rules incur comparative losses that increase fairly rapidly with the available hop SNR for values of γ_H above 2 - 3 dB. Since this is the dominant range of importance in TH applications, optimal devices (albeit complex) should attract due attention.

---

[19] However, this margin will probably disappear if the loss due to asynchronism is accounted for in an asynchronous, noncoherent, optimal detector.
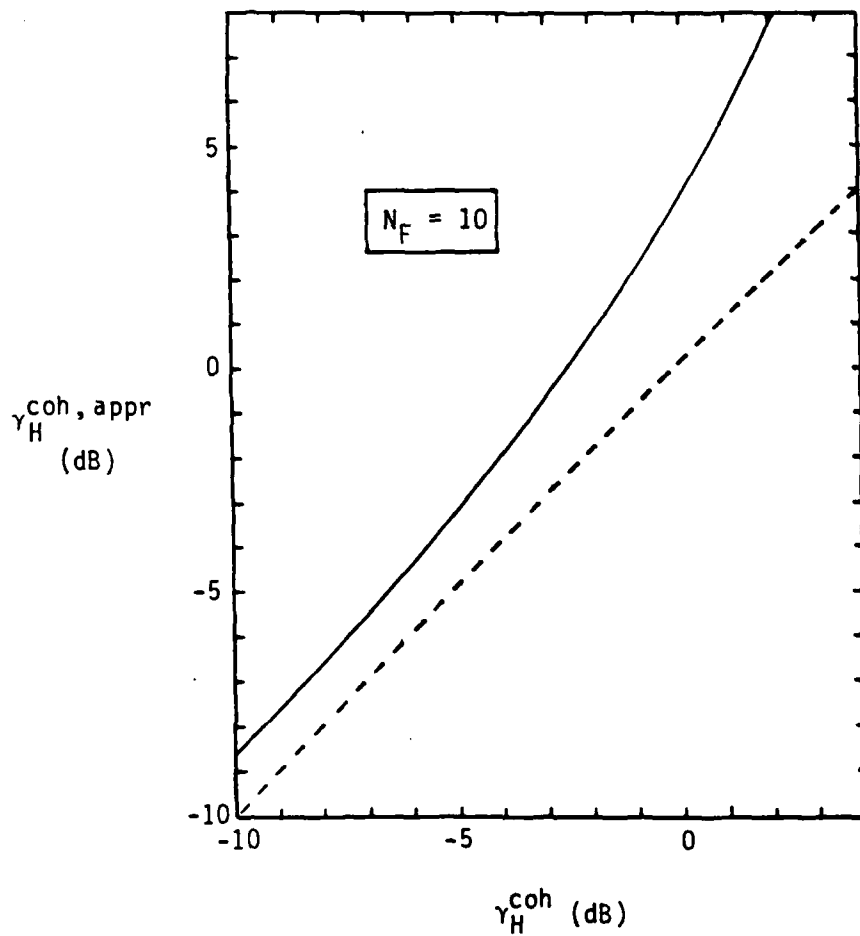
Figure 14. Comparison of the Exact (4.2) versus the Approximate (4.5) Coherent Time-Hopping Rules in Terms of Slot SNR's

72
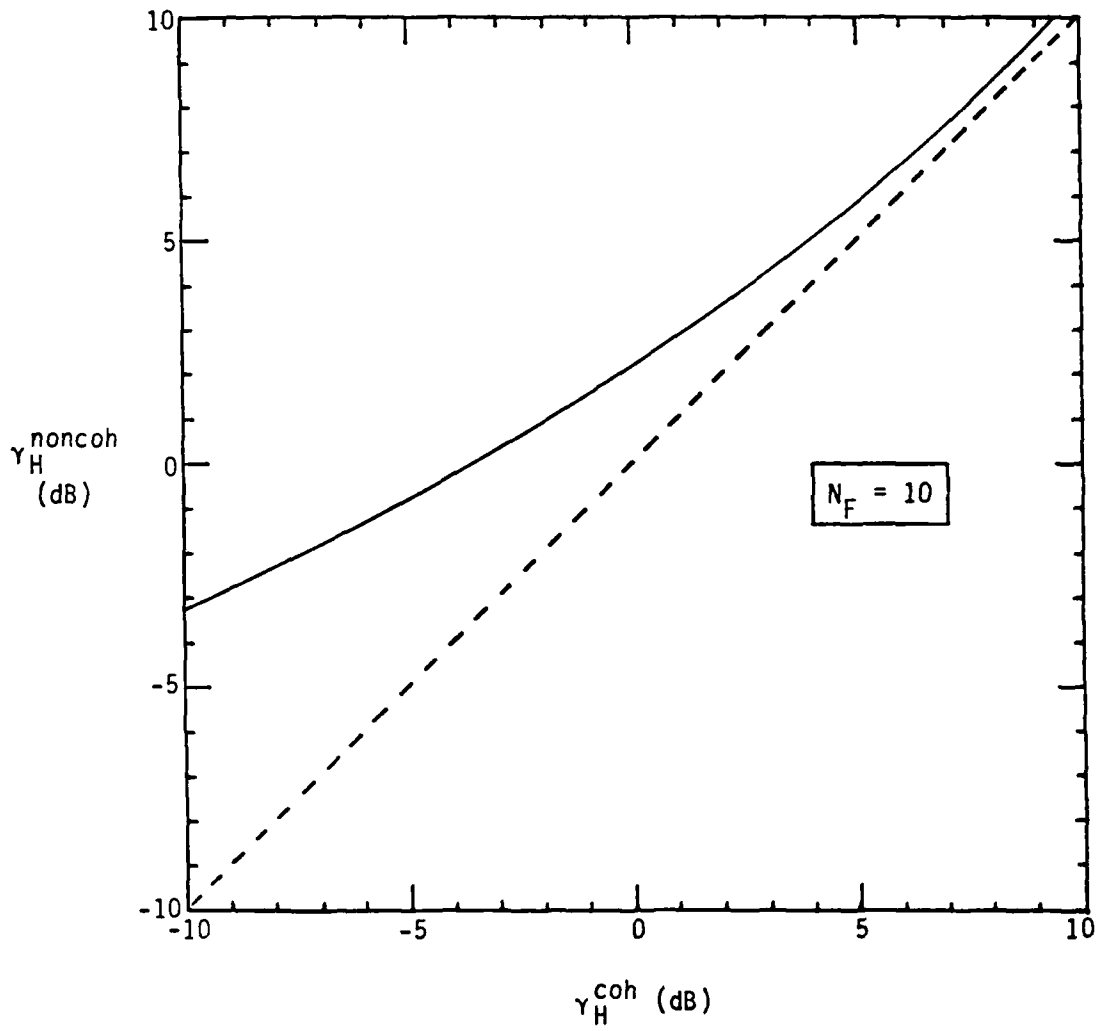
Figure 15 . Comparison of the Coherent (4·2) versus the Noncoherent (4.10)
Time-Hopping Rules in Terms of Slot SNR's
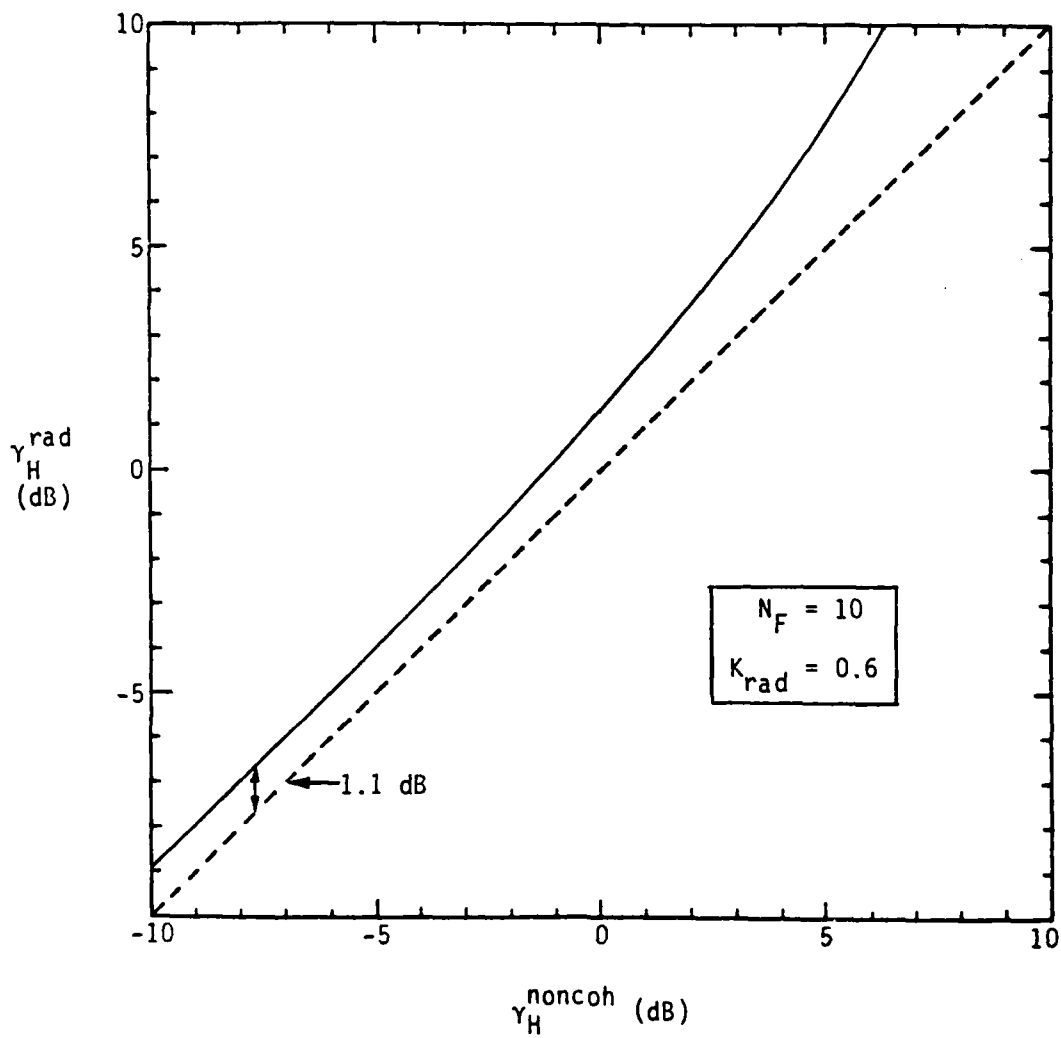
Figure 16. Comparison of the Noncoherent Rule (4.10) versus the Radiometer

So far a multitude of optimal and suboptimal receiver structures for the wideband detection of DS and TH waveforms in AWGN were derived and evaluated in this report. The starting points were those receivers resulting from the assumed knowledge of many pertinent parameters (except the codes themselves); upon gradual removal of these assumptions, a family of suboptimal structures emerge whose associated losses furthered them from the globally optimal performance towards the simple lower-bounding performance of the radiometer. It is generally concluded that the higher degree of sophistication and complexity for such detectors is more justifiable in the TH case than in DS, both because of the prevailing SNR values and the signal structure of TH versus DS.

5.0 FREQUENCY-HOPPING SIGNALS

For FH systems, the main challenge in implementing optimal receivers is the large number of hopping frequencies (as many as available by the FH system) that must be simultaneously observed and measured per hop before an optimal decision is reached. Contrary to that, the two systems considered previously utilize a single carrier frequency; stated differently, the instantaneous bandwidth[20] of those waveforms effectively comprises the overall spread-spectrum bandwidth. The implication is that any additional benefit (always with respect to the radiometer) brought about by the optimal detectors in the DS and TH cases must be extracted from the intelligent time-domain processing of the received waveform, rather than from increasing hardware complexity. In FH/LPI, however, we shall see that detection performance improves as the channelized width of the spectral observables decreases towards the optimal hopping-rate width which, of course, implies more filters.

The FH/LPI problems are mathematically formulated as detection of a complex sinusoid of unknown frequency in additive white Gaussian noise (AWGN). This is a problem common to diverse fields such as Doppler radar and sonar [22-26], spread spectrum communications [27-33], robust detection in the presence of signal perturbations ("slewing")[34], unknown colored noise [35], unknown signal spectrum [36-37], unknown bandwidth due to digital modulation [38] (see also [39] for some simulation results), etc. Unfortunately, the wide diversity of the underlying models precludes the extraction of firm, universal conclusions about the relative merit of the different techniques, either among themselves or with respect to the simplest hypothesis-discriminating device, namely the energy detector (radiometer). Here, we shall address the problem from a basic

---

[20]By this, we mean the bandwidth associated with the single chip pulse of the spreading code.

communications viewpoint, cautiously establishing the discrete-space detection model, and we shall subsequently explore a variety of possible approaches to its solution.

5.1 Waveform-Processing Alternatives

Let $s(t)$ be the FH signal to be detected solely in AWGN within a total spread bandwidth of W_s Hz. If $R_H \triangleq T_H^{-1}$ is the hopping rate and hopping frequencies are contiguous and equispaced by the minimum noncoherent orthogonal separation of $f = R_H$, it follows that the total number M of possible hopping locations is $M = W_s / R_H = W_s T_H$ -- typically, a very large number. Let the total observation time T be N_T hops, i.e., $T = N_T T_H$.

We restrict attention here to the broadband, AWGN case, which is the only observable waveform under hypothesis H_0:

$$r(t) = n(t); \; 0 \leq t \leq T \quad\quad (H_0) \quad\quad\quad\quad (5.1a)$$

If, under the alternative hypothesis H_1,

$$r(t) = s(t) + n(t); \; 0 \leq t \leq T \quad\quad (H_1) \quad\quad\quad\quad (5.1b)$$

the signal $s(t)$ is itself broadband ("white") and Gaussian, the energy detector is tantamount to the optimal likelihood ratio (LR) test

$$\Lambda(r(t)) = \frac{f(r(t)|H_1)}{f(r(t)|H_0)} \underset{H_0}{\overset{H_1}{\underset{<}{\gtrless}}} \text{threshold} \quad\quad\quad\quad (5.2)$$

When, however, the signal of interest is inherently narrowband, as is the case of interest here, it possesses sufficient structure so that parametric approaches warrant attention, whether optimal and theoretically justifiable or not.

Implementation of (5.2), or any variant thereof, over the total RF bandwidth W_s might result in unacceptable complexity. One way to alleviate the problem is shown in Figure 17 wherein the total bandwidth W_s is subdivided into large contiguous segments of
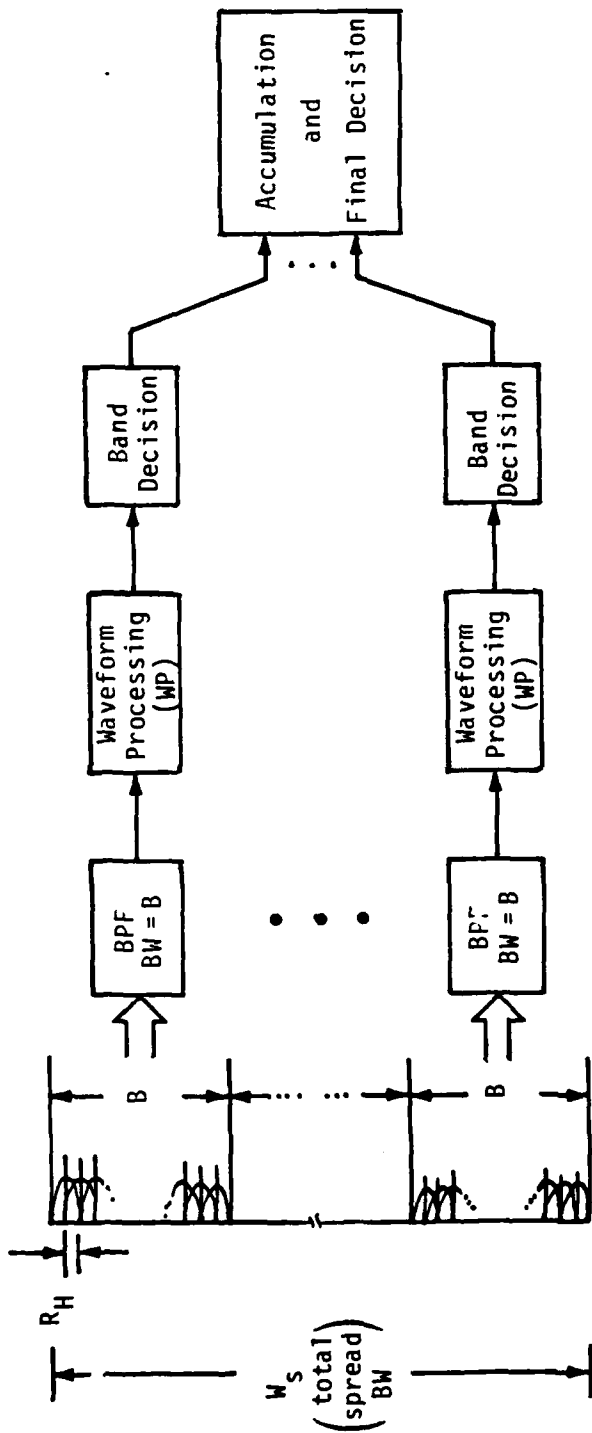
Figure 17. Suboptimal Processing: Segmenting W_s into B-Hz Bands $(B \gg R_H)$

B Hz, each being much larger than the optimal bandwidth of R_H Hz. Appropriate processing produces a per-band decision which is then fed into an overall accumulator (e.g., a majority-logic combiner) for a final decision (H_1 versus H_0). Let us note that alternate reduced configurations have also appeared in the literature [40,41], such as the partial-band filter-bank combiner. There, only a fraction of the total number M of the hopping slots is being observed, but the observation bandwidth per slot is optimal ($B=R_H$).

The focus of the following sections is on the waveform-processing (WP) aspect on a per-band basis. Clearly, algorithms that improve performance on that level will also increase the overall system performance. We shall assume throughout this development that the hop time-bandwidth product

$$G = B T_H = B/R_H \gg 1 \qquad (5.3)$$

is very large, i.e., of the order of hundreds or more. The factor G also measures the order of the reduction in complexity when implementing the suboptimal structure of Figure 17 instead of the optimal. As a consequence, the input SNR per band γ_{in}, defined as

$$\gamma_{in} \triangleq \frac{S}{N_0 B} \qquad (5.4)$$

is typically very small compared to unity ($\gamma_{in}, \ll 1$).

Now, two questions arise immediately:

(a) Into how many bands should the spectrum be divided?

(b) What kinds of WP alternatives are available or could be used?

With respect to (a), it is intuitively clear that one should use as many bands as the number of devices which can be afforded since, by decreasing B and thus increasing γ_{in} from (5.4), more reliable decisions on a per-band bases can be achieved; an elaborate cost-versus-payoff study is of significant interest in this area, but will not be pursued here. As for the second question, we note that the device which immediately comes to mind is the familiar radiometer, designed to measure energy in the band of B Hz. Under the Gaussian

assumption for the output-decision statistic (which is well justified for very large G via a central-limit-type argument), its performance is easily derived to be (see Sections 3.4, 4.3)

$$d_{\lambda,\text{rad}} = Q^{-1}[P_{FA}] - Q^{-1}[P_D] \triangleq \sqrt{\text{SNR}_{\text{out}}} \tag{5.5a}$$

$$\text{SNR}_{\text{out}} = \text{SNR}_{\text{out}}^{\text{rad}} = (N_T)\,\gamma^2_{\text{in}} \approx (N_T G)^{-1}\,\gamma^2_H \tag{5.5b}$$

(P_D, P_{FA}) are the detection and false alarm probabilities, respectively, and $Q^{-1}(x)$ is the inverse of the Gaussian integral function, and

$$\gamma_H \triangleq \frac{ST_H}{N_0} \tag{5.5c}$$

is the hop SNR. Note, that the second equality in (5.5b) signifies the small-signal suppression effect of square-law detectors [42, page 267]. We emphasize again the (P_D, P_{FA}) pertain to the per-band decision, not the overall scheme.

The radiometer solution is implementationally simple, but otherwise unacceptable in most cases from a performance viewpoint; we shall soon have a chance to establish this latter fact. Alternatively, more sophisticated approaches must be sought, and that is what the following sections are about, namely to establish and analyze families of advanced detection rules (waveform-processing schemes).

A major aspect of this detection problem is to choose the domain in which the decision algorithm is to operate, namely the spectral versus the correlation domain. Of course, by virtue of the Wiener-Kinchine theorem the two domains contain, in principle, the same amount of second-order information. However, how this information can be best exploited from a detection viewpoint, when a finite length data record is available and certain parameters in the signal and/or noise models are not completely known (in either a statistical or a deterministic sense), remains still a challenging question. It has prompted researchers to look beyond the traditional spectral approach (which is motivated mostly

81

from likelihood ratio considerations) into the correlation domain [43, 44, 26, 30-38]; the results reported exhibited a varying degree of success, depending on the assumptions made and the nature of the adopted decision rule. An added degree of motivation for the correlation domain comes from the recent advances in the technology of real-time, large time-bandwidth-product autocorrelation devices (see [45] and refs, therein).

5.2 Single-Hop, Spectral-Domain Algorithms

Now we shall explore single-hop algorithms ($N_T = 1$); in other words, the data record consists of single-hop $0 \leq t \leq T_H$ of a perfectly epoch-synchronized.signal. The results should give an indication of the relative merit of the different algorithms, their capabilities, complexity limitations, etc. Futhermore, we shall assume throughout this section a noncoherent environment, which is mostly dictated by practical considerations of the FH modulation.

Let us first consider algorithms in the spectral-domain. In order to motivate them, let us assume that the signal (under H_1) is just a sinusoid of known power S but unknown frequency f_s and phase θ; frequency f_s lies in an RF bandwidth of B Hz, centered at the known frequency f_c, i.e.

$$r(t) = \sqrt{2S} \cos(\omega_s t + \theta) + n(t) \qquad (H_1) \qquad\qquad (5.6)$$

where $|f_s - f_c| \leq B/2$ and $T_H \gg B^{-1}$, i.e. $G = BT_H \gg 1$. This situation is depicted in Figure 18. The one-sided noise power spectral density (PSD) N_0 W/Hz is also known. Under the broadband asssumption for the noise and modeling the unknown frequency f_s as a random variable, uniformly distributed in ($f_c - B/2$, $f_c + B/2$), leads to the optimal LR test

$$\Lambda(r(t)) = \mathscr{E}_{f_s}\{\Lambda(r(t)|f_s)\}$$

$$= \frac{\exp\left\{-\dfrac{ST}{N_0}\right\}}{B} \int_{f_c - B/2}^{f_c + B/2} I_0\left(\frac{2\sqrt{S}}{N_0}\, R(f_s)\right) df_s \underset{H_0}{\overset{H_1}{\gtrless}} \text{threshold} \qquad (5.7a)$$

where $I_0(\cdot)$ is the zero[th]-order Bessel function, $\mathscr{E}\{\cdot\}$ stands for expectation and $R(f_s)$ is the real envelope at frequency f_s,

83
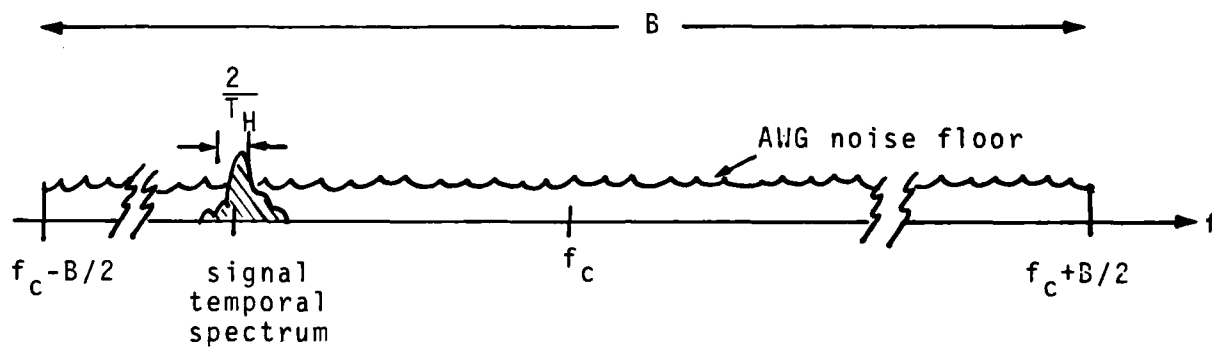
Figure 18   A pictorial representation of the RF spectrum
around center frequency f_c under H_1 (signal present).

$$R(f_s) = \sqrt{R_I^2(f_s) + R_Q^2(f_s)} \qquad (5.7b)$$

with

$$R_I(f_s) = \sqrt{2} \int_0^T r(t) \cos 2\pi f_s t \ dt \qquad (5.7c)$$

$$R_Q(f_s) = \sqrt{2} \int_0^T r(t) \sin 2\pi f_s t \ dt \qquad (5.7d)$$

the inphase and quadrature components, respectively. This optimal rule(5.7a) averages the nonlinear transformations of the envelopes at all frequencies in the band. This being overly demanding to implement, one discretizes the frequency uncertainty region in $G = B/(T^{-1})$ candidates f_m; $m = 0,...,G - 1$, spaced T_H^{-1} Hz apart, and approximates (5.7a) as

$$\Lambda = \frac{\exp\{-\gamma_H\}}{G} \sum_{m=0}^{G-1} I_0\left(\frac{2\sqrt{S}}{N_0} R(f_m)\right) \underset{H_0}{\overset{H_1}{\underset{<}{\overset{>}{\gtrless}}}} \text{threshold} \qquad (5.8)$$

with $R(f_m)$ as per (5.7). The set of $2G = 2BT_H$ orthogonal function $\{\sin \omega_m t, \cos \omega_m t\}_{m=0}^{G-1}$ can be approximately interpreted as a predominant set of eigenfunctions of the broadband noise with a rectangular spectrum [12]. Note, that if the candidate hopping frequencies were known exactly _a priori_, rule (5.8) could be derived directly from rule (4.9), (with $Q = 1$) by exploiting the duality between TH and FH. In fact, both spreading techniques belong to a larger class of orthogonal signal sets.

From a theoretical standpoint, any mechanism which provides reliable envelope estimates[21] $|R_m| = R(f_m)$ or, equivalently, spectral estimates $S_m = |R_m|^2$; $m = 0,...,G-1$ can

---

[21]Since both real and complex quantities will be encountered in the sequel, the symbol "n" will denote a complex number, while $|\cdot|$ will stand for the complex norm: Plain letters refer to the real counterparts.

be coupled with the aforementioned LR-type test or any other approximations thereof. Possible choices include the aforementioned quadrature analog implementation (5.7b)-(5.7d) a bank of narrowband filters, chirp-transform (SAWD) devices [45] or a complex FFT operating on the baseband complex envelope $\tilde{r}(t)$ of the real bandpass observation $r(t)$:

$$\tilde{r}(t) = r(t) \exp(-j2\pi f_c t)|_{LP} \tag{5.9a}$$

$$\tilde{r}_k \triangleq \tilde{r}(kB^{-1}); \quad k=0,\ldots,G-1 \tag{5.9b}$$

$$\{\tilde{R}_m\}_{m=0}^{G-1} = FFT\{\tilde{r}_k\}_{k=0}^{G-1} \tag{5.9c}$$

$$S_m = |\tilde{R}_m|^2; \quad m=0,\ldots,G-1 \tag{5.9d}$$

As indicated, this requires sampling the baseband complex signal $\tilde{r}(t)$ at the Nyquist rate of B complex samples/sec, and is based on the fact that $r(t)$ and $\tilde{r}(t)$ possess identical spectral envelopes, as per (5.9d). The information loss incurred in the sampling operation (5.9b) is negligible for large G; furthermore, denser spectral sampling can be obtained by padding $\{r_k\}$ with an appropriate number of zeros, although such is not required for implementing (5.8). Issues associated with the standard generation of the "periodogram" (5.9d) such as data windowing, segmentation (Welch method), etc. have been studied extensively in the context of spectral estimation (see, for instance, [46] and refs therein) and will not be discussed here any further.

Let us now return to the performance of rule (5.8). It is clear from the above problem formulation that, for G large, the LR statistic, Λ of (5.8) should be modeled as Gaussian (under a central-limit-theorem type of argument) which, in turn, negates the

modeling assumption of a Gaussian LLR ℓ. As a result, the more traditional measure d_ℓ is not applicable; instead a "Gaussian" measure d_Λ must be derived and employed.

Let us define d_Λ via the standard expression (2.7)

$$d_\Lambda^2 \triangleq \frac{[\mathscr{E}\{\Lambda|H_1\} - \mathscr{E}\{\Lambda|H_0\}]^2}{\text{var}\{\Lambda|H_0\}}$$

Where $\mathscr{E}\{\Lambda|H_i\}$ is the expectation of Λ under hypothesis H_i; $i = 0,1$ and var $\{\Lambda|H_0\}$ is its variance under H_0. Let us further note that, under H_0, all G observables $\{R_m\}_{m=0}^{G-1}$ are just noisy envelopes, while under H_1 there is one "signal-plus-noise" envelope and (G-1) noisy ones (recall the orthogonality assumption). Thus, for large G, it is reasonable to assume that $\text{var}\{\Lambda|H_1\} \approx \text{var}\{\Lambda|H_0\}$, which reinforces the utility of d_Λ^2 as a reliable distance measure between the two (approximately Gaussian) distributions of Λ under either hypothesis.

It is straightforward to show that (see also Appendix H)

$$\mathscr{E}\left\{I_0\left(\frac{2\sqrt{S}}{N_0}R\right)\right\} = \begin{cases} e^{\gamma_H} & \text{;noise only} \\ e^{\gamma_H}I_0(2\gamma_H) & \text{;signal-plus-noise} \end{cases} \tag{5.10a}$$

$$\mathscr{E}\left\{I_0^2\left(\frac{2\sqrt{S}}{N_0}R\right)\right\} = e^{2\gamma_H}I_0(2\gamma_H) \text{ ; noise only} \tag{5.10b}$$

so that

87

$$\text{var}\{I_0 \ (\frac{2\sqrt{S}}{N_0} \ R)|H_0\} = e^{2\gamma_H}(I_0(2\gamma_H)-1)$$

(5.10c)

where γ_H is the hop-SNR as per (5.5c). Thus,

$$\mathscr{E}\{\Lambda|H_1\} = (G-1) \ e^{\gamma_H} + e^{\gamma_H}I_0(2\gamma_H)$$

(5.11a)

$$\mathscr{E}\{\Lambda|H_0\} = G \cdot e^{\gamma_H}$$

(5.11b)

Combining the above and the independence assumption between observables we conclude that

$$d_\Lambda^2 = G^{-1}[I_0(2\gamma_H)-1]$$

(5.12)

Equation (5.12) will be used for evaluating the performance of decision rule (5.8) under the assumption that the signal does indeed come on one of the candidate frequencies (no frequency offset); we term this Case I. Clearly, the same rule can be employed, neglecting the fact that there can be an offset. Use of (5.3) under the assumption of a worst-case frequency offset $\Delta f = R_H/2$, i.e. the signal arriving amidst two candidates is termed Case II.

Two more cases arise from the possibility of adjusting the power factor S in (5.8) by a coefficient $\alpha < 1$, which accounts for the power loss on the signal measurement due to worst-case offset:

$$\alpha = \left(\frac{\sin \pi(\Delta f)T_H}{\pi(\Delta f)T_H}\right)^2 = \left[\frac{\sin \frac{\pi(R_H T_H)}{2}}{\frac{\pi R_H T_H}{2}}\right]^2$$

(5.13a)

or

88

$$\alpha = \left(\tfrac{2}{\pi}\right)^2 = -3.9 \ dB \tag{5.13b}$$

Thus, Case III refers to the power-adjusted rule (5.14)

$$\sum_{m=0}^{G-1} I_0 \left(\frac{2\sqrt{\alpha S}}{N_0} \ R_m \right) \underset{H_0}{\overset{H_1}{\gtrless}} \ threshold \tag{5.14}$$

when there actually is an offset $\Delta f = R_H/2$, while Case IV refers to the adjusted rule(5.13) when there actually is not an offset ($\Delta f = 0$). All four cases are summarized in Table 1, along with their defining features (first four columns). The last column lists the associated distances, in analogy to (5.12). To illustrate the steps involved, Case II is analyzed more thoroughly in Appendix I; the other two involve similar calculations.

Let us note here that the amplitude adjustment in (5.13) is only a partial, ad-hoc remedy towards the frequency-misalignment problem: an exact approach should account for the fact that, whenever $\Delta f = R_H/2$, two adjacent spectral slots simultaneously receive significant signal power (albeit reduced α) and should proceed to construct the LR from there. However, the resulting "optimal rule" is overly complex and not measurably better than the alternatives examined herein.

The optimal rule (5.8) might be overly demanding to implement. An alternative and popular rule is the spectral-maximum detector, which selects the maximum from the envelope observables $R_m = |\tilde{R}_m|$ and compares it to a threshold [25, 26, 34, 39, etc.]

Table 1. Definitions and Distance Results for the 4 Cases Examined

Case	Rule	Power Adjusted by α	Actual Offset Δf	Mismatch between Rule and Reality	Distance d_Λ^2
I	(2)	No	Zero	No	$G^{-1}[I_0(2\gamma_H)-1]$
II	(2)	No	$R_H/2$	Yes	$4G^{-1}\left[\dfrac{(I_0(2\sqrt{\alpha}\gamma_H)-1)^2}{I_0(2\gamma_H)-1}\right]$
III	(8)	yes	$R_H/2$	No	$4G^{-1}[I_0(2\alpha\gamma_H)-1]$
IV	(8)	yes	Zero	Yes	$G^{-1}\left[\dfrac{(I_0(2\sqrt{\alpha}\gamma_H)-1)^2}{I_0(2\alpha\gamma_H)-1}\right]$

$$\max_m \quad R_{,m} \quad \underset{H_0}{\overset{H_1}{\underset{<}{\gtrless}}} \quad \text{threshold; } m = 0,...,G-1 \tag{5.15}$$

Rule (5.15) affords a generalized-likelihood-ratio tests [12] interpretation: If the narrowband (hop) SNR $\gamma_H = ST_H/N_0$ is large, the spectral observable corresponding to the signal location can be expected to rise well above the noise floor and be the maximum with high probability; thus, it can serve both as a frequency estimator, as well as a detection statistic for a now narrowband (matched filter) hypothesis testing. The performance associated with (5.15) can be determined exactly (i.e., no distance need be evaluated) by noting that rule (5.15) is exactly equivalent to the rule

$$\left\{ \begin{array}{ll} \text{if all } R_m < T_{max} \quad , & \text{decide } H_0 \\ \text{if at least one } R_m \geq T_{max} \quad , \text{decide } H_1 \end{array} \right\} \tag{5.16}$$

which involves the comparison of each R_m; $m = 0,...,G-1$ with the same threshold T_{max}. Let P_{fa} denote the <u>slot false alarm</u> probability

$$P_{fa} \triangleq \text{prob} \left\{ R_m > T_{max} \middle| \begin{array}{l} \text{signal absent} \\ \text{in slot } m \end{array} \right\} \tag{5.17a}$$

and P_d denote the <u>slot detection</u> probability

$$P_d \triangleq \text{Prob} \left\{ R_m > T_{max} \middle| \begin{array}{l} \text{signal} \\ \text{in slot } m \end{array} \right\} \tag{5.17b}$$

The slot probabilities (P_d, P_{fa}) are then related to the DOC (system) probabilities (P_D, P_{FA}) via

$$P_{FA} = 1-(1-P_{fa})^G \tag{5.18}$$

91

$$P_D = 1-(1 - P_d)(1-P_{fa})^{G-1} \quad \text{(no offset)} \tag{5.19a}$$

where it is assumed that only one slot contains the signal under H_1 (no frequency offset). If, on the other hand, a worst-case offset is assumed, (5.19a) is modified to

$$P_D = 1-(1-P_{d;\,\alpha})^2(1-P_{fa})^{G-2} \quad \text{(worst offset)} \tag{5.19b}$$

where the notation $P_{d;\alpha}$ is adopted to indicate the signal-power loss by α (i.e., a hop SNR of $\alpha\gamma_H$).

The slot probabilities of eq. (5.17) are related through the standard Marcum's Q function [15, 16]

$$Q(a,\beta) = \int_{\beta}^{\infty} r e^{-\frac{r^2+a^2}{2}} I_0(ar)\,dr \tag{5.20}$$

as

$$P_d = Q\left[\sqrt{2\gamma_H}\,,\,\sqrt{2\ln P_{fa}^{-1}}\right] \tag{5.21}$$

Equations (5.18)-(5.21) can be used to relate P_{FA} and P_D directly: from (5.18) it follows that

$$P_{fa} = 1-(1 - P_{FA})^{1/G} \tag{5.22a}$$

wherefrom

92

$$(1-P_{f_a})^{G-1} = (1-P_{FA})^{\frac{G-1}{G}} \tilde{=} 1-P_{FA} \tag{5.22b}$$

since $G \gg 1$. Thus, substituting (5.21), (5.22) into (5.19a) yields

$$P_D \underset{\text{(no offset)}}{\tilde{=}} 1-\left(1-P_{FA}\right)\left\{1-Q\left[\sqrt{2\gamma_H},\sqrt{2\ \ln\left[1-(1-P_{FA})^{1/G}\right]^{-1}}\ \right]\right\} \tag{5.23}$$

for no offset; the expression for worst-case offset induces minor changes as per (5.19b).

A satisfactory approximation to (5.23) can be derived when $G^{-1}P_{FA} \ll 1$ (the typical case of interest), since then

$$(1-P_{FA})^{1/G} \approx 1 - \frac{P_{FA}}{G}$$

which, upon substitution to (5.23 yields)

$$P_D \approx 1-\left(1-P_{FA}\right)\left[1-Q\left(\sqrt{2\gamma_H},\sqrt{2\ \ln\left(\frac{G}{P_{FA}}\right)}\right)\right] \tag{5.24}$$

Finally, if $P_{FA} \ll 1$, so that $1 - P_{FA} < 1$, a tight lower bound to (5.24) is

$$P_D \gtrsim Q\left[\sqrt{2\gamma_H},\sqrt{2\ \ln\frac{G}{P_{FA}}}\ \right] \tag{5.25}$$

93

Approximation (5.25) is identical to the performance of a narrowband (known frequency) noncoherent detector, whose slot false alarm probability P_{fa} is G^{-1} times the overall system (broadband) false alarm probability P_{FA}.(compare with (5.21)). In other words, if γ_H is sufficiently high so that the overall detection probability is primarily due to the slot containing the signal (i.e. $P_d \approx P_D$) and G is, say, 10^3, then in order to have the overall $P_{FA} = 10^{-3}$ we must have $P_{fa} \approx 10^{-6}$ per slot.

As mentioned, all detection schemes can be compared to the lower-bounding performance of the radiometer

$$\int_0^T r^2(t)dt = (\frac{1}{2}) \int_0^T |\tilde{r}(t)|^2 dt \underset{H_0}{\overset{H_1}{\gtrless}} \text{threshold}$$

(5.26a)

or in a discrete-time version,

$$\sum_{k=0}^{G-1} |\tilde{r}_k|^2 = \frac{1}{G} \sum_{n=0}^{G-1} |\tilde{R}_n|^2 \underset{H_0}{\overset{H_1}{\gtrless}} \text{threshold}$$

(5.26b)

Whose lower-bounding performance is given by (5.5) with $N_T = 1$. For the wideband case of interest, radiometric methods become progressively more inadequate as G increases. Note, that as the slot SNR $\gamma_H \to 0$, then $I_0(x) \approx 1 + \frac{x^4}{4}$ and the decision rule (5.8) becomes the radiometer (5.26b).

The spectral detection problem presented so far can be summarized as follows: Given the complex baseband envelope $r(t)$; $0 \le t \le T$, of an unknown-frequency sinusoid in complex additive Gaussian noise, approximately white, bandwidth $B \gg T^{-1}$,

94

$$\tilde{r}(t) = \sqrt{2} \, [\sqrt{S} \, e^{j\Delta\omega t} + n_I(t) + jn_Q(t)]; \quad |\Delta\omega| \triangleq |\omega_s - \omega_c| \le B/2,$$
$$0 \le t \le T$$

$$(5.27a)$$

or its sampled version

$$\tilde{r}_k = \sqrt{2} \, [\sqrt{S} \, e^{j(\frac{\Delta\omega}{B})k} + n_I(\frac{k}{B}) + jn_Q(\frac{k}{B})]; \quad k = 0, \ldots, G-1$$

$$(5.27b)$$

under H_1, and noise only under H_0, create a set of spectral estimates $|\tilde{R}_m|^2; \, m = 1, \ldots, G$ and use them in conjunction with any one of the rules (5.8), (5.15) or (5.26) to obtain a binary decision (H_0 vs. H_1). These spectral estimates can be created by any judicious mechanism. A particularly attractive class of such novel spectral estimators is based on autoregressive (AR) models [46]. Those could be employed to produce the desired spectral observables in an efficient manner, according to the formula[22]

$$|\tilde{R}_n|^2 = \left. \frac{1}{\left| 1 + \sum_{m=1}^{M} \hat{a}_{M,m} \, e^{-j\omega m} \right|^2} \right|_{\omega = 2\pi f_n} \qquad n = 1, \ldots, G$$

$$(5.28)$$

Here, M is the order of the adopted AR model and $\hat{a}_m; \, m = 1, \ldots, M$ are the estimated coefficients derived from a nonlinear operation on the raw data $\tilde{r}_k$ of (5.9b) and/or a weighted (filtered) version of the linear prediction residuals [47]. Note, that for the AR spectrum, it is the area under a peak which actually reflects the power of the corresponding harmonic component.

---

[22]This is the AR spectrum normalized by the estimated variance of the linear prediction errors.

The question of identifying good spectral generators from a detection viewpoint, of which the FFT and AR models of (5.9c) and (2.28) are two examples, is indeed quite open and therefore exciting in its own merit. This is particularly so, because most of the efforts in the literature address the improvement of spectral estimators (in terms of bias, resolution, smoothness, line-splitting, sidelobe behavior, etc.), which says nothing of their detection capability. Here, however, we leave that question aside and proceed to examine decision rules which do not explicitly utilize spectral information; instead, these rules operate directly on data from the correlation domain, thus constituting the field of correlation detection.

96

5.3 Single Hop, Correlation Domain Algorithms in AWGN

Let the finite-record sample correlation function [23] be

$$y(\tau) = \int_\tau^{T_H} r(t)r(t-\tau)dt; \quad 0 \le \tau \le T_H \tag{5.29}$$

where $r(t)$ is as per (5.1) or, more specifically, (5.6). Since $r(t)$ is a BP process, so is $y(\tau)$. Combining (5.6), (5.29) and rejecting double-frequency terms leads to the complex envelope $\tilde{y}(\tau)$ of $y(\tau)$ as

$$\tilde{y}(\tau) = \frac{1}{2} \int_\tau^T \tilde{r}(t)\tilde{r}^*(t-\tau)dt \tag{5.30}$$

where "*" means "complex conjugate." Sampled every B^{-1} sec, (5.30) yields

$$\tilde{y}_k \triangleq \tilde{y}(kB^{-1}) = \frac{1}{2} \int_{k/B}^{T_H} \tilde{r}(t)\tilde{r}^*(t-kB^{-1})dt; \quad k=0,...,G-1 \tag{5.31a}$$

Furthermore, if the integral in (5.31) is approximated by a finite sum in terms of samples $\tilde{r}_k$ of $\tilde{r}(t)$, we arrive at the biased estimates of the correlation sequence

$$\tilde{y}_k = (\frac{1}{2B}) \sum_{\ell=k}^{G-1} \tilde{r}_\ell \tilde{r}^*_{\ell-k} \quad : \quad k=0,\ldots,G-1 \tag{5.31b}$$

which could have also been derived by direct quadrature demodulation of $r(t)$ and complex sampling of the resulting $\tilde{r}(t)$; whether this approach is preferable to the sequence (5.29)-

---

[23]From now on, the term "sample" will be omitted; "correlation" will always pertain to time averaging, not ensemble averaging.

(5.31) is a matter of implementational convenience. From a constant-false-alarm-rate (CFAR) viewpoint, it is typically advantageous to use the normalized correlation observables

$$\tilde{\rho}_k \triangleq \frac{\tilde{y}_k}{\tilde{y}_0} = \frac{\sum_{\ell=k}^{G-1} \tilde{r}_\ell \tilde{r}_{\ell-k}^*}{\sum_{\ell=0}^{G-1} |\tilde{r}_\ell|^2} \quad ; \quad k=0,\dots,G-1$$

(5.32)

It is well known that, within a constant, the sequence $\{\tilde{y}_k\}_{k=0}^{G-1}$ and the periodogram $\{|\tilde{R}_m|^2\}_{m=0}^{G-1}$ are Discrete Fourier Transform (DFT) pairs. Thus, given (5.31), a DFT operation would allow the application of the spectral algorithms discussed in Section 5.2. However, it is possible to find meaningful detection statistics in terms of the $\tilde{y}_k$'s without an explicit evaluation of the spectrum. In other words, we can state the following (single-hop) correlation-detection problem: Based on the sequence $\{y_k\}_0^{G-1}$ of (5.31) or equivalently, on the set $[\tilde{y}_0, \{\tilde{\rho}_k\}_0^{G-1}]$ of (5.32), formulate a detection statistic without explicit evaluation of the spectrum $\{|R_m|^2\}_{m=0}^{G-1}$.

Simple examples of ad-hoc detector choices proposed in the past are the "Semicoherent Detection Statistical Test"

$$|\tilde{y}_k| \underset{H_0}{\overset{H_1}{\gtrless}} \text{threshold.} \qquad \text{(for some k)} \qquad (5.33)$$

in a radar environment (see [26]), the RF correlation statistic.

$$Y = \sum_{k=1}^{\lambda G} d_k \, |\tilde{y}_k|^2 \underset{H_0}{\overset{H_1}{\gtrless}} \text{threshold} \qquad (5.34)$$

of [32], with $0 < \lambda \le 1$ and $\{a_k\}_{k=1}^{\lambda G}$ an appropriate set of coefficients, the statistic $|\tilde{\rho}_1|^2$ of [34], etc. Some more advanced choices will be discussed later in this section. For the time

98

being let us concentrate on the analysis of (5.34), whereupon it will be shown that significant gains can result with respect to the radiometer. Let us note that the zero[th] term $|\tilde{y}_0|^2$, which is in fact the radiometric output, could have been included in (3.54) with a marginal improvement in the detector's discriminatory power; on the other hand, this would make the detector much more sensitive to the (possibly fluctuating) noise variance and is, therefore, omitted.

Decision rule (5.34) can be rephrased in terms of the continuous-argument correlation function $y(\tau)$ of (5.29) as

$$Y = \sum_{k=1}^{\lambda G} a_k \; W_k \; \underset{H_0}{\overset{H_1}{\gtrless}} \; \text{threshold} \tag{5.35a}$$

where

$$W_k = y^2(\tau_k)|_{Lowpass} \qquad \tau_k = k \; B^{-1}$$

$$(k=1,...,\lambda G) \tag{5.35b}$$

by virtue of the fact that $y^2(\tau)|_{LP} = |y(\tau)|^2/2$. In other words, the complex baseband rule (5.34) can be reconfigured in terms of power measurements (around τ_k) on the real-time correlation output at an RF or IF frequency as shown in Figure 19. Again, whether the rule is actually implemented at RF or baseband in discrete continuous time,etc.,is a matter of practical convenience.

The set of coefficients $\{a_k\}_1^{G-1}$ can be chosen according to any particular philosophy and is subject to optimization. It can be shown that performance of the summation (5.35) is insensitive to the exact value of a_k's and a number of reasonable choices would work, as long as the upper limit of the summation is properly truncated at a level $S = \lambda G$, which is
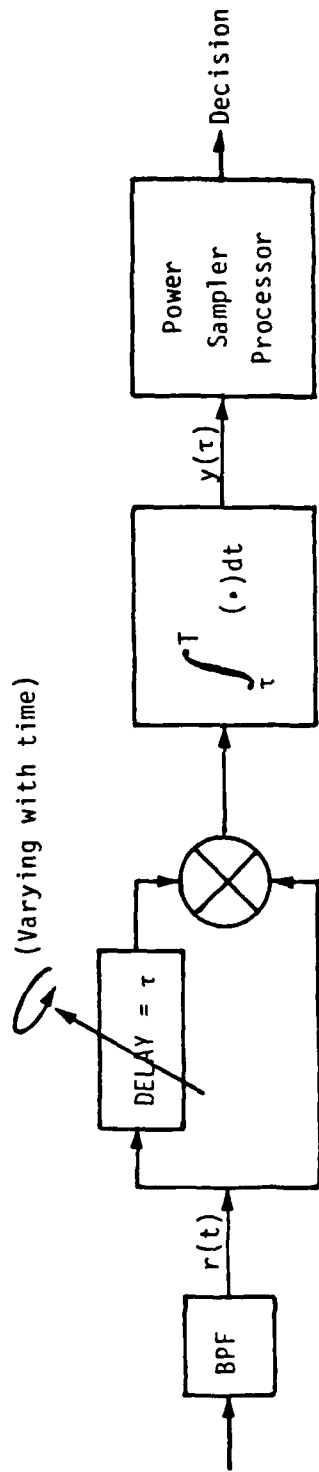
Figure 19. Mathematical Model of a Real-Time Autocorrelation Detector, Implemented in Continuous Time.

100

less than G (i.e., $\lambda < 1$). This is because the last samples possess such an increased variance that their inclusion in the summation is detrimental. Analytically, this is equivalent to letting $a_k = 0$ for $k = S + 1,...,G$. Thus, a proper choice of λ is rather crucial, while that of $\{a_k\}_{k=1}^{\lambda G}$ is not. For reasons that will soon be clear, it is mathematically convenient to let

$$a_k = \begin{cases} \left(T_H - \tau_k\right)^{-2} & ; \ k=1,\ldots,\lambda G \\ 0 & ; \ k=\lambda G+1,\ldots,G \end{cases}$$

(5.36)

in the following calculations. We note, that this set of a_k's, corresponding to the inverse of a triangular window on the correlation samples y_k of (5.31), is such that the latter samples become <u>unbiased</u> estimates of the true (ensemble) correlation function of the underlying discrete-time process[24] [46,48].

To pursue the analysis of (5.35), with $y(\tau)$ as per (5.29), let us assume that, under H_1, the input to the correlator $r(t)$ consists of a sinusoid $\sqrt{2S} \cos(\omega_c t + \theta)$, whose frequency coincides with the center frequency of the observed band, plus bandpass Gaussian noise with the standard quadrature expansion,

$$r(t) = \sqrt{2S} \cos(\omega_c t + \theta) + \sqrt{2} \left[n_I(t) \cos(\omega_c t + \theta) - n_Q(t) \sin \omega_c t + \theta \right]$$
$$0 \le t \le T_H \qquad\qquad (5.37)$$

In (5.37), $n_I(t)$ and $n_Q(t)$ are the inphase and quadrature lowpass noise processes, respectively, which are i.i.d., zero-mean, with a flat PSD of $N_0/2$ W/Hz and two-sided

---

[24]Such unbiased correlation estimates lead to power-spectral-density estimates which are not warranted to be non-negative, an undesirable feature in spectral estimation [46]. Yet, they are quite appropriate for our detection procedure (5.35), which further illuminates the aforementioned distinction between the detection and estimation goals.

bandwidth of B Hz each (total power per component = $N_0B/2$). The assumption about the signal's frequency is just mathematically convenient; it will be shown later that it does not alter the results in any way.(see the baseband complex formulation in Appendix K as well as the results of Section 5.4.

Filtering out double frequencies, the autocorrelator output $y(\tau)$ around the center frequency is

$$y(\tau) = \int_{\tau}^{T_H} r(t)r(t-\tau)dt = y_{SS}(\tau) + y_{SN}(\tau) + y_{NS}(\tau) + y_{NN}(\tau)$$

(5.38)

with

$$y_{SS}(\tau) = S(T_H-\tau) \cos \omega_c\tau \tag{5.39a}$$

$$y_{SN}(\tau) = \sqrt{S} \ (N_I^d(\tau) \cos \omega_c\tau + N_Q^d (\tau) \sin \omega_c\tau) \tag{5.39b}$$

$$y_{NS}(\tau) = \sqrt{S} \ (N_I(\tau) \cos \omega_c\tau - N_Q (\tau) \sin \omega_c\tau) \tag{5.39c}$$

$$y_{NN}(\tau) = (N_{II}(\tau) + N_{QQ}(\tau)) \cos \omega_c\tau + (N_{IQ}(\tau) - N_{QI}(\tau)) \sin \omega_c\tau \tag{5.39d}$$

where the correlation-domain noise processes have been introduced, i. e.,

$$N_{\begin{bmatrix}I\\Q\end{bmatrix}}^d(\tau) = \int_{\tau}^{T_H} n_{\begin{bmatrix}I\\Q\end{bmatrix}}(t-\tau)dt \tag{5.40a}$$

$$N_{\begin{bmatrix}I\\Q\end{bmatrix}}(\tau) = \int_{\tau}^{T_H} n_{\begin{bmatrix}I\\Q\end{bmatrix}}(t)dt \tag{5.40b}$$

$$N_{II}(\tau) = \int_{\tau}^{T_H} n_I(t) \ n_I(t-\tau)dt \tag{5.40c}$$

$$N_{QQ}(\tau) = \int_\tau^{T_H} n_Q(t)\, n_Q(t-\tau)dt \tag{5.40d}$$

$$N_{IQ}(\tau) = \int_\tau^{T_H} n_I(t)\, n_Q(t-\tau)dt \tag{5.40e}$$

$$N_{QI}(\tau) = \int_\tau^{T_H} n_Q(t)\, n_I(t-\tau)dt \tag{5.40f}$$

Much of the following analysis deals with the statistical characterization of the above noise processes. For instance, it is clear that the first four processes in (5.40a) and (5.40b) are zero mean and Gaussian, while the remaining are not Gaussian. However, they will be approximately treated as such in the analysis, particularly for $0 < \tau \ll T_H$, by virtue of the following central-limit-type argument: The bandwidth B of $n_I(t)$ and $n_Q(t)$ is much larger than T_H^{-1}; thus, each integral in (5.40c) through (5.40f) can be approximated by a large sum of noise-product samples, each sample taken B^{-1} seconds apart. Since we shall be interested in values of τ that are multiples of B^{-1}, it can be shown that those samples are mutually uncorrelated. Although this does not imply statistical independence (which is a prerequisite for a rigorous application of the central-limit theorem), it nonetheless reinforces the argument. This will permit us to calculate higher moments using Gaussian identities whose exact evaluation would otherwise be unwieldy. We furthermore note that simulation has confirmed the validity of the approximation (see Section 5.4)

The first point of interest is the mean value of $y(\tau)$ in (5.38). We shall assume that the input BP filter in Figure 19 has a perfectly rectangular transfer function ("brick wall"), which implies that the autocorrelation function $R_{nn}(\tau)$ for both $n_I(t)$ and $n_Q(t)$ is given by

$$R_{nn}(\tau) \triangleq \mathscr{E}\left\{n_I(t)n_I(t-\tau)\right\} = \mathscr{E}\left\{n_Q(t)n_Q(t-\tau)\right\} = \left(\frac{N_0 B}{2}\right)S_a(\pi B \tau) \tag{5.41}$$

where $S_a(x) \triangleq (\sin x)/x$. Using the fact that

$$\mathscr{E}\left\{N_I\right\} = \mathscr{E}\left\{N_I^d\right\} = \mathscr{E}\left\{N_Q\right\} = \mathscr{E}\left\{N_Q^d\right\} = \mathscr{E}\left\{N_{IQ}\right\} = \mathscr{E}\left\{N_{QI}\right\} = 0 \qquad (5.42a)$$

and

$$\mathscr{E}\{N_{II}(\tau)\} = \{N_{QQ}(\tau)\} = (T_H - \tau)R_{nn}(\tau), \qquad (5.42b)$$

we conclude from (5.38) through (5.40) that

$$\mathscr{E}\{y(\tau)\} = [S + (N_0 B) \, S_a(\pi B \tau)](T_H - \tau) \cos \omega_c \tau \qquad (5.43)$$

Certain interesting observations can be made on (5.43). First, although the quadrature component ($\sin \omega_c \tau$) has been eliminated, the mean $\mathscr{E}\{y(\tau)\}$ still includes an unknown oscillation [25]; that is why noncoherent (power) sampling must be performed at the signal-processing unit. Second, we note that the mean value at zero offset $\mathscr{E}\{y(0)\} = (S + N_0 B)T_H$ is just the average energy measured by the radiometer at the end of T_H second, as it should be. *Since we have assumed that $\gamma_{in} \ll 1$, implying that $S \ll N_0 B$,* it follows that the radiometer output is dominated by the noise contribution. Third, if the output $y(\tau)$ is power sampled at multiples of B^{-1}, i.e., $\tau_k = kB^{-1}$; k an integer, the contribution of the mean noise will be eliminated due to the nulls of the $S_a(x)$ function. This fact will be exploited in the following.

Let us return to (5.38) for a moment. Since we shall be interested in low-SNR case, we make the simplifying assumption that the "signal times noise" terms $y_{SN}(\tau)$ and $y_{NS}(\tau)$ are negligible compared to the "noise times noise" term $y_{NN}(\tau)$. For γ_{in} below -15 dB, or so, such a simplification is quite justified. Then, $y(\tau)$ can be expressed as

$$y(\tau) = C(\tau) \cos \omega_c \tau + N_I^{eq}(\tau) \cos \omega_c \tau + N_Q^{eq}(t)\sin \omega_c \tau \qquad (5.44)$$

---

[25]Recall that the signal's carrier frequency is truly unknown, randomly placed in the B-Hz band. It was modeled here to coincide with the known center frequency of the band just for analytical convenience.

where

$$C(\tau) = \begin{cases} S(T_H-\tau) & (H_1) \\ 0 & (H_0) \end{cases}$$

(5.45a)

is the envelope of the signal component and the equivalent noises are defined by

$$N_I^{eq}(\tau) \triangleq N_{II}(\tau) + N_{QQ}(\tau)$$

(5.45b)

and

$$N_Q^{eq}(\tau) \triangleq N_{IQ}(\tau) - N_{QI}(\tau)$$

(5.45c)

As mentioned, $y(\tau)$ will be power sampled at $\tau_k = kB^{-1}$; at which points,

$$\mathscr{E}\left\{N_I^{eq}(\tau_k)\right\} = \mathscr{E}\left\{N_Q^{eq}(\tau_k)\right\} = 0$$

(5.46)

According to our previous discussion, N_I^{eq} and N_Q^{eq} will be treated as Gaussian noises. Furthermore, it is shown in Appendix J that $N_I^{eq}(\tau_k)$ and $N_Q^{eq}(\tau_j)$ are uncorrelated for every $k,j = 1,...,G$; similarly, the pairs $\left(N_I^{eq}(\tau_{k_1}), N_I^{eq}(\tau_{k_2})\right)$ and $\left(N_Q^{eq}(\tau_{k_1}), N_Q^{eq}(\tau_{k_2})\right)$ are uncorrelated as long as $\tau_{k_1} \neq \tau_{k_2}$. Coupling this result with the approximate Gaussian assumption, it follows that the sequences of noise samples $\left\{N_I^{eq}(\tau_k)\right\}_{k=1}^G$ and $\left\{N_Q^{eq}(\tau_k)\right\}_{k=1}^G$ contain $2G$ Gaussian rv's which are zero mean and approximately independent. Thus, to complete their statistical description, the second moments (or variances, for this case) are required. Those are obtained in Appendix J, wherein it is shown that

$$\mathscr{E}\left\{\left(N_I^{eq}(\tau_k)\right)^2\right\} = \left(N_0B\right)^2\left(T_H-\tau_k\right)^2\left(F_1(k) + F_2(k)\right)$$

(5.47a)

and

$$\mathscr{E}\left\{\left(N_Q^{eq}(\tau_k)\right)^2\right\} = \left(N_0B\right)^2\left(T_H-\tau_k\right)^2\left(F_1(k) - F_2(k)\right)$$

(5.47b)

where

$$F_1(k) = \int_0^1 (1-\rho') \, S_a^2\left[\pi G(1 - \zeta_k)\rho'\right] d\rho' \tag{5.48a}$$

$$F_2(k) = \int_0^1 (1-\rho') S_a\left[\pi G\left((1 - \zeta_k)\rho' + \zeta_k\right)\right] S_a\left[\pi G\left((1-\zeta_k)\rho' - \zeta_k\right)\right] d\rho' \tag{5.48b}$$

and the normalized parameter ζ_k is defined as

$$\zeta_k \overset{\Delta}{=} \frac{\tau_k}{T_H} = \frac{k}{BT_H} = \frac{k}{G} \; ; \; k=1,\ldots,G-1 \tag{5.48c}$$

so that $0 < \zeta_k < 1$. Some meditation on the functional form of $F_2(k)$ reveals that it has a negligible contribution compared to $F_1(k)$, so it will henceforth be dropped. From (5.47), we then have that

$$\sigma_N^2(k) \overset{\Delta}{=} \mathscr{E}\left\{\left(N_I^{eq}(\tau_k)\right)^2\right\} \approx \mathscr{E}\left\{\left(N_Q^{eq}(\tau_k)\right)^2\right\}$$

$$\approx (N_0 B)^2 (T_H-\tau_k)^2 \, F_1(k) = (N_0 BT_H)^2 (1 - \zeta_k)^2 \, F_1(k) \tag{5.49}$$

which is a fairly simple expression, but also fundamental for the following. In deriving the above, it was assumed that (a) timing epoch is known, e.g., under H_1, the signal occupies exactly the observation period and, (b) the input BP filter is a rectangular one with bandwidth B. The first assumption can be removed with some SNR loss, while the

106

second is only analytically convenient; the results can easily be modified to account for any actual filter shape.

Let us now return to the noncoherent sampling indicated by (3.35b). Such sampling can be implemented via a square-law device, followed by a wideband lowpass filter; its bandwidth should be several times B, but still much narrower than twice the carrier frequency. Again, neglecting "signal x noise terms"[26], we have from (5.44) and (5.45a) that

$$W_k = (ST_H)^2(1 - \xi_k)^2 + \left(N_I^{eq}(\tau_k)\right)^2 + \left(N_Q^{eq}(\tau_k)\right)^2; k=1,\ldots,G-1$$

(5.50)

By virtue of the approximate statistical independence of the second and third noise terms in (22), $\{Wk\}_{k=1}^{G-1}$ is a sequence of approximately independent noisy samples, upon which

the decision is based. As mentioned, this valuable property of independence gradually diminishes as $k \rightarrow G-1$ because the fundamental assumption in assessing it (i.e., Gaussian equivalent noise) weakens toward the end; this is also why those latest samples should be ignored. Nonetheless, such a property is the key factor in the anticipated superiority of the correlator versus the radiometer -- namely, the fact that additional data can be exploited by incorporating all these new samples in the decision. Their approximate independence prevents these samples from being statistically useless.

In order to proceed with the evaluation of rule (3.35), we need the mean and variance of the W_k's. From (5.47) and (5.50), we have that the difference of the means under the two hypotheses, $\Delta\mathscr{E}\{W_k\}$, is given by

$$\Delta\mathscr{E}\{W_k\} \overset{\Delta}{=} \mathscr{E}\{W_k|H_1\} - \mathscr{E}\{W_k|H_0\} = (ST_H)^2(1-\zeta_k)^2$$

(5.51)

---

[26]A more exact analysis is provided in the discrete-time model of Section 5.4 without any significant deviation in the results.

107

Furthermore, using the independence between $N_I^{eq}(\tau_k)$ and $N_Q^{eq}(\tau_k)$ along with the Gaussian assumption yields the variance as

$$\text{var}\{W_k\} = 2\text{var}\left\{\left(N_I^{eq}(\tau_k)\right)^2\right\} = 2\left[\mathscr{E}\left\{\left(N_I^{eq}(\tau_k)\right)^4\right\} - \mathscr{E}^2\left\{\left(N_I^{eq}(\tau_k)\right)^2\right\}\right]$$

$$= 2\left[3\sigma_N^4(k) - \sigma_N^4(k)\right] = \left(2\sigma_N^2(k)\right)^2 \qquad (5.52)$$

with σ_N^2 as per (5.49).

As seen in (5.51), (5.52) and (5.49), the quantities of interest for W_k include a multiplicative factor $(1- \zeta_k)^2$, a reflection of the fact that the integration time reduces proportionally to τ_k as $\tau_k \to T_H$. Insertion of the coefficients a_k in (5.36) purported to remove this factor without essentially altering the results. Thus, if we define

$$W_k' \triangleq \frac{W_k}{(T_H - \tau_k)^2} = \frac{W_k}{T_H^2(1 - \zeta_k)^2}$$

$$(5.53)$$

it follows from (5.51) and (5.52) that

$$\Delta \mathscr{E}\{W'_k\} = S^2 \qquad (5.54a)$$

and

$$\text{var}\{W_k'\} = 4(N_0 B)^4 F_1^2(k) \qquad (5.54b)$$

while the decision rule (5.35a) reads:

$$Y = \sum_{k=1}^{\lambda G} W_k'$$

$$(5.55)$$

If we now define the output SNR for the correlator in the familiar way

$$SNR_{out}^{corr} \triangleq d_Y^2 = \frac{(\epsilon\{Y|H_1\} - \epsilon\{Y|H_0\})^2}{var\{Y|H_0\}}$$

(5.56)

then, using the uncorrelatedness of each W_k, we conclude that

$$SNR_{out}^{corr} = \frac{(\lambda GS^2)^2}{4(N_0B)^4 \sum_{k=1}^{\lambda G} F_1^2(k)} = \frac{\lambda^2 G^2}{4 \sum_{k=1}^{\lambda G} F_1^2(k)} \cdot \gamma_{in}^4$$

(5.57a)

or, using the fact that $\gamma_H = G \cdot \gamma_{in}$,

$$SNR_{out}^{corr} = A(\lambda,G) \, G^{-1} \cdot \gamma_H^4$$

(5.57b)

where the coefficient $A(\lambda, G)$ is defined as

$$A(\lambda,G) \triangleq \frac{\lambda^2}{4G \sum_{k=1}^{\lambda G} F_1^2(k)}$$

(5.57c)

Equations (5.5b) and (5.7b) can be combined into a ratio

109

$$\frac{SNR_{out}^{corr}}{SNR_{out}^{rad}} = A(\lambda,G) \cdot \gamma_H^2 \qquad (5.58)$$

The interpretation of (5.58) is that, within the framework of performance established herein, the correlator will outperform the radiometer if the product $A(\lambda,G) \cdot \gamma_H^2$ is above unity and vice versa. We note that this product signifies some kind of utility factor and is separated into two components: (a) $A(\lambda,G)$, depends on features of the device used (G) and the signal-processing algorithm employed (λ), and (b) $\gamma_H = ST_H/N_0$, depends on scenario parameters (signal and noise strength, hopping duration).

Exact evaluation of $A(\lambda,G)$ requires numerical integration by computer. However, we shall develop a lower bound and an approximation, which are quite useful for a wide range of λ. This minimum value (or lower bound) can be used in conjunction with (5.58) to guarantee a minimum gain for the correlator versus the radiometer. The argument is based on the observation that the quantity $F_1(k)$ in (5.48a) is a monotonically increasing function of the argument ζ_k; thus,

$$F_1(k) \leqslant F_1(\lambda G) = \int_0^1 (1-\rho') S_a^2\left[\pi G(1-\lambda)\rho'\right]d\rho' \quad ; \quad k=1,\ldots,\lambda G \qquad (5.59)$$

since $\zeta_{\lambda G} = \lambda$ from (5.48c). The inequality in (5.59) can be strengthened by the following steps:

$$\int_0^1 (1-\rho') S_a^2\left[\pi G(1-\lambda)\rho'\right]d\rho'$$

$$< \int_0^1 S_a^2\left[\pi G(1-\lambda)\rho'\right]d\rho' = G^{-1}(1-\lambda)^{-1}\int_0^{G(1-\lambda)} S_a^2[\pi x]dx$$

$$< G^{-1}(1-\lambda)^{-1}\int_0^\infty S_a^2[\pi x]dx$$

$$= G^{-1}(1-\lambda)^{-1}(1/2) \qquad (5.60)$$

110

Thus, from (5.59) and (5.60),

$$\sum_{k=1}^{\lambda G} F_1^2(k) \ < \ \lambda G \ F_1^2(\lambda G) \ < \ \frac{\lambda}{4G(1-\lambda)^2}$$

which, when combined with (5.57c), yields

$$A(\lambda, G) > A_{min}(\lambda, G) = A_{min}(\lambda) = \lambda(1-\lambda)^2 \tag{5.61}$$

We note that the lower bound A_{min} depends only on λ, while the exact gain $A(\lambda, G)$ also depends on G. This is just a fortunate coincidence, and indicates that A_{min} can be used for every G, as long as G >> 1. Thus, we arrive at the following inequaility

$$\frac{SNR_{out}^{corr}}{SNR_{out}^{rad}} \ > \ \lambda(1-\lambda)^2 \ \gamma_H^2 \tag{5.62}$$

which, as mentioned, should be tight for small λ.

In addition to this general bound, we can create a good approximate formula for the above ratio when $G(1 - \lambda) >> 1$, as follows: since the steps used to derive (5.50) are, in fact, tight successive approximations, we conclude that $F_1(k) \approx G^{-1}(1-kG^{-1})^{-1}(1/2)$, which leads to

$$\sum_{k=1}^{\lambda G} F_1^2(k) \approx \frac{1}{4} \sum_{k=1}^{\lambda G} \frac{1}{(G-k)^2} = \frac{1}{4} \sum_{m=G(1-\lambda)}^{G} \left(\frac{1}{m^2}\right)$$

The last summation can be well approximated by the integral

$$\sum_{m=G(1-\lambda)}^{G} \frac{1}{m^2} \approx \int_{G(1-\lambda)}^{G} \frac{dx}{x^2} = \frac{1}{G}\left[\frac{1}{1-\lambda} - 1\right] = \frac{\lambda}{G(1-\lambda)}$$

provided that $G(1 - \lambda) \gg 1$. Substitution into (5.57c) leads to

$$\frac{SNR_{out}^{corr}}{SNR_{out}^{rad}} \approx \lambda(1-\lambda) \gamma_H^2 \tag{5.63}$$

which differs from the bound (5.62) in the exponent of $(1 - \lambda)$. For low λ, (5.62) and (5.63) agree closely. In any case, those two equations indicate that the relative merit of the correlator increases proportionally to the square of the hop SNR and could, therefore, reach significant levels, depending on the application (coded or uncoded systems, slow or fast hopping, etc.)

The RF algorithm (5.34) - (5.35) analyzed above is but one attempt to exploit the information imbedded in the correlation coefficient $\{\widetilde{y}_k\}_1^G$. In fact, it can be viewed as a nonparametric algorithm, in that no particular model for the underlying process has been assumed in formulating it; the algorithm simply measures the total "power" of the correlation lags. As an attempt at a more structured approach, consider modeling the time domain process $\{r_k\}_{k=0}^{G-1}$ as an autoregressive (AR) process of order M, i.e.

$$\widetilde{r}_k = - \sum_{m=1}^{M} \hat{\alpha}_{M,m} \widetilde{r}_{k-m} + \widetilde{\epsilon}_k \; ; \quad k=M+1,...G-1 \tag{5.64}$$

In (5.64), $\{\widetilde{\epsilon}_k\}$ represents the zero mean i.i.d. ("white") driving noise process with estimated variance σ^2_ϵ and $\alpha_M = [\alpha_{M,1},...,\alpha_{M,M}]^T$ is the estimated AR parameter vector;

112

the normalized AR spectrum (by σ_ε^2) resulting from (5.64) is expressed in (5.28). The fact that (5.64) can spectrally model arbitrarily closely any second-order ergodic process of finite variance as $G \rightarrow \infty$ (and possibly as $M \rightarrow \infty$) serves as a motivation for this approach. Furthermore, since the estimation of parameters for an AR model results in linear equations, it has a computational advantage over moving-average (MA) or ARMA formulations.

From the detection viewpoint, the postulation of (5.64) poses the interesting problem of determining decision statistics associated with it. One such approach was outlined in Section 5.2; furthermore, Kay [34] showed that, for a one-pole $(M = 1)$ modeling, the spectral-maximum rule (5.15) is equivalent to the threshold comparison of the estimated (single) pole magnitude

$$|\hat{\alpha}_{1,1}|^2 = \left|\frac{\tilde{y}_1}{\tilde{y}_0}\right|^2 \equiv |\tilde{p}_1|^2 \underset{H_0}{\overset{H_1}{\underset{<}{\gtrless}}} \text{threshold} \tag{5.65}$$

which is a normalized variant to rule (5.33). This fact of exact equivalence, which constitutes an interesting conceptual bridge between the spectral and correlation detection domains, is hard to generalize to higher M. Unfortunately, the parametric performance of the one-pole spectral model is inferior to the nonparametric FF/spectral-maximum combination for the narrowband signal case [34]. Similarly discouraging simulation results were obtained in [38, 39] for higher order $M \geq 1$. In the case of [38], a straightforward extension of the statistic (5.65) was attempted in the form

$$\sum_{k=1}^{M} |\hat{\alpha}_{M,k}|^2 \underset{H_0}{\overset{H_1}{\underset{<}{\gtrless}}} \text{threshold} \tag{5.66}$$

wherein it was found that for a small time-bandwidth product performance somewhat worsens for increasing M; on the other hand, when the signal spectrum broadened, due to

113

random phase modulation, performance of (5.66) was superior to the periodogram. The conclusion from the above should not necessarily be that AR modeling is inappropriate; rather, that a search for more meaningful detection statistics is in order. For more detailed information see Appendix K.

Let us, also, note that AR modeling of either the colored alone [35] or ARMA modeling of a Gaussian signal plus noise [36] has been recently employed as a tool for signal detection under modeling uncertainties. In the latter case, the classification of the algorithm in the context of this report is not clear, since the periodogram is used as an intermediate step in a spectral matching procedure for the estimation of the ARMA parameters. In both cases, however, a LR is formed, either in its GLRT form or as a whitening matched filter (asymptotically equal to an SNR measure). When the signal is Gaussian and broadband (but not exactly white), Kay [37] suggests the use of a GRLT, based again on estimating a_M.

We conclude this part by suggesting an alternative modeling approach which has been shown to be promising in the very broadband case. *(See Appendix K)*. The approach consists of modeling the correlation sequence $\tilde{y}_k$ as an AR process itself

$$\tilde{y}_k = \sum_{n=1}^{M} \hat{\beta}_{M,n} \tilde{y}_{k-n} + \eta_k \quad k=M+1,\ldots,G-1$$

(5.67)

and creating decision statistics associated with this model. For instance, an $M = 1$ model could give rise to a decision rule similar to (5.65)

$$\left| \frac{\bar{R}_y(1)}{\bar{R}_y(0)} \right| \underset{H_0}{\overset{H_1}{\underset{<}{\gtrless}}} \text{threshold}$$

(5.68)

114

where now $\{\widetilde{R}_y(k)\}_{k=0}^{\lambda G}$ pertains to the correlation of the sequence $\{\widetilde{y}_k\}$. In this correlation-of-the-correlation domain (C^2D), the aforementioned rule (5.34) can be interpreted as

$$Y \equiv \widetilde{R}_y(0) \underset{H_0}{\overset{H_1}{\gtrless}} \text{threshold} \tag{5.69}$$

with $a_k = 1$. We note that (5.68), or any other similar rule in the C^2D domain involves nonlinear operations on the data $\widetilde{y}_k$, in contrast with the linear operation of the FFT, required to produce the spectrum $S_n = |R_n|^2$. The tradeoff between the merit resulting from such nonlinear operations versus the computational burden implicit in them is examined further in Appendix K.

115

5.4 Comparative Results

In order to substantiate the value of the different approaches discussed so far, we compare the performance of certain algorithms in detecting a sinusoid in a wideband scenario (large G). The comparison here is by no means exhaustive; rather, its purpose is to give a preliminary flavor of the differences in performance between approaches. A more comprehensive comparison is offered in Appendix K, along with a discussion of the associated computational load of each algorithm, both for low and high TB products. We note that the large-TB case fits well the spread-spectrum frequency hopping detection model described without, of course, being confined to that.

We first look at the performance of rule (5.34), an order to assess the accuracy of our analysis.

The algorithm has been simulated on a digital computer. In the simulation, the autocorrelation function $y(\tau)$ of (5.38) has been carried out by its discrete-time equivalent in terms of noise samples of $n_I(t)$ and $n_Q(t)$. Since the input process is bandlimited to B, the analog operation of (5.38) can be simulated by its equivalent discrete-time system with sampling intervals equaling B^{-1}.

In terms of discrete-time samples, the radiometer output in (5.26) is modeled as

$$Y_{RAD} = \frac{2}{G} \sum_{k=1}^{G} \left[S + 2\sqrt{S}\, n_I\left(\frac{k}{B}\right) + n_I^2\left(\frac{k}{B}\right) + n_Q^2\left(\frac{k}{B}\right) \right]$$

$$(5.69)$$

where $G = BT_H$ is an integer and $n_I(k/B)$, $n_Q(k/B)$ are quadrature noise samples. Equation (5.69) is easily seen to be proportional to the time average of the squared envelope of $r(t)$ over the hop time T_H.

116

Similarly, the discrete-time simulation equation for the autocorrelation detector can be expressed as follows:

$$Y_{CORR} = \sum_{k=2}^{\lambda G} \left| \frac{1}{G-k+1} \left[(G-k+1)S + \xi(k) + j\,\eta(k) \right] \right|^2 \tag{5.70}$$

where $j = \sqrt{-1}$, $|\cdot|^2$ is complex magnitude squared, and $\xi(k)$, $\eta(k)$ are contributions from the SxN and NxN terms given in (5.39),

$$\xi(k) = \sum_{\ell=k}^{G} \left\{ n_I\left(\frac{\ell}{B}\right) n_I\left(\frac{\ell-k+1}{B}\right) + n_Q\left(\frac{\ell}{B}\right) n_Q\left(\frac{\ell-k+1}{B}\right) + \sqrt{S}\left[n_I\left(\frac{\ell-k+1}{B}\right) + n_I\left(\frac{\ell}{B}\right) \right] \right\} \tag{5.71a}$$

and

$$\eta(k) = \sum_{\ell=k}^{G} \left\{ n_I\left(\frac{\ell-k+1}{B}\right) n_Q\left(\frac{\ell}{B}\right) - n_I\left(\frac{\ell}{B}\right) n_Q\left(\frac{\ell-k+1}{B}\right) + \sqrt{S}\left[n_Q\left(\frac{\ell}{B}\right) - n_Q\left(\frac{\ell-k+1}{B}\right) \right] \right\} \tag{5.71b}$$

which are zero-mean noise processes for the assumed filter characteristics of Figure 19. Note that this discrete-time model incorporates all possible terms without any simplification.

For the discrete-time models (5.69) - (5.71), we have analytically evaluated the *means and variances of the decision variable* γ under either hypothesis H_i; $i = 0,1$. This not only allows for a step-by-step comparison with the corresponding simulation outcomes, but also permits a more precise performance description in terms of (P_D, P_{FA}). The theoretical results appear on Table 2. The simulation results, along with their theoretical (numerical) counterparts from Table 2, appear in Tables 3 and 4 for the radiometer and the autocorrelator, respectively. The last entry of Tables 3 and 4, SNR_{out}, is calculated on the basis of (5.56), which evidently neglects $var\{Y| H_1\}$. The close

117

Table 2. Moments of Detector-Output Variables Evaluated from the Discrete-Time Model Equations (5.69) and (5.70)

Moments of Detector-Output Variables	Radiometer	Autocorrelator*
$\mathscr{E}(Y\|H_0)$	$2N_0B$	$(N_0B)^2 \sum\limits_{k=1}^{\lambda G} \dfrac{1}{G-k} \approx (N_0B)^2 \ln\left(\dfrac{1}{1-\lambda}\right)$
$\mathscr{E}(Y\|H_1)$	$2(S + N_0B)$	$\lambda GS^2 + \left[2SN_0B + (N_0B)^2\right] \sum\limits_{k=1}^{\lambda G} \dfrac{1}{G-k}$ $= \lambda GS^2 + \left[2SN_0B + (N_0B)^2\right] \ln\left(\dfrac{1}{1-\lambda}\right)$
$\text{var}(Y\|H_0)$	$\dfrac{1}{G}(2N_0B)^2$	$(N_0B)^4 \sum\limits_{k=1}^{\lambda G} \left(\dfrac{1}{G-k}\right)^2 \approx \dfrac{1}{G}\left(\dfrac{\lambda}{1-\lambda}\right)(N_0B)^4$
$\text{var}(Y\|H_1)$	$\dfrac{(2N_0B)^2}{G}\left(1 + 2\dfrac{S}{N_0B}\right)$	$\approx \dfrac{1}{G}\left(\dfrac{\lambda}{1-\lambda}\right)(N_0B)^4 + \lambda^2 G\,(N_0B)^4\left(\dfrac{2S}{N_0B}\right)^3$ $+ 2\lambda\,(N_0B)^4\left(\dfrac{S}{N_0B}\right)\left(1 + 4\dfrac{S}{N_0B}\right)$

*Autocorrelator variance under H_1 given here is an approximation which consists of only the significant terms in its computation.

118

Table 3. Comparison of Radiometer Simulation Results to Theory (200 Trials)

$$BT_H = 1000$$

Input SNR	−20 dB		−15 dB		−10 dB	
Theory or Simulation	Theory	Simulation	Theory	Simulation	Theory	Simulation
$\mathcal{E}\left(Y\|H_0\right)$	4.00	4.003	4.00	4.003	4.00	4.003
$\mathcal{E}\left(Y\|H_1\right)$	4.04	4.044	4.126	4.132	4.40	4.407
$var\left(Y\|H_0\right)$	16.00	16.14	16.00	16.14	16.00	16.14
$var\left(Y\|H_1\right)$	16.3	16.20	17.0	16.69	19.2	18.57
Radiometer SNR_0 (dB)	−10.00	−9.73	0.00	0.14	10.0	10.06

Table 4. Comparison of Autocorrelation Detector Simulation Results to Approximate Analysis

$$BT_H = 1000; \lambda = 0.1$$

Y_{in} (dB)	−20 dB		−15 dB		−10 dB	
Theory or Simulation	Theory	Simulation	Theory	Simulation	Theory	Simulation
$\mathcal{E}\left(Y\vert H_0\right)$	0.417	0.419	0.417	0.419	0.417	0.42
$\mathcal{E}\left(Y\vert H_1\right)$	0.47	0.472	0.84	0.863	4.46	4.57
$var\left(Y\vert H_0\right)$	1.76×10^{-3}	2.61×10^{-3}	1.76×10^{-3}	2.6×10^{-3}	1.76×10^{-3}	2.61×10^{-3}
$var\left(Y\vert H_1\right)$	3.37×10^{-3}	4.97×10^{-3}	4.58×10^{-2}	5.34×10^{-2}	1.322	1.41
Autocorrelation Detector SNR_0 (dB)	1.16	0.17	20.06	18.76	39.7	38.2

numerical agreement between theory and simulation, over a wide range of γ_{in} values, can be observed from the tables.

It is further interesting to note that the difference in variance of γ under the two hypotheses is virtually negligible for the radiometer, while it becomes quite pronounced for the correlator as γ_{in} increases. The implication is that SNR_{out} is well suited as a performance measure for the former, but not so much for the latter. A comparison between theory and simulation, in terms of the SNR_{out} difference

$$(\Delta SNR)_{dB} = (SNR_{out}^{corr})_{dB} - (SNR_{out}^{rad})_{dB}$$

$$\approx [\lambda(1-\lambda)]_{dB} + 2[(\gamma_{in})_{dB} + G_{dB}] \tag{5.72}$$

as derived in (5.63), is provided in Table 5. Certain parameters were chosen so that the theoretical assumptions involved in the analysis would be well justified: (1) large time-bandwidth product (G = 1000 or 30 dB), (2) small input SNR ($\gamma_{in} \leq -10$ dB), (3) small $\lambda(\lambda = 0.1)$ and, (3) large number of trials (200), so as to assume statistical confidence. Since those numbers were in accordance with the assumptions made, any deviations of the simulation from the theory would indicate an error in the modeling process (Gaussianness, etc.). Fortunately, that was not the case, as evidenced by the closeness of the theoretical and simulation results in Table 5. It is, also, clear that significant gains can be attained over the radiometer, particularly as γ_{in} increases.

Next, we look at the sensitivity of the decision rule (5.55) with respect to the choice of λ. This is illustrated in Figure 20, where the detection probability P_D is plotted versus λ ($0 < \lambda \leq 1$) for two values of γ_{in} while G = 100 is constant; for each set of three curves associated with a value of γ_{in}, the corresponding values of P_{FA} are 10^{-2}, 10^{-4} and 10^{-6}, from top to bottom, respectively. In all cases examined, the trend is clear: performance is insensitive to change of λ over a very wide range, as long as λ is neither

121

Table 5. Theoretical and Simulation Values for $(\Delta SNR)_{dB} = \left(SNR_{out}^{corr}\right)_{dB} - \left(SNR_{out}^{rad}\right)_{dB}$

For Various Values of γ_{in} (dB)

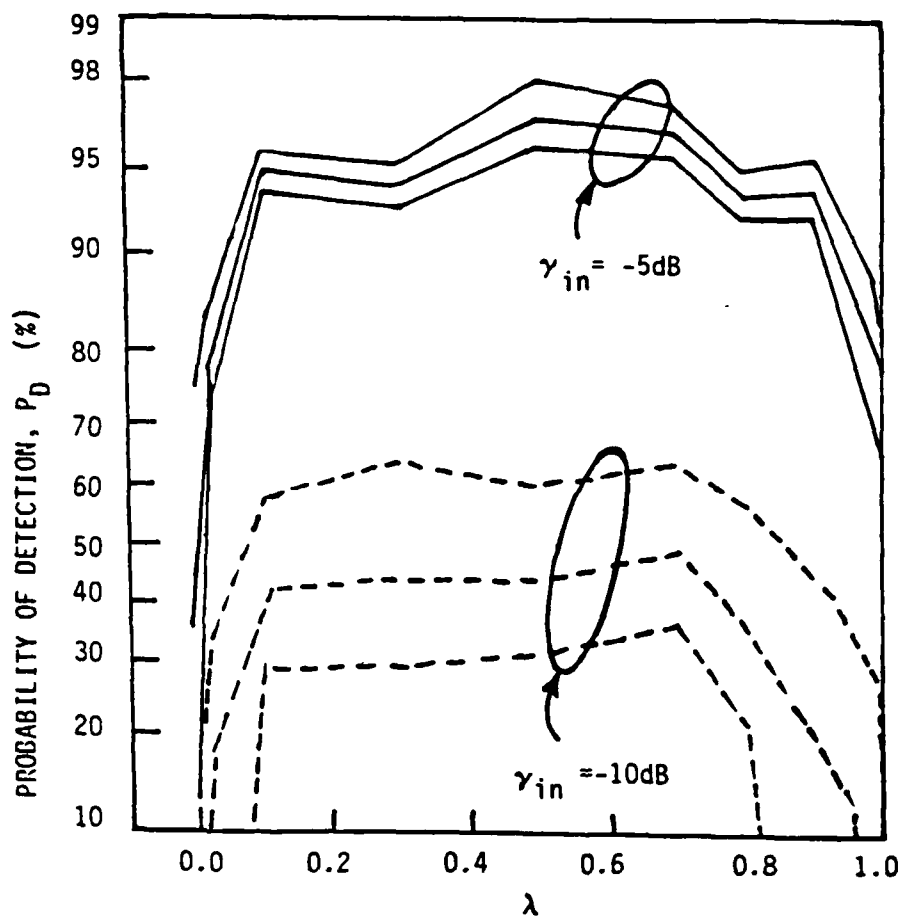| $G = 10^3, \lambda = 0.1$			
γ_{in} (dB)	-10	-15	-20
ΔSNR (dB) theoretical (lower bound)	29	19	9
ΔSNR (dB) Simulation	28	18.5	10

Figure 20. Simulation Results: Effects of λ on Detector Performance; $BT_H = 100$, (Curves shown are for $P_{FA} = 10^{-2}, 10^{-4}$, and 10^{-6} respectively.)

too small nor too large. So, any λ in the range (0.1, 0.8) would be a suitable choice. Although the curves illustrated in Figure 5 are for a particular choice of a_k's from (5.36); an identical kind of behavior was, also, found for other choices. This is a rather convenient conclusion since one does not have to be concerned about optimizing λ whenever the constants are changed. Furthermore, it was found as a more general conclusion that the overall performance (P_D, P_{FA}) was insensitive to the particular choice of a_k's. Thus, one can set $a_k = 1$, $k = 1,2,...,\lambda G$, which would simplify the decision rule to a mere accumulation of the power samples W_k and a threshold comparison.

A suitable set of design curves for both the radiometer and the correlator are provided in Figures 21 and 22. In these figures, the input SNR's (γ_{in}) required to achieve certain detector operating characteristics are shown for both algorithms. The probabilities of false alarm (P_{FA}) and detection (P_D) are computed directly from the first two moments of the detector-output variables under either hypothesis (Tables 3 and 4). Gaussian approximation is used, which is justifiable since in either algorithm the detector output consists of the sum of a large number of random variables. With this assumption, P_D is given in terms of P_{FA} and the moments of γ as

$$P_D = Q\left[\frac{\mathcal{E}\{Y|H_0\} - \mathcal{E}\{Y|H_1\} + \sqrt{\mathrm{var}\{Y|H_0\}} \cdot Q^{-1}[P_{FA}]}{\sqrt{\mathrm{var}\{Y|H_1\}}} \right]$$

(5.73)

From Figures 21 and 22, the relative gains of the correlator over the radiometer in terms of γ_{in} can be assessed. These results are plotted in Figures 23 , 24 and, also, summarized in Table 6. Note, that the performance improvement of the correlator over the radiometer is significant in the (P_D, P_{FA}) range of interest. For example, for $BT_H = 1000$, $P_D = 0.9$, $P_{FA} = 10^{-3}$, the correlator will require 6.8 dB less γ_{in} than the radiometer. This performance

124
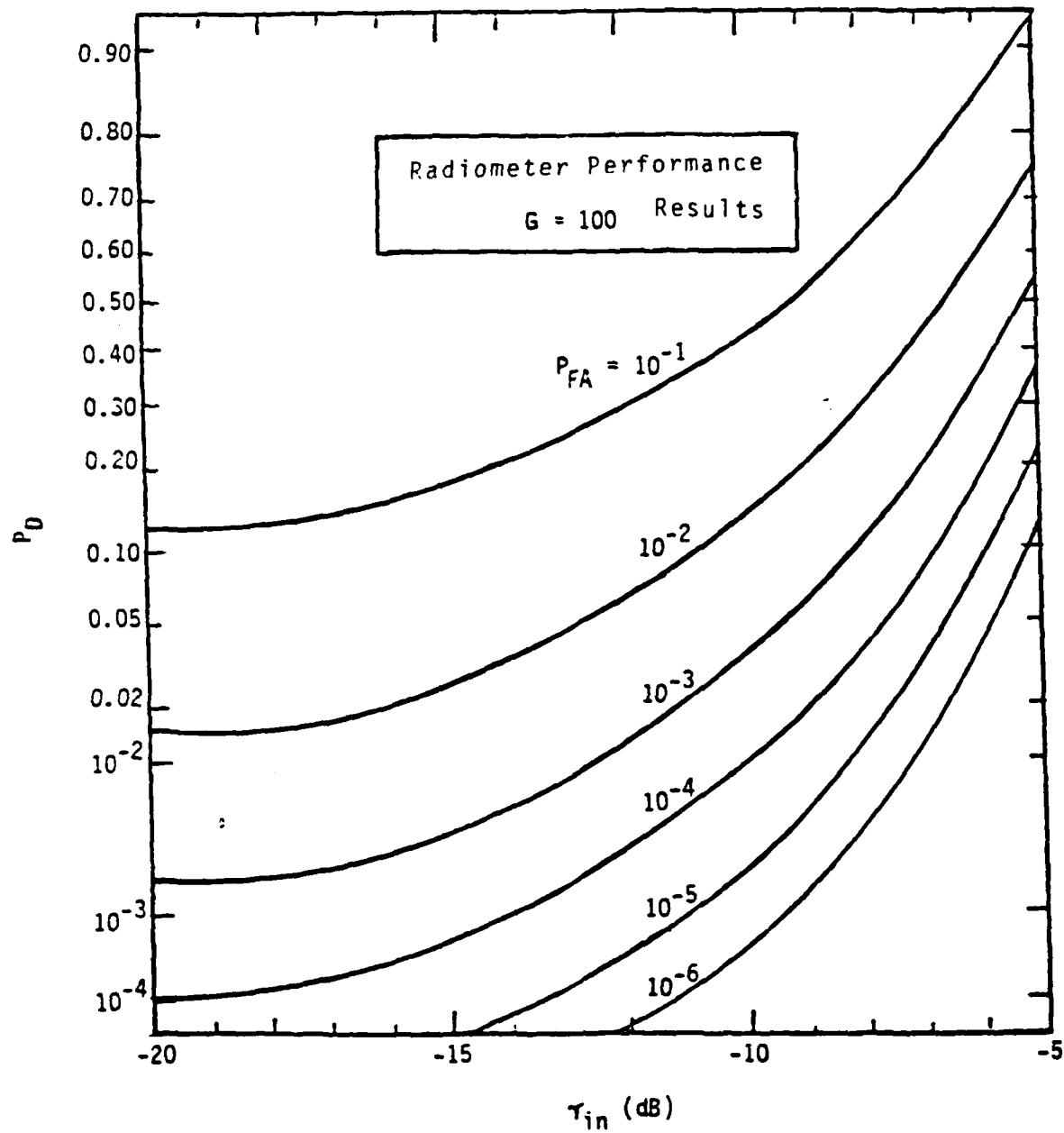
Figure 21. Plot of P_D Versus γ_{in} for the Radiometer, Parameterized by P_{FA}
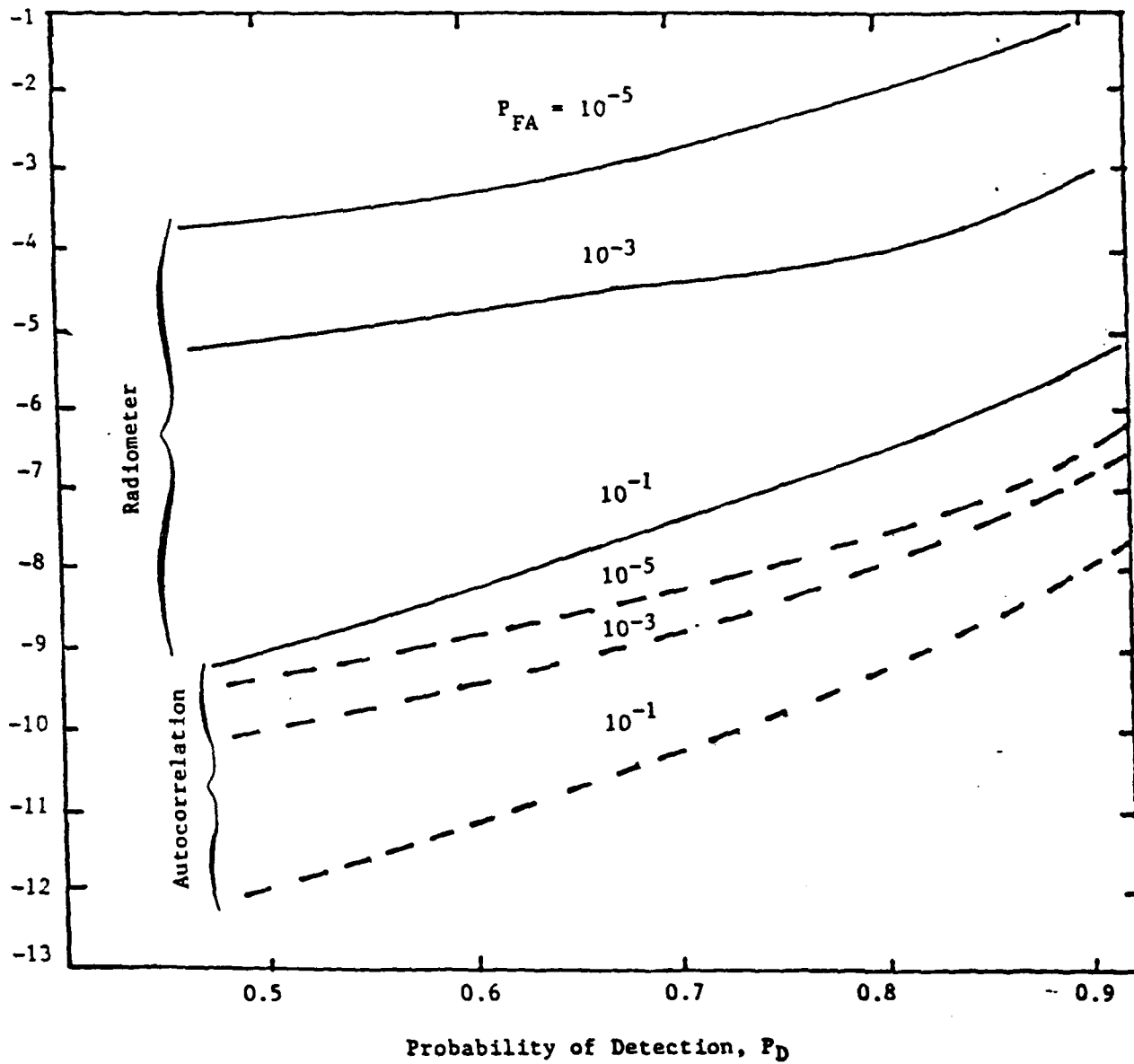
Figure 23. Relative Comparison of Radiometer and Correlation-Detector Performance; $BT_H = 100; \lambda = 0.1$

127
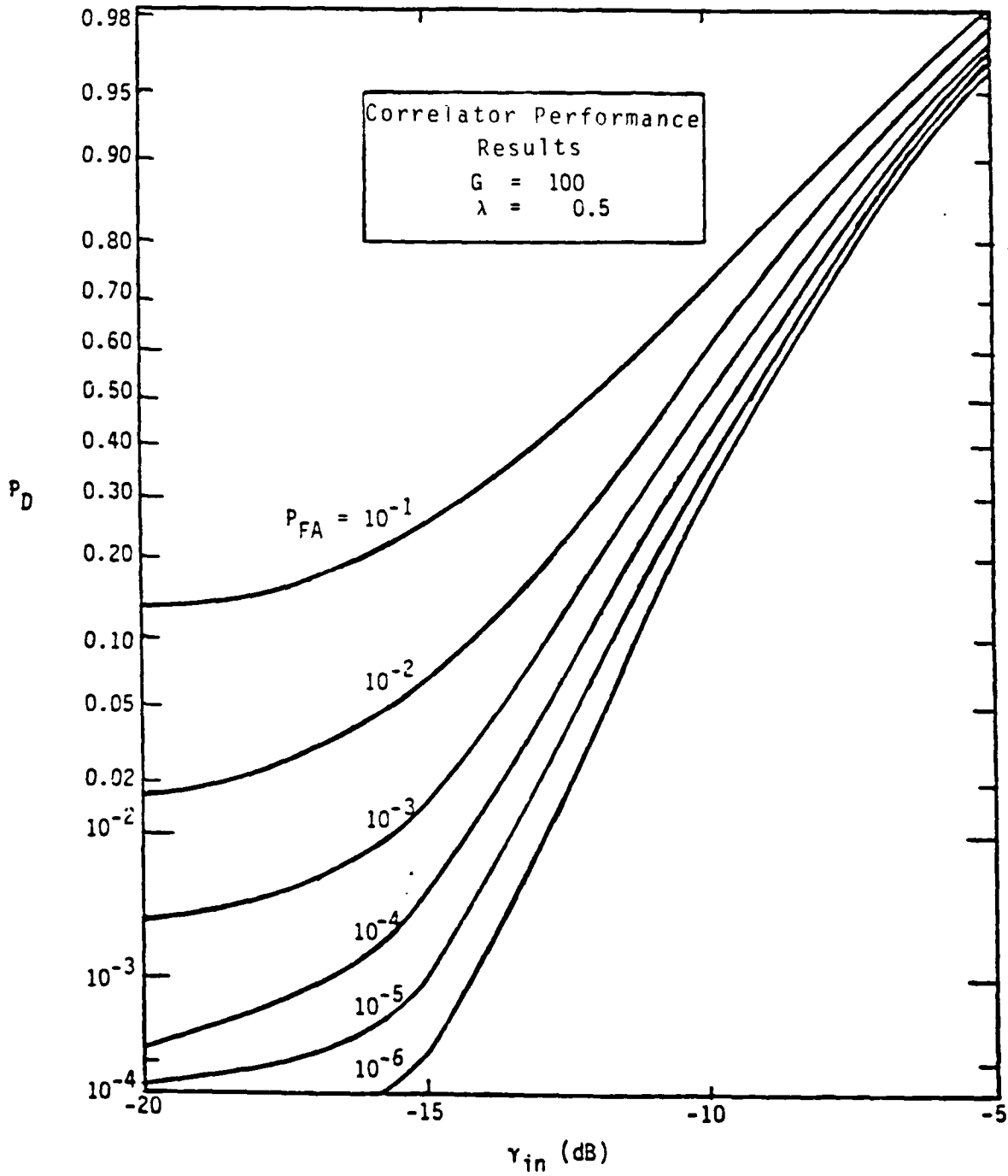
Figure 22.   Plot of P_D Versus γ_{in} for the Correlator, Parameterized by P_{FA}
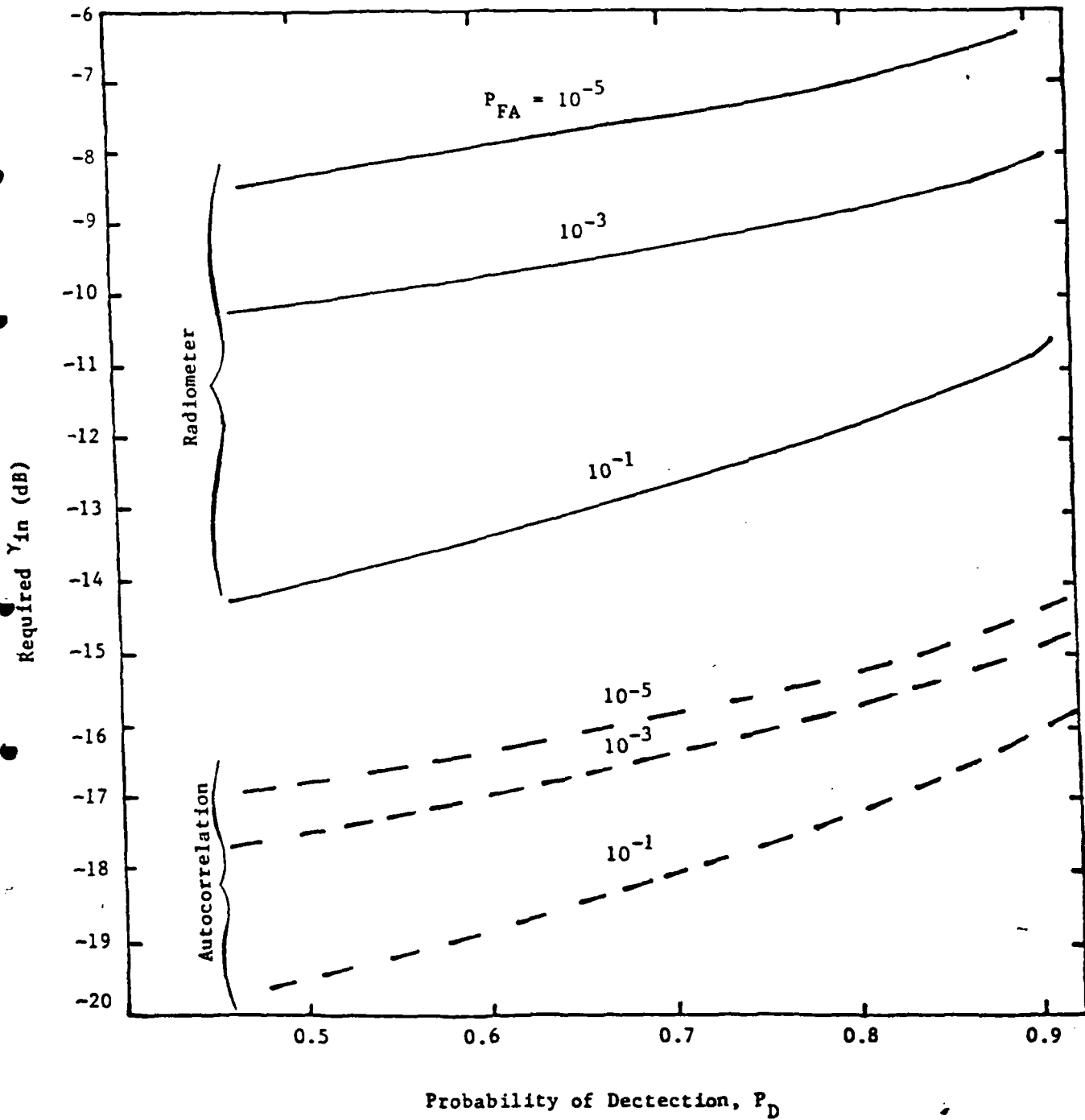
Figure 24. Relative Comparison of Radiometer and Correlation-Detector Performances; $BT_H = 1000$; $\lambda = 0.1$

128

Table 6. Relative Improvement of the Autocorrelation Technique Over the Radiometer Approach in terms of Required Input SNR γ_{in} For Desired P_D and P_{FA} Performance level.

BT_H	P_{FA}	Improvement of Autocorrelation Technique Over Radimeter (dB)				
		$P_D = 0.9$	$P_D = 0.8$	$P_D = 0.7$	$P_D = 0.6$	$P_D = 0.5$
	10^{-5}	5.4	5.5	5.5	5.6	5.7
100	10^{-3}	3.8	4.0	4.4	4.6	4.8
	10^{-1}	2.6	2.7	2.8	2.9	3.0
	10^{-5}	8.3	8.3	8.4	8.4	8.5
1000	10^{-3}	6.8	7.0	7.1	7.3	7.5
	10^{-1}	5.2	5.3	5.4	5.4	5.5

improvement will be 8.3 dB for the operating characteristic $P_D = 0.9$, $P_{FA} = 10^{-5}$ (which requires a higher γ_{in} than $P_D = 0.9$, $P_{FA} = 10^{-3}$) .

Finally, the RF correlation and radiometric results are compared with the various spectral algorithms of section (5.2) in Figures 25 a,b,c ($BT_H = 100$) and 26 a,b,c ($BT_H=1000$) for various P_{FA} levels. In particular, the curves on these figure designate the following cases:

Curve 1:   Optimal LR algorithm with $\Delta f = 0$ (Case I of Table 1)

Curve 2:   Power Adjusted Rule with $\Delta f = 0$ (Case IV of Table 1)

Curve 3:   Power Adjusted Rule with $\Delta f = R_H/2$ (Case III of Table 1)

Curve 4:   Optimal LR Algorithm with $\Delta f = R_H/2$ (Case II of Table 1)

Curve 5:   Spectral-Maximum Detector with $\Delta f = 0$ (eqn. 5.16)

Curve 6:   Spectral-Maximum Detector with $\Delta f = R_H/2$ (eqn. 5.16)

Curve 7:   The Autocorrelator (which is basically not affected by Δf)

Curve 8:   The Radiometer(which is not affected by Δf).

The performance of the LR algorithm, as illustrated in these figures, is optimal if $\Delta f = 0$ only. With the worst-case frequency offset ($\Delta f = R_H/2$) a degradation close to 5 dB will be suffered. With the power-adjusted rule this degradation can be somewhat minimized: resulting in degradations (from optimal) of approximately 0.7 dB and 3.5 dB, respectively, for $\Delta f = 0$ and $R_H/2$.

The performance of the spectral-maximum detector, also, suffers a significant (approximately 3 dB) degradation when $\Delta f = R_H/2$.

The LR algorithm exhibits a pronounced threshold behavior: when the hop SNR γ_H is above a threshold value (which depends on the BT_H and P_{FA} setting), the probability of signal detection P_D approaches unity rapidly. On the other hand, if γ_H is below this threshold value, P_D diminishes to zero.

The other algorithms' (i.e., the spectral-maximum, the autocorrelator, and the radiometer) performances are more robust, they do not exhibit pronounced threshold behavior like the LR detector. In fact, for large BT_H ($BT_H = 1000$), moderate γ_H ($\gamma_H < 10$ dB) and acceptable $P_{FA}(\leq 10^{-3})$, the performance of the spectral-maximum detector and the autocorrelator both exceed that of the LR detector, when worst-case Δf is considered.

Since the cases of interest in a LPI detection environment actually correspond to large BT_H, moderate γ_H, and $P_{FA} < 10^{-3}$, and since Δf cannot be expected to be zero, it appears that spectral-maximum detector and the autocorrelator are "better" LPI detectors than the LR detector, due to their robustness, though the LR detector is "optimal" in the theoretical sense, assuming perfect frequency and power alignments.

The most interesting observation to be made on these figures is that in the region of interest, described above, the autocorrelator appears to be the best choice, since it is not affected by Δf and, thus, performs better than the spectral-maximum detector when the worst-case $\Delta f = R_H/2$ is considered.

For a numerical discussion and simulation comparisons involving the aforementioned novel AR schemes, the interested reader is referred to Appendix K.

131

Figure 25a

Performance of Various LPI Detection Algorithms for
FH Signals

132

$BT_H = 100 \qquad P_{FA} = 10^{-3}$

Figure 25b

Performance of Various LPI
Detection Algorithms for FH
Signals

$\gamma_H(dB)$

$\gamma_{in}(dB)$

133

$$BT_H = 100, \quad P_{FA} = 10^{-5}$$

Figure 25c

Performance of Various LPI Detection Algorithms
for FH Signals

134

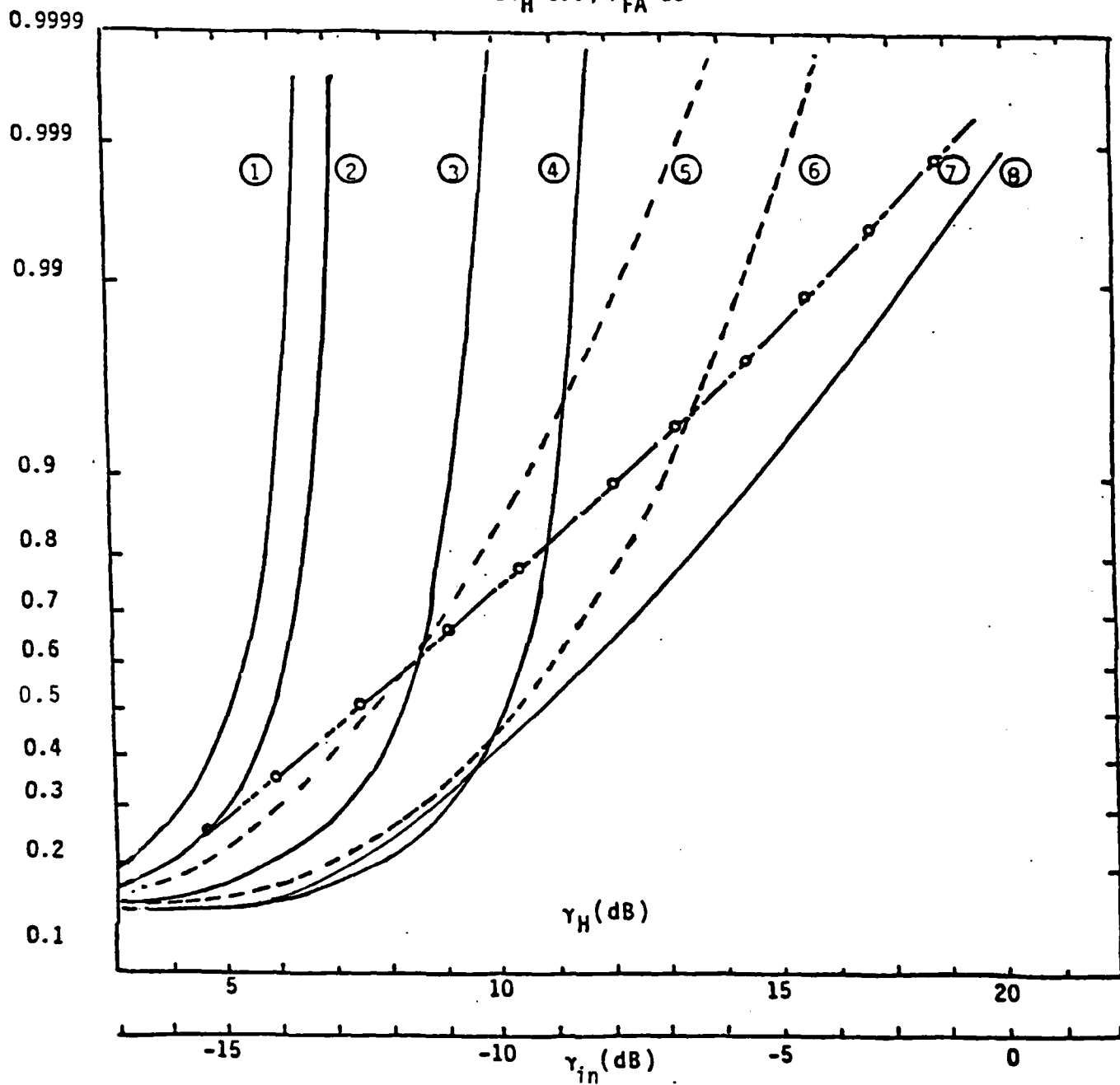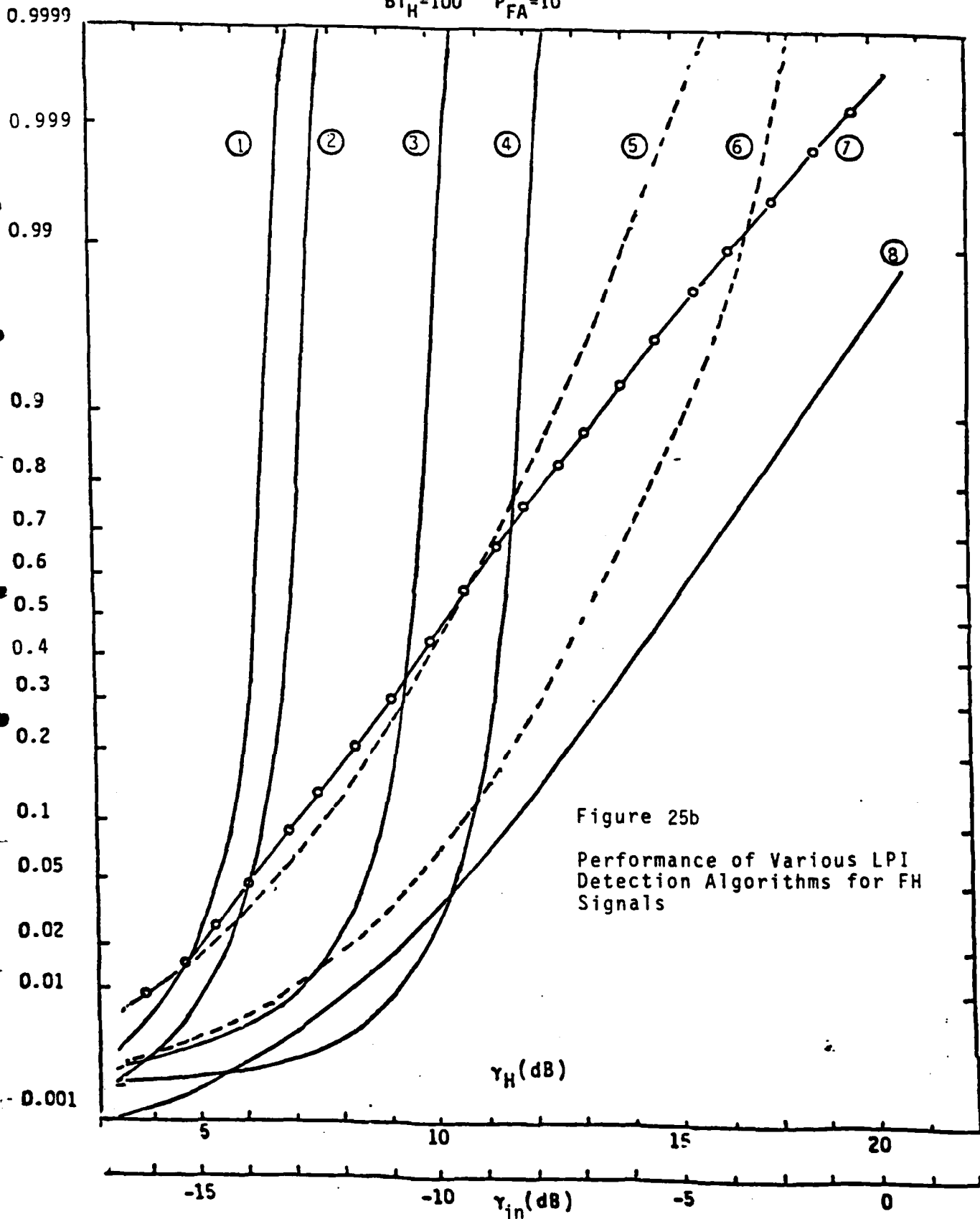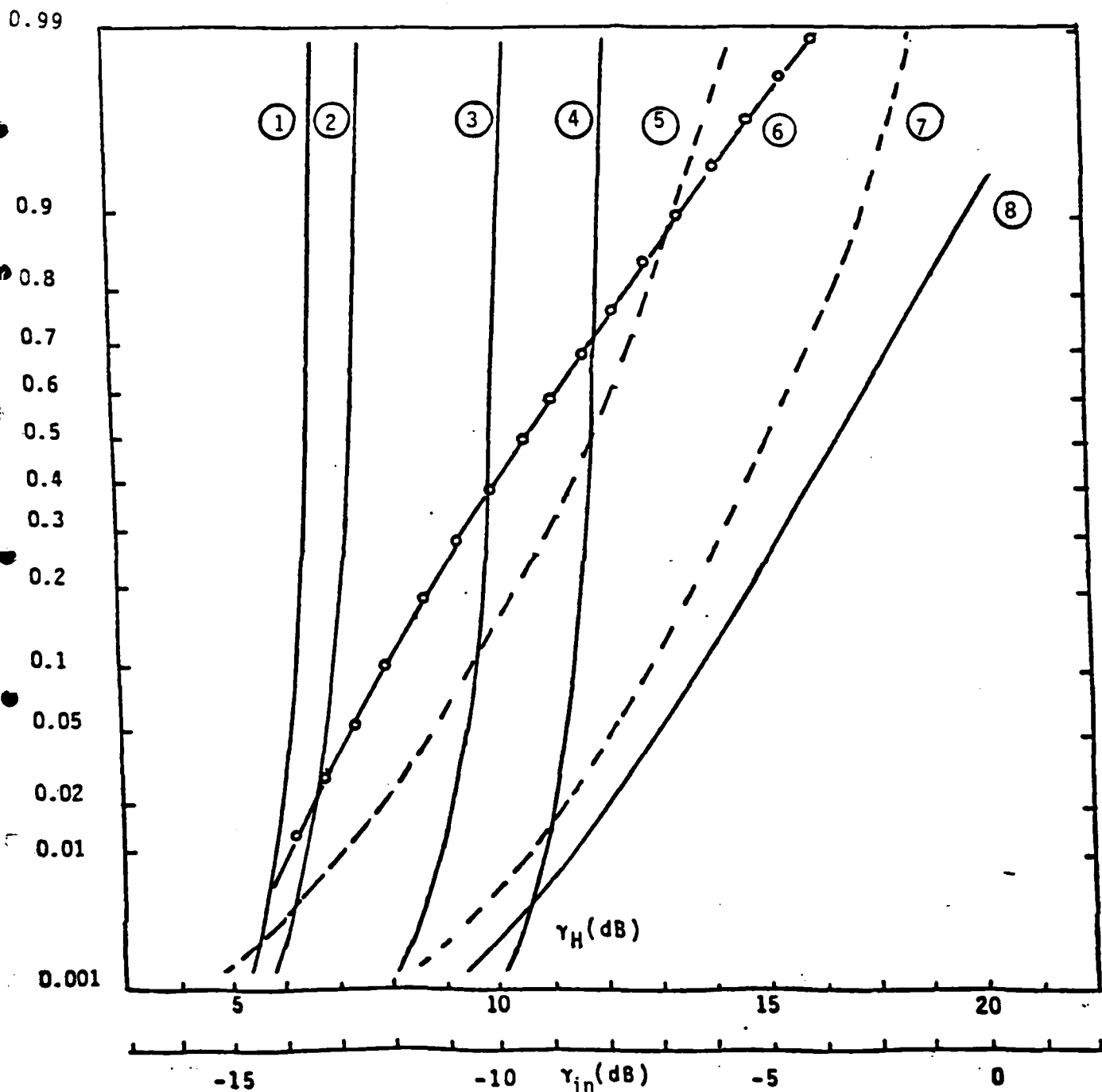$BT_H = 1000$, $P_{FA} = 10^{-1}$

Figure 26a

Performance of Various LPI Detection Algorithms for FH Signals

135

$BT_H = 1000$, $P_{FA} = 10^{-3}$

Figure 26b

Performance of Various LPI Detection Algorithms
for FH Signals

136

Figure 26c
Performance of Various
Detection Algorithms
for FH Signals

$BT_H = 1000$, $P_{FA} = 10^{-5}$

137
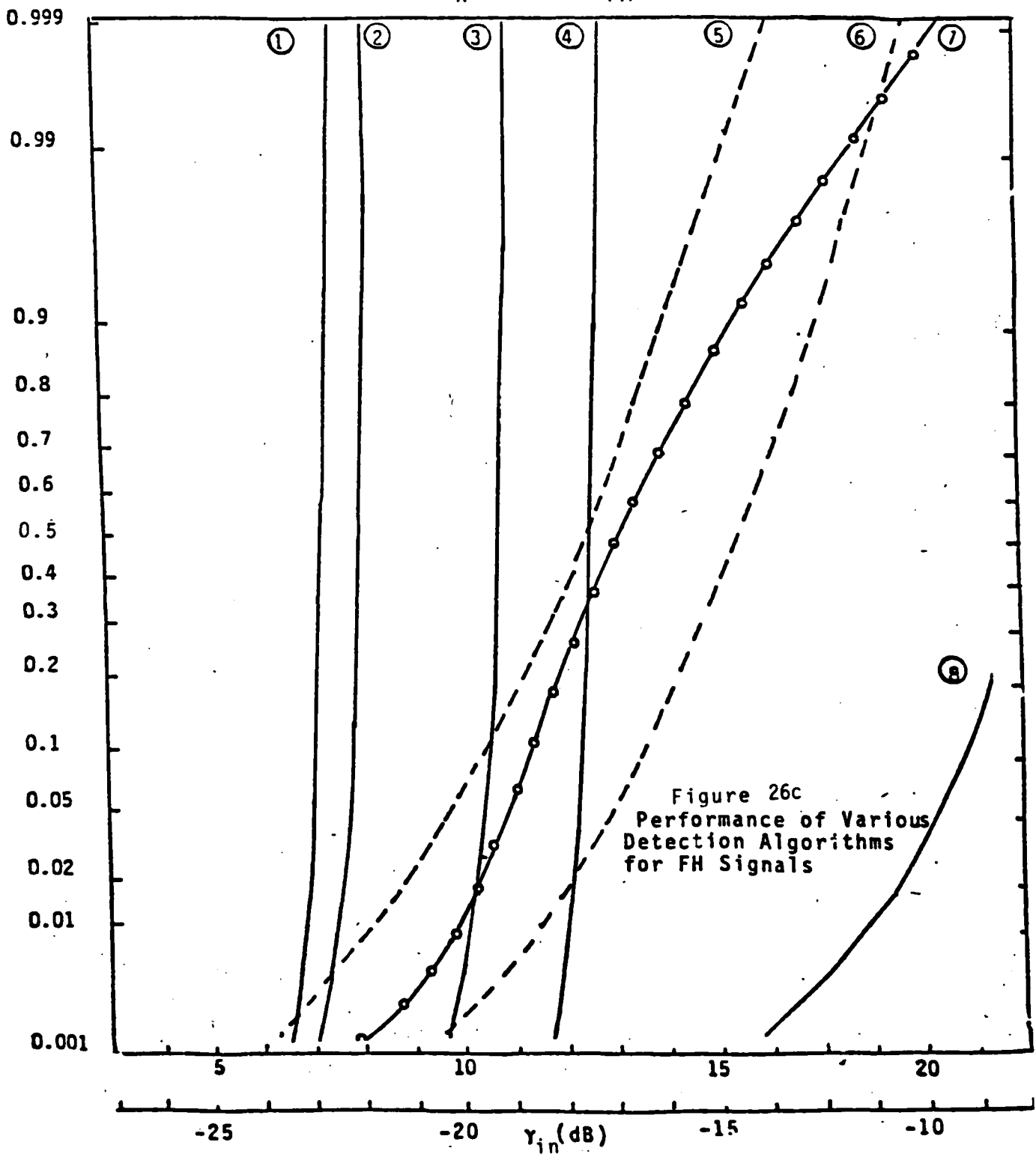
5.5 Narrowband Interference

Thus far, the interference model has consistently been additive broadband Gaussian noise. As mentioned in the Introduction, this is hardly expected to be the case in a dense environment where the sought signal coexists with a variety of narrowband and wideband waveforms, some of which vary quite unpredictably with time. Interference excision can work well whenever sufficient discrimination exists between the wanted and unwanted signals. Such discrimination results from distinctive features, be those long-term (multihop) spectral information, directional information, different rates, etc. In this section, we shall assume that everything possible (from an excision viewpoint) has been done, and what is left is some random, unpredictable narrowband interference. Our purpose is to show that, even in such an environment, intelligent processing can provide good detection capability while brute-force radiometric detection could fail miserably. For illustrative purposes we shall assume that the thermal noise level is negligible compared to the narrowband interference power. Furthermore, the sought signal will have a DS modulation on it, either by itself or in a hybrid DS/FH form. In the latter case, the spectral segments of Figure 17 must have enough bandwidth to accommodate the DS modulation. Since we are interested here in single-hop, per-band waveform processing, it follows that the FH part of the modulation does not explicitly enter in the mathematical model, except through the center frequency of the observed band. In that sense, both pure DS and per-band DS/FH (single-hop) in narrowband interference result in the same mathematical model. Let us remark that the present model (wideband signal in narrowband noise) is, in a sense, the inverse to the problem tackled in Section 5.2 - 5.4, therein, having a narrowband signal (FH) in wideband Gaussian noise. In view of the encouraging results, in these previous sections, it is to be expected that a good algorithm could also exploit the difference between signal and "noise" in the present case, too. In fact, it will then be shown that for observation data with a large time-bandwidth-product G, a very simple

138

algorithm operating on the output of a real-time autocorrelation device can achieve almost perfect performance--in stark contrast with the poor performance of the radiometer.

Hybrid modulation schemes have become increasingly popular spread-spectrum communication choices, due to the enhanced antijam margin which they offer. Adding DS modulation to FH, also, improves the anti-intercept capability because the "noiselike" appearance of DS makes detection more difficult. On the other hand, multiple tones constitute a common model of nonwhite interference and can emerge in a number of scenarios, i.e., it can be intentional (jamming of the band) or unintentional (multiple users in a broadcast environment, adjacent radar sources, etc.). It is, also, conceivable that the tone interference has been deliberately inserted by the communicator in a pseudorandom manner, so as to impede the interceptor's task, while it can be pseudorandomly avoided by the intended receiver.

Let the FH/DS hybrid signal to be detected be represented by $s(t) = \sqrt{2S}\, c(t) \cos \omega_0 t$, where ω_0 is an unknown frequency within the observed spectral band, $c(t)$ is the DS code of rate $R_c = T_c^{-1}$ and S is the signal power. The unknown interference consists of M tones (M is a random variable in each observation interval, which is equal to the hop time $T_H = R_H^{-1}$), with I_k, ω_k and ϕ_k denoting, respectively, the power, radian frequency and phase of the kth tone. The total received signal in $(0, T_H)$, under hypothesis H_1 (signal present), is given by

$$r(t) = \sqrt{2S}\, c(t) \cos \omega_0 t + \sum_{k=1}^{M} \sqrt{2I_k} \cos(\omega_k t + \phi_k) \tag{5.74}$$

Note, the absence of thermal noise in (5.74), as previously discussed. The code $c(t)$ can be modeled as either a random sequence of independent, identically distributed ± 1's with $\Pr[c(t) = 1] = 0.5$, or a PN code with a full period equal to T_H. As the ratio

139

$N \triangleq T_H/T_c = R_c/R_H$ increases (N denotes the number of code chips per hop), the performance difference becomes insignificant, a fact also verified by simulation.

Let B denote the input observation bandwidth. The presence of the DS code implies that B should be at least equal to R_c or higher, but definitely much larger than R_H. Equivalently, the time-bandwidth product $G \triangleq BT_H \gg 1$. Furthermore, for simplicity, we shall assume that all tones have equal power $I_k = I/M$, $k = 1,...,M$, where I is the total interference power, and they are equi-spaced within the bandwidth B. In other words, the frequency separation $|f_k - f_{k+1}|$ between adjacent tones equals $B/(M + 1)$, which is much greater than T_H, i.e., $|f_k - f_{k+1}| \gg T_H$. None of the above assumptions are critical in the forthcoming conclusions; they simply ease the analytical burden.

The real-time autocorrelation operation produces the output

$$y(\tau) = \int_{\tau}^{T_H} r(t) \, r(t - \tau) dt \quad ; \quad 0 \leqslant \tau \leqslant T_H$$

(5.75)

Substituting (5.74) into (5.75) and rearranging redefines $y(\tau)$ as

$$y(\tau) = Sy_c(\tau) \cos \omega_0 \tau + \left(\frac{I}{M}\right)(T_H - \tau) \sum_{m=1}^{M} \cos \omega_m \tau + \sqrt{\frac{SI}{M}} \left(\sum_{k=1}^{M} n_k^c(\tau) + n_0^\beta(\tau) \right)$$

(5.76)

where $y_c(\tau)$ is the code partial-correlation function (a random variable)

$$y_c(\tau) = \int_{\tau}^{T_H} c(t) \, c(t - \tau) dt$$

(5.77)

and $n_0^\beta(\tau), n_k^\alpha; k = 1,...,M$ are approximately Gaussian (via a central limit theorem-type argument), bandpass noise processes (signal x interference terms) defined by

$$n_k^\alpha(\tau) = \alpha_k^I(\tau) \cos \omega_k \tau - \alpha_k^Q(\tau) \sin \omega_k \tau$$

(5.78a)

and

$$n_0^\beta(\tau) = \left(\sum_{k=1}^M \beta_k^I(\tau) \right) \cos \omega_0 \tau + \left(\sum_{k=1}^M \beta_k^Q(\tau) \right) \sin \omega_0 \tau$$

(5.78b)

where

$$\alpha_k^I(\tau) = \int_\tau^{T_H} c(t) \cos\left[(\omega_0 - \omega_k)t - \phi_k \right] dt \qquad ,$$

(5.79a)

$$\alpha_k^Q(\tau) = \int_\tau^{T_H} c(t) \sin\left[(\omega_0 - \omega_k)t - \phi_k \right] dt \qquad ,$$

(5.79b)

$$\beta_k^I(\tau) = \int_\tau^{T_H} c(t - \tau) \cos\left[(\omega_0 - \omega_k)t - \phi_k \right] dt \qquad ,$$

(5.79c)

and

$$\beta_k^Q(\tau) = \int_\tau^{T_H} c(t - \tau) \sin\left[(\omega_0 - \omega_k)t - \phi_k \right] dt$$

(5.79d)

Before discussing the statistical characterization of the above noise processes , let us examine the noiseless (mean) part of $y(\tau)$ in (5.76), as shown in Figure 27. Of particular interest here are the envelopes of the useful signal (small shaded triangle) and the

141
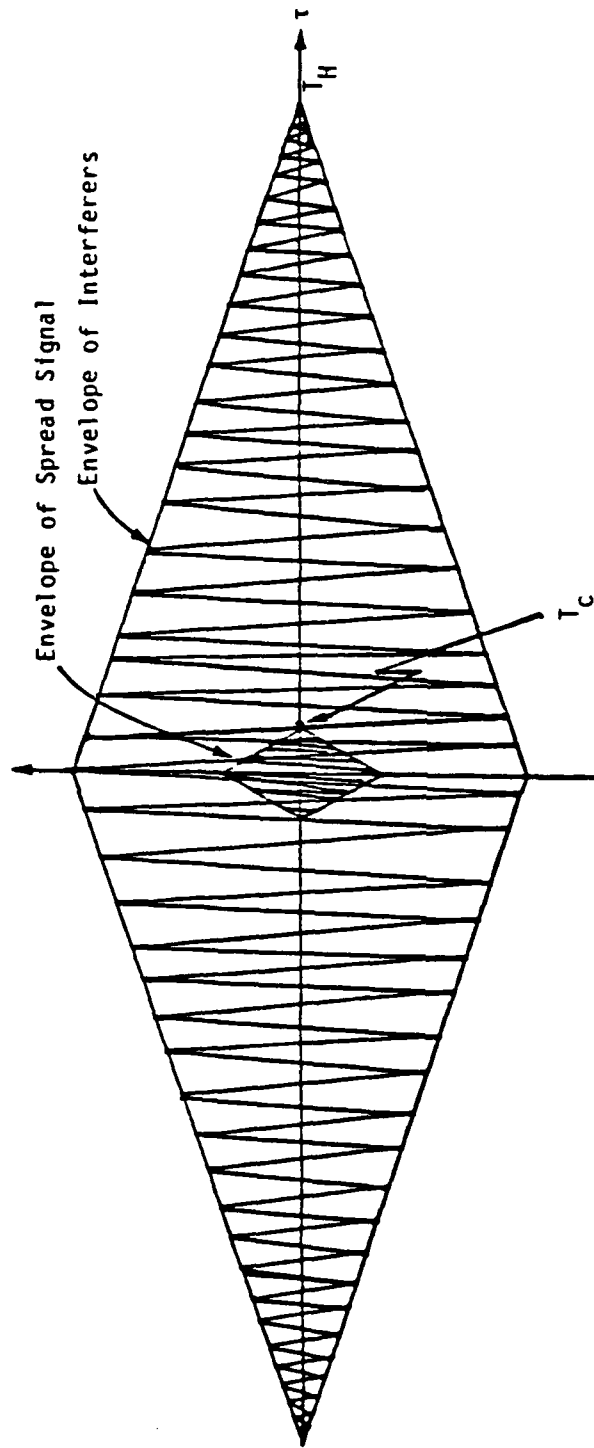
Figure 27. Mean of Output y(τ): The Signal and Interference Additive Components

142

interference (large triangle), respectively, since the actual components, e.g., the first two terms in (5.76), are modulated by the unknown frequencies. The structural difference between the two correlations is evident: the DS code superimposed on each hop creates a narrow mean autocorrelation function, since the expected value of the function $y_c(\tau)$ in (5.77) is zero for $|\tau| \geq T_c$. Contrary to that, the interfering tones correlate for the whole interval $[0,T_H]$. Clearly, then, a power (noncoherent) sample $\tau_1 = T_c$ would measure interference only[27] this sample could be subtracted from the corresponding one at $\tau_0 = 0$, so that under H_1, contains the full signal power plus interference. This subtraction would approximately cancel the interference contribution at $\tau_0 = 0$ so that, under H_1, only the signal would emerge while, under H_0, the statistic would be almost zero. Thus, the adopted decision rule is (see Figure 28)

$$\Delta = y^2(0)\Big|_{LP} - y^2(T_c)\Big|_{LP} \mathop{\gtrless}_{H_0}^{H_1} \Delta_0$$

(5.80)

where Δ_0 is a fixed threshold. In the absence of thermal noise Δ_0 can be set at a very small (positive) level in order to maximize the detection probability

We shall now investigate the performance of rule (5.80). Let us first address the statistics of $n_k^\alpha(\tau)$ and $n_0^\beta(\tau)$, defined in (5.78) and (5.79). Let $\mathscr{E}\{\cdot\}$ and var$\{\cdot\}$ indicate the mean and variance, respectively. *It is then easily shown that*

$$\mathscr{E}\left\{\alpha_k^j(\tau)\right\} = \mathscr{E}\left\{\beta_k^j(\tau)\right\} = 0 \quad ; \quad j=I,0$$

(5.81)

and that

---

[27] Any $\tau_1 = T_c$ would, also, do especially in the face of some uncertainty about T_c.
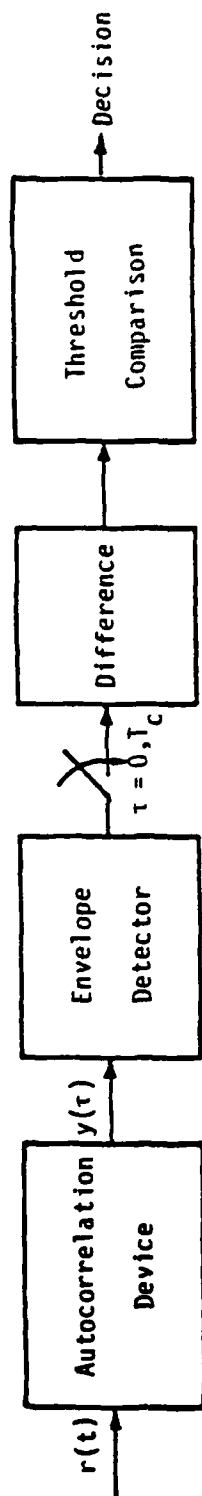
Figure 28. Block Diagram of the Decision Rule in the Autocorrelation Domain

$$\text{var}\left\{\alpha_k^j(\tau)\right\} = \text{var}\left\{\beta_k^j(\tau)\right\} = \mathscr{E}\left\{\left(\alpha_k^I(\tau)\right)^2\right\} \tag{5.82}$$

In the following, we shall concentrate on offsets $\tau = mT_c$; $m = 0,1,2,...,N$. In fact, only $\tau = 0$ and $\tau = T_c$ are of interest (see (5.80)). Then, lengthy manipulations can establish the following facts:

(a) The variance of (5.82) is given by

$$\mathscr{E}\left\{\left(\alpha_k^I(mT_c)\right)^2\right\} = \frac{(N-m)T_c^2}{2} S_a^2\left[\pi(f_0 - f_k)T_c\right] \tag{5.83}$$

where $S_a(x) = \sin x/x$ is the sampling function.

(b) The components $\alpha_k^j(mT_c)$ and $\beta_k^\ell(mT_c)$; $j = I,Q$; $\ell = I,Q$; are mutually uncorrelated which, by the Gaussian assumption, renders them independent; then the noises $n_k^\alpha(mT_c)$ and $n_0^\beta(mT_c)$ are also independent.

(c) Each noise porcess has mutually uncorrelated inphase and quadrature components (therefore, by the Gaussian assumption, independent).

(d) Noises corresponding to different frequencies (e.g., $n_k^\alpha(\tau)$ and $n_\ell^\alpha(\tau)$ with $k \neq \ell$) are approximately uncorrelated

(e) Processes $n_k^\alpha(\tau)$ and $n_0^\beta(\tau)$, however, have different properties, i.e., $n_k^\alpha(\tau)$ is a highly correlated process (as a function of τ), while $n_0^\beta(\tau)$ generally is not; in fact, samples of $n_0^\beta(\tau)$ taken T_c apart could be uncorrelated.

Of the above conclusions, (e) is probably the most interesting from a performance viewpoint: If the noise $n_0^\beta(\tau)$ had been as highly correlated as $n_k^\alpha(\tau)$, the decision rule (5.44) performance would have been perfect, since the same[28] random noise sample would be obtained at $\tau = 0$ and $\tau = T_c$; thus, they would cancel out. This not being true, a slight degradation in performance is expected, as was, also, observed in the simulation.

---

[28]Same within a totally insignificant change.

Nonetheless, since the mean part of the interference (second term in (5.26)) does cancel out, the performance of this scheme is far superior to that of the radiometer, which is oblivious to that term. In fact, the radiometer output is merely the value $y(0)$, which is dominated by the power of the random interference (Figure 27). Without further assistance, it is impossible to determine if there is any signal in the total observed power since the interference contribution is random and, hence, unknown.

As mentioned above, the high correlation of $\alpha_k(\tau)$ implies that $\alpha_k^j(0) \approx \alpha_k^j(T_c)$; $j = I,Q$. On the other hand, the degree of correlation between $\beta_k(0)$ and $\beta_k(T_c)$ varies with the frequency difference $\Delta f_k = f_0 - f_k$. For the special case, wherein one of the interfering frequencies f_{k_0} coincides with f_0, it is easily seen that $\beta_{k_0}^j(0) \approx \beta_{k_0}^j(T_c)$; $j = I,Q$. Those facts are used in the subsequent analysis.

We can now turn to the decision rule (5.80): upon squaring, taking the difference, lowpass filtering (e.g., rejecting double-frequency terms), assuming that $f_k = f_0$ for one frequency[29] and using the above conclusions, it follows that

$$\Delta = \frac{S^2}{2}\left(T_H^2 - y_c^2(T_c)\right) + \left(\frac{SI}{M}\right)\left(n^2(0) - n^2(T_c)\right)\Big|_{LP}$$

$$+ S\sqrt{\frac{SI}{M}}\left[\left(\alpha_{k_0}^I(0) + \sum_{k=1}^{M}\beta_k^I(0)\right)T_H - \left(\alpha_k^I(T_c) + \sum_{k=1}^{M}\beta_k^I(T_c)\right)y_c(T_c)\right]$$

$$+ \left(\frac{I}{M}\right)T_H\sqrt{\frac{SI}{M}}\left[\sum_{k=1}^{M}\left(\beta_k^I(0) - \beta_k^I(T_c)\right)\right] + ST_H\left(\frac{I}{M}\right)\left(T_H - y_c(T_c)\right) \quad (5.84)$$

where

---

[29]For the case of a single interferer, it can be shown that worst-case signal detectability happens when the interferer's frequency coincides with the signal frequency.

$$\eta(\tau) = \sum_{k=1}^{M} n_k^{\alpha}(\tau) + n_0^{\beta}(\tau)$$

$$(5.85)$$

is the total BP equivalent noise. Let us note that, at least for the case of a full PN code period per hop, $y_c(T_c)$ is approximately zero, which considerably simplifies (5.84). Furthermore, even for the random-code model, a comparison between analysis and simulation for the one-tone case (see next section) has indicated that the impact of the rv $y_c(T_c)$ is unnoticeable; hence, setting $y_c(T_c) = 0$ seems to be a reasonable approximation for the general case. Still, a full analysis of (5.84) without further simplifying assumptions is extremely complicated. In order to gain some insight here, we shall focus on the one-tone random interference ($M = 1$), with the reasonable conjecture that the multi-tone case should provide analogous conclusions.

Since, in this case, $\beta_1^I(T_c) \approx \beta_1^I(0) = a_1^I(0) \approx a_1^I(T_c) \triangleq a_1$ and $\eta^2(0) = \eta^2(T_c))$, it follows from (5.84) that

$$\Delta = \frac{(ST_H)^2}{2} \left[1 + 2\gamma_I^{-1} \left(1 + 2\sqrt{\gamma_I} \ a_{1,norm} \right) \right]$$

$$(5.86)$$

where we have defined the signal-to-interference ratio $\gamma_1 \triangleq S/I$ and the normalized random variable

$$a_{1,norm} \triangleq \frac{a_1}{T_H} = \left(\frac{T_c}{T_H} \right) \cos \phi_1 \sum_{n=1}^{N} c_n$$

$$(5.87)$$

In (5.87), c_n; $n = 1,...,N$ are the code chips and ϕ_1 is the random phase of the interference. Clearly, under H_0, $\Delta = 0$ with probability 1. Under H_1, it can be shown that

147

$$\mathscr{E}\left\{\Delta\middle|H_1\right\} = \frac{(ST_H)^2}{2}\left(1 + 2\gamma_I^{-1}\right)$$

(5.88a)

and

$$\text{var}\left\{\Delta\middle|H_1\right\} = 2(ST_H)^4(N\gamma_I)^{-1}$$

(5.88b)

Based on (5.88) and the Gaussian assumption about Δ, the performance of this decision scheme is predicted by the detection probability

$$P_D^{corr} = 1 - Q\left[\sqrt{\frac{N\gamma_I}{2}}\left(\frac{1}{2} + \gamma_I^{-1} - \Delta_0^*\right)\right]$$

(5.89)

where $\Delta_0^* = \Delta_0/(ST_H)^2$ is a normalized threshold and $Q(x)$ is the Gaussian integral function. In the absence of thermal noise, Δ_0^* can be set arbitrarily close to zero; thus, it always yields the zero false-alarm rate $P_{FA} = 0$. In practice, Δ_0^* would be set according to the thermal noise level and the degree of uncertainty about the power S of the detected signal.[30]

The performance predicted by (5.89) is indeed excellent.. We note that increasing the interference power (hence, increasing γ_I^{-1}) actually helps detection instead of deterring it, while it has no effect on false alarm. For instance, it can be shown that, if $N > 60$, then $P_D^{corr} > 99\%$ independently of γ_I, as long as $\Delta_0^* \leq 0.4$, i.e., one can tolerate 40% uncertainty about the signal power and still expect excellent detection capabilities, regardless of the interference power. The above conclusion is rather insensitive to N in that, for $N = 10$, the corresponding minimum P_D^{corr} is 90%.

---

[30]Alternatively, this can be expressed in terms of the uncertainty regarding the transmitter/intercept receiver's true distance.

The radiometer performance is easier to analyze for an arbitrary M and is based on the fact that its output $\gamma_{rad} = y(0)$ can be written as

$$Y_{rad} = ST_H + IT_H + 2\sqrt{S\frac{I}{M}}\left(\sum_{k=1}^{M} a_k^I(0)\right) \tag{5.90}$$

Let M_{max} be the maximum number of tones which can be expected in any hop. Here, for simplicity, we consider only the case $M_{max} = 1$, where Prob[one interfering tone] = Pr[no interfering tone] = 1/2 for each hop. Assuming that the threshold y_0 is set at $y_0 = I_1T_H$, so that [31] $P_{FA} = 0$, it can then be shown that

$$P_D^{rad} = \begin{cases} 1 - \frac{1}{2}Q\left[\sqrt{\frac{N\gamma_I}{2}}\right], & \text{if } \gamma_I > 1 \\ \frac{1}{2}\left(1 - Q\left[\sqrt{\frac{N\gamma_I}{2}}\right]\right), & \text{if } \gamma_I < 1 \end{cases} \tag{5.91}$$

Thus, the obtainable performance decreases with decreasing signal-to-interference ratio γ_I and in the limit

$$\lim_{\gamma_I \to 0} P_D^{rad} = \frac{1}{4} \qquad \left(M_{max} = 1\right) \tag{5.92}$$

which is certainly poor compared to P_D^{corr}. It can also be shown that the radiometer performance is a decreasing function of M_{max}, so that the above results constitute an upper bound for the general case. Finally, we note that the question of threshold setting is much more crucial for the radiometer than the correlator, since the performance of the latter is effectively independent of the jamming power.

---

[31] This is selected so as to match the zero P_{FA} of the correlator: another choice of y_0 would lead to $P_{FA} = 0.5$.

The correlator with one tone interference was simulated by computer; the results shown in Figure 29 are based on 10,000 independent trials. Also, shown in this figure are the analytical predictions (dotted lines) whose agreement with the simulation is quite striking, even for such low values of N as $N = 3$ and $N = 10$. Since detection probability is monotonically increasing with N (see (5.89)), those values represent worst-case designs which nonetheless yield excellent performance results. It was somewhat surprising to find that the Gaussian model provides such an accurate analytical prediction, even for $N = 3$; furthermore, setting $y_c(T_c)$ equal to zero proved to be a well-justified simplification. Note, that no false alarm was observed ($P_{FA} = 0$) and that performance is practically insensitive to the amount of interference inserted. In contrast, the radiometer performance (as evidenced by (5.91)) deteriorates rapidly with decreasing S/I, as expected. Finally, let us mention that the performance shown in Figure 29 is for a nonoptimized (arbitrarily chosen) threshold $\Delta_0^* = S^2 T^2_H/N$. In the absence of thermal noise, further improvement can be attained for the correlator by decreasing Δ_0^* to a very small (but positive) value.

Although analysis and simulation are not yet available for the multitone case, it is anticipated that the gap between the radiometer and the correlator performance will increase as the interference-to-noise ratio increases, independently of M_{max}. That gain is due to the relative insensitivity of the correlator to the interference nuisance parameters.

As mentioned, the theory of this section does not include thermal noise. The determination, analytical evaluation and simulation of algorithms which operate satisfactorily in a mixed environment (i.e., both thermal noise and random interference), will be the topic of future research.
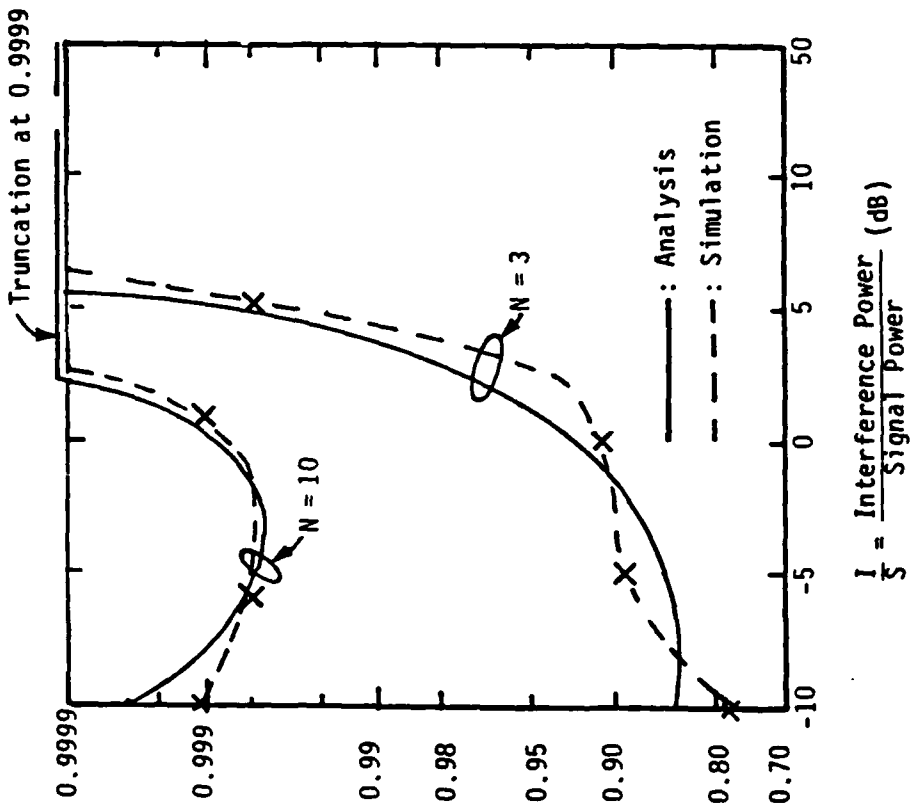
Figure 29. P_D Versus I/S for the Real-Time Autocorrelator (Nonoptimized Threshold)

151

APPENDIX A

ON MOMENT- GENERATING FUNCTIONS AND LIKELIHOOD RATIOS

A lot of powerful results in statistical decision theory rely upon the judicious use of transform-domain techniques and, in particular, on characteristic functions (CF) or moment-generating functions (MGF). Given the CF $\Phi_x(\omega)$ of a rv X,

$$\Phi_x(\omega) = \mathscr{E}\{e^{j\omega x}\} \tag{A.1}$$

assuming it exists, threshold-exceedance probabilities for X can be evaluated via the formula [10]

$$Pr[X > x_0] = \frac{1}{2} + \frac{1}{\pi} \int_0^\infty \frac{Im\{\Phi_x(\omega)e^{-j\omega x_0}\}}{\omega} \, d\omega$$

$$\tag{A.2}$$

where x_0 is the fixed threshold and $Im\{\cdot\}$ denotes the imaginary part of the enclosed quantity. Expressions (A.1) and (A.2) are particularly amenable to numerical evaluation by appropriate algorithms (c.f.[11]). For the purpose of proving the BFT results of Section 2 and deriving certain Chernoff bounds, we shall find it convenient to deal with the moment-generating functions

Let

$$M_x(s) \overset{\Delta}{=} \mathscr{E}\{e^{sx}\} = \Phi_x(-js) \tag{A.3}$$

denote the MGF of X, where s is a real variable; in fact, it is typically adequate to restrict attention to the $s \geq 0$ range.

When the averaging in (A.3) is over the pdf $f|_{x|H_i}(x)$ under hypothesis H_i; i = 0,1, it will be explicitly indicated as a subindex. Furthermore,

let

$$\mu_x(s) \overset{\Delta}{=} \ln M_x(s) \tag{A.4}$$

152

denote the second moment-generating function of X

and

$$g_X(s) \triangleq \frac{d}{ds} \mu_X(s) = \frac{\dot{M}_X(s)}{M(s)}$$

(A.5)

its derivative.[1] Whether one works with $\mu_x(s)$ (see, for instance, [12]) or $g_x(s)$, as we shall do here, is a matter of notational preference. From (A.4), (A.5) it follows that

$$M_x(s) = \exp \left\{ \int_0^s g_x(s')ds' + C_g \right\}$$

(A.6)

Since, however $M_x(0) = 1$, the constant $C_g = 0$ in (A.6), so that

$$M_x(s) = \exp \left\{ \int_0^s g(s')\,ds' \right\}$$

(A.7)

which is used extensively below.

Functions $\mu_x(s)$ and $g_x(s)$ possess some interesting properties. For instance, the Taylor series expansion of $\mu_x(s)$ around $s = 0$ has the form

$$\mu_x(s) = \sum_{m=0}^{\infty} \frac{s^m}{m!} C_m^{(X)}$$

(A.8)

where $C_m^{(X)}$ is the mth cumulant of X (see ref.[10]). Furthermore, it is easily shown that

---

[1]The dot indicates differentiation with respect to s.

$$g_x(0) = \mathscr{E}\{X\}$$

$$\dot{g}_x(0) = \text{var}\{X\}$$

$$\dot{g}_x(s) \geq 0 \tag{A.9}$$

i.e. the function $g_x(s)$ is monotonically increasing.

Let X be some decision statistic for the binary test

$$X \overset{H_1}{\underset{H_0}{\gtrless}} x_0 \tag{A.10}$$

(not necessarily an LR or LLR), with the corresponding pdf's $f_{X|H_i}(x)$ as shown in Figure A.1. Then the performance quantities

$$P_{FA} = Pr\{X > x_0 | H_0\} = \int_{x_0}^{\infty} f_X|_{H_0}(x)\,dx \tag{A.11a}$$

$$P_D = Pr\{X > x_0 | H_1\} = \int_{x_0}^{\infty} f_X|_{H_1}(x)\,dx \tag{A.11b}$$

can be bounded as follows (Chernoff bound): If the r.v. W is defined as

$$W \overset{\triangle}{=} \begin{cases} 0, & \text{if } X \leq x_0 \\ 1, & \text{if } X > x_0 \end{cases} \tag{A.12}$$

then, for every $s \geq 0$,

$$\exp(-s(X - x_0)) \leq W \leq \exp(s(X - x_0)) \tag{A.13}$$

as it is evident from Figure A.1. Furthermore, from (A.11), (A.12),

$$P_{FA} = \mathscr{E}\{W|H_0\} \tag{A.14a}$$
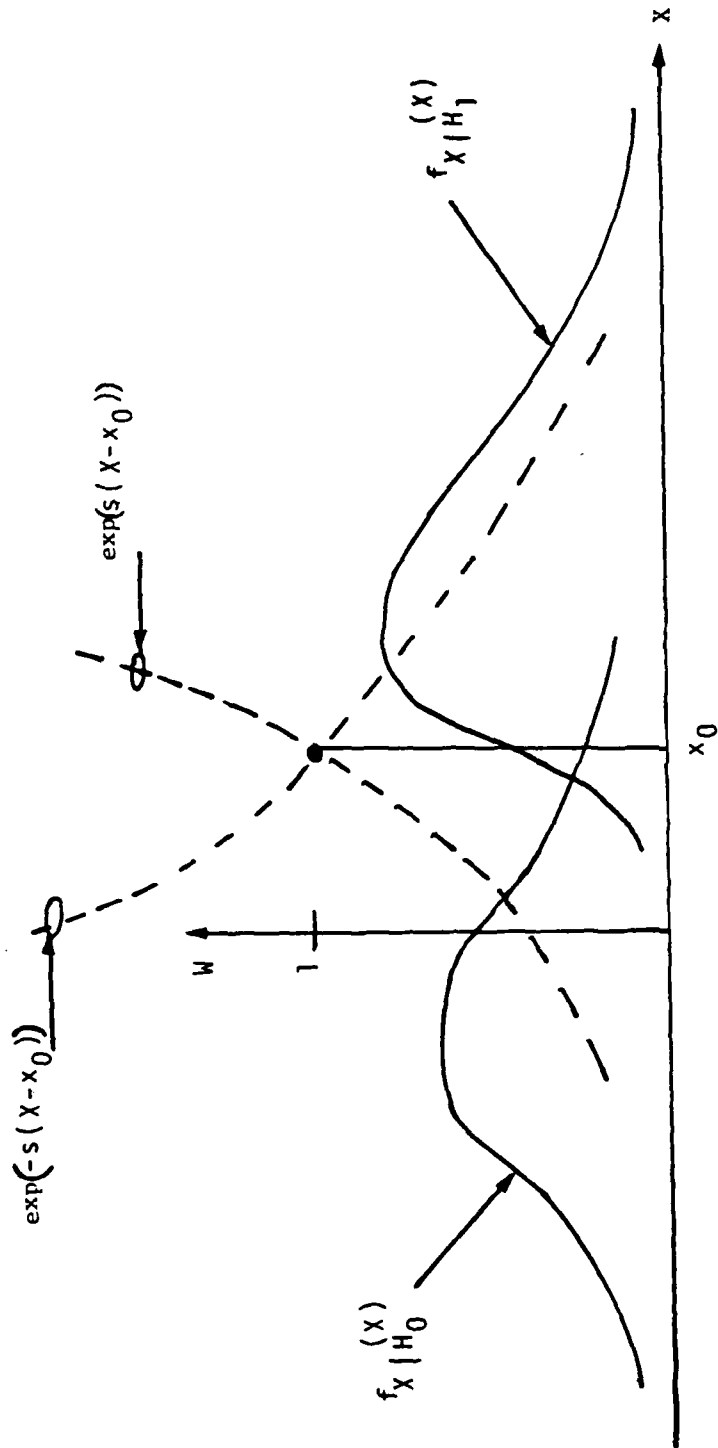
Figure A.1   Plot of the pdf's $f_{X|H_i}(X)$; $i=0,1$, the threshold x_0, the new variable W and the exponential bounds

155

and

$$P_D = \mathscr{E}\{W|H_1\} \tag{A.14b}$$

From (A.13), (A.14.a) we conclude that

$$P_{FA} \le \mathscr{E}\{e^{s(X - x_0)} |H_0\} = e^{-sx_0} M_{X|H_0}(s)$$

or using (A.7),

$$P_{FA} \le \exp\{-sx_0 + \int_0^s g_0(s')ds'\} \tag{A.15}$$

where $g_0(s) \triangleq g_{x|H_0}(s)$. Because of the monotonicity of the exp($\cdot$) function, the extremum of (A.15) occurs at the extremum of the exponent E(s)

$$\dot{E}(s) \triangleq \frac{d}{ds} [-sx_0 + \int_0^s g_0(s')ds'] = 0$$

or at $s = s_*$ where

$$g_0(s_*) = x_0 \tag{A.16}$$

Furthermore, since $\ddot{E}(s) = \dot{g}(s) \ge 0$ from (A.9), it follows that the extremum is actually a minimum, yielding the tightest (or lowest) upper bound on P_{FA} of (A.15),

$$\boxed{\begin{array}{l} P_{FA} \le (P_{FA})_{uB} = \exp\{E_*\} = \exp\{\int_0^{s_*} g_0(s')ds' - s_* g_0(s_*)\} \\[2ex] g_0(s_*) = x_0 \end{array}} \tag{A.17}$$

A lower bound on P_D in terms of of $g_{X|H_1}(s)$ can also be derived following similar steps; however, its most utility is for the particular case of interest, whereby X stands for some LLR. Then, all the previous conclusions (which of course still hold) can be enriched with some additional ones, owing to the fact that the MGF $M_{\ell|H_0}(s)$ of ℓ under H_0 is.

156

$$M_{\ell|H_0}(s) \triangleq \mathscr{E}\{e^{s\ell} | H_0\} = \mathscr{E}\{\Lambda^s | H_0\}$$

(A.18)

which links the properties of $M_{\ell|H_0}(s)$ to those of a LR Λ. We conclude that

$$M_{\ell|H_1}(s) \triangleq \mathscr{E}\{e^{s\ell} | H_1\} = \mathscr{E}\{\Lambda^s | H_1\} = \mathscr{E}\{\Lambda^{1+s} | H_0\}$$

or

$$M_{\ell|H_1}(s) = M_{\ell|H_0}(s+1)$$

(A.19)

which implies that <u>all the statistical properties of any LLR under H_1 can be determined, once its distribution under H_0 (equivalently, $M_{\ell|H_0}(s)$ is provided.</u> This interesting aspect of LLR's is, also, manifested in the statement of the PBF theorem (Section 2) for the special Gaussian case. Since $M_{\ell|H_1}(s)$ is just a "shifted" replica of $M_{\ell|H_0}(s)$, the latter contains all the necessary information through (A.7), it suffices to know $g_0(s) = g_{\ell|H_0}(s)$. An immediate corollary of (A.19) is that

$$M_{\ell|H_0}(1) = M_{\ell|H_1}(0) = M_{\ell|H_0}(0) = 1$$

(A.20)

which, in turn, yields from (A.7)

$$\int_0^1 g_0(s') \, ds' = 0$$

(A.21)

The monotonic increase of $g_0(s)$ (recall (A.9)) along with the fact (A.21) implies that $g_0(s)$ should look something like the curve of Figure A.2, since, from (A.9), (A.19), $g_0(1) = g_{\ell|H_1}(0) = \mathscr{E}\{\ell|H_1\}$, etc. In particular, any LLR ℓ must satisfy.

157
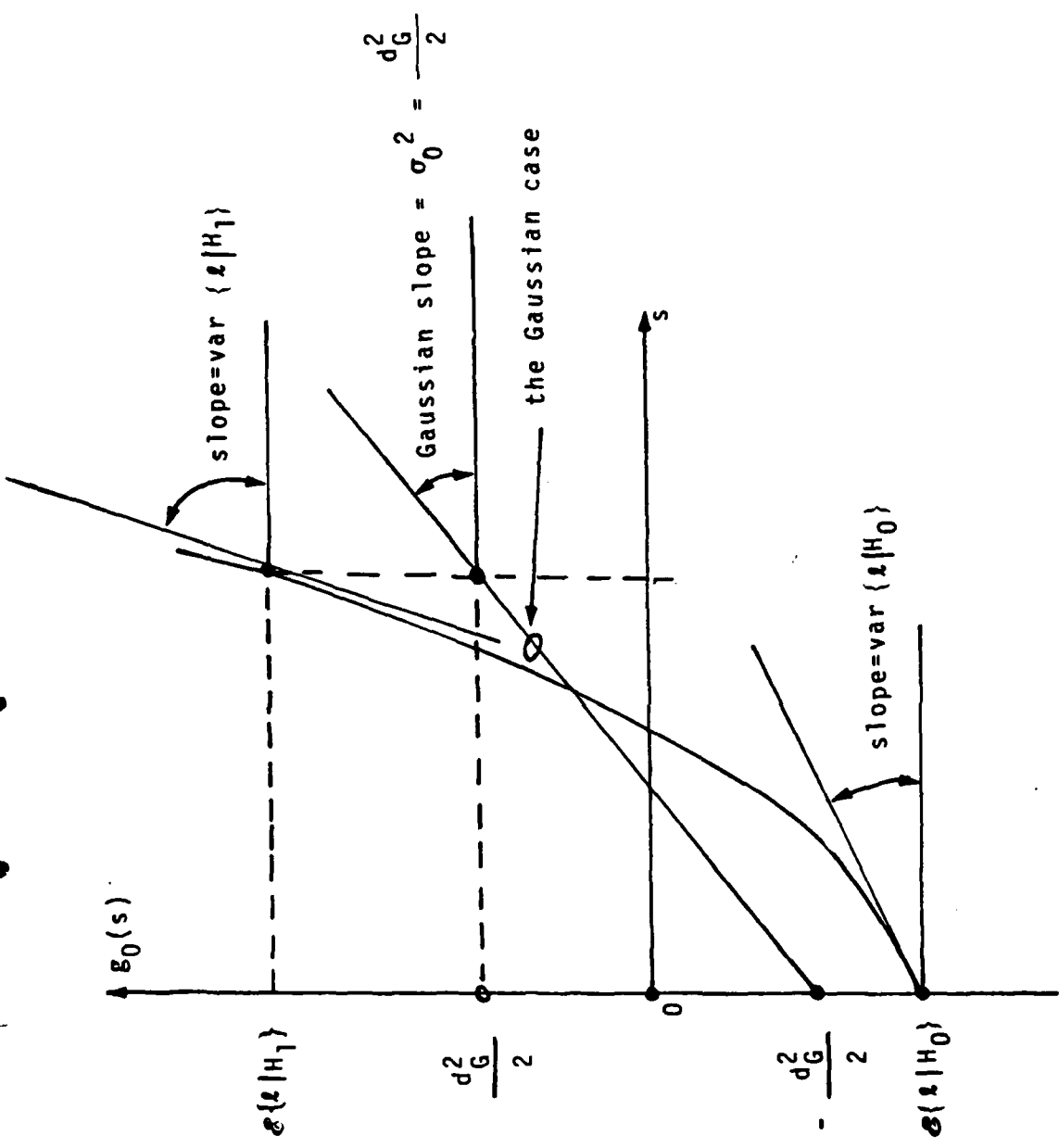
Figure A.2: A plausible form of the function $g_0(s)$.

$$\mathscr{E}\{\ell|H_0\} \leq 0 \leq \mathscr{E}\{\ell|H_1\} \qquad (A.22)$$

as a result of Figure A.2. Equalities in (A.22) apply only to the trivial case where $\Lambda = 1$ almost everywhere. An alternative proof of (A.22) can be found in ref [13] where $\mathscr{E}\{\ell|H_1\}$; $i = 0$, are termed <u>directed divergences</u> and the difference $J = \mathscr{E}\{\ell|H_1\}\} - \mathscr{E}\{\ell|H_0\}\}$ is called <u>J-divergence.</u>

Another byproduct of (A.19) is a lower bound for P_D in (A.11b) in a form dual to (A.17). Indeed, from (A.14.b),

$$P_D = \mathscr{E}\{W|H_1\} \geq \mathscr{E}\{e^{-s(X-x_0)}|H_1\}$$

$$= e^{-sx_0} M_X|_{H_1}(-s) = e^{-sx_0} M_{X|H_0}(1-s)$$

or, changing the variable s into (1-s) without loss.[2]

$$P_D \geq e^{(1-s)x_0} M_{X|H_0}(s) = \exp\{(1-s)x_0 + \int_0^s g_0(s')ds'\} \qquad (A.23)$$

Again, by differentiation of the exponent, the extremum (which is easily shown to be a maximum) occurs at $s = s_*$ where $g_0(s_*) = x_0$, resulting in the tightest (highest, lower bound)

$$P_D \geq \exp\{(1-s_*) g_0(s_*) + \int_0^s g_0(s')ds'\}$$
$$\qquad (A.24a)$$

or

---

[2] Since we are restricting attention to the $0 \leq s \leq 1$ range and $0 \leq 1 - s \leq 1$, the substitution is legitimate

$$\boxed{P_D \geq (P_D)_{LB} = e^{x_0}(P_{FA})_{UB}}$$

(A.24b)

with $(P_{FA})_{UB}$ as per (A.17).

Equipped with this brief expose on the useful properties of the LLR moment-generating functions, we can now prove the BPF theorem in a rather compact fashion. Indeed, assume that ℓ is Gaussian under H_0, with $\mathscr{E}\{\ell|H\} = m_0$ and $var\{\ell|H_0\} = \sigma^2$ its second-order statistics. Since the MGF of a Gaussian r.v. is well-known to be,

$$M_{\ell H_0}(s) = exp\{m_0 s + \frac{\sigma^2 s^2}{2}\}$$

(A.25)

it follows that the associated $g_0(s)$ is simply

$$g_0(s) \triangleq \frac{d}{ds}(\ln M_{\ell H_0}(s)) = m_0 + \sigma^2 s$$

(A.26)

In other words, $g_0(s)$ is a straight line as shown in Figure A.2 with a constant slope

$$g_0(s) = \sigma_0^2 = var\{\ell|H_0\} = var\{\ell|H_1\}$$

(A.27)

From (A.20), (A.25) we have that

$$M_{\ell H_0}(1) = exp\{m_0 + \frac{\sigma_0^2}{2}\} = 1$$

or

$$m_0 = -\frac{\sigma_0^2}{2} \tag{A.28}$$

i.e. the mean and variance of ℓ under H_0 cannot be arbitrary within the Gaussian model, but rather related as per (A.28). Inserting (A.28) into (A.25) results in

$$M_{\ell|H_0}(s) = \exp\{\frac{\sigma^2}{2}(s-1)s\} \tag{A.29}$$

We can now use (A.19) to assess that

$$M_{\ell|H_1}(s) = \exp\{\frac{\sigma^2}{2}s + \frac{\sigma^2}{2}s^2\} \tag{A.30}$$

But this is exactly the MGF of a Gaussian ℓ under H_1, with $\mathrm{var}\{\ell|H_1\} \triangleq \sigma_0^2$ (in accordance with (A.27)) and

$$\mathscr{E}\{\ell|H_1\} = \frac{\sigma^2}{2} = -\mathscr{E}\{\ell|H_0\} \tag{A.31}$$

as shown in Figure A.2. We conclude from (A.27), (A.31) that the variance $\mathrm{var}\{\ell|H_0\} \triangleq \sigma_0^2$ describes fully the Gaussian pdf's of ℓ under either hypothesis. In order to complete the statement of the PBF theorem, let us note that, for any LLR ℓ ,

$$M_{\ell|H_0}^{(2)} = \mathscr{E}\{\Lambda^2|H_0\} = 1 + \mathrm{var}\{\Lambda|H_0\}$$

so that the "Gaussian" distance d_G, defined as

$$d_G^2 \triangleq \ln(1 + \text{var}\{\Lambda|H_0\}) - \ln M_{\ell|H_0}(2) \qquad (A.32)$$

However, for the particular Gaussian model, (A.29) yields

$$M_{\ell|H_0}(2) = \exp\{\sigma^2\} \qquad (A.33)$$

which, when compared with (A.32) results in

$$\sigma^2 = d^2 = \ln(1 + \text{var}\{\Lambda|H_0\}) \qquad (A.34)$$

Note that the LR $\Lambda = e^{\ell}$ in (A.34) is obviously not Gaussian.

The content of this Appendix could provide the basis for exploring the properties of LLR's beyond what is presented here.

162

APPENDIX B

PROOF OF EQUATION (3.7)

Let us start from (3.4), i.e.,

$$\Lambda\left(r(t)\right) = \frac{\exp\left\{-N\gamma_c\right\}}{2^N} \sum_{i=1}^{2^N} \exp\left\{\frac{2\sqrt{S}}{N_0} \sum_{j=1}^{N} r_j \, c_{ij}\right\} \underset{H_0}{\overset{H_1}{\gtrless}} \Lambda_0$$

(B.1)

with γ_c as per (3.5), c_{ij} denoting the jth chip of the ith code pattern and r_j as per (3.6). Consider the N-dimensional linear space consisting of all binary patterns $\underline{c}_i$; $i=1,...,2^N$ of length N. Now observe that this space can be divided into two disjoint complementary subsets, each of cardinality 2^{N-1}, by the rule that, for each possible vector $\underline{c}_i$ belonging to one of the subsets, $-\underline{c}_i$ belongs to the other subset. Exactly which vectors $\underline{c}_i$ are included in which subset is immaterial as long as the above rule holds. We can now perform the summation in (B.1) over one of the two complementary subsets instead of the whole linear space, with the equivalent rule.

$$\sum_{\substack{i=1 \\ i \in \mathscr{G}}}^{2^{N-1}} \cosh\left[\left(\frac{2\sqrt{S}}{N_0}\right) \underline{r} \cdot \underline{c}_i\right] \underset{H_0}{\overset{H_1}{\gtrless}} \Lambda_0'$$

(B.2)

where $\underline{r} = (r_1,...,r_N)$, $\mathscr{G}$ is one of the aforementioned disjoint subsets and any resulting scale factors are absorbed into the threshold Λ_0'. In (B.2), cosh(x) is the hyperbolic cosine function

$$\cosh(x) = \frac{e^x + e^{-x}}{2}$$

(B.3)

163

Since $\cosh(x)$ is an even function of x, the summation in (B.2) can be extended over the whole linear space

$$\sum_{i=1}^{2^N} \cosh\left(\frac{2\sqrt{5}}{N_0}\ \underline{r}\cdot\underline{c}_i\right) \begin{array}{c} H_1 \\ \gtrless \\ H_0 \end{array} \Lambda_0$$

(B.4)

In order to proceed, we first need to introduce the superscripts $\underline{r}^{(N)}$ and $\underline{c}_i^{(N)}$, which will indicate the length of the corresponding vectors, and then prove the following:

Lemma 1. It is true that:

$$\sum_{i=1}^{2^N} \cosh\left(\underline{r}^{(N)}\cdot\underline{c}_i^{(N)}\right) = 2^N \prod_{i=j}^{N} \cosh(r_j)$$

(B.5)

Proof: The proof is by induction. First, let $N = 1$. Then,

$$\sum_{i=1}^{2} \cosh\left(\underline{r}^{(1)}\cdot\underline{c}_i^{(1)}\right) = \cosh(r_1) + \cosh(-r_1) = 2\cosh(r_1)$$

(B.6)

since $\cosh(x)$ is even function. Thus, (B.5) is satisfied for $N = 1$. Next, assume that it is true for $N = k$, i.e.,

$$\sum_{i=1}^{2^k} \cosh\left(\underline{r}^{(k)}\cdot\underline{c}_i^{(k)}\right) = 2^k \prod_{j=1}^{k} \cosh(r_j)$$

(B.7)

and prove it for $N - k + 1$. Indeed,

164

$$2^{k+1} \sum_{i=1}^{2^k} \cosh\left(\underline{r}^{(k+1)} \cdot \underline{c}_i^{(k+1)}\right) = \sum_{i=1}^{2^k} \left[\cosh\left(\underline{r}^{(k)} \cdot \underline{c}_i^{(k)} + r_{k+1}\right) + \cosh\left(\underline{r}^{(k)} \cdot \underline{c}_i^{(k)} - r_{k+1}\right)\right]$$

(B.8)

But,

$$\cosh(a+b) + \cosh(a-b) = \frac{e^{a+b} + e^{-a-b} + e^{a-b} + e^{-a+b}}{2}$$

$$= e^a\left(\frac{e^b + e^{-b}}{2}\right) + e^{-a}\left(\frac{e^n + e^{-b}}{2}\right) = \left(e^a + e^{-a}\right)\left(\frac{e^b + e^{-b}}{2}\right)$$

$$= 2\cosh(a)\cosh(b)$$

(B.9)

which, upon substitution in (B.8), yields

$$2^{k+1} \sum_{i=1}^{2^k} \cosh\left(\underline{r}^{(k+1)} \cdot \underline{c}_i^{(k+1)}\right) = \sum_{k=1}^{2^k} 2 \cosh\left(\underline{r}^{(k)} \cdot \underline{c}_i^{(k)}\right) \cosh(r_{k+1})$$

$$= 2 \cosh(r_{k+1}) \sum_{i=1}^{2^k} \cosh\left(\underline{r}^{(k)} \cdot \underline{c}_i^{(k)}\right)$$

$$= 2 \cosh(r_{k+1}) 2^k \prod_{j=1}^{k} \cosh(r_j) = 2^{k+1} \prod_{j=1}^{k+1} \cosh(r_{j+1})$$

(B.10)

where the truth of (B.8) has been used. Equation (B.10) completes the proof of Lemma 1.

If Lemma 1 is applied to (B.4), it renders it equivalent to

$$2^N \prod_{j=1}^{N} \cosh\left(\frac{2\sqrt{S}}{N_0} r_i\right) \underset{H_0}{\overset{H_1}{\gtrless}} \Lambda'_0$$

(B.11)

which is (3.7a).

165

APPENDIX C

PROOF OF EQUATIONS (3.9) - (3.10)

Let us rewrite the decision rule (3.8) as

$$\lambda = \sum_{j=1}^{N} y_j \underset{H_0}{\overset{H_1}{\gtrless}} \Lambda'_0$$

(C.1)

where the independent, identically distributed random variables (iid rv's) $y_j = r_j^2$ assume the form

$$y_j = \begin{cases} n_j^2 & \text{under } H_0 \\ (\sqrt{S}T_c c_j + n_j)^2 & \text{under } H_1 \end{cases}$$

(C.2)

In (C.2), n_j represents the Gaussian rv

$$n_j = \int_{(j-1)T_c}^{jT_c} n_I(t) \, dt$$

(C.3)

whose statistics are independent of j.

A precise analysis should account for the exact distribution of y_j under either hypothesis. So, for instance, under H_0 y_j is chi-squared rv with N degrees of freedom. For large N (of the order of hundreds or more, that is the practical case), very satisfactory approximate results can be obtained which circumvent the difficulties of an exact, but enormously complicated, analysis . This is done by invoking a central-limit-type argument: The decision statistic λ being the sum of a large number of iid rv's y_j, is approximately Gaussian distributed, with mean

$$\mathscr{E}\left\{\lambda|H_k\right\} = N\mathscr{E}\left\{y_j|H_k\right\} ; \quad k=0,1$$

(C.4a)

and variance

$$\text{var}\left\{\lambda\middle|H_k\right\} = N \,\text{var}\left\{y_j\middle|H_k\right\} ; \quad k=0,1$$

$$(\text{C.4b})$$

under either hypothesis. Thus, having the second-order statistics of the individual rv's y_j and, subsequently, of λ from (C.1) enables us to determine performance immediately.

Let

$$m = \sqrt{S}\ T_c\, c_j\, \delta_{k1} \tag{C.5}$$

so that

$$y_j = (m+n_j)^2 = m^2 + n_j^2 + 2mn_j \tag{C.6}$$

Furthermore, the Gaussian rv n_j has zero mean and variance

$$\sigma_n^{\,2} = \mathscr{E}\left\{n_j^2\right\} = \frac{N_0 T_c}{2} \tag{C.7}$$

Thus, from (C.6),

$$\begin{aligned}
\mathscr{E}\left\{y_j\right\} &= m^2 + \sigma_n^{\,2} = ST_c^{\,2}\,\delta_{k1} + \frac{N_0\, T_c}{2} \\
&= \left(N_0\, T_c\right)\left(\frac{1}{2} + \frac{ST_c}{N_0}\,\delta_{k1}\right) = \left(N_0\, T_c\right)\left(\frac{1}{2} + \gamma_c \delta_{k1}\right)
\end{aligned}$$

$$(\text{C.8})$$

Finally,

$$\text{var}\{y_j\} = \text{var}\,\{m^2+n_j^2+2mn_j\} = \text{var}\{n_j^2+2mnj\} = \text{var}\{n_j^2\} + 4m^2\,\text{var}\{n_j\} \tag{C.9}$$

since the random variables n_j^2 and n_j are uncorrelated ($\mathscr{E}\{n_j^3\} = 0$). Thus,

$$\text{var}\{y_j\} = (3\sigma_n^4 - \sigma_n^4) + 4m^2\sigma_n^2 = 2\sigma_n^2[\sigma_n^2 + 2m^2] = (N_0T_c)^2[1/2 + 2\gamma_c\delta_{k1}] \qquad (C.10)$$

Equation (3.9) results from combining (C.8) and (C.10) with (C.4).

APPENDIX D

PERFORMANCE OF RULE (3.19)

A Gaussian-approximation-based analysis of the low-SNR, chip-noncoherent detector (3.19) can be performed following guidelines similar to those in Appendix C, as follows: Let the bandpass AWGN $n(t)$ be represented by

$$n(t) = \sqrt{2} \left\{ n_I(t) \cos \omega_0 t - n_Q(t) \sin \omega_0 t \right\} \tag{D.1}$$

where $n_I(t)$ and $n_Q(t)$ are baseband, independent, Gaussian processes with a flat one-sided PSD of N_0 W/Hz each. Conditioned on the unknown phase ϕ_j and the ± 1-chip c_j of the interval $(j-1) T_c \geq t \geq j T_c$, the inphase and quadrature variables r_{I_j} and r_{Q_j} of (3.15c) are Gaussian with means

$$\mathscr{E}\left\{ r_{I_j} \big| \phi_j, c_j \right\} = \sqrt{S} \; T_c \; c_j \; \delta_{k1} \cos \phi_j$$

$$\begin{array}{l} j=1,2,\ldots,N \\ k=0,1 \end{array}$$

$$\mathscr{E}\left\{ r_{Q_j} \big| \phi_j, c_j \right\} = \sqrt{S} \; T_c \; c_j \; \delta_{k1} \sin \phi_j$$

$$\tag{D.2}$$

and common variance σ_n^2

$$\sigma_n^2 \triangleq \text{var}\left\{ r_{I_j} \right\} = \text{var}\left\{ r_{Q_j} \right\} = \frac{N_0 T_c}{2} \tag{D.3}$$

Thus, averaging the phase [1] ϕ_j, it follows that each of the independent envelope rv's r_j of (3.18) has, under H_1, a Rician distribution

---

[1] Again it is easily seen that the value of c_j becomes irrelevant due to the squaring.

$$f\left(r_j \big| H_1\right) = \frac{r_j}{\sigma^2} \exp\left[-\frac{1}{2}\left(\frac{r_j^2}{\sigma^2} + 2\gamma_c\right)\right] I_0\left(\frac{r_j}{\sigma}\sqrt{2\gamma_c}\right) (r_j \geqslant 0) \quad j=1,2,\ldots,N$$

$$\text{(D.4)}$$

where γ_c is the predetection SNR while, under H_0 (i.e., signal absent, $\gamma_c = 0$), (D.4) reduces to a Rayleigh distribution

$$f\left(r_j \big| H_0\right) = \frac{r_j}{\sigma^2} \exp\left[-\frac{r_j^2}{2\sigma^2}\right] (r_j \geqslant 0)$$

$$\text{(D.5)}$$

Therefore, the statistics of the decision rv λ in (3.19), being the sum of N iid rv's, can be precisely found (see (3.21 a,b) in text).

Although those results are exact, they are cumbersome to use from a computational viewpoint, especially for large N (N > 100). Besides, the Gaussian approximation about λ becomes suffficiently tight in that region and, thus, emerges as an attractive and simple tool.

Let us start from the fact that

$$r_{I_j} = \sqrt{S}\, T_c\, c_j\, \delta_{k1} \cos\phi_j + n_{I_j}$$

$$\text{(D.6a)}$$

and

$$r_{Q_j} = \sqrt{S}\, T_c\, c_j\, \delta_{k1} \sin\phi_j + n_{Q_j}$$

$$\text{(D.6b)}$$

In (D.9), the Gaussian rv's n_{I_j} and n_{Q_j} are defined by

$$n_{I_j} = \int_{(j-1)T_c}^{jT_c} n_I(t) \, dt$$

(D.7a)

and

$$n_{Q_j} = \int_{(j-1)T_c}^{jT_c} n_Q(t) \, dt$$

(D.7b)

and are, therefore, mutually independent, each with zero mean and variance σ_N^2.

Then, the squared envelope r_j^2 is

$$r_j^2 = r_{I_j}^2 + r_{Q_j}^2 = ST_c^2 \, \delta_{k1} + n_{I_j}^2 + n_{Q_j}^2 + 2\sqrt{S} \, T_c \, c_j \, \delta_{k1}\left(n_{I_j} \, \phi_j + n_{Q_j} \sin \phi_j\right)$$

(D.8)

It immediately follows that

$$\mathscr{E}\left\{r_j^2\right\} = ST_c^2 \, \delta_{k1} + 2\sigma_n^2 = ST_c^2 \, \delta_{k1} + N_0 T_c = \left(N_0 T_c\right)\left(1 + \gamma_c \, \delta_{k1}\right)$$

(D.9)

which is (3.22d)

In order to calculate the variance of r_j in (D.8), we note that the first term is a constant (thus, it can be neglected), while the second, third and fourth terms are pairwise uncorrelated. This is because: (a) $n_{I_j}^2$ and $n_{Q_j}^2$ are functions of independent rv's and, (b) the fourth term includes both c_j and ϕ_j, which are independent of the noise and zero mean. As a conclusion,

$$\text{var}\left\{r_j^2\right\} \triangleq \mathscr{E}\left\{\left(r_j^2 - \mathscr{E}\left\{r_j^2\right\}\right)^2\right\} = \text{var}\left\{n_{Ij}^2\right\} + \text{var}\left\{n_{Qj}^2\right\}$$

$$+ 4ST_c^2 \delta_{k1} \text{var}\left\{n_{Ij} \cos\phi_j + n_{Qj} \sin\phi_j\right\}$$

$$= 4\sigma_n^4 + 4ST_c^2 \sigma_n^2 \delta_{k1} = \left(N_0 T_c\right)^2 + 2 ST_c^3 N_0 \delta_{k1}$$

$$= \left(N_0 T_c\right)^2 \left(1 + 2\gamma_c \delta_{k1}\right)$$

$$(D.10)$$

since

$$\text{var}\left\{\cos\phi_j\right\} = \text{var}\left\{\sin\phi_j\right\} = \frac{1}{2}$$

Equation (D.10) is identical to equation (3.22b).

172

where noises n_{j2} and $n_{j+1,1}$, are mutually independent, as are c_j and c_{j+1}.

Thus,

$$\mathscr{E}\left\{r_{j2}\ r_{j+1,1}\right\} = S\left(\frac{T_c}{2}\right)^2 \delta_{k1}\ \mathscr{E}\left\{c_j\ c_{j+1}\right\} + \mathscr{E}\left\{n_{j2}\ n_{j+1,1}\right\} = 0$$

In an analogous way,

$$r_{j1} = \sqrt{S}\left(\frac{T_c}{2}\right)c_j\ \delta_{k1} + n_{j1}$$

(E.5)

which, combined with (E.3) yields

$$\mathscr{E}\left\{r_{j1}\ r_{j2}\right\} = \frac{ST_c^2}{4}\ \delta_{k1} + \mathscr{E}\left\{n_{j1}\ n_{j2}\right\} = \frac{ST_c^2}{4}\ \delta_{k1}$$

(E.6)

by virtue of independence between n_{j1} and n_{j2}. Finally, substituting the above into (3.41) yields

$$\mathscr{E}\left\{\lambda_2\ |H_k\ ;\ \epsilon=0\right\} = N\left[2\ \mathscr{E}\left\{r_{j1}^2\right\} + \mathscr{E}\left\{r_{j1}\ r_{j2}\right\}\right]$$

$$= N\left[\frac{\left(N_0 T_c\right)}{2}\left(1 + \gamma_c\ \delta_{k1}\right) + \frac{ST_c^2}{4}\ \delta_{k1}\right]$$

$$= N\left(\frac{N_0 T_c}{2}\right)\left[1 + \gamma_c\ \delta_{k1} + \frac{\gamma_c}{2}\ \delta_{k1}\right]$$

$$= N\left(\frac{N_0 T_c}{2}\right)\left[1 + \left(\frac{3}{2}\right)\gamma_c\ \delta_{k1}\right]$$

(E.7)

Before we proceed with var $\{\lambda_2|\ H_0\}$, let us for a minute turn to the worst-case mean of (3.41) as explained in the report. However, the picture now is changed to Figure E.2, under the assumption of a worst epoch $\epsilon = 1/4$. Then, we can write that

$$r_{j2} = \sqrt{S}\left(\frac{T_c}{2}\right)c_j\ \delta_{k1} + n_{j2}$$

(E.8)

175
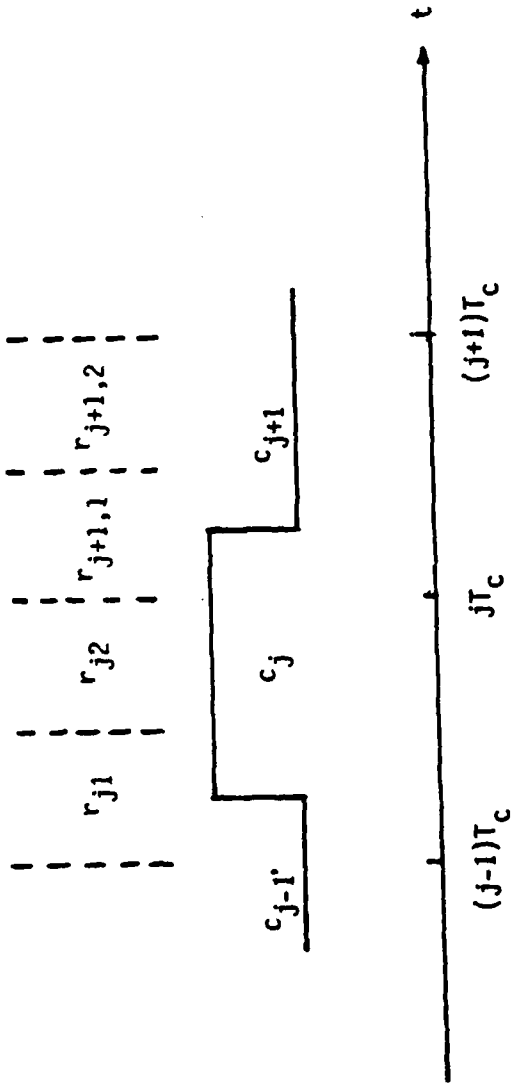
Figure E.2   Definition of r_j's, Assuming H_1 and $\epsilon = 1/4$.

176

and

$$r_{j1} = \sqrt{S}\left(\frac{T_c}{4}\right)\left[c_{j-1} + c_j\right] + n_{j1}$$

(E.9)

Note that r_{j2} is identical to (E.3); thus, $\mathscr{E}\{r_{j2}{}^2|H_k; \varepsilon = 1/4\}$ is the same as above.

Futhermore

$$\mathscr{E}\left\{r_{j1}{}^2\Big|H_k;\varepsilon=1/4\right\} = \left(\tfrac{1}{2}\right)\left[\mathscr{E}\left\{r_{j1}{}^2\Big|H_k;\varepsilon=1/4;A_{same}\right\} + \mathscr{E}\left\{r_{j1}{}^2\Big|H_k;\varepsilon=1/4;A_{diff}\right\}\right]$$

(E.10)

where the conditioning events A_{same} and A_{diff} refer to c_{j-1} and c_j having the same or a different sign. Clearly,

$$P_r\{A_{same}\} = P_r\{A_{diff}\} = 1/2$$

(E.11)

a fact used in (E.10). Let us now note that, under A_{diff}, the mean of r_{ji} is zero while, under A_{same}, it is equal to $\sqrt{S}\ T_c/2$. Thus,

$$\mathscr{E}\left\{r_{j1}{}^2\Big|H_k;\varepsilon=1/4\right\} = \left(\tfrac{1}{2}\right)\left[\left(\frac{N_0 T_c}{4}\right)\left(1 + \gamma_c\ \delta_{k1}\right) + \left(\frac{N_0 T_c}{4}\right)\right] = \left(\frac{N_0 T_c}{4}\right)\left[1 + \tfrac{1}{2}\ \gamma_c\ \delta_{k1}\right]$$

(E.12)

In exactly the same way,

$$\mathscr{E}\left\{r_{j1}\ r_{j2}\Big|H_k;\varepsilon=1/4\right\} = S\left(\frac{T_c{}^2}{8}\right)\mathscr{E}\left\{c_j\left(c_{j-1} + c_j\right)\right\}\delta_{k1} + \mathscr{E}\left\{n_{j1}\ n_{j2}\right\}$$

$$= \left(\frac{S T_c}{N_0}\right)\left(\frac{N_0 T_c}{8}\right)\delta_{k1} = \left(\frac{N_0 T_c}{4}\right)\left(\frac{\gamma_c}{2}\right)\delta_{k1}$$

(E.13)

which is identical to $\mathscr{E}\{r_{j2}r_{j+1,1}\ |\ H_k;\varepsilon = 1/4\}$.

Put together, the above result in

$$\mathcal{E}\{\lambda_2|H_k;\epsilon = 1/4\} = N\left(\frac{N_0T_c}{2}\right)\left[1 + \frac{5}{4}\gamma_c\delta_{kl}\right]$$

(E.14)

In both cases, var $\{\lambda_2|H_0\}$ is the same. A straight-forward calculation can show it to be

$$\text{var}\{\lambda_2|H_0\} = \left(\frac{3}{4}\right) \ N \ \frac{(N_0T_c)2}{2}$$

(E.15)

Combining (E.7) and (E.14) with (E.15) results in (3.42) and (3.43), respectively.

178

APPENDIX F

ANALYSIS OF THE RADIOMETRIC DETECTOR

Here we briefly develop the LPI performance of the radiometer, as shown in Figure 9, when the input $r(t)$ is as per (3.2). The output $r_{BP}(t)$ of the rectangular BP filter is

$$r_{BP}(t) = \sqrt{2S}\,\bar{c}(t)\,\cos(\omega_0 t + \phi) + n_{BP}(t) \qquad \text{(F.1)}$$

where $n_{BP}(t)$ is filtered AGN with the typical BP representation

$$n_{BP}(t) = \sqrt{2}\left[n_I(t)\,\cos\,\omega_0 t + n_Q(t)\,\sin\,\omega_0 t\right] \qquad \text{(F.2)}$$

In (F.2), $n_I(t)$ and $n_Q(t)$ are independent zero-mean jointly Gaussian low-pass noise processes, each with a flat PSD of N_0 W/Hz (one-sided) and bandwidth of $W_{BP}/2$ Hz (one-sided). The code signal, filtered by the BPF, is designated $c(t)$ in (F.1). The zonal LPF (shown for analytical purposes only) rejects the $2f_0$ components of the square-law output $z(t)$ and has an output given by

$$z_{LP}(t) = S\left(\bar{c}(t)\right)^2 + n_I^{\,2}(t) + n_Q^{\,2}(t) + 2\sqrt{S}\,\bar{c}(t)\,n_I(t) \qquad \text{(F.3)}$$

In order to maintain analytical tractability, we approximate and model $\bar{c}(t)$ as an attenuated, but undistorted, version of $c(t)$, namely,

$$\bar{c}(t) \triangleq \alpha c(t) \qquad \text{(F.4)}$$

179

where the "attenuation factor" α^2 measures the (normalized) power reduction due to filtering

$$\alpha^2 \triangleq \frac{\int_{-\infty}^{\infty} |H_L(f)|^2 S_c(f) df}{\int_{-\infty}^{\infty} S_c(f) df} = \left(\frac{2}{\pi}\right) \int_0^{\pi W_{BP} T_c / 2} \left(\frac{\sin x}{x}\right)^2 dx$$

(F.5)

since, for a ± 1-valued code, the denominator of (F.5) equals $c^2(t) = 1$. In the previous expression, $S_c(f)$ is the PSD of the random code signal $c(t)$ and $H_L(f)$ is the low-pass equivalent of the BPF $H_{BP}(f)$, i.e.,

$$H_L(f) = \begin{cases} 1 & |f| \leq W_{BP}/2 \\ 0 & , \text{ otherwise} \end{cases}$$

(F.6)

By suitably adjusting $H_L(f)$, (F.5) can be generalized to filters other than the perfectly rectangular one considered above.

From the above definitions, it follows that $(\bar{c}(t))^2 = \alpha^2$

Thus,

$$z_{LP}(t) = \alpha^2 S + n_I^2(t) + n_Q(t) + 2\sqrt{S} \alpha c(t) n_I(t)$$

(F.7)

under H_1. Under the alternative H_0, $z_{LP}(t)$ is given by the above expression with $S = 0$. It follows that

$$\mathscr{E}\left\{z_{LP}(t)|H_k\right\} = \alpha^2 S \delta_{k1} + N_0 W_{BP}; \quad k = 0, 1$$

(F.8)

with δ_{k1} as per (3.9c). Thus, the expected value of $E\{\lambda|H_k\}$ of test statistic λ at the output of the integrator in Figure 9 can be calculated under either hypotheses H_k; $k = 0,1$, as

$$\mathscr{E}\{\lambda|H_k\} = \int_0^{NT_c} \mathscr{E}\{z_{LP}(t)|H_k\}dt = NT_c\left[N_0W_{BP} + \alpha^2S\delta_{k1}\right]; \ k=0,1$$

(F.9)

The next step is to obtain the second-order statistics of $z_{LP}(t)$ and λ. The typical approach, based on the assumption $W_{BP}NT_c \gg 1$, is to model $z_{LP}(t)$ as a very wide-band ("delta-correlated") process with respect to the approximate bandwidth $(NT_c)^{-1}$ of the integrator. Thus, one needs to evaluate only the PSD of $z_{LP}(t)$ at the origin $f = 0$, distinguishing between the average (constant) contribution and the random contribution. Using the fact that $n_I(t)$ and $n_Q(t)$ are Gaussian, the autocorrelation function of $z_{LP}(t)$ can be obtained directly, from which its PSD under H_1 is given by

$$S_{z_{LP}}(f) = \left(\alpha^2S + N_0W_{BP}\right)^2 \delta(f) + 4S_{n_I}(f) \circledast S_{n_Q}(f) + 4\alpha^2 S S_c(f) \circledast S_{n_I}(f)$$

(F.10)

where $\circledast$ means "convolved with." The coefficient of the Dirac delta function $\delta(f)$ agrees with the first-order statistics of $z_{LP}(t)$ obtained directly in (F.7). The two-sided PSD of $z_{LP}(t)$ at $f = 0$ measures its random contribution and is obtained by evaluating the last two terms $S_{z_{LP}}(f)$ in (F.9) with $f = 0$, resulting in

$$S_{z_{LP}}(f)\Big|_{f=0} = N_0^2 W_{BP} + 2\alpha^4 SN_0 \delta_{k1} \ ; \ k=0,1$$

(F.11)

The delta-correlated random part of $z_{LP}(t)$ contributes to the variance of λ as

$$\text{var}\{\lambda|H_k\} = \left(NT_c\right)S_{z_{LP}}(0) = \left(NT_c\right)\left(N_0^2W_{BP} + 2\alpha^4 SN_0 \delta_{k1}\right)$$

(F.12)

181

The mean and variance of λ in (F.8) and (F.11) suffice to characterize performance under the Gaussian assumption which hinges on the fact that $W_{BP}NT_c \approx N >> 1$. The result is (3.10a) with

$$a = \sqrt{\frac{\alpha^4}{W_{BP}T_c}} \; ; \; b = 2a^2$$

(F.13)

Clearly, the choice of W_{BP} has an impact on α through (F.12) and α^2 in (F.5). The quantity

$$a = \frac{\alpha^2}{\sqrt{W_{BP}T_c}} = \frac{\left(\frac{2}{\pi}\right) \int_0^{\pi W_{BP}T_c/2} \left(\frac{\sin x}{x}\right)^2 dx}{\sqrt{W_{BP}T_c}}$$

(F.14)

has been plotted in Figure F.1 as a function of the product $W_{BP}T_c$. The maximum $\alpha_{max} \approx 0.77$ (or -1.1 dB) is attained at $W_{BP}T_c \approx 1$.
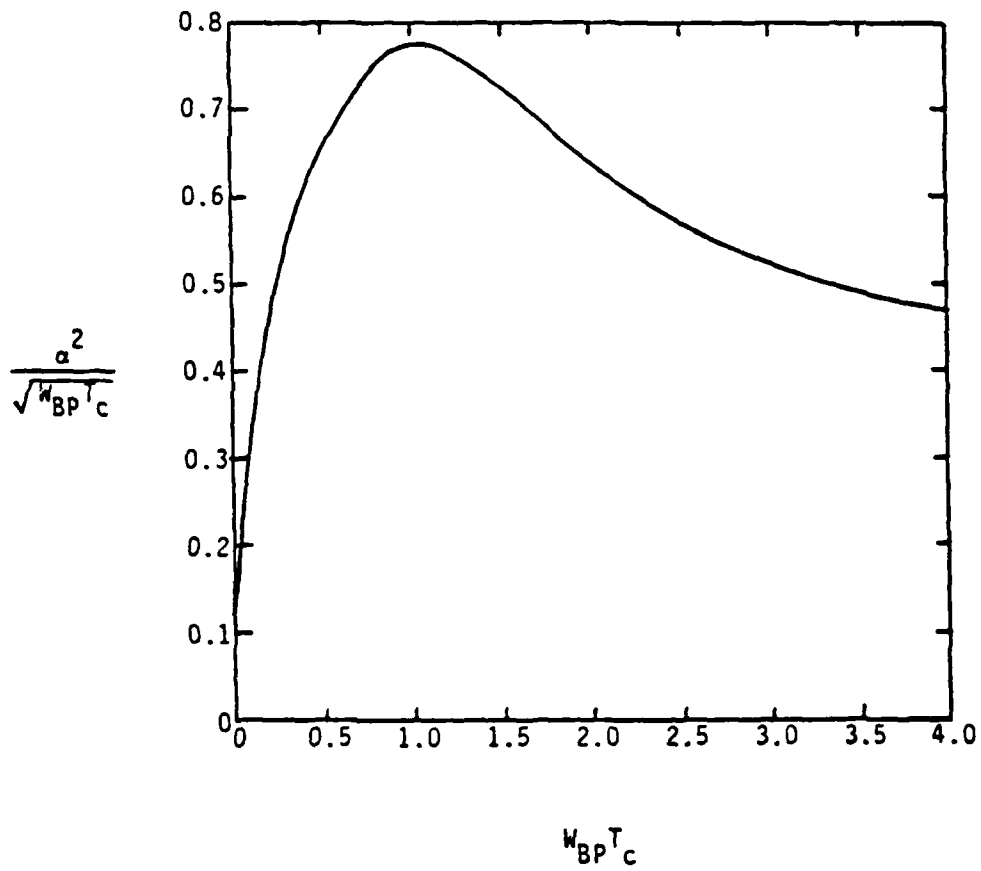
Figure F.1. SNR Attenuation Due to the Choice of W_{BP} in the Radiometer

183

APPENDIX G

DERIVATION OF EQUATION (3.50)-(3.52)

Let

$$\lambda = \sum_{j=1}^{N} y_j \underset{H_0}{\overset{H_1}{\gtrless}} \Lambda_0'$$

(G.1)

be the decision rule (3.48), where

$$y_j = r^{(1)} r_j^{(2)}$$

(G.2)

and $r_j^{(i)}$; $i = 1,2$ is given by (3.49). Then,

$$r_j^{(i)} = \sqrt{S}\, T_c\, c_j\, \delta_{k1} + n_j^{(i)}$$

(G..3)

where $n_j^{(1)}$ and $n_j^{(2)}$ are zero mean, mutually independent Gaussian rv's with common variance $\sigma_n^2 = N_0 T_c/2$. From (G.2) and (G.3), it follows that

$$y_j = S\, T_c^2\, \delta_{k1} + \sqrt{S}\, T_c\, c_j\, \delta_{k1}\left(n_j^{(1)} + n_j^{(2)}\right) + n_j^{(1)}\, n_j^{(2)}$$

(G.4)

Thus,

$$\mathscr{E}\left\{y_j\right\} = S\, T_c^2\, \delta_{k1} = \left(N_0 T_c\right)\gamma_c\, \delta_{k1}$$

(G.5)

which justifies (3.50). Futhermore

184

$$\text{var}\left\{y_j\right\} = S \, T_c^2 \, \delta_{k1} \, \text{var}\left\{n_j^{(1)} + n_j^{(2)}\right\} + \text{var}\left\{n_j^{(1)} \, n_j^{(2)}\right\}$$

$$= S \, T_c^2 \, \delta_{k1} \, 2\sigma_n^2 + \sigma_n^4 = 4\sigma_n^4\left[\left(\frac{1}{4}\right) + \frac{S T_c^2}{2\sigma_n^2} \, \delta_{k1}\right]$$

$$= \left(N_0 T_c\right)^2\left[\frac{1}{4} + \gamma_c \, \delta_{k1}\right]$$

as per (3.51). From (3.50), (3.51), equation (3.52) follows immediately.

APPENDIX H

DERIVATION OF (4.13)

Let $R = R_{km}$ in (4.10) and (4.11). Then, following steps identical to (4.7) yields (4.10)

$$d_{l,\text{noscod}}^2 = Q \ln\left[1 + \frac{\exp\{-2\gamma_H\}}{N_F} \operatorname{var}_{H_0}\left\{I_0\left(\frac{2\sqrt{S}}{N_0}R\right)\right\}\right]$$

(H.1)

where the density of R under H_1 is the Rician

$$f(R|H_1) = \frac{R}{\sigma_n^2}\exp\{-\gamma_H\}\exp\left\{-\frac{1}{2}\frac{R^2}{\sigma_n^2}\right\}I_0\left(\frac{2\sqrt{S}}{N_0}R\right)$$

(H.2a)

with

$$\sigma_n^2 = \frac{N_0 T_H}{2}$$

(H.2b)

and $\gamma_H = ST_H/N_0$. We note further that

$$\Lambda(R) = \exp\{-\gamma_H\}I_0\left(\frac{2\sqrt{S}}{N_0}R\right)$$

(H.3)

is an LR. Thus, from the known properties of LR's

$$\mathscr{E}\{\Lambda|H_0\} = 1 \Rightarrow \mathscr{E}\left\{I_0\left(\frac{2\sqrt{S}}{N_0}R\right)\Big|H_0\right\} = e^{\gamma_H}$$

(H.4)

and

$$\mathscr{E}\{\Lambda^2|H_0\} = \mathscr{E}\{\Lambda|H_1\} = \int_0^\infty \Lambda(R)f(R|H_1)\,dR.$$

(H.5)

Substituting (H.2), (H.3) into (H.5) and letting $x = R/\sigma_n$ yields

$$\mathscr{E}\left\{\Lambda^2|H_0\right\} = \exp\left\{-2\gamma_H\right\}\int_0^\infty x \exp\left\{-\frac{x^2}{2}\right\} I_0^2\left[\sqrt{2\gamma_H}\,x\right] dx.$$

(H.6)

From [21, pp. 718, 6.633.2].

$$\int_0^\infty e^{-\rho^2 x^2} J_p(\alpha x) J_p(\beta x) x\, dx$$
$$= \frac{1}{2\rho^2}\exp\left\{-\frac{\alpha^2+\beta^2}{4\rho^2}\right\} I_p\left(\frac{\alpha\beta}{2\rho^2}\right)$$

(H.7)

Letting $\rho^2 = 1/2$, $\alpha = \beta = \sqrt{2\gamma_H}$, $\rho = 0$ (here $j = \sqrt{-1}$) and using the fact that $I_0(x) = J_0(jx)$ in (H.6) and (H.7) results in

$$\mathscr{E}\left\{I_0^2\left(\frac{2\sqrt{S}}{N_0}R\right)\Big|H_0\right\} = \exp\left(2\gamma_H\right) I_0(2\gamma_H)$$

(H.8)

Combining (H.1), (H.4) and (H.8) provides (4.12). As a byproduct, we note from (H.3), (H.5), and (H.8) that

$$\mathscr{E}\left\{I_0\left(\frac{2\sqrt{S}}{N_0}R\right)\Big|H_1\right\} = \exp\left(\gamma_H\right) I_0(2\gamma_H)$$

(H.9)

187

APPENDIX I

EVALUATION OF d_A FOR CASE II

We consider here the Case II, where no power adjustment takes place in the decision rule (i.e., (5.8) is used), but the actual frequency offset of the incoming signal with respect to the observed spectral points is the worst, namely $\Delta f = R_H /2$. The case is depicted in Figure I.1. Note that, in principle, a residual signal power can be measured in frequencies beyond the two adjacent ones (f_i, f_{i+1}), but that amount is insignificant and can be neglected. On the other hand, each of the adjacent spectral slots observes a tone of power αS (α as per (5.13)) in noise, so that the the probability density function (pdf) of the envelope R in each adjacent slot is the Rician pdf

$$f_R\left(R \middle| \begin{array}{c} signal \\ present \end{array}\right) = \frac{R}{\sigma_n^2} e^{-\alpha \gamma_H} e^{-\frac{1}{2}\frac{R^2}{\sigma_n^2}} I_0\left(\frac{2\sqrt{\alpha S}}{N_0} R\right)$$

(I.1)

where γ_H is the hop SNR and $\sigma_n^2 = N_0 T_H/2$ is the noise variance in each quadrature component of the bandpass additive Gaussian noise. Since, in the absence of the signal, the mean and variance of $I_0(2\sqrt{S} R/N_0)$ remain as per (5.11a,b), we only need to evaluate

$$\mathscr{E}\left\{I_0\left(\frac{2\sqrt{S}}{N_0} R\right)\middle| \begin{array}{c} signal \\ present \end{array}\right\} = \int_0^\infty I_0\left(\frac{2\sqrt{S}}{N_0} R\right) f_R\left(R \middle| \begin{array}{c} signal \\ present \end{array}\right) dR$$

(I.2)

with the pdf as in (I.1). Setting $R \stackrel{\Delta}{=} R/\sigma_n$ in (I.2) yields

$$\mathscr{E}\left\{I_0\left(\frac{2\sqrt{S}}{N_0} R\right)\middle| \begin{array}{c} signal \\ present \end{array}\right\} = e^{-\alpha \gamma_H} \int_0^\infty r e^{-\frac{r^2}{2}} I_0\left(\sqrt{2\gamma_H} r\right) I_0\left(\sqrt{2\alpha\gamma_H} r\right) dr$$

(I.3)

188
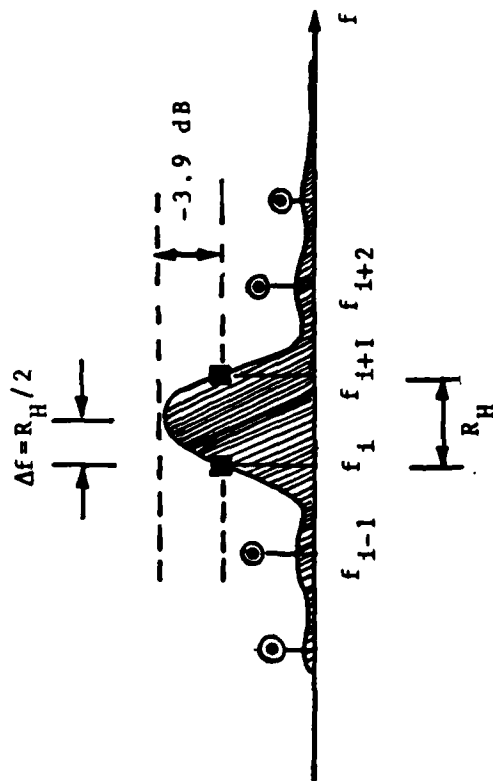
Figure I1: Worst-case frequency offset where $f_n; n=i-1, i, i+1, \ldots$ are the measured spectral positions.

■ = signal-plus-noise measurement
⊙ = effectively noise-only measurement

189

The latter integral can be evaluated by proper modification of the expression in [21, p.718], yielding

$$\mathscr{E}\left\{I_0\left(\frac{2\sqrt{S}}{N_0}\ R\middle|\ \begin{matrix}\text{signal}\\\text{present}\end{matrix}\right)\right\} = e^{-\alpha\gamma_H}\left[I_0(2\sqrt{\alpha}\ \gamma_H)e^{(1+\alpha)\gamma_H}\right]$$

$$= e^{\gamma_H}I_0\left(2\sqrt{\alpha}\ \gamma_H\right)$$

(I.4)

Fianlly, noting from Figure (I.1) that the expression (I.4) pertains to 2 slots (under H_1), while the remaining (G-2) are only noise, yields

$$\mathscr{E}\{\Lambda|\ H_1;\text{Case II}\} = 2e^{\gamma_H}\ I_0(2\sqrt{\alpha}\ \gamma_H) + (G-2)e^{\gamma_H}$$

(I.5)

instead of (5.11a). Putting (I.5), (5.1b), (5.10c) and d_Λ^2 together results in

$$d_\Lambda^2 = 4G^{-1}\left[\frac{(I_0(2\sqrt{\alpha}\ \gamma_H)-1)^2}{I_0(2\gamma_H)-1}\right]$$

(I.6)

as per Table 1 in Section 5.2.

A final note is in regard to the notation in (I.1)-(I.4): we condition on "signal present", as opposed to "H_1", because the above expectations pertain to the slots which truly contain a signal component, while "H_1" simply means "signal in some slots in the bandwidth B".

APPENDIX J

STATISTICAL CHARACTERIZATION OF NOISE PROCESSES
$N_I^{eq}(\tau)$ AND $N_Q^{eq}(\tau)$

We define $N_I^{eq}(\tau)$ and $N_Q^{eq}(\tau)$ as per (5.45) and (5.40). It then follows from (5.41), (5.42) and (5.43) that $N_I^{eq}(\tau_k)$, $N_Q^{eq}(\tau_k)$; $\tau_k = KB^{-1}$ are zero-mean random variables, i.e., (5.46). Furthermore, by virtue of a central-limit-type argument (summations of a large number of rv's), they are assumed to be approximately Gaussian.

We shall first show that $N_I^{eq}(\tau_k)$ and $N_Q^{eq}(\tau_j)$ are uncorrelated for every k and j; in which case, they are also approximately independent (due to the Gaussian assumption). Indeed, from (5.45a).

$$\mathcal{E}\left\{N_I^{eq}(\tau_k)\, N_Q^{eq}(\tau_j)\right\} = \mathcal{E}\left\{N_{II}(\tau_k)\, N_{IQ}(\tau_j)\right\} + \mathcal{E}\left\{N_{QQ}(\tau_k)\, N_{IQ}(\tau_j)\right\}$$
$$- \mathcal{E}\left\{N_{II}(\tau_k)\, N_{QI}(\tau_j)\right\} - \mathcal{E}\left\{N_{QQ}(\tau_k)\, N_{QI}(\tau_j)\right\}$$

$$(J.1)$$

Let us consider the first term on the right-hand side of (J.1); a similar line of argument applies to the next three terms. By definition,

$$\mathcal{E}\left\{N_{II}(\tau_k)\, N_{IQ}(\tau_j)\right\} = \int_{\tau_k}^{T_H} \int_{\tau_k}^{T_H} \mathcal{E}\left\{n_I(t_1)n_I(t_1-\tau_k)n_I(t_2)n_Q(t_2-\tau_j)\right\} dt_1 dt_2$$

$$(J.2)$$

However, $n_Q(t)$ is independent of $n_I(t)$, which implies that the integrand of (J.2) contains the factor $\mathcal{E}\{n_Q(t_2-\tau_j)\}$, which is zero. Thus,

$$\mathcal{E}\left\{N_{II}(\tau_k)\, N_{IQ}(\tau_j)\right\} = 0$$

$$(J.3)$$

191

Along with (J.1) and the above remarks, (J.3) establishes the uncorrelatedness of $N_I^{eq}(\tau_k)$ and $N_Q^{eq}(\tau_j)$.

Let us now consider $N_I^{eq}(\tau_{k_1})$ and $N_I^{eq}(\tau_{k_2})$ for $\tau_{k_1} \neq \tau_{k_2}$. We have that

$$\mathscr{E}\left\{N_I^{eq}(\tau_{k_1})N_I^{eq}(\tau_{k_2})\right\} = \mathscr{E}\left\{N_{II}(\tau_{k_1})N_{II}(\tau_{k_2})\right\} + \mathscr{E}\left\{N_{QQ}(\tau_{k_1})N_{QQ}(\tau_{k_2})\right\}$$

$$+ \mathscr{E}\left\{N_{II}(\tau_{k_1})N_{QQ}(\tau_{k_2})\right\} + \mathscr{E}\left\{N_{QQ}(\tau_{k_1})N_{II}(\tau_{k_2})\right\}$$

$$(J.4)$$

But,

$$\mathscr{E}\left\{N_{II}(\tau_{k_1})N_{II}(\tau_{k_2})\right\}_{\tau_{k_1} \neq \tau_{k_2}} = \int_{\tau_{k_1}}^{T_H}\int_{\tau_{k_2}}^{T_H} \mathscr{E}\left\{n_I(t_1)n_I(t_1 - \tau_{k_1})n_I(t_2)n_I(t_2 - \tau_{k_2})\right\}dt_1 dt_2$$

$$(J.5)$$

We shall approximate the integral (J.5) as the double sum

$$\mathscr{E}\left\{N_{II}(\tau_{k_1})N_{II}(\tau_{k_2})\right\}_{k_1 \neq k_2} = (\Delta\tau)^2 \sum_{k=k_1}^{G}\sum_{m=k_2}^{G}\mathscr{E}\left\{n_I(k)n_I(k-k_1)n_I(m)n_I(m-k_2)\right\}$$

$$(J.6)$$

where $\Delta\tau = \tau_1 = B^{-1}$. We note that $n_I(k)$ and $n_I(k)$ and $n_I(k-k_1)$ are independent rv's since $k_1 \neq 0$, as are $n_I(m)$ and $n_I(m-k_2)$. Furthermore, due to the independence of the rv's involved, the expectation in (J.6) will be zero whenever all four sampling times k, $k-k_1$, m, $m-k_2$ are pairwise different, as shown in Figure J.1(a). If we assume that $k_1 < k_2$, we then observe that the three remaining cases depicted in Figure J.1 are (b) $k-k_1 = m-k_2$; in which case, $k \neq m$, or (c) $k = m$; in which case, $k-k_1 \neq m-k_2$, or (d) $k=m-k_2$; in which case, $k-k_1 \neq m$. In all those cases, the common conclusion is that at least two rv's exist which do not coincide with the others. The net result is that the expectation in (J.6) will always be zero, establishing the approximate uncorrelatedness of $N_{II}(\tau k_1)$ and $N_{II}(\tau k_2)$. The same exact argument establishes that $\mathscr{E}\{N_{QQ}(\tau k_1) N_{II}(\tau k_2)\} \cong 0$, while it is even easier to

192
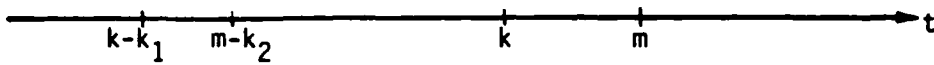
(a) All sampling times different
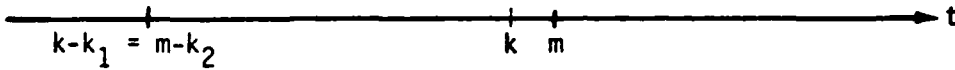
(b) $k - k_1 = m - k_2$

(c) $k = m$
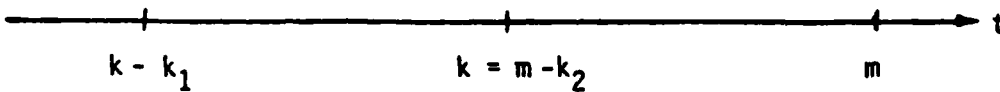
(d) $k = m - k_2$

Figure J.1. Some Possible Combinations of Sampling Times in (J.6)

show that $\mathscr{E}\{N_{II}(\tau_{k1})\, N_{QQ}(\tau_{k2})\} \cong \mathscr{E}\{N_{QQ}(\tau_{k1})N_{II}(\tau_{k2})\} \cong 0$. Thus all of the above can be combined in (J.4) to illustrate that different samples ($\tau_{k_1} \neq \tau_{k_2}$) of the same process N_I^{eq} are approximately uncorrelated. It can similarly be demonstrated that the same is true for $N_Q^{eq}(\tau)$, defined in (5.45c).

Finally, we are concerned with the variance of $N_I^{eq}(\tau_k)$ and $N_Q^{eq}(\tau_k)$. Clearly, since the respective means are zero, those variances coincide with the second moments. Furthermore,

$$\mathscr{E}\left\{\left(N_I^{eq}(\tau_k)\right)^2\right\} = \mathscr{E}\left\{N_{II}^2(\tau_k)\right\} + \mathscr{E}\left\{N_{QQ}^2(\tau_k)\right\} = 2\mathscr{E}\left\{N_{II}^2(\tau_k)\right\}$$

(J.7)

But,

$$\mathscr{E}\left\{N_{II}^2(\tau_k)\right\} = \int_{\tau_k}^{T_H} \int_{\tau_k}^{T_H} \mathscr{E}\left\{n_I(t_1)n_I(t_1-\tau_k)n_I(t_2)n_I(t_2-\tau_k)\right\} dt_1 dt_2$$

$$= \int\int_0^{T_H-\tau_k} \mathscr{E}\left\{n_I(t_1'+\tau_k)n_I(t_1')n_I(t_2'+\tau_k)n_I(t_2')\right\} dt_1' dt_2'$$

(J.8)

where a simple change of variables has been performed. We shall now use a familiar property of four jointly Gaussian rv's $\{x_i\}_{i=1}^4$, namely,

$$\mathscr{E}\left\{\prod_{i=1}^4 x_i\right\} = \mathscr{E}\{x_1 x_2\}\,\mathscr{E}\{x_3 x_4\} + \mathscr{E}\{x_1 x_3\}\mathscr{E}\{x_2 x_4\} + \mathscr{E}\{x_1 x_4\}\mathscr{E}\{x_2 x_3\}$$

(J.9)

Applying (J.9) into (J.8) results in (for any τ):

194

$$\mathcal{E}\left\{N_{II}^2(\tau)\right\} = \int\!\!\!\int_0^{T_H-\tau} \mathcal{E}\left\{n_I(t_1'+\tau)n_I(t_1')\right\}\ \mathcal{E}\left\{n_I(t_2'+\tau)n_I(t_2')\right\}\ dt_1'dt_2'$$

$$+ \int\!\!\!\int_0^{T_H-\tau} \mathcal{E}\left\{n_I(t_1'+\tau)n_I(t_2'+\tau)\right\}\mathcal{E}\left\{n_I(t_1')\ n_I(t_2')\right\}dt_1'dt_2'$$

$$+ \int\!\!\!\int_0^{T_H-\tau} \mathcal{E}\left\{n_I(t_1'+\tau)n_I(t_2')\right\}\mathcal{E}\left\{n_I(t_1')\ n_I(t_2'+\tau)\right\}\ dt_1'dt_2'$$

$$= R_{nn}^2(\tau)\ (T_H-\tau)^2 + \int\!\!\!\int_0^{T_H-\tau} R_{nn}^2(t_1'-t_2')\ dt_1'dt_2'$$

$$+ \int\!\!\!\int_0^{T_H-\tau} R_{nn}(t_1'-t_2'+\tau)\ R_{nn}(t_1'-t_2'-\tau)\ dt_1'dt_2'$$

$$(J.10)$$

where $R_{nn}(\tau) = \mathcal{E}\{n_I(t)n_I(t+\tau)\}$ is the correlation function of $n_I(t)$.

Equation (J.10) can be further simplified. First, we note that, for $\tau = \tau_k = kB^{-1}$, $R_{nn}(\tau_k) = 0$, so the first term drops out. Furthermore, one can employ the even symmetry of $R_{nn}(\tau)$, i.e., the fact that $R_{nn}(\tau) = R_{nn}(-\tau)$, in order to reduce the two-dimensional integrals to one-dimensional ones (see [49, page 325] for details). The result is then

$$\mathcal{E}\left\{N_{II}^2(\tau_k)\right\} = 2\int_0^{T_H-\tau_k}(T_H-\tau_k-\rho)\left(\frac{N_0 B}{2}\right)^2\ S_a^2(\pi B\rho)\,d\rho$$

$$+ 2\int_0^{T_H-\tau_k}(T_H - \tau_k - \rho)\left(\frac{N_0 B}{2}\right)^2\ S_a\left[\pi B(\rho+\tau_k)\right]\ S_a\left[\pi B(\rho-\tau_k)\right]d\rho$$

$$(J.11)$$

With the change of variables

$$\rho' = \frac{\rho}{T_H - \tau_k}$$

$$(J.12)$$

and defining the normalized parameter ζ_k as

195

$$\zeta_k \triangleq \frac{\tau_k}{T_H} = \frac{k}{BT_H} = \frac{k}{G} \tag{J.13}$$

we can rewrite (J.11) as

$$\mathscr{E}\{N_{II}^2(\tau_k)\} = \frac{(N_0B)^2}{2}(T_H-\tau_k)^2\left[\int_0^1 (1-\rho')S_a^2\left[\pi B\rho'(T_H-\tau_k)\right]d\rho'\right.$$

$$\left. + \int_0^1 (1-\rho')S_a\left[\pi B\left(\rho'(T_H-\tau_k)+\tau_k\right)\right]S_a\left[\pi B\left(\rho'(T_H-\tau_k)-\tau_k\right)\right]d\rho'\right]$$

$$= \frac{(N_0B)^2(T_H-\tau_k)^2}{2}(F_1(k) + F_2(k)) \tag{J.14}$$

where

$$F_1(k) = \int_0^1 (1-\rho')S_a^2\left[\pi BT_H\left(1 - \frac{\tau_k}{T_H}\right)\rho'\right]d\rho' = \int_0^1 (1-\rho')S_a^2\left[\pi G(1-\zeta_k)\rho'\right]d\rho' \tag{J.15}$$

and

$$F_2(k) = \int_0^1 (1-\rho') S_a\left[\pi G\left(\rho'(1-\zeta_k) + \zeta_k\right)\right]S_a\left[\pi G\left(\rho'(1-\zeta_k) - \zeta_k\right)\right]d\rho' \tag{J.16}$$

Combining (J.14) with (J.7) yields (5.47a).

Quite similarily, it follows from (5.45c).

$$\mathscr{E}\left\{\left(N_Q^{eq}(\tau)\right)^2\right\} = 2\mathscr{E}\left\{N_{IQ}^2(\tau)\right\} - 2\mathscr{E}\left\{N_{IQ}(\tau)N_{QI}(\tau)\right\} \tag{J.17}$$

But,

196

$$\mathscr{E}\left\{N_{IQ}^2(\tau)\right\} = \iint\limits_{\tau}^{T_H} \mathscr{E}\left\{n_I(t_1)n_Q(t_1-\tau)n_I(t_2)n_Q(t_2-\tau)\right\}dt_1dt_2$$

$$= \iint\limits_{\tau}^{T_H} R_{nn}^2(t_1-t_2)dt_1dt_2 = \iint\limits_{0}^{T_H-\tau} R_{nn}^2(t_1'-t_2')\,dt_1'dt_2'$$

$$(J.18)$$

since $n_I(\tau)$ and $n_Q(\tau)$ are independent, with the same correlation function. The integral in (J.18) is identical to the second term in (J.10), which corresponds to the $F_1(k)$ term in (J.14). Furthermore,

$$\mathscr{E}\left\{N_{IQ}(\tau)\,N_{QI}(\tau)\right\} = \iint\limits_{\tau}^{T_H} \mathscr{E}\left\{n_I(t_1)n_Q(t_1-\tau)n_Q(t_2)\,n_Q(t_2-\tau)\right\}dt_1dt_2$$

$$= \iint\limits_{0}^{T_H-\tau} R_{nn}\left(t_1'-t_2'+\tau\right)R_{nn}\left(t_1'-t_2'-\tau\right)dt_1'dt_2'$$

$$(J.19)$$

which is identical to the third term in (J.10) corresponding to the $F_2(k)$ term in (J.14). Combining the above with (J.17) (note the minus sign of the second term) results in

$$\mathscr{E}\left\{N_Q^{eq}(\tau)^2\right\} = (N_0B)^2\left(T_H - \tau_k\right)^2\left(F_1(k) - F_2(k)\right)$$

$$(J.20)$$

as per (5.47b)

APPENDIX K

DETECTION OF FREQUENCY-HOPPING SIGNALS
VIA
AUTOREGRESSIVE MODELING

KI. INTRODUCTION

The purpose of this Appendix is to present a number of methodologies that can be used for the detection of frequency-hopping signals in AWGN. These methods operate in the autocorrelation-domain (ACD) and are based on autoregressive (AR) power spectrum estimation concepts. They are simple to implement and have low computational complexity, i.e., they have properties that make them very suitable for real-time implementations. Specifically, four different methods will be discussed and their performance demonstrated and compared with that of the conventional radiometer and the Correlator-Detector [see section 5.4].

The organization of the Appendix is as follows. Section KII establishes the problem formulation and its imposed constraints. Section KIII presents the four different detection methods, which are all based on AR models. The discussion emphasizes the methods mathematical description, performance evaluation and computational complexity. Concluding remarks and recommendations for future research are given in Section KIV.

KII. PROBLEM FORMULATION

Assume that the output of the correlator $y(\tau)$ can be expressed as in equation (5.44), where now we allow the signal frequency $f_0 = \omega_0/2\pi$ to be arbitrary (i.e., different from the center frequency f_c)

$$y(\tau) = C(\tau) \cos \omega_0 \tau + N_I^{eq}(\tau) \cos \omega_0 \tau + N_Q^{eq}(\tau) \sin \omega_0 \tau \qquad (K.1)$$

198

where

$$C(\tau) = \begin{cases} S(T_H - \tau), & H_1 \\ 0 & H_0 \end{cases}$$

if we mix $y(\tau)$ down to baseband by

$$y_c(\tau) = 2 \cos \omega_0 \tau \, y(\tau)|_{LP}$$

$$y_s(\tau) = 2 \sin \omega_0 \tau \, y(\tau)|_{LP}$$

then

$$y_c(\tau) = c(\tau) \cos \Delta\omega\tau + N_I^{eq}(\tau)$$

$$y_s(\tau) = c(\tau) \sin \Delta\omega\tau + N_Q^{eq}(\tau)$$

where $\Delta\omega \triangleq \omega_c - \omega_0$, $|\Delta\omega| \leq 2\pi B/2$, B is the observation bandwidth. By sampling the signals $y_c(\tau), y_s(\tau)$ (2) at $\tau_k = k\, B^{-1}$ points, the data records become

$$\begin{cases} y_c(k) = \dfrac{S}{B} (B\, T_H - k) \cos\dfrac{\Delta\omega}{B} k + N_I^{eq}(k) & (H_1) \\ y_c(k) = N_I^{eq}(k) & (H_0) \end{cases} \qquad (K.3)$$

$$\begin{cases} y_s(k) = \dfrac{S}{B} (B\, T_H - k) \sin\dfrac{\Delta\omega}{B} k + N_Q^{eq}(k) & (H_1) \\ y_s(k) = N_Q^{eq}(k) & (H_0) \end{cases} \qquad (K.4)$$

$$k = 0,1,2,..., G = BT_H$$

where $\mathscr{E}\{N_I^{eq}(k)\} = \mathscr{E}\{N_Q^{eq}(k)\} = 0$ for $k = 1,2,...,G$ and
$\text{var}\{N_I^{eq}(k)\} = \text{var}\{N_Q^{eq}(k)\} \approx (N_0 B)^2 (T_H - \frac{k}{B})^2 F_1(k)$.
Defining

$$W_0(k) \triangleq y_c(k)/(T_H - \tau_k)$$

$$W_s(k) \triangleq y_s(k)/(T_H - \tau_k), \qquad (K.5)$$

then from (K.3), (K.4) and (K.5) we can get the following analytic signal

$$W(k) = W_c(k) + j\, W_s(k) \qquad (K.6)$$

or

$$W(k) = S \exp(j\Omega k) + n(k) \qquad (H_1)$$

$$W(k) = n(k) \qquad (H_0) \qquad (K.7)$$

199

where

$$\Omega = \frac{\Delta\omega}{B}(|\Omega| \leq \pi)$$

$$n(k) = n_I(k) + jn_Q(k)$$

$$n_I(\cdot), n_Q(\cdot) \sim \text{Gaussian distributed, i.i.d}$$

$$\mathscr{E}\{n_I(k)\} \cong \mathscr{E}\{n_Q(k)\} \simeq 0 \quad \text{for } k = 1,2,\dots, G$$

$$\text{var}\{n_I(k)\} \cong \text{var}\{n_Q(k)\} \simeq (N_0B)^2 F_1(k) \quad \text{for } k = 1,2,\dots,G$$

and

$$\mathscr{E}\{n_I(0)\} = N_0B, \quad \mathscr{E}\{N_Q(0)\} = 0$$

Note, that the Gaussianess assumption for $\{n(k)\}$ weakens as $k \to G$. Therefore, we will concentrate on the observation interval $k = 0,1,2,\dots,\lambda G$ where $\lambda = 0.1 \sim 0.5$. Under these assumptions, $(G(1 - \lambda) \gg 1)$ a good approximate formula for $F_1(k)$ can be obtained, i.e.,

$$F_1(k) \cong \frac{1}{2 G\left(1 - \frac{k}{G}\right)} \qquad \text{(K.8)}$$

<u>Problem:</u> Given $\{W_c(k)\}$, $(W_s(k))$ $k=0,1,\dots, \lambda G$, $G \gg 1$, decide between H_1 (signal plus noise) and H_0 (noise).

A simple autocorrelation-domain (ACD) algorithm is desired that can be of low complexity and very suitable for real-time implementation.

<u>Important Observation:</u> The SNR in the ACD, is generally higher than that in the time domain. For example, take the case where $\Omega = 0$. Given the input SNR per band

$$\gamma_{in} \triangleq \frac{S}{(N_0B)}$$

which typically is very small ($\gamma_{in} = 10^{-1}, 10^{-2}$), we observe that the local SNR in the ACD-Baseband γ_B, is given by

$$\gamma_B(k) = \frac{S^2}{2(N_0B)^2 F_1(k)} \quad ,$$

or equivalently

$$\gamma_B(k) = \gamma_{in}^2 (G-k)$$

$$k=0,1,2,...,\lambda G.$$

if $\gamma_{in} = 10^{-1}$ (=-10dB), $G = 10^3, \lambda = 0.1$, then

$$9.54 \text{ dB} \leq \gamma_B(k) \leq 10\text{dB}$$

which indicates a significant increase in SNR.

The $\gamma_B(k)$ decreases as k increases. So, the problem here is how to employ the first λG samples of {W(k)} so that significant gains can be obtained. For example, the radiometer uses the first sample W(0), and the method of Kay [34] uses the first two samples, W(0), W(1) to form a detection parameter.

KIII. DETECTION METHODS BASED ON AR MODELING

Three different methods have been investigated and their performance evaluated via Monte-Carlo simulations. The first one is based on complex data ({W(k)}), whereas the other two are on real data ({W_c(k)}). All methods employ an autoregressive (AR) model in which AR coefficients are used to form a detection parameter in the ACD without forming an AR spectrum estimate. An important result obtained during our research is that the first method, which is based on complex data, does not exhibit any sensitivity to angle, whereas the other two methods do.

KIII A: METHOD I; COMPLEX DATA

(i) Preliminaries

Suppose we are given the following set of data samples, {R(0), R(1),..., R(m)} that have the properties of an autocorrelation sequence. Note that $R(\tau) = R^*(-\tau)$.

An equivalent unique representation of this set of samples can be obtained in terms of reflection coefficient $\{k_i\}$, i.e., $\{R(0), k_1, k_2,..., k_m\}$ where $|k_i| \le 1$, $i = 1,2,..,M$ [46]. This is achieved by fitting an Mth-order AR model to the data $\{R(0),..., R(M)\}$ in the MSE sense, and solving the resulting linear system of equations via the Levinson-Durbin algorithm. The steps are as follows:

i.1)   Normal Equations

$$
\begin{bmatrix}
R(0) & R(-1) & R(-2) & \ldots & R(-M) \\
R(1) & R(0) & R(-1) & \ldots & R(1-M) \\
\cdot & \cdot & \cdot & & \cdot \\
\cdot & \cdot & \cdot & & \cdot \\
\cdot & \cdot & \cdot & & \cdot \\
R(M) & R(M-1) & R(M-2) & \ldots & R(0)
\end{bmatrix}
\begin{bmatrix}
1 \\
a_1^{(M)} \\
\cdot \\
\cdot \\
\cdot \\
a_M^{(M)}
\end{bmatrix}
=
\begin{bmatrix}
P_M \\
0 \\
\cdot \\
\cdot \\
\cdot \\
0
\end{bmatrix}
$$

(K.9)

The unknowns are the AR coefficients $\{a_1^{(M)},...,a_M^{(M)}\}$ and the variance P_M of the linear prediction error. Once the above linear system of equations is solved, then the resulting AR spectrum of the data is

$$
S_{AR}(\omega) = \frac{P_M}{\left| 1 + \sum_{i=1}^{M} a_i^{(M)} \exp j(-\omega i) \right|^2}
$$

(K.10)

i.2)   Levinson-Durbin Algorithm [50], [51].

There is an elegant, recursive and fast procedure for solving the normal equations in (K.9), the so-called Levinson-Durbin algorithm. The method requires $\sim M^2$ operations only comparing to more general methods that require $\sim M^3$ operations. Note that the R matrix in (K.9) is Toeplitz and Hermitian. The algorithm proceeds as follows:

$$k_i = \frac{-\left[R(i) + \sum_{m=1}^{i-1} a_m^{(i-1)} R(i-m)\right]}{P_{i-1}} \quad i = 1,2,...,M$$

$$a_j^{(i)} = a_j^{(i-1)} + k_i\, a_{i-j}^{(i-1)*} \quad j = 0,1,...,i-1$$

$$P_i = P_{i-1}(1 - |k_i|^2) \tag{K.11}$$

Note that

$$\left.\begin{array}{l} a_0^{(i)} = 1 \\ a_i^{(i)} = k_i \end{array}\right\}, \quad i=1,2,...,M$$

and $a_\lambda^{(i)} = 0$ for $\lambda > i$. So, in obtaining the solution for an AR model of order M, one actually computes the solutions for all AR models of orders less than M, i.e., i-1,2,...,M^{-1}, M. The quantities $\{k_i\}\ 1 \le i \le M$ are known as reflection coefficients or partial correlation coefficients. A necessary and sufficient condition for the stability of the resulting Mth-order AR model is that [51], [52].

$$P_i > 0,\ 1 \le i \le M$$

or equivalently

$$|k_i| < 1,\ 1 \le i \le M \tag{K.12}$$

It can be shown that iff $\underline{R}_m > 0$ in (K.9), then (K.12) is satisfied [51]. It can also be shown that

$$0 \le P_i \le P_{i-1},\ i = 1,2,...,M \tag{K.13}$$

i.3) Detection Parameter

The detection parameter that will be adopted corresponds to the geometric over the arithmetic mean of the Mth-order AR spectrum given by (K10). It is described by [52]

$$V_M = \frac{GM}{AM} = \frac{\exp\left(1/2\pi\int_{-\pi}^{+\pi} n S_{AR}^{(M)}(\omega)\ d\omega\right)}{1/2\pi\int_{-\pi}^{+\pi} S_{AR}^{(M)}(\omega)\ d\omega}$$

$$\tag{K.14}$$

203

It is, therefore, clear the V_M depends completely on the shape of the AR model spectrum. Since GM ≤ AM, it follows that

$$0 \leq V_M \leq 1 \tag{K.15}$$

It is easy to see that when $S_{AR}^{(M)}(\omega)$ is flat, i.e., white noise, then $v_M = 1$ (FigureK.1(a)). On the other hand, if the spectral data spread is large, such as the pattern shown below in Figure K.1(b),
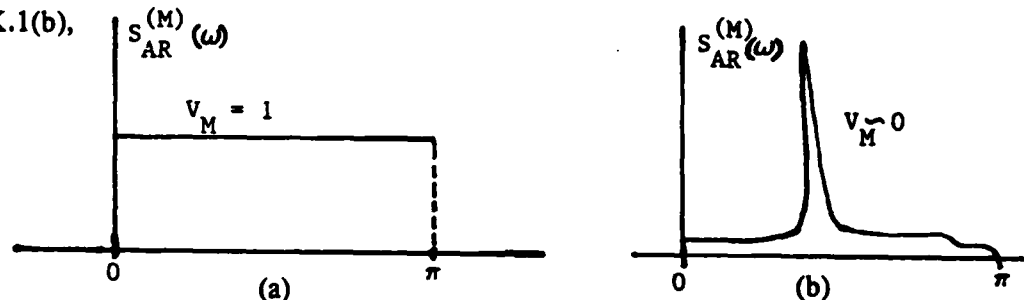
Figure K.1. Spectral spread: (a) white noise , (b) sinusoid in noise

then $V_M \approx 0$. So, another way of looking at V_M is in terms of the flatness of the spectrum [52].

It can be shown that V_M can be easily expressed in terms of the reflection coefficient of an Mth-order AR model as follows [52].

$$V_M = \prod_{i=1}^{M} (1 - |k_j|^2) \tag{K.16}$$

However, a closer examination of (K.16) and (K.11) reveals that

$$V_M = \frac{P_M}{R(0)} \tag{K.17}$$

which is the normalized by the signal energy variance of the linear prediction error associated with the Mth-order AR model. Since $P_0 = R(0)$, it is apparent that from (K.17) and (K.13), equation (K.15) follows.

The detection schemes described in this section will be based on comparison of V_M to a specified threshold value, i.e.,

$$V_M \quad \begin{matrix} < \gamma \quad (H_1) \\ \\ > \gamma \quad (H_0) \end{matrix}$$

$$(K.18)$$

where γ is a number between zero and one.

i.4)   M = 1 AR CASE: Equivalent Detection Parameters

If we are given the two first samples only $\{R(0), R(1)\}$, $|R(1)| \leq R(0)$, $R(0) > 0$, then a 1st-order (M = 1) AR model can be obtained with the detection parameter

$$V_1 = [1 - |k_1|^2]$$

or

$$V_1 = \frac{P_1}{R(0)}$$

$$(K.19)$$

However, $|k_1|^2$ can also be used as an equivalent detection parameter as follows

$$|k_1|^2 \quad \begin{matrix} > \delta \quad (H_1) \\ \\ < \delta \quad (H_0) \end{matrix}$$

$$(K.20)$$

This is the scheme suggested by Kay [34] (note t' $_{AL}$ a$_1^{(i)}$ = k_1) and shown to be equivalent to a comparison of a <u>normalized</u> spectral peak with a threshold v, i.e.

$$\max_{|\omega| \leq \pi} \left[\frac{S_{AR}^{(1)}(\omega^*)}{P_1} \right] \begin{array}{c} > \ v \ (H_1) \\ < \ v \ (H_0) \end{array} \qquad (K.21)$$

Another equivalent interpretation of the detection parameter V_1 in (K.19) can be established using the determinant of the matrix

$$\underline{R}_1 = \begin{bmatrix} R(0) & R(1) \\ R(1) & R(0) \end{bmatrix}$$

normalized by $R^2(0)$. Specifically, the detection parameter is

$$\widetilde{H}_1 = \frac{\det[\underline{R}_1]}{R(0)^2} = \left[1 - \frac{|R(1)|^2}{R^2(0)} \right]$$

or

$$\widetilde{H}_1 = [1 - |k_1|^2] = V_1 \qquad (K.22)$$

It is important to note that in the case where $\{R(0), R(1)\}$ are autocorrelation samples of a Gaussian weakly stationary random process then H_1 corresponds to a normalized entropy measure. Under H_0 (white noise) the entropy is higher than that H_1 (signal+noise). This, in the case of a Gaussian signal, in Gaussian white noise, the detection scheme in (K.22) compares a normalized entropy measure of the process to a threshold.

We, therefore, conclude that V_1(i.e., GM/AM of the spectrum or normalized variance of the linear prediction error), $|a_1^{(1)}|^2$, $\max[S_{AR}^{(1)}(\omega)/P_1]$ and $\widetilde{H}_1$ (i.e., normalized determinant of the covariance matrix) are all equivalent detection parameters for a 1st-order AR model and complex data $\{R(0), R(1)\}$. Their generalization to higher-order AR models, however, does not generally provide equivalent detection schemes.

i.5)   Mth-order AR case: Generalizations

If we are given the first $M + 1$ samples $\{R(0), R(1),...,R(M)\}$, then the following detection parameters can be obtained from the Mth-order AR model:

$$V_M = \frac{P_M}{R(0)} = \prod_{i=1}^{M} (1 - |k_i|^2, \quad (GM/AM)$$

$$R_M = |a_M^{(M)}|^2 = |k_M|^2, \quad (Magnitude\ of\ the\ poles)$$

$$\Gamma_M = \sum_{i=1}^{M} |a_i^{(M)}|^2; \quad [38],$$

$$C_M = \sum_{i=1}^{M} |k_i|^2,$$

$$PEAK_M = \max_{|\omega| \le \pi} \left| \frac{S_{AR}^{(M)}(\omega^*)}{PM} \right|$$

$$\widetilde{H}_M = \frac{\prod_{i=0}^{M} P_i}{R^M(0)} = \frac{P_0}{R(0)} \cdot \frac{P_1}{R(0)} \cdots \frac{P_M}{R(0)} = \prod_{i=0}^{M} V_i$$

The detection parameters R_M, Γ_M, and C_M may be seen as generalizations of $|k_1|^2$ shown in (K.20). However, they are not generally equivalent with each other nor with (K.23e), (K.23f) and (K.23a). For finite length data N and order M > 1, each one of the detection parameters given by (K.23 a - K.23f) is expected to have different performance. Some asymptotic results (N→∞) related with (K.23a), (K.23c) and (K23e) are given in Addendum I.

(ii) The Method

The method employs V_M as a detection parameter ((K.16), (K.17)) and compares that to a specific threshold value as shown in (K.18). However the V_M is estimated by performing AR modeling in the autocorrelation of autocorrelation domain AACD. This is because the the AR coefficients of an Mth-order model are computed using (K.9) or (K.11) with "data" $\{R(0),...,R(M)\}$ generated as follows:

$$R(\tau) = \frac{1}{\lambda G} \sum_{n=1}^{\lambda G - \tau} W(n) \; W^*(n+\tau)$$

$$\tau = 0,1,...,M$$

(K.24)

where $W(n)$ is given by (K.7). Since $W(n)$ is the output of the correlator, $\{R(\tau)\}$ represents an estimate of the autocorrelation of the autocorrelation of the original time sequence (i.e., the input to the correlator). Equation (K.24) corresponds to the biased autocorrelation formula, which has been shown to guarantee a stable Mth-order AR model (i.e. $|k_i| < 1$, $i = 1,2,...,M$) [51]. It is for stability reasons that the biased estimates are used here instead of the unbiased ones.

In summary the method proceeds as follows: a) Given the data in (K.7), compute $R(\tau)$, $\tau = 0,1,...,M$ from (K.24). b) Use the Levinson-Durbin algorithm in (K.11) to compute P_M c). The detection parameter is $V_M = P_M/R(0)$. Note that the first sample $W(0)$ in (K.7) is not taken into account when computing $\{R(\tau)\}$ in (K.24).

(iii) Performance

The detection performance of Method I has been tested via Monte Carlo simulations for $G = 1000$, $\lambda = 0.1$-0.5, and input SNR $\gamma_{in} = 0$ dB down to -25 dB. The probability of detection P_D was computed for $P_{FA} = 10^{-1}$. To assume statistical confidence, a very large number of trials (1000) was performed. These results are illustrated in Figure K2. Several features can be noted from Figure K2:

208

Figure **K.2** Monte Carlo Simulation results on
Method I with G=1000

209
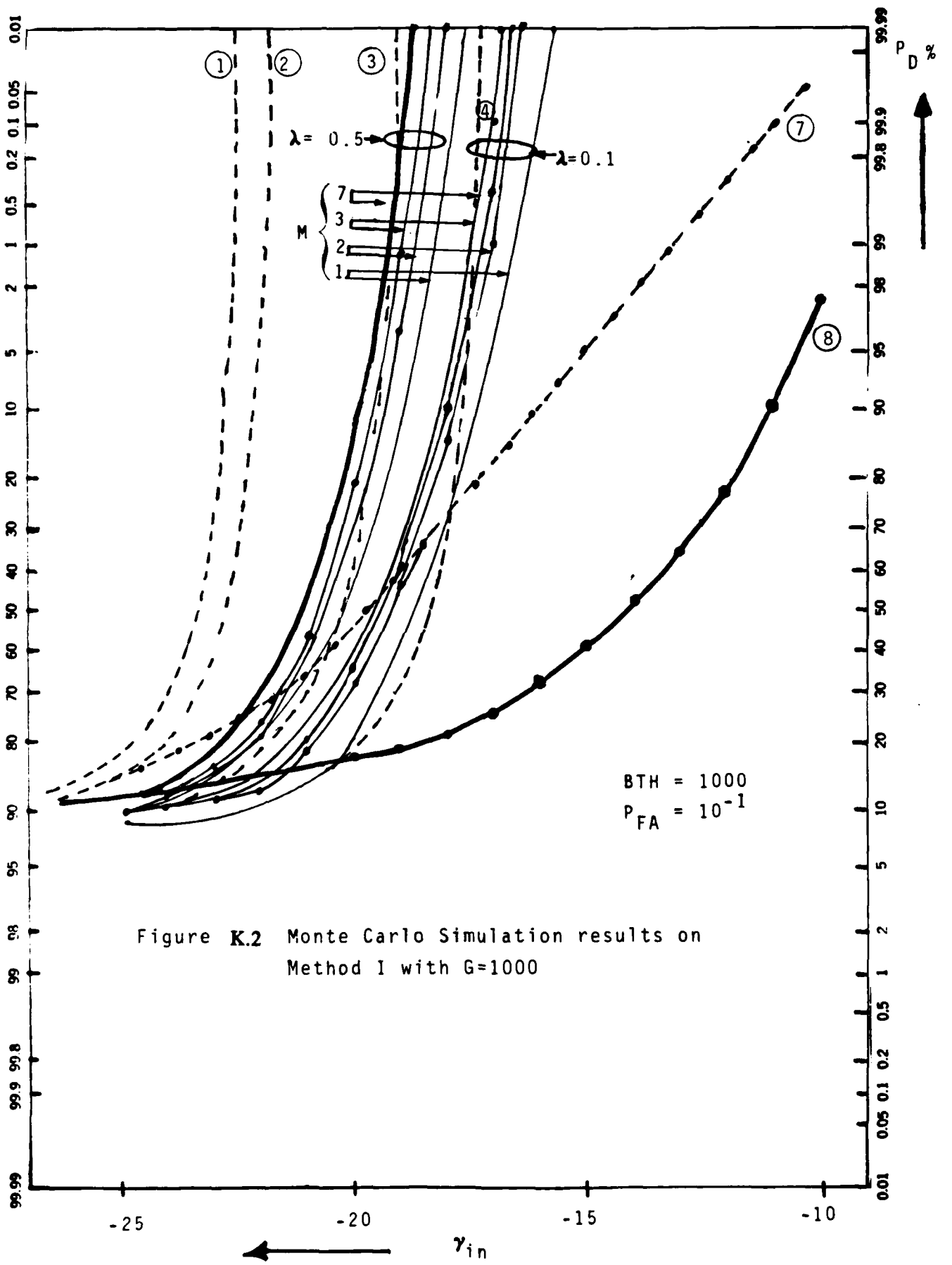
a) For a constant order M, the performance of the AR detector I improves as λ increases.

b) For a constant λ, the performance also improves as the model order M increases.

c) For M=2 and λ=0.5, Method I outperforms the radiometer detector (⑧) when $\gamma_{in} \leq$ -23.4 dB and the correlator detector (⑦) when $\gamma_{in} \leq$ -21.4

d) For G = 1000, P_D= 0.95, P_{FA}= 0.1, M=1, λ = 0.5, the AR detector I will require   3.6 dB and 8.2 dB less than the correlator ⑦ and radiometer ⑧ detectors, respectively.

e) There is approximately 0.4 dB improvement if M changes from M=1 to M=2. Furthermore, an additional improvement of ~0.4 dB is achieved by changing the order from M=2 to M=7.

Figure K3 illustrates similar improvements but for the case where G =.100. For example, if M = 1, λ = 0.5 then Method I outperforms the correlator-detector (⑦) for $\gamma_{in} \leq$ -14dB. Furthermore, Table K.I summarizes the effect of λ (length of the data), model order M and input SNR γ_{in} on the distance d = $|m_0 - m_1|$ between the two means and on the variances σ_0^2 , σ_1^2 of the detection parameter V_M. From Table KI, it is apparent that:

a) if M=const, γ_{in}=const and $\lambda\uparrow$ then d$\downarrow$, $\sigma_0^2\downarrow$, $\sigma_1^2\downarrow$

b) if λ=const, γ_{in}=const and M$\uparrow$ then d$\uparrow$ $\sigma_0^2\downarrow$, $\sigma_1^2\downarrow$

c) if M=const, λ=const and $\gamma_{in}\uparrow$then d$\downarrow$, σ_0^2=const, $\sigma_1^2\downarrow$

The AR detector is therefore independent of the noise variance (γ_{in}) for a given order M and length of data λG. It is, thus, unnecessary to estimate the noise variance in order to set a threshold at the receiver.

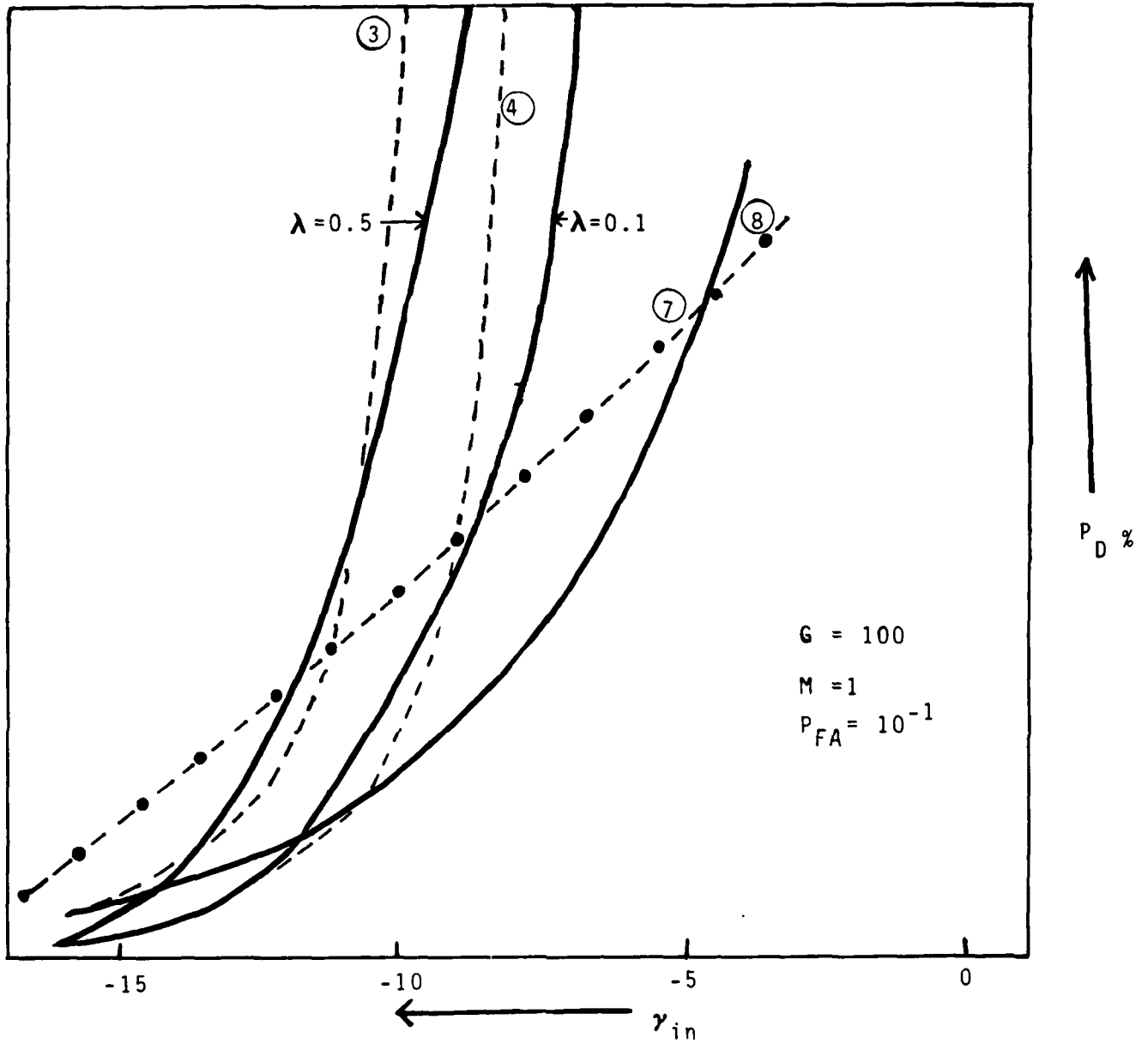Figure **K.3**   Monte-Carlo Simulation Results on
Method I with G=100.

TABLE K.I

AR DETECTOR I: Model order (M), sample mean under $H_0(m_0)$, sample mean under $H_1(m_1)$, sample variances σ_0^2 (H_0) and σ_1^2 (H_1) of V_M (M=P)

γ_{in}	G=1000	M = 1		M = 2		M = 3	
		$\lambda=0.1$	$\lambda=0.5$	$\lambda=0.1$	$\lambda=0.5$	$\lambda=0.1$	$\lambda=0.5$
-20dB	m_0-m_1	0.00611	0.00435	0.0125	0.0083	0.018	0.0117
	σ_0^2	0.937×10^{-4}	0.039×10^{-4}	2.751×10^{-4}	0.989×10^{-4}	3.77×10^{-4}	1.033×10^{-4}
	σ_1^2	2.094×10^{-4}	0.229×10^{-4}	5.623×10^{-4}	1.382×10^{-4}	8.0×10^{-4}	1.65×10^{-4}
-18dB	m_0-m_1	0.0332	0.0234	0.0576	0.0403	0.0730	0.0532
	σ_0^2	0.937×10^{-4}	0.039×10^{-4}	2.751×10^{-4}	0.991×10^{-4}	3.77×10^{-4}	1.033×10^{-4}
	σ_1^2	7.662×10^{-4}	1.059×10^{-4}	15.266×10^{-4}	2.820×10^{-4}	19.43×10^{-4}	3.503×10^{-4}
-16dB	m_0-m_1	0.132	0.0971	0.195	0.148	0.22645	0.179
	σ_0^1	0.937×10^{-4}	0.039×10^{-4}	2.756×10^{-4}	0.981×10^{-4}	3.77×10^{-4}	1.038×10^{-4}
	σ_1^2	22.807×10^{-4}	3.775×10^{-4}	31.055×10^{-4}	5.801×10^{-4}	32.532×10^{-4}	6.394×10^{-4}

(iv)   Computational Complexity

The computational complexity of the AR detector I is compared with that of the
Periodogram (FFT based), using as a figure of merit the number of complex multiplications
(which are the most expensive). Note that a complex multiplication is equivalent to 4 real
multiplications and 2 real additions. The results are summarized in Table KII. From this
table several important features can be noted:

a) If the length of the data is $\lambda G = 2^a$, then the Periodogram detector requires
   $Mu = (a + 1) \cdot \lambda G$, whereas the AR detector requires $Mu \sim (M + 1) \lambda G$.

b) The AR detector requires less multiplications than the Periodogram for $M < a$.

Note that a rectanglar window on the data has been assumed for the Periodogram in Table KII.
If any other window is used, which is usually the case, then Mu (Periodogram) =
$(a + 1) \lambda G$ complex muiltiplications plus $2\lambda G$ real multiplications.

KIII. B METHOD II: REAL DATA IN AR MODEL

This method employs real data to form a detection parameter using a second-order
AR model. The sequence of samples is given by (K.3) and (K.5), i.e.,

$$W_c(k) = S \cos \Omega k + n_I(k) \qquad (H_1)$$
$$k = 0,1,...,G \qquad ; |\Omega| \le \pi$$
$$W_c(k) = \qquad n_I(k) \qquad (H_0) \qquad\qquad (K.25)$$

with the statistics of $\{n_I(k)\}$ given in (K.7) and (K.8). The approach taken here models
$\{W_c(k)\}_1^{\lambda G}$ as a 2nd-order AR process of which the parameters are estimated using the
least-squares (LS) method for spectral estimation [46]. The detection parameter is the

213

TABLE K.II

COMPLEX MULTIPLICATIONS

$AG = 2^{\alpha}$	PERIODOGRAM (FFT BASED)	AR DETECTOR			
		$M = 1$	$M = 2$	$M = 3$	$M = \alpha$
$\alpha = 6$	448	132	200	279	482
$\alpha = 7$	1024	260	392	525	1067
$\alpha = 8$	2304	516	776	1037	2357
$\alpha = 9$	5120	1028	1544	2061	5184

AR DETECTOR: $(M+1) \; G + [M^2+3M+1] - [\frac{M(M+1)}{2}]$

Periodogram: $(\alpha+1) \lambda G^*$

*Rectangular window on the data.

214

coefficient of the AR model, which corresponds to the product of the poles' magnitude. It is given by

$$P_{II} = |a_2^{(2)}| = \left| \frac{R_{12} r_1 - R_{11} r_2}{R_{11} R_{22} - R_{12}^2} \right|$$

(K.26)

where

$$R_{11} = \sum_{k=1}^{\lambda G-2} W_c^2(k+1) \quad , \quad R_{22} = \sum_{k=1}^{\lambda G-2} W_c^2(k)$$

$$R_{12} = \sum_{k=1}^{\lambda G-2} W_c(k) W_c(k+1) \quad , \quad r_1 = \sum_{k=1}^{\lambda G-2} W_c(k+1) W_c(k+2)$$

$$r_2 = \sum_{k=1}^{\lambda G-2} W_c(k) W_c(k+2)$$

(K.27)

It is important to note that for the signal only case, $P_{II} = 1$ exactly. Furthermore, for λG large ($\lambda G \geq 100$) the Burg technique [53] and the Yule-Walker (YW) method [54] for spectrum estimate, both give estimates very close, if not identical to those of LS[46]. This is because as $\lambda G \rightarrow \infty$ the LS, Burg and YW methods become the same.

The detection scheme compares P_{II} to a threshold value γ, i.e.,

$$P_{II} \begin{array}{l} > \gamma \quad (H_1) \\ \\ < \gamma \quad (H_0) \end{array}$$

(K.28)

We have tested the performance of this scheme for $\gamma_{in} = 0$ dB down to -20 dB, $G = 1000$, $\lambda = 0.1, 0.5$, and signal angles $\Omega = 11.25° \mu$, $\mu = 1,2,...,10$. The sample mean of the detection parameter P_{II} was computed from 1000 sample trials under H_1. The key result obtained from this group of simulations was that P_{II} is very sensitive to the values of the signal angle Ω(i.e., μ). This high dependence of P_{II} (H_1) on Ω may cause P_{II} (H_1) $\cong 0$ not only using the LS method but also the Burg or YW techniques. The

results are illustrated in Figure K.4(a,b) for the LS and Burg techniques, respectively. A theoretical justification of this phenomenon can be established using asymptotic ($\lambda G \rightarrow \infty$) results. As $\lambda G \rightarrow \infty$, the detection parameter P_{II} in (K.26) becomes (LS or Burg or YW method)

$$\hat{P}_{II} = \frac{R^2(1) - R(0) \, R(2)}{R^2(0) - R^2(1)} = \frac{N}{D}$$

(K.29)

with $R(0) \cong 1/2 + Q_B$, $R(1) \cong 1/2 \cos \Omega$, $R(2) \cong \cos 2\Omega$

Thus

$$N = 1 - \cos 2\Omega - 4 \, Q_B \cos 2\Omega, \text{ and}$$

$$D = 2 - \cos 2\Omega + 8[Q^2_B + Q_B].$$

where Q_B is the "average" variance of the additive WGN. Note that if $Q_B = 0$, then $N = D$ and therefore $P_{II} = 1$. However, when $Q_B \neq 0$ then $N = 0$ if

$$\cos 2\Omega = \frac{1}{1 + 4Q_B}$$

(K.30)

So, for those values of Ω for which (K.30) is satisfied, $\hat{P}_{II}(H_1) = 0$. Table KIII illustrates the cases where $N = 0$ for various γ_{in} using (K.30) and Figure K.4. Apparently the simulation results (Figure K.4) are in good agreement with the asymptotic results (K.30).
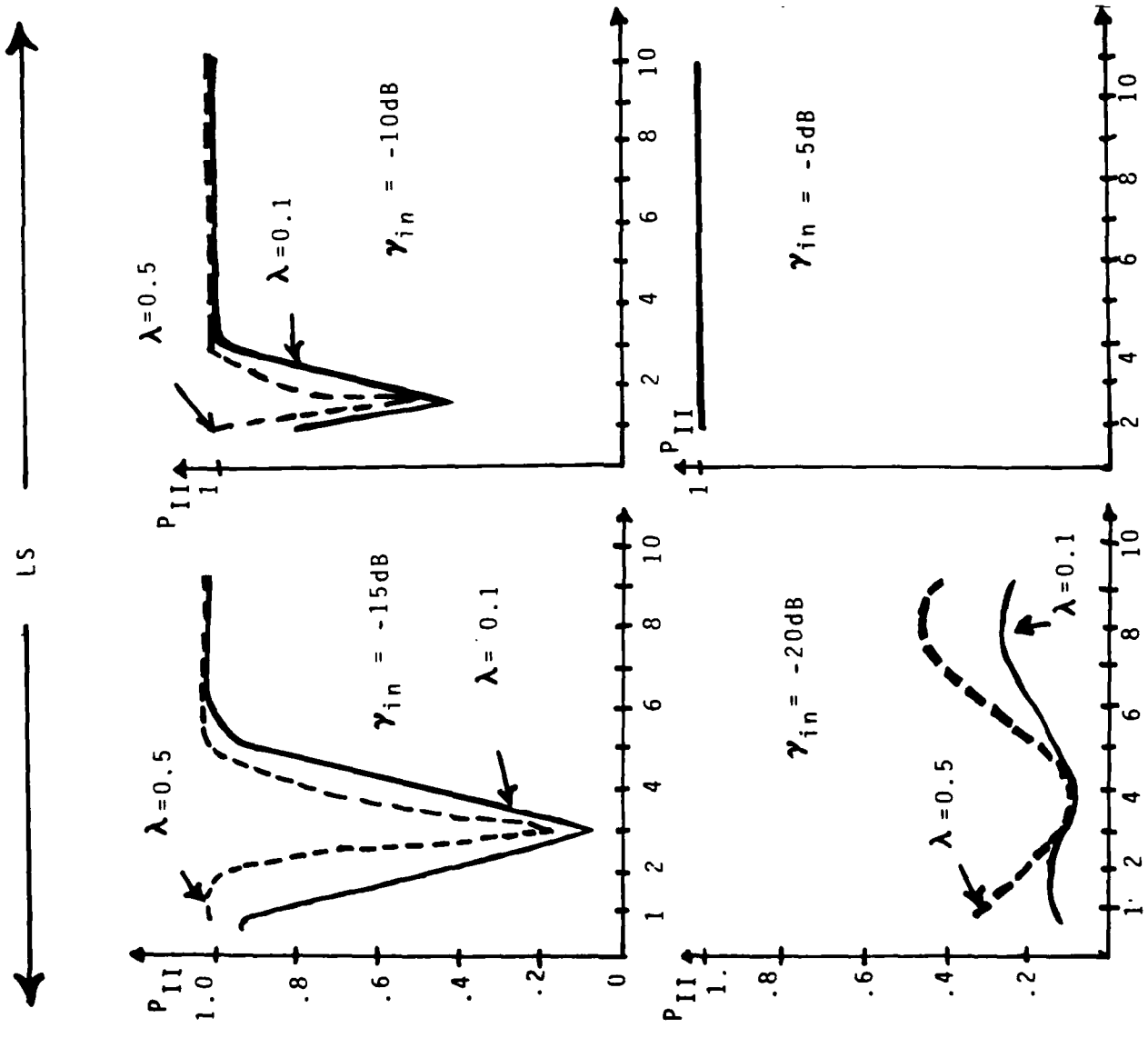
G=1000 P_{II} under H_1 vs signal angle (μ)

LS

P_{II} under H_1 vs signal angle (μ)

Figure K.4a

Effect of normalized signal frequency offset $\Omega = (11.25°) \times \mu$; $\mu = 1,\ldots,10$; on the detection probability P_{II} for the least squares (LS) algorithm, with γ_{in} as a parameter (G = 1000)

$\gamma_{in} = -10$dB

$\lambda = 0.5$

$\lambda = 0.1$

$\gamma_{in} = -5$dB

$\gamma_{in} = -15$dB

$\lambda = 0.5$

$\lambda = 0.1$

$\gamma_{in} = -20$dB

$\lambda = 0.5$

$\lambda = 0.1$

217
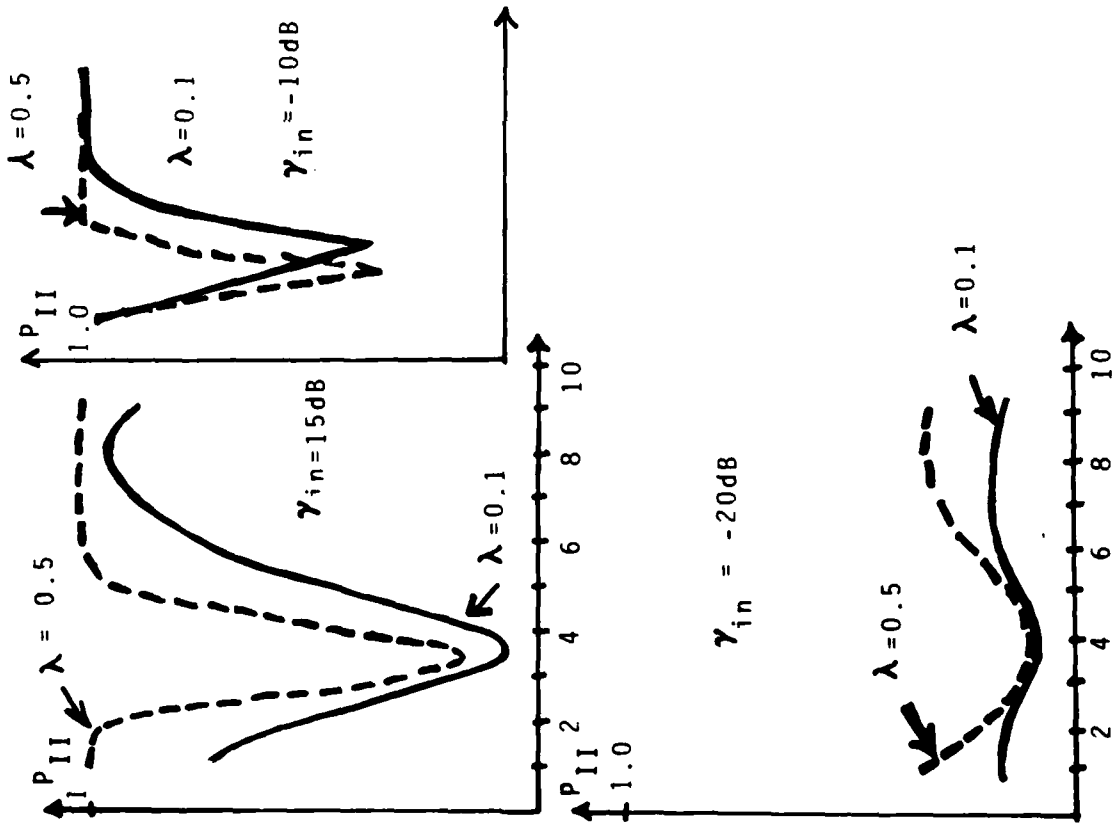
Figure K.4b

Effect of normalized signal frequency offset $\Omega = (11.25°) \times \mu$; $\mu = 1,...,10$; on the detection probability P_{II} for the Burg algorithm, with γ_{in} as a parameter (G = 1000)

Table KIII. Values of $\Omega = 11.25°$ μ for which $\hat{P}_{II} = 0$ under various γ_{in}.

$\gamma_{in}(dB)$	Q_B	Ω (theory)	μ (theory)	μ(simulation,Fig. K.4)
0	5×10^{-4}	$1.81°$	0.16	~ 0
-5	5×10^{-3}	$5.68°$	0.5	~ 0
-10	5×10^{-2}	$16.77°$	1.49	~ 1.5
-15	5×10^{-1}	$35.26°$	3.134	~ 3
-20	5	$43.63°$	3.87	~ 4

Due to the high dependence on the signal angle Ω, Method II was not pursued any further. It is important to note, however, that while Methods I and II are equivalent from the spectrum estimation viewpoint, they have diverse performance as far as the detection scheme in (K.28) is concerned.

III.c   METHOD III; REAL DATA IN ARMA MODEL

This method is a modification of the LS approach and employs the same real data record $\{W_c(k)\}^{\gamma G}$. It models the data as an ARMA (2,2) process from which the magnitude of the second AR coefficient serves as the detection parameter, i.e.,

$$|a_2| = \left| \frac{z_{21} \ t_1 - z_{11} t_2}{z_{11} z_{22} - z_{12} z_{21}} \right|$$

(K.31)

where

$$z_{11} = \sum_{k=1}^{M-2} W_c(k+1) \ W_c(k+3) \quad , \quad z_{22} = \sum_{k=1}^{M-2} W_c(k) \ W_c(k+4)$$

$$z_{12} = \sum_{k=1}^{M-2} W_c(k) \ W_c(k+3) \quad , \quad z_{21} = \sum_{k=1}^{M-2} W_c(k+1) \ W_c(k+4)$$

$$t_1 = \sum_{k=1}^{M-2} W_c(k+1) \ W_c(k+3) \quad , \quad t_2 = \sum_{k=1}^{M-2} W_c(k+2) \ W_c(k+4)$$

219

In the "signal only" case, $|a_2| = 1$ exactly. Furthermore under H_1 (signal plus noise), as the length of the data record $M \to \infty$ then

$$z_{11} = 1/2 \cos 2\Omega, \quad z_{22} = 1/2 \cos 2\Omega, \quad z_{12} = 1/2 \cos \Omega,$$

$$z_{21} = 1/2 \cos 3\Omega, \quad t_1 = 1/2 \cos 3\Omega \text{ and } t_2 = 1/2 \cos 4\Omega.$$

Thus,

$$|a_2| = \left| \frac{1/8[1 - \cos 2\Omega]}{1/8[1 - \cos 2\Omega]} \right| = 1,$$

i.e.,

asymptotically ($M \to \infty$), the parameter $|a_2|$ is free of the AWGN. However, the price paid is that under H_0 equation (K.31) becomes a very bad estimator of $|a_2|$ which as $M \to \infty$ becomes undefined ($|a_2| = \frac{0}{0}$). To remedy this problem, we sacrifice a part of the method's good performance under H_1 by using as detection parameter

$$\hat{P}_{III} = \left| \frac{z_{21} \, t_1 - z_{11} \, t_2}{z_{11} \, z_{22} - z_{12} \, z_{21} + Q} \right|$$

(K.32)

where $Q = \dfrac{W_c^4(0)}{4G^2}$. The detection scheme is the same as that shown in (K.28).

We have tested the performance of this approach for $\gamma_{in} = -10$ dB down to -20 dB, $G = 1000$, $\lambda = 0.1$, 0.5 and signal angles $\Omega = 11.25° \, \mu$, $\mu = 1,2,...,10$. The P_D was computed for $P_{FA} = 10^{-1}$ and the results are illustrated in Figure K5. From this figure, it is apparent that the performance of Method III is determined by the angle signal Ω, having as a lower bound curve the AR (min) and an upper bound curve the AR (max). Thus, while the angle dependence of Method III is much less than that of Method II, it is still large enough to degrade the performance of the detector. We, therefore, did not pursue any further Method III.
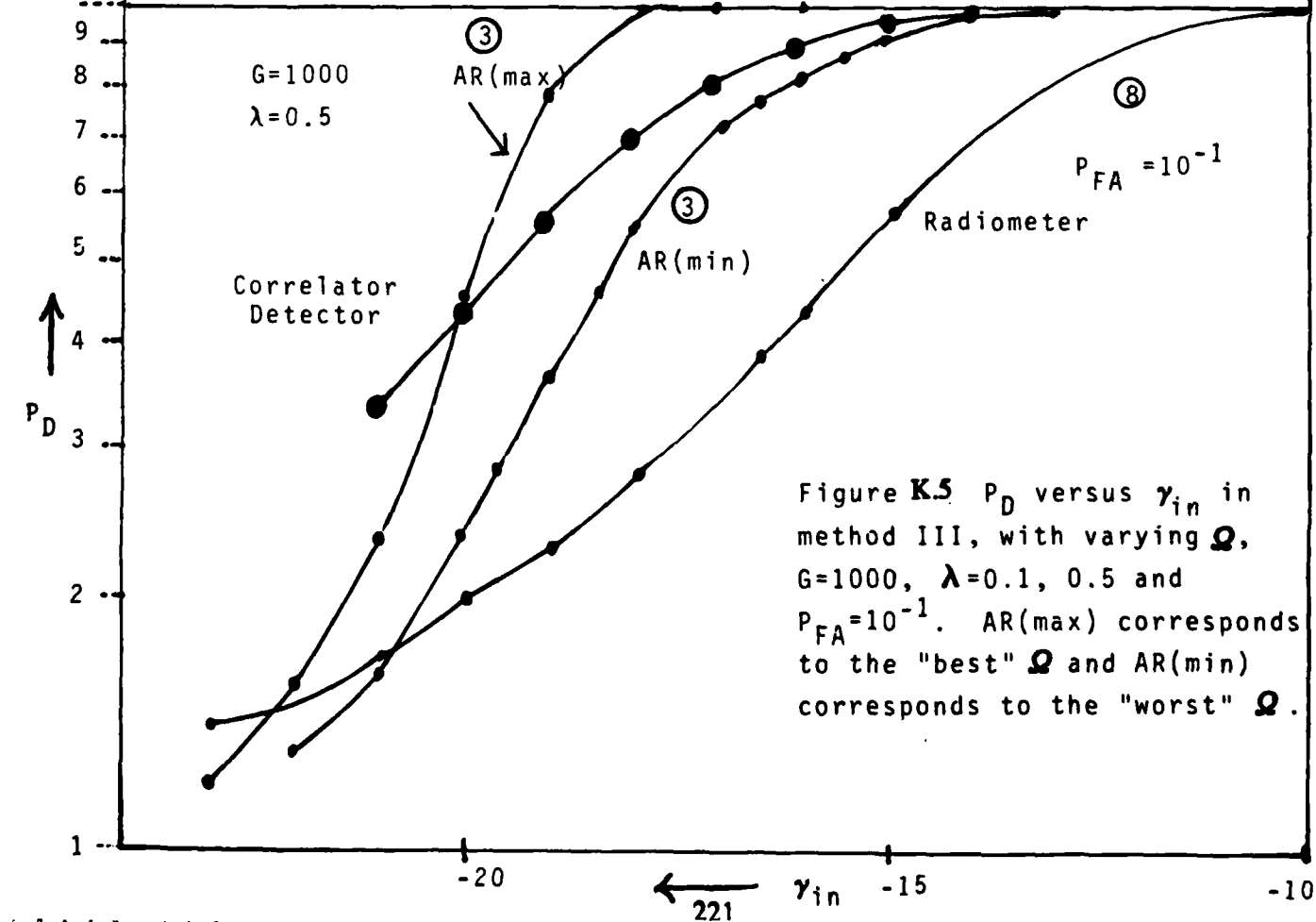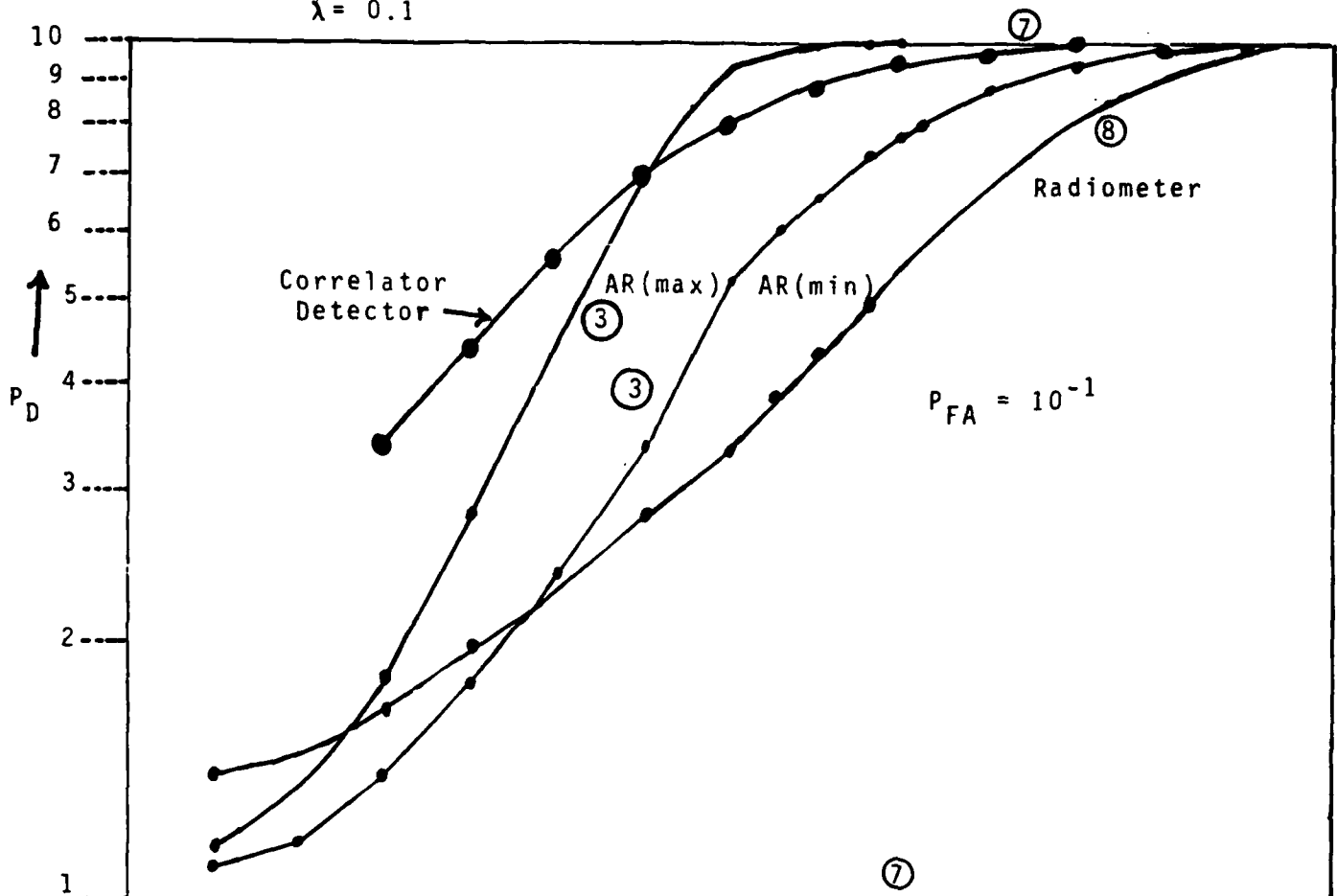
Figure K.5 P_D versus γ_{in} in method III, with varying Ω, G=1000, λ=0.1, 0.5 and P_{FA}=10^{-1}. AR(max) corresponds to the "best" Ω and AR(min) corresponds to the "worst" Ω.

221

IV. CONNECTION WITH OTHER DETECTION SCHEMES

Given the data $r(k)$, $k = 0,1,2,..,L$ in the <u>time-domain</u> where

$$r(k) = \exp(j\Omega k) + \varepsilon(k) \qquad (H_1)$$

$$r(k) = \varepsilon(k) \qquad (H_0) \qquad (K.33)$$

various detection schemes have been developed to decide between H_0 and H_1.

1) <u>Radiometer:</u> The detection statistic is

$$W(0) = \frac{1}{L} \sum_{k=0}^{L} |r(k)|^2 \qquad (K.34)$$

which is the <u>first lag</u> of the autocorrelation of $\{(k)\}$.

2) <u>AR(1) Method of Kay [34]:</u> The detection statistic here is the magnitude of the parameter of a 1st-order AR model, as explained in section III.A (i.4). The method estimates the first two autocorrelation lags

$$W(0) = 1/L \sum_{k=0}^{L} |r(k)|^2$$

$$W(1) = 1/L \sum_{k=0}^{L-1} r(k) r^*(k+1) \qquad (K.35)$$

and forms the parameter

$$|a|^2 = \left| \frac{W(1)}{W(0)} \right|^2$$

(K.36)

which is compared to a threshold.

3) <u>Adaptive AR Detection Scheme [55]</u>: Considering the binary detection problem

$$r(k) = s(k) + \varepsilon(k) \qquad (H_1)$$

$$r(k) = \quad \varepsilon(k) \qquad (H_0) \qquad \text{(K.37)}$$

the method models the unknown signal as an AR process

$$s(k) + \sum_{i=1}^{P} a_i \, s(k - i) = u(k)$$

and uses as detection parameter the

$$\text{SNR} = \frac{\sigma_u^2}{\sigma_\varepsilon^2} \qquad \text{(K.38)}$$

The method estimates from the observations $\{r(k)\}$ the $\{\hat{a}_i\}_i^P$, $\hat{\sigma}_u^2$ $\hat{\sigma}_\varepsilon^2$ using a <u>nonlinear optimization technique.</u>

4) <u>Broadband Detection of Signals [37]</u>.

Considering the binary detection problem

$$r(k) = s(k) + n(k) \qquad (H_1)$$

$$r(k) = \quad n(k) \qquad (H_0)$$

where $\{s(k)\}$ is assumed to be stationary Gaussian random process with a <u>broadband</u> unknown PSD, the method models $\{r(k)\}$ as an AR process of order P, i.e.,

$$r(k) + \sum_{i=1}^{P} a_i \, r(k - i) = u(k)$$

and uses as detection parameter

$$G = \frac{\sigma_u{}^2}{W(0)}$$

which actually is the GM/AM of the signal spectrum.

5) RF Correlator-Detector [Section 5.3]

This is a detection scheme that employs <u>all</u> autocorrelation samples of $\{r(k)\}$ i.e.,

$$W(\tau) = -\frac{1}{L} \sum_{K=0}^{L-\tau} r(k)\, r^*(k+2)$$

$$\tau = 0,1,...\lambda G$$

by forming the following detection parameter:

$$R(0) = \frac{1}{\lambda G} \sum_{\tau=1}^{\lambda G} W(\tau)\, W^*(\tau)$$

which is actually the first lag of the autocorrelation of the autocorrelation sequence. Thus, the Correlator Detector may be seen as the radiometer operating in a different domain (AACD).

224

ADDENDUM I

In the asymptotic case ($\lambda G \to \infty$), the "data" generated by (K.24) becomes.

H_0: $\{R(0)=Q, \ R(1)=...=R(M)= 0\}$

H_1: $\{R(0)=1+Q, R(1)=e\text{-}j^\Omega \ , ..., R(M)=e^{-jM\Omega} \}.$ (I.1)

The AR parameters generated via the Levinson recursion take the values: (Mth-order Model)

H_0: $\alpha_i^{(M)} = 0 \ , \ i=1,2,...,M$

$k_i = 0, \ i=1,2,...,M$

$P_i = Q, \ i=0,1,...,M$ (I.2)

H_1: $a_\lambda^{(M)} = -\dfrac{1}{(Q + M)} \ e^{-j\Omega\lambda}, \ \lambda=1,2,...,M$

$k_i = -\dfrac{1}{(Q + i)} \ e^{-j\Omega i}, \ i=1,2,...,M$

$P_i = +Q \ \dfrac{(Q+i+1)}{(Q+i)}, \ i=1,2,...,M$

(I.3)

Therefore, the detection parameter Γ_M (Ketchum, [38]) (K.23c) becomes

H_0: $\Gamma_M = 0$

H_1: $\Gamma_M = \dfrac{M}{(Q+M)^2}$

(I.4)

and thus the distance $\gamma_M = |\Gamma_M(H_1)\text{-}\Gamma_M(H_0)|$ is given by

225

$$\gamma_M = \frac{M}{(Q+M)^2}$$

On the other hand, V_M becomes

H_0: $\quad V_M = 1$

H_1: $\quad V_M = \dfrac{Q(Q + M + 1)}{(Q+1)(Q+M)}$

and therefore, the distance $v_M = |V_M(H_1) - V_M(H_0)|$ takes the value

$$v_M = \frac{M}{(Q+1)(Q+M)} \tag{I.5}$$

Comparing v_M with γ_M, it is apparent that $v_M > \gamma_M$ for M>1 and $v_M = \gamma_M$ for M=L.

For the asymptotic case ($\lambda G \to \infty$), we can also find equivalent detection parameters

to a normalized AR spectrum peak. If we define as

$$\frac{S_{AR}^{(M)}(\omega)}{P_M} \triangleq \frac{1}{|D(\omega)|^2} \tag{I.6}$$

where $D(\omega)$ is obtained from (I.3) and (K.10) as

$$D(\omega) = 1 - \sum_{\lambda=1}^{M} \frac{1}{(Q+M)} e^{-j[\omega+\Omega]\lambda}$$

then

$$J(\omega) = |D(\omega)|^2 = 1 - \frac{1}{(Q+M)} \sum_{\lambda=1}^{M} e^{j(\omega+\Omega\lambda)} - \frac{1}{(Q+M)} \sum_{\mu=1}^{M} e^{j(\omega+\Omega)\mu}$$

$$+ \frac{1}{(Q+M)^2} \sum_{\lambda=1}^{M} \sum_{\mu=1}^{M} e^{j(\omega+\Omega)(\mu-\lambda)}$$

By differentiating and forcing $\dfrac{\partial J(\omega)}{\partial \omega} = 0$, we obtain

226

$$\frac{1}{Q + M} \sum_{\lambda=1}^{M} \sum_{\mu=1}^{M} (\mu-\lambda) e^{j(\omega+\Omega)(\mu-\lambda)} = \sum_{\mu=1}^{M} e^{j(\omega+\Omega)\mu} - \sum_{\lambda=1}^{M} \lambda e^{-j(\omega+\Omega)\lambda}$$

(I.7)

After some algebra, we find that the solution of (I.7) which corresponds to minimum $J(\omega)$ is

$$\omega^* + \Omega = 0$$

and, thus, the spectrum peak is given by

$$\frac{1}{|D(\omega^*)|^2} = \frac{1}{\left(1 - \dfrac{M}{Q + M}\right)^2}$$

(I.8)

We conclude that equivalent detection parameters to (I.8) can be

$$\frac{M}{Q + M} = \sum_{i=1}^{M} |a_i^{(M)}| \quad \text{or} \quad \frac{M}{(Q + M)^2} = \Gamma_M \quad \text{or} \quad \frac{1}{Q + M} = |a_M^{(M)}|.$$

For example, when M=2 equation (I.7) becomes

$$2 \sin 2(\omega + \Omega) + \left[1 - \frac{1}{Q + 2}\right] \sin(\omega + \Omega) = 0$$

or

$$\sin(\omega + \Omega) \left[4 \cos(\omega + \Omega) + 1 - \frac{1}{Q + 2}\right] = 0$$

Therefore $\quad \omega^* + \Omega = 0 \rightarrow \dfrac{1}{|D(\omega^*)|^2} = \dfrac{1}{\left(1 - \dfrac{2}{Q + 2}\right)^2}$

and $\qquad\qquad = \dfrac{(Q + 2)^2}{Q^2}$

$$\cos(\omega^* + \Omega) = -\frac{1}{4}\left(\frac{Q + 1}{Q + 2}\right) \rightarrow \frac{1}{|D(\omega^*)|^2} = \frac{(Q + 2)^2}{(Q + r)^2}$$

where r>2.

227

REFERENCES

[1] H. Urkowitz, "Energy detection of unknown deterministic signals," _Proc. IEEE_, Vol. 55, pp. 523-531, April 1967.

[2] R. A. Dillard, "Detectability of spread spectrum signals," _IEEE Trans. Aerosp. Electron. Systems_, Vol. AES-15, pp. 526-537, July 1979.

[3] W.W. Peterson, T.G. Birdsall and W.C. Fox, "The theory of signal detectability," _IRE Trans._, PGIT-1954.

[4] S. L. Berstein, "Optimum detectors of pseudonoise waveforms," MIT Lincoln Laboratory Technical Note No. 1974-37, June 1984.

[5] J.D. Edell, "Wideband, noncoherent, frequency-hopped waveforms and their hybrids in low-probability-of-intercept communications," NRL Report, Code 8025, November 1976.

[6] D. Woodring and J. Edell, "Detectability calculation techniques," NRL Report, Code 5480, September 1977.

[7] A. Polydoros and C.L. Weber, "Optimal detection considerations for low probability of intercept," _MILCOM '82 Proceedings_, pp. 2.1.1-2.15, October 1982.

[8] N. F. Krasner, "Optimal detection of digitally modulated signals," _IEEE Trans. Comm._, Vol. Com-30, No. 5, pp. 885-895, May 1982.

[9] N.F. Krasner, "Maximum likelihood parameter estimation for LPI signals," _MILCOM '82 Proceedings_, pp. 2.3-1 to 2.3-4, October 1982.

[10] M.G. Kendall and A. Stuart, _"The Advanced Theory of Statistics"_ , Vol. 1, Third Edition, Hafner Publishing Co., N.Y. 1969.

[11] A.H. Nuttall, "Accurate efficient evaluation of cumulative or exceedance probability distributions directly from characteristic functions," NUSC Technical Report No. 7023, October 1, 1983.

[12] H.L. Van Trees, _Detection, Estimation and Modulation Theory_, Part I, J. Wiley, 1968.

[13] S. Kullback, _"Information Theory and Statistics"_, Dover, New York, 1968.

[14] R. Hogg and A. Craig, _"Introduction to Mathematical Statistics"_, Second Edition, McMillan, New York, 1965.

[15] J. I. Marcum, "A Statistical theory of target detection by pulsed radar: mathematical appendix", The Rand Corp., July 1948, also reprinted in _Trans IRE-IT_, April 1960.

[16] J. Di Franco and W. Rubin, _Radar Detection_, Artech House, 1980.

[17] Special Issue on Synchronization, IEEE Trans. on Communications, Vol. COM-28, August 1980.

[18] J.K. Holmes, Coherent Spread Spectrum Systems, John Wiley, 1982.

[19] M. Schwartz, Information, Transmission, Modulation and Noise, Mc-Graw Hill, Second Edition, 1970.

[20] P. Wong, "Delay chip-rate detector analysis", GTE-Governments Systems, Western Division, Report No. PRE-1242, June 1985.

[21] I.S. Gradshteyn and I.M. Ryzhik, Tables of Integrals, Series and Products, New York, Acdemic Press, 1980.

[22] E. J. Kelly, I.S. Reed and W.L. Root, "The detection of radar echoes in noise," J. SIAM, Vol. 8, pp. 309-341, June 1960.

[23] I. S. Reed, "On a moment theorem for complex Gaussian processes," IRE Trans. Inform. Theory, Vol. IT-8, pp. 194-195, April 1962.

[24] I. Selin, "Detection of coherent radar returns of unknown Doppler shift," IEEE Trans. Inform. Theory, Vol. IT-11, pp. 396-400, July 1965.

[25] L.E. Brennan, I.S. Reed and W. Sollfrey, "A comparison of average-likelihood and maximum-likelihood ratio tests for detecting radar targets of unknown Doppler frequency," IEEE Trans. Inform. Theory, Vol. IT-14, pp. 104-110, January 1968.

[26] G.W. Lank, I.S. Reed and G.E. Pollon, "A semicoherent detection and Doppler estimation statistic," IEEE Trans. Aerosp. Electron. Systems, Vol. AES-9, No. 2, pp. 151-165, March 1973.

[27] J.D. Edell, "Wideband, noncoherent, frequency-hopped waveforms and their hybrids in low-probability-of-intercept communications," NRL Report, Code 8025, November 1976.

[28] R.A. Dillard, "Detectability of spread spectrum signals," IEEE Trans. Aerosp. Electron. Systems, Vol. AES-15, pp. 526-537, July 1979.

[29] N.F. Krasner, "Optimal detection of digitally modulated signals," IEEE Trans. Comm., Vol. Com-30, No. 5, pp. 885-895, May 1982.

[30] A. Polydoros and J.K. Holmes, "Autocorrelation techniques for wideband detection of FH waveforms in white noise," MILCOM '83 Proceedings, pp. 776-780, October 1983.

[31] A. Polydoros and J.K. Holmes, "Autocorrelation techniques for wideband detection of FH/DS waveforms in random tone interference," MILCOM '83 Proceedings, pp. 781-785, October 1983.

[32] A. Polydoros and K.T. Woo, "LPI detection of frequency-hopping signals using autocorrelation techniques," IEEE Trans. Commun., Special Issue on Spread Spectrum Communications, October 1985.

[33] A. Polydoros and K.T. Woo, "Wideband spectral detection of unknown frequency signals," presented at the Intern. Symposium on Information Theory, Brighton, England, June 1985

[34] S.M. Kay, "Robust detection of autoregressive spectrum analysis," IEEE Trans.Acoust., Speech and Signal Processing, Vol. ASSP-30, No.2, pp. 256-269, April 1982.

[35] S.M. Kay, "Asymptotically optimal detection in unknown colored noise via autoregressive modeling," IEEE Trans. Acoust., Speech and Signal Processing, Vol. ASSP-31, No. 4, pp. 927-940, August 1983.

[36] B. Porat and B. Friedlander, "Parametric techniques for adaptive detection of Gaussian signals," IEEE Trans. Acoust, Speech and Signal Processing, Vol. ASSP-32, No. 4, pp. 780-790, August 1984.

[37] S. Kay "Broadband detection of signals with unknown spectra," Intern. Conf. ASSP Proceedings, Tampa, Florida, pp. 331.1-33.1.3, April 1985.

[38] J.W. Ketchum and D. Herrick, "Signal detection using autoregressive parameters," Intern. Conf. ASSP Proceedings, Tampa, Florida, pp. 9.8.1-9.8.4, April 1985.

[39] E.K.L. Hung and R.W. Herring, "Simulation experiments to compare the signal detection properties of DFT and MEM spectra," IEEE Trans. Acoust., Speech and Signal Processing, Vol. ASSP-29, No. 5, pp. 1084-1089, October 1981.

[40] "System tradeoffs for LPI communications", Axiomatix Final Report R7911-1, November 5, 1979.

[41] M.K. Simon, J.K. Omura, R.A. Scholtz and B.K. Levitt, Spread Spectrum Communication, Vol. III, Computer Science Press, 1985.

[42] W.B. Davenport and W.L. Root, An Introduction to the Theory of Random Signals in Noise, N.Y. McGraw Hill, 1958.

[43] L. Kleinrock, "Detection of the peak of an arbitrary spectrum," IEEE Trans. Inform. Theory, July 1964.

[44] D. McGinn and D.H. Johnson, "Reduction of all-pole parameter estimation bias by successive autocorrelation," Proc. ICASSP'83, pp. 1088-1091, Boston, MA, April 1983.

[45] L.B Milstein and P.K. Das, "Spread spectrum receiver using surface acoustic wave technology," IEEE Trans. Commun., Vol. COM-25, pp. 841-847, August 1977.

[46] S. Kay and L. Marple, "Spectrum analysis - A modern perspective, "Proc. IEEE, Vol. 69, No. 11, pp. 1380-1419, November 1981.

[47] B.I. Helme and C.L. Nikias, "Improved spectrum performance via a data-adaptive weighted Burg technique," IEEE Trans. Acoust., Speech and Signal Processing, Vol. ASSP-33, No. 4, August 1985.

[48] A.V. Oppenheim and R.W. Schafer, "Digital Signal Processing, Prentice-Hall, New Jersey, 1975.

[49] A. Papoulis, Probability, Random Variables and Stochastic Processes, McGraw-Hill, New York, 1965.

[50] S. Haykin (ed.), Nonlinear Methods of Spectral Analysis, Vol. 34, Springer-Verlag, New York, 1979.

[51] S. Orphomides, Optimum Signal Processing, McMillan Publishing, Co., New York, 1985.

[52] J. Makhoul, "Linear prediction: A tutorial review", Proc. IEEE, Vol. 63, pp. 561-580, April 1975.

[53] J.P. Burg, "Maximum entropy spectral analysis", PhD Thesis, Stanford Univ., 1975.

[54] T. Ulrych and T. Bishop, "Maximum entropy spectral analysis and AR decomposition", Rev. Geophysics and Space Phys., Vol. 13, pp. 1983-200, Feb. 1985.

[55] B. Porata and B. Friedlander, " Parametric techniques for adaptive detection of Gaussian signals" IEEE Trans. ASSP, Vol. 32, pp. 780-790, August 1984.